MICRO-AEROBIC PRODUCTION OF ISOBUTANOL WITH *PSEUDOMONAS PUTIDA* AND INVESTIGATION OF ITS RESILIENCE TO SUBSTRATE LIMITATIONS

Dissertation

Von der Fakultät Energie-, Verfahrens- und Biotechnik der Universität Stuttgart zur Erlangung der Würde eines Doktor-Ingenieurs (Dr.-Ing.) genehmigte Abhandlung
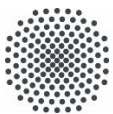
Vorgelegt von:

Andreas Ankenbauer

aus München

Hauptberichter: Prof. Dr.-Ing. Ralf Takors

Mitberichter: Prof. Dr.-Ing. Lars M. Blank

Tag der mündlichen Prüfung: 03. Mai 2022

Universität Stuttgart

Institut für Bioverfahrenstechnik der Universität Stuttgart

2022

Titel in deutscher Sprache:

MIKRO-AEROBE PRODUKTION VON ISOBUTANOL IN *PSEUDOMONAS PUTIDA* UND UNTERSUCHUNGEN ZU DESSEN WIDERSTANDSFÄHIGKEIT GEGEN SUBSTRATLIMITIERUNGEN

What we know is a drop, what we don't know is an ocean.

Sir Isaac Newton

Acknowledgements

DECLARATION OF AUTHORSHIP

I declare that this thesis has been written by me. Thoughts, results, and citations from other authors have been marked with references according to scientific standards. The presented results are based on my own research activities or on joint activities with other scientists in which case I have indicated my individual contributions.

Hiermit erkläre ich, dass ich die vorliegende Arbeit selbstständig angefertigt habe. Gedanken, Forschungsergebnisse und Zitate anderer Autoren wurden wissenschaftlichen Standards entsprechend im Text mit Quellenangaben gekennzeichnet. Die präsentierten Forschungsergebnisse beruhen auf meiner eigenen Forschungsaktivität oder gemeinsamen Forschungsaktivitäten mit anderen Wissenschaftlern, in welchem Fall ich die einzelnen Beiträge kenntlich gemacht habe.

_____   _____
            Ort, Datum   Andreas Ankenbauer

CONTENTS

NOMENCLATURE

Table 1 Abbreviations and descriptions

Abbreviation	Description
µ	Biomass specific growth rate
2-KG	2-ketogluconic acid
3-HA	3-hydroxyalkanoate
ADH	Alcohol dehydrogenase
ADP	Adenosine diphosphate
AlsS	Acetolactate synthase
AMP	Adenosine monophosphate
approx.	approximately
ATP	Adenosine triphosphate
B. subtilis	*Bacillus subtilis*
c_i	Concentration of a component i
$\tilde{c}$	Steady-state concentration
C. cellulolyticum	*Clostridium cellulolyticum*
C. glutamicum	*Corynebacterium glutamicum*
C. ljungdahlii	*Clostridium ljungdahlii*
C. thermocellum	*Clostridium thermocellum*
C10	3-hydroxydecanoic acid
C12	3-hydroxydodecanoic acid
cDNA	Complementary DNA
CO_2	Carbon dioxide
CoA	Coenzyme A
CDW	Cell dry weight
CTR	Carbon transfer rate
D	Dilution rate
d	Differential
DEG	Differentially expressed genes

Abbreviation	Description
DHAD	Dihydroxyacid dehydratase
DNA	Deoxyribonucleic acid
DOT	Dissolved oxygen tension
e	Exponential function
E. coli	*Escherichia coli*
e.g.	*exempli gratia* (= for example)
ED	Entner-Doudoroff
EDEMP	Combination of ED, EMP, and PP pathway in *Pseudomonas putida* KT2440
EMP	Embden-Meyerhof-Parnas
et al.	*et alii* (= and others)
F	Feed flow rate
FAD	flavin adenine dinucleotide
Fig.	Figure
G. thermoglucosidasius	*Geobacillus thermoglucosidasius*
GA3P	Glyceraldehyde-3-phosphate
GAM	Growth associated maintenance demand
Gcd	Glucose dehydrogenase
Glk	Glucokinase
KARI	Ketol-acid reductoisomerase
KDC	Ketoacid decarboxylase
KIV	2-ketoisovaleric acid
K_S	Saturation constant of substrate S
L. lactis	*Lactococcus lactis*
MON	Motor octane number
mRNA	Messenger RNA
m_S	Maintenance coefficient
NAD(H)	Nicotinamide adenine dinucleotide
NADP(H)	Nicotinamide adenine dinucleotide phosphate

Abbreviation	Description
ncRNA	Non-coding RNA
NGAM	Non-growth associated maintenance demand
OTR	Oxygen transfer rate
P. putida	*Pseudomonas putida*
Pfk	6-phospho-fructo-1-kinase
PFR	Plug flow reactor
pH	Negative decadic logarithm of the proton concentration
PHA	Poly(3-hydroxyalkanoate)
PhaZ	PHA depolymerase
PP	Pentose phosphate
ppGpp	Guanosine pentaphosphate
PQQ	Pyrroloquinoline quinone
R. eutropha	*Ralstonia eutropha*
r	Reaction speed
RL	Rhamnolipids
RON	Research octane number
S. cerevisiae	*Saccharomyces cerevisiae*
S. elongatus	*Synechococcus elongatus*
S	Substrate
STR	Stirred tank reactor
t	Time
TCA	Tricarboxylic acid cycle
V	Volume
$\dot{V}$	Gas flow rate
v/v	Volume to volume proportion
vvm	Volume per volume per minute
WT	Wild type
X	Biomass

Abbreviation	Description
Y	Yield
Z. mobilis	*Zymomonas mobilis*
τ	Residence time

Table 2 Indices and descriptions

Index	Description
in	Inflowing
out	Outflowing
max	Maximum
P	Product
i	Arbitrary component
X	Biomass
S	Substrate
P	Product
0	Time point 'zero'

Table 3 Units and descriptions

Unit	Description
m	meter
g	gram
mg	milligram
mL	milliliter
s	second
min	minute
h	hour
L	liter
%	Percent as part of 100 parts
C-mol	Mol of carbon atoms
mmol	Milli mol (10^{-3})
μ	Micro (10^{-6})

LIST OF FIGURES

LIST OF TABLES

ZUSAMMENFASSUNG

Der Wandel von einer auf fossilen Ressourcen basierenden Wirtschaft zu einer regenerativen Wirtschaft steht unmittelbar bevor, ist zugleich aber auch äußerst ungewiss. Ungeachtet des Wissens um die Verknappung fossiler Brennstoffe und die Zunahme von Naturkatastrophen infolge des Klimawandels beläuft sich der Anteil der erneuerbaren Energien an der weltweiten Energieversorgung immer noch auf weniger als 20 %. Die Förderung eines globalen nachhaltigen Energiemanagements obliegt nicht nur der Politik, sondern auch der Forschung und der Industrie, deren Aufgabe es ist, neue Technologien für erneuerbare Energien zu nutzen. Biokraftstoffe der nächsten Generation, wie beispielsweise Ethanol oder Isobutanol, besitzen das Potenzial den Verkehrssektor zu revolutionieren, um den Kohlenstoff-Fußabdruck der Menschheit zu senken. Derartige Biokraftstoffe können in großen Bioreaktoren mit Hilfe von Mikroorganismen aus erneuerbaren Rohstoffen gewonnen werden. Inhomogenitäten wie Kohlenstoff- oder Sauerstoffgradienten in großen Bioreaktoren beeinträchtigen jedoch häufig die Effizienz solcher industriellen Bioprozesse. Das Bodenbakterium *Pseudomonas putida* hat aufgrund seiner natürlichen Toleranz gegenüber Alkoholen, seiner vielseitigen Stressregulationen und seiner Affinität für ein breites Spektrum von Substraten das Potenzial, die häufig in der Industrie eingesetzten Organismen wie *Escherichia coli* oder *Corynebacterium glutamicum* abzulösen.

Im Rahmen der vorliegenden Arbeit soll die Fähigkeit von *P. putida* KT2440 zur Synthese von Isobutanol und dessen Leistungsfähigkeit unter Stress, wie er in großen Bioreaktoren verursacht wird, untersucht werden. Das Wachstum von *P. putida* wurde anhand kontinuierlicher Kulturen in einem herunterskalierten Versuchsaufbau analysiert, bestehend aus einem Rührkesselreaktor (STR) und einem damit verbundenen Pfropfenströmungsreaktor (PFR). Das System ermöglichte eine definierte Hungerzone im PFR, um großvolumige Glukose- oder Sauerstoffgefälle zu imitieren und die metabolische und transkriptionelle Reaktion der Zelle auf kurzfristige Nährstoffschwankungen zu erfassen. In *P. putida* wurde eine durch die stringente Antwort hervorgerufene Regulierung identifiziert, die zur sofortigen Wiederherstellung

der energetischen Ladung der Zelle durch den Abbau von intrazellulären 3-Hydroxyalkanoaten bei vorübergehender Glukoseauszehrung führte. Durch die Berechnung stöchiometrischer Bilanzen konnte nachgewiesen werden, dass 80 % des Bedarfs der Zelle an ATP durch den sofortigen Abbau von 3-Hydroxyalkanoaten bereitgestellt wurde. Diese Erkenntnis lässt sich durch Transkriptomanalysen belegen, da die für die Oxidation dieser Kohlenstoffverbindungen zuständigen Gene signifikant exprimiert waren. Im Gegensatz zu einer intensiven kurzfristigen Reaktion auf den Kohlenstoffmangel in dem PFR mit über 900 signifikant exprimierten Genen, passten sich die Zellen langfristig an diese Schwankungen an. Nach 25 Stunden des fortlaufenden Glukosemangels konnten lediglich minimale transkriptionelle und metabolische Veränderungen festgestellt werden und die Energieladung der Zelle blieb auf einem physiologischen Niveau in Höhe von 0,8. Ein weiteres Ergebnis der Transkriptomanalyse war der Nachweis von 725 exprimierten kleinen nichtkodierenden RNAs, die bisher nicht für *P. putida* annotiert waren. Angesichts der Tatsache, dass nichtkodierende RNAs auf Protein- und mRNA-Ebene agieren, trägt diese Prognosestudie zur Aufdeckung weiterer Regulationsmuster bei.

Trotz seines streng aeroben Wesens zeigte *P. putida* auch bei Sauerstofflimitierung eine stabile Wachstumsleistung. Die maximale Wachstumsrate von *P. putida* KT2440 und die Produktionsrate des rhamnolipidbildenden *P. putida* SK4-Stamms verringerten sich, wenn gelöster Sauerstoff in STR-Kulturen oszillierte, während die endgültige Biomasse und der Rhamnolipidertrag mit den Referenzbedingungen bei idealer Belüftung vergleichbar blieben. Ähnliche Ergebnisse wurden durch Begrenzung der Sauerstoffzufuhr durch oszillierendes Schütteln von Mikrotiterplatten festgestellt. Bei Nachahmung von Sauerstoffgradienten mit dem STR-PFR-Versuchsaufbau ergab sich eine mit den Kontrollbedingungen durchaus vergleichbare Wachstumsleistung, trotz des wiederholten Absinkens der Energieladung von 0,7 auf einen kritischen Wert von 0,3 innerhalb des PFR. Durch nicht zielgerichtete Proteomik konnte eine erhöhte Abundanz von Proteinen im Zusammenhang mit Replikation, Rekombination und Reparatur nachgewiesen werden. Aus der verringerten Häufigkeit der Acetyl-CoA-Synthase und der Isocitrat-Lyase konnte auf eine mögliche Herunterregulierung des Citratsäurezyklus und des Glyoxylat-Shunts geschlossen werden.

Um das Potenzial der Isobutanolsynthese aus Glukose zu ermitteln, wurden der L-Valin- und der rekombinante Ehrlich-Weg, die beide NADPH verbrauchen, in *P. putida* überexprimiert. Von mehreren erfolgreichen Produktionsklonen wies *P. putida* Iso2 die höchste Isobutanolbildung auf, nämlich $120 \, \text{mg} \, \text{L}^{-1}$ bei einem Ertrag von $22 \, \text{mg}_{isobutanol} \, \text{g}_{glucose}^{-1}$ in Schüttelkolbenkulturen. Die Isobutanolsynthese ging jedoch stets mit der beträchtlichen Bildung des Nebenprodukts 2-Ketogluconsäure (2-KG) einher. Um die Isobutanolproduktion weiter zu optimieren und die Ursache für die 2-KG-Ausscheidung zu untersuchen, wurde der Produktionsprozess auf eine Fed-Batch-Kultur mit getrennten Wachstums- und Produktionsphasen in einem kontrollierten 30-Liter-Bioreaktor hochskaliert. Auf diese Weise konnte ein maximaler Titer von $3.35 \, \text{g}_{isobutanol} \, \text{L}^{-1}$ erreicht werden. Das Metabolomprofil und die Berechnung der Stoffwechselflüsse in diesen Phasen lieferten Hinweise auf NADPH-Limitierungen während der Isobutanolproduktion. Das für die Isobutanolsynthese benötigte NADPH konkurrierte mit dem NADPH-Bedarf für anabole Prozesse, was das Wachstum verlangsamte. Die Zellen reagierten auf die NADPH Verknappung offenbar mit der Verlagerung von Protonen aus NADH, was wiederum den Elektronentransport für die oxidative ATP-Synthese beeinträchtigte. Durch diesen Energiemangel war die Zelle gezwungen, Elektronen aus der direkten Oxidation von Glukose zu 2-KG zu gewinnen, wodurch die erhöhte Bildung von Nebenprodukten zu erklären ist. Die Verwendung einer mikro-aeroben Umgebung im Bioreaktor verhinderte die 2-KG-Bildung fast vollständig und verbesserte die Versorgung mit NADPH zur Bildung von Isobutanol, was eine Verdreifachung der Ausbaute auf $60 \, \text{mg}_{isobutanol} \, \text{g}_{glucose}^{-1}$ erzielte. Die Erkenntnisse dieser Arbeit dienen als wissenschaftlicher Nachweis für die Eignung von *P. putida* KT2440 in industriellen Produktionsanlagen eingesetzt zu werden aufgrund seiner vielseitigen Stressregulation, die anderen von der Industrie bevorzugten Mikroorganismen überlegen ist.

ABSTRACT

The transition from an economy based on fossil resources to a regenerative economy is imminent yet uncertain. Despite an awareness of the scarcity of fossil fuels and the increasing natural disasters due to climate change, the world's renewable energy supply still constitutes less than 20% of the total energy supply. Advancing global sustainable energy management lies not only in the hand of policies but also in the hand of research and industry to exploit new renewable energy technologies. To reduce humankind's carbon footprint, next-generation biofuels, such as ethanol or isobutanol, have the potential to revolutionize the transportation sector. These biofuels can be produced from renewable feedstock in large bioreactors using microorganisms. However, inhomogeneities, such as carbon or oxygen gradients in large-scale bioreactors, often limit the efficiency of such industrial bioprocesses. The soil bacterium *Pseudomonas putida* has the potential to supersede existing industrial workhorses like *Escherichia coli* or *Corynebacterium glutamicum* due to its natural tolerance towards alcohols, its versatile repertoire of stress responses, and its affinity to a broad range of substrates.

This thesis aims to investigate the capability of isobutanol production in *P. putida* KT2440 and to explore its performance during large-scale stress. The growth of *P. putida* was analyzed with continuous cultures in a scale-down system consisting of a stirred tank reactor (STR) and a connected plug flow reactor (PFR). The system allowed a defined starvation zone inside the PFR to mimic large-scale glucose or oxygen gradients and to resolve the cell's metabolic and transcriptional response to short-term nutrient fluctuations. In *P. putida*, a regulation mediated by the stringent response was identified which resulted in the immediate restoration of the cell's energy charge by degrading intracellular 3-hydroxyalkanoates during transient starvation. The computation of stoichiometric balances revealed that 80% of the cell's ATP maintenance demand was covered by the immediate degradation of the 3-hydroxyalkanoates. Transcriptomic analyses supported this finding as genes belonging to the oxidation of these carbon compounds were significantly upregulated. In contrast to an intense short-term response to carbon starvation inside the PFR with

over 900 significantly expressed genes, the cells adapted to the recurring fluctuations in the long term. Only minor transcriptional and metabolic changes were detected after 25 hours of repeated glucose starvation and the energy charge was at a physiological level of 0.8. A further output of transcriptome analysis was the detection of 725 expressed small non-coding RNAs that were not yet annotated for *P. putida.* Since non-coding RNAs act on protein and mRNA levels this prediction study contributes to unraveling further regulation patterns.

Despite its strict aerobic nature, *P. putida* also showed stable growth performance during oxygen limitations. The maximal growth rate of *P. putida* KT2440 and the production rate of the rhamnolipid producing *P. putida* SK4 strain were reduced when dissolved oxygen was oscillated in STR batch cultivations, but the final biomass and product yield remained comparable to the reference condition with ideal aeration. Similar results were obtained by limiting the oxygen supply through oscillating shaking of microtiter plates. When large-scale oxygen gradients were mimicked using the STR-PFR scale-down system, the overall growth performance was still comparable to the undisturbed condition even though energy charges repeatedly dropped from 0.7 to a critically low level of 0.3 inside the PFR. Untargeted proteomics revealed the increased abundance of proteins related to replication, recombination, and repair. A possible downregulation of the TCA and the glyoxylate shunt was concluded from the reduced abundance of acetyl-CoA synthase and isocitrate lyase.

To examine the potential of isobutanol synthesis from glucose, the L-valine and the recombinant Ehrlich pathway, both NADPH-consuming, were overexpressed in *P. putida*. Among several successful production clones, *P putida* Iso2 exhibited the highest isobutanol formation of 120 mg L^{-1} with a yield of 22 $mg_{isobutanol}$ $g_{glucose}^{-1}$ in shake-flask cultures. However, isobutanol synthesis was always accompanied by an immense by-product formation of 2-ketogluconic acid (2-KG). To further improve isobutanol production and investigate the cause of 2-KG excretion, the production process was scaled up to fed-batch cultivation in a 30 L controlled bioreactor with separated growth and production phases. Thus, a maximum titer of 3.35 $g_{isobutanol}$ L^{-1} was achieved. The metabolome profile and the calculation of metabolic fluxes in these phases allowed the identification of NADPH limitations during isobutanol production. The NADPH for the isobutanol pathway competed with the NADPH demand for

anabolic processes which reduced growth. The cells apparently counteracted the NADPH limitation by translocating protons from NADH which, in turn, impeded the electron transport for oxidative ATP synthesis. This energy shortage forced the cell to generate electrons from the direct oxidation of glucose to 2-KG, explaining the high by-product formation. Using a micro-aerobic environment in the bioreactor prevented the 2-KG formation almost completely and improved the NADPH supply for isobutanol formation, resulting in a nearly triple yield of 60 $mg_{isobutanol}$ $g_{glucose}^{-1}$. The outputs of this thesis provide scientific evidence of the suitability of *P. putida* KT2440 for large-scale applications due to its versatile stress regulation, which is superior to other industrial favored microorganisms.

1. INTRODUCTION

1.1. INDUSTRIAL BIOTECHNOLOGY – CHANCES AND CHALLENGES

In general, industrial biotechnology summarizes the efforts to generate valuable chemical molecules by using microorganisms. This field of industry originates from the ancient technology of brewing beer and wine or transforming milk into food and beverages (Campbell-Platt, 1994). Thus, it has been a key part of our daily nutrition for several thousands of years. These classical processes of converting raw products into valuable comestibles using microbes are referred to as fermentation processes. Besides the mass production of beer in large fermentation vessels, the first industrial-scale microbial fermentation began with the production of penicillin in the late 1940s (Fleming, 1929). This evolution paved the way for further biotechnological production of different pharmaceuticals such as insulin. Furthermore, new fields like red biotechnology evolved, an industry branch that aims to supply therapeutic antibodies against different diseases by using human cells instead of bacterial or yeast cells. Nevertheless, white biotechnology has also evolved into an indispensable part of our everyday life as streamlined bacteria are exploited to secrete specialty chemicals or even sustainable biofuels like bioethanol (Hermann and Patel, 2007; M. Patel et al., 2006).

An increasingly important product in the means of white biotechnology is biofuels. Already 70% of the total renewable energy supply (14% in 2018) can be attributed to biofuels (c.f. Figure 1). The exploration of next-generation biofuels is of utmost interest to achieve global climate protection goals. For example, the European Union declared a target of at least 10% of transportation fuels from renewable biofuels by the end of 2020 though in 2018 only 5.5% of transportation fuels were biofuels. However, the production of renewable fuels in the EU is steadily increasing, reaching over 15 million

tons in 2018. Compared to the 260 million tons of fossil fuel-based consumption in the transportation sector within Europe, there is still enough potential for developing biofuel production strategies (European Commission, 2020). The classical approach for first-generation biofuels relies on the transformation of field crops into ethanol using yeast fermentation. Thus, the growing biofuel market is another important part of industrial biotechnology. However, the use of potential food for transportation fuels competes with the increasing malnutrition and food shortages in many parts of the world. Therefore, intensive research must be done on second-generation biofuels which use agricultural byproducts such as lignocellulosic biomass that serves as a substrate for microbes (Timilsina, 2014). In addition, microbial production of alcohols with higher energy density and lower corrosive impacts compared to ethanol is of important industrial interest to pave the way for a sustainable energy future. In summary, the essential fields of industrial biotechnology contribute significantly to everyone's life, be it nutrition, health, transportation, or energy supply. Hence, we must take the chances that arise with this industry branch and explore further optimization of the existing processes and industrial hosts.
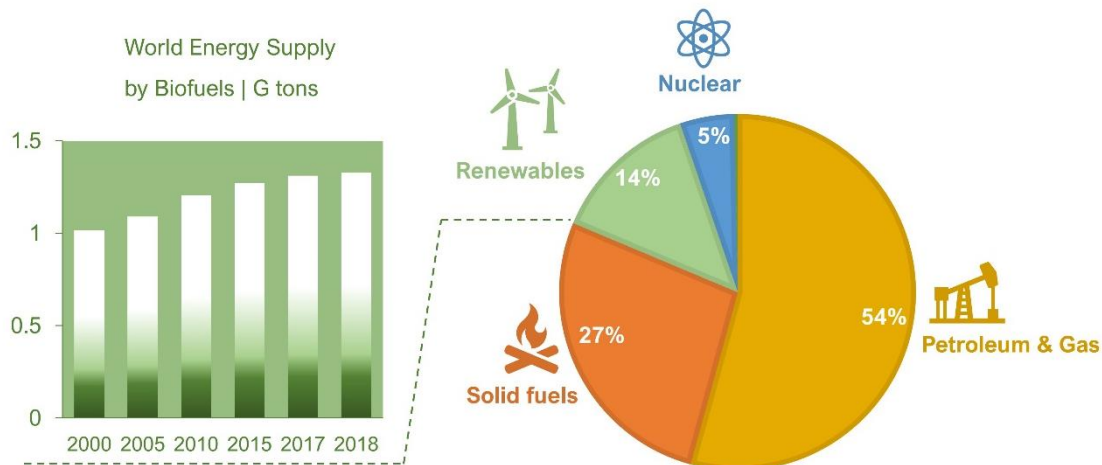
Figure 1 The proportion of the different origins of the world's total energy supply in 2018 is illustrated in the pie chart. Approx. 0.3% (not visible) derives from other, not mentioned sources. The energy supply by biofuels accounts for approx. 70% of all renewable sources (in total 14%) +in 2018 and its production has been constantly increasing since 2000 according to the European Commission (2020).

Today, industrial host organisms are cultivated mostly in large stainless-steel bioreactors with working volumes up to 20 m³ for human cell cultures or fine chemicals

and even 100 m^3 for commodities (Takors, 2012). The propagation of cells involves the stepwise increase of the cell density and the working volume in different cultivation systems and scales. Thus, a typical scale-up strategy can imply a volume factor of 10^8 from the working cell bank to the final production scale (Crater and Lievense, 2018). Efficient and economic industrial bioprocesses require that cells perform equally well on a lab scale and on a large scale. It is not unusual that promising innovative bioprocesses fail when they are transferred from lab-scale to pilot-scale or above. Often, process transfers are accompanied by performance losses regarding biomass, product yields, and plasmid amplification of up to 94% (Lara et al., 2006a). Takors (2012) summarized several stress factors for the cell culture that only arise during the process of scale-up but usually not in lab-scale experiments. Among these are biological impacts like the increased number of cell divisions or chemical factors comprising modified media concentration of salts and gas solubility. In addition, physical impacts such as high hydrostatic pressures at the bottom of large-scale bioreactors are further sources of bioprocess disturbances and affect the solubility of process gases (oxygen and carbon dioxide). In combination with inefficient mixing and high microbial consumption rates, substrate gradients often occur (Takors, 2012). Several research projects revealed productivity issues due to a variety of inhomogeneities in cubic meter scale fermenters (Enfors et al., 2001; Humphrey, 1998; Lara et al., 2006a; Schweder et al., 1999). The authors identified gradients regarding dissolved oxygen and carbon dioxide, pH, temperature, carbon substrates as well as shear stress as major crucial impacts. Typically, these gradients arise due to increasing mixing times dependent on the working volume. To be precise, the duration of homogenic mixing can range from 3 seconds in a 5 L stirred tank reactor (Xing et al., 2009) to 1000 seconds in a 150 m³ bubble column reactor (Sweere et al., 1987). Lara et al. (2006a) list a comprehensive overview of determined mixing times in different types of bioreactors. Consequently, overcoming the negative effects of large-scale inhomogeneities constitutes one of the major challenges in industrial biotechnology. This requires the holistic understanding of physiological, metabolic, and transcriptomic reactions of industrial microbes aiming to streamline the production host and optimize the bioprocess.

1.2. MOTIVATION AND OBJECTIVES

The hunger for energy on the Earth is constantly increasing due to the growth of our population combined with ongoing globalization. The world's energy production has increased since 1979 by approximately 2% every year (IEA, 2020). In contrast to a small but emerging proportion of renewable-based energies, such as solar, wind, geothermal, and biofuels (in total 13.5% in 2018), the world's total energy demand was mainly (81% in 2018) supplied by the finite resources petroleum, gas and solid fuels (c.f. Figure 1) (European Commission, 2020). This leaves a high carbon footprint since the carbon compounds that were stored and transformed in a natural process over millions of years are now burned within decades. This burning process leaves, besides useable energy and toxic oxygen compounds, water vapor and carbon dioxide which are responsible for the greenhouse effect (Hsiang and Kopp, 2018; King, 2004). To create a bioeconomy that thrives on renewable production of energy sources, industries and research institutions are focusing on the exploration of alternatives for fuels and for other petrol-based bulk chemicals. One promising candidate among renewable fuels is isobutanol since it can be used as a drop-in additive to gasoline and as a precursor for jet fuels. There is a strong worldwide demand for isobutanol with an expected growth of 6.4% per year reaching USD 1.6 billion by 2027. (Brownstein, 2015; Marketysers Global Consulting LLP, 2020).

Thus, in terms of a circular bioeconomy, the sustainable production of isobutanol as a next-generation biofuel from renewable feedstock is of paramount interest within this market. Several microorganisms such as *Escherichia coli* or *Corynebacterium glutamicum* were already engineered for efficient overproduction of isobutanol from glucose as a carbon source (Blombach and Eikmanns, 2011; Chen and Liao, 2016; Lan and Liao, 2013). However, the toxicity of isobutanol to said microbial producers constrained high production titers and thereby the efficient industrial application so far (Blombach et al., 2011; Chen and Liao, 2016; Jones and Woods, 1986). Since a natural tolerance towards solvents, alcohols, and aromatics was discovered for *Pseudomonas putida* KT2440 (c.f. chapter 2.2.3), engineering this microbe to become an isobutanol producer might overcome the problem of product inhibition and pave the way for industrial application. This also requires ensuring the practicality and feasibility of *P. putida* being cultivated in large-scale stirred tank reactors. Only few studies cover

a process transfer of *P. putida* into pilot scale (400 – 500 L) (Elbahloul and Steinbuchel, 2009; Gorenflo et al., 2001). Thus, limited knowledge of the performance of *P. putida* in cubic-scale bioprocesses is currently available. Another issue that has restricted the widespread industrial use of *P. putida* so far is its obligate aerobic nature, which results in high oxygen demand during high cell density cultivations (c.f. chapter 2.3.2). As previously mentioned, industrial microbial production processes typically suffer from growth and productivity losses due to reactor inhomogeneities such as pH gradients, hydrostatic pressures, and nutrient starvation zones (Lara et al., 2006a; Takors, 2012). Hence, the suitability of *P. putida* as industrial production platform will be unraveled in the present thesis. The objectives are illustrated in Figure 2 and comprise the following research topics:
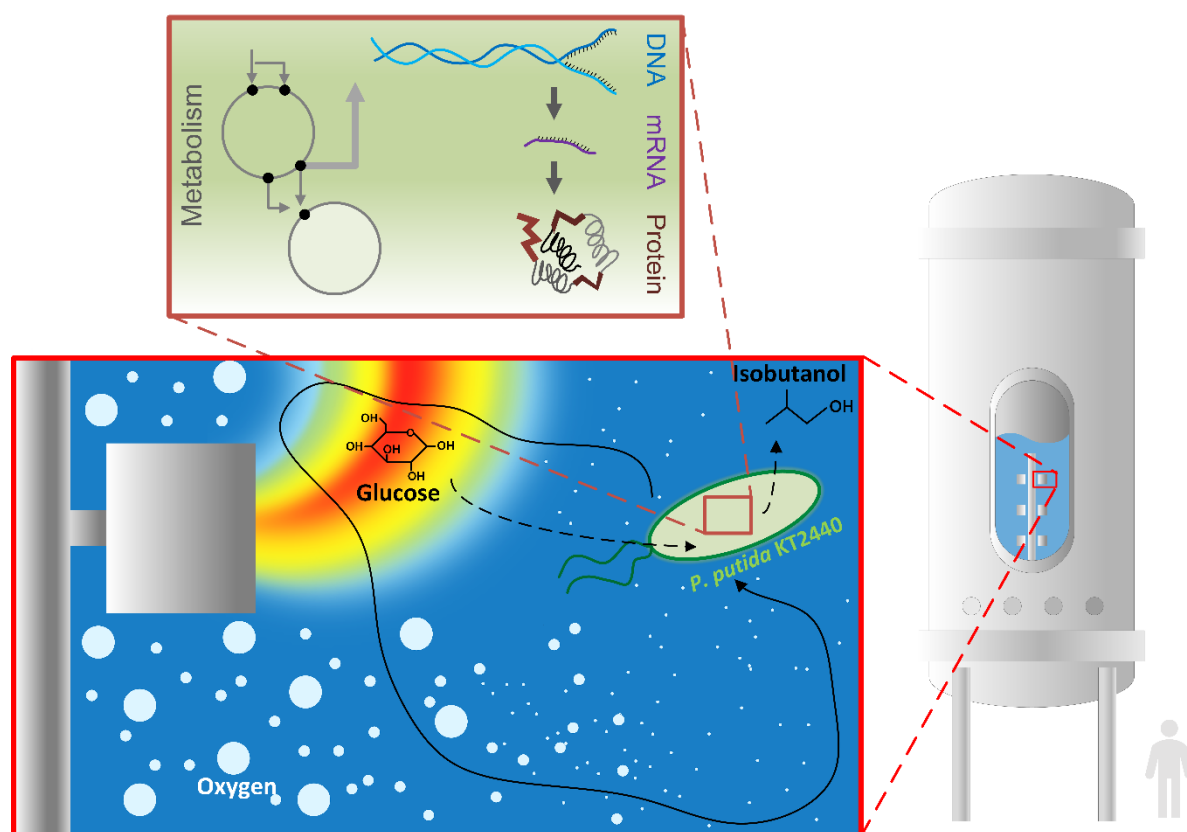
Figure 2 At a glance: the different research topics to unravel the large-scale performance of P. putida and its suitability as an isobutanol producer are illustrated within this figure. The objectives of this thesis comprise the conversion of glucose to isobutanol using P. putida and the identification of stress regulation patterns in the metablic and transcriptional profile during short-term glucose and oxygen starvation, that are likely to occur in large-scale stirred tank reactors due to inhomogeneities.

❖ Cultivate *P. putida* KT2440 under controlled growth conditions with defined starvation zones and evaluate the phenotypical performance during typical large-scale stresses such as oxygen and glucose gradients. The exposure to repeated starvation zones will stimulate the cells' growth during glucose- and oxygen-limited chemostat cultivations and thereby mimic inhomogeneities that are likely to occur in large-scale bioreactors.

❖ Decipher *P. putida's* stress mechanisms to cope with transient nutrient starvations on transcriptional, protein and metabolic level. Hereby, multi-omics studies will elucidate the short- and long-term strategies of the cells to manage these stress factors. The analysis of differential gene expression levels and the cell's adenylate energy charge based on intracellular levels of AMP, ADP, and ATP will be used to compare its performance to that of *E. coli* under similar conditions. The alteration of intracellular metabolite levels such as the alarmone ppGpp and 3-hydroxyalkanoates will contribute to a deeper understanding of *P. putida's* stringent response during carbon starvation.

❖ Elucidate the response of the strict aerobic organism to low oxygen environments. Metabolic profiles aim to identify pathways and stress responses that enable *P. putida* to cope with oxygen stress. The findings can contribute to increasing the industrial application of *P. putida* since microorganisms with low oxygen demand are preferred in industry.

❖ Evaluate the potential and constraints of recombinant isobutanol production with *P. putida*. The plasmid-based implementation of the Ehrlich pathway in a strain that is unable to degrade isobutanol will enable the production of this alcohol with *P. putida.* The scale-up of the best producer strain with separated growth and induction phases aims to identify metabolic constraints during isobutanol synthesis. The aerobic isobutanol production will be compared to micro-aerobic conditions regarding side product formation and the product conversion yield.

2. THEORETICAL BACKGROUND

2.1. THE NEXT-GENERATION BIOFUEL ISOBUTANOL

The production of first-generation biofuels like bioethanol or biodiesel relies on sugar-containing substrates or plant-based fatty acids, thus depends on valuable agricultural products and arable land. To overcome the competitive bias that arises from the transformation of food into fuel, the research for fuel alternatives promotes next-generation biofuels that can be produced from renewable sources and predominantly from agricultural side products. The biomass-to-liquid (BtL) approach uses lignocellulosic biomass, mostly from wood, to create synthesis gas that is then chemically processed to yield liquid alkanes, alkenes, and alcohols according to the Fischer-Tropsch method (Dürre, 2007). However, industrial usage of BtL fuels currently focuses on biodiesel (SunFuel® and SunDiesel®, cooperation of Choren Industries, Shell, Volkswagen, and Daimler). Moreover, several companies such as Clariant (Hortsch and Corvo, 2020; Rarbach and Söltl, 2013) and Iogen (Tolan, 2002) offer technologies for the conversion of cereal and corn straw into bioethanol using microbial fermentation.

2.1.1. CHEMICAL PROPERTIES OF ISOBUTANOL

As an alternative to ethanol, butanol and isobutanol offer several important advantages as biofuels. Besides its limited miscibility with water (8.5%) and thus lower hygroscopicity, isobutanol has a higher blending capacity with gasoline and works with existing combustion engines. Moreover, its lower vapor pressure makes it safe to handle and it poses no risk when transported in existing pipelines due to reduced corrosivity. Most importantly, the energy content of iso-/butanol is significantly higher, e.g., isobutanol has a net energy content of 82% of gasoline in contrast to ethanol that reaches 65% of gasoline energy (Brownstein, 2015; Dürre, 2007). As isobutanol has a

higher "research octane number" (RON = 113) and "motor octane number" (MON = 94) than n-butanol (RON = 94; MON = 78), it is more attractive as a supplement for gasoline. In 2005, the practical utility of the alternative fuel was demonstrated when a car powered by 100% isobutanol was driven for 10,000 miles (Brownstein, 2015).

2.1.2. CHEMICAL AND MICROBIAL SYNTHESIS OF ISOBUTANOL

Conventionally, isobutanol and other C4 alcohols can be synthesized chemically by hydroformylation of propylene and synthesis gas. Propen reacts with carbon monoxide and hydrogen to butanal and 2-methylpropanal. Latter is hydrated to form 2-methyl-1-propanol, also known as isobutanol or isobutyl alcohol (Chianelli et al., 1994; Verkerk et al., 1999).

According to recent market estimations, the global demand for isobutanol is expected to grow with an annual growth rate of 6.4%, reaching a market volume of USD 1.6 billion in 2027. In the past, isobutanol was mainly produced from petroleum and used both as a solvent and a precursor in butyl rubber production. However, the relatively high costs for synthetic isobutanol production limit its use as a fuel additive (Brownstein, 2015; Marketysers Global Consulting LLP, 2020). Nevertheless, several efforts have already been undertaken regarding microbial isobutanol production. Louis Pasteur and Chaim Weizmann were pioneers that discovered the anaerobic production of acetone/butanol/ethanol (ABE) by *Clostridium acetobutylicum* from starch over 100 years ago (Pasteur, 1862; Sauer et al., 1993; Weizmann, 1916). This discovery paved the way for commercial ABE production. However, critical issues such as low yields and product inhibition constrained the first industrial approaches for microbial ABE production during the first half of the 20th century (Brownstein, 2015).

Different host organisms and cultivation strategies have already been established for microbial isobutanol production (Chen and Liao, 2016; Lan and Liao, 2013). So far, the highest isobutanol titer was achieved with an engineered *E. coli* strain that produced more than 50 g L^{-1} within 72 hours in an aerobic fed-batch process with *in situ* gas stripping yielding 0.68 mol$_{isobutanol}$ mol$_{glucose}^{-1}$ (Baez et al., 2011). The authors further showed that gas stripping of isobutanol through increased aeration in the bioreactor (1.2 vvm) is an effective strategy to avoid toxic product levels in the broth and energy-intensive distillation. Furthermore, Blombach et al. (2011) developed a two-phase

fermentation comprising aerobic growth on glucose and acetate followed by anaerobic production of isobutanol with *Corynebacterium glutamicum*. This approach with the tailored *C. glutamicum* Iso7 strain resulted in 180 mM (13.3 g L^{-1}) isobutanol with a volumetric isobutanol productivity of 4.4 mmol L^{-1} h^{-1}. However, the high final isobutanol concentration in the broth probably constrained higher titers due to product toxicity (Blombach et al., 2011). Table 4 lists an overview of recent metabolic engineering approaches for the production of isobutanol in different host organisms.

2.1.3. THE METABOLIC PATHWAY FOR MICROBIAL ISOBUTANOL PRODUCTION

The metabolic pathway for isobutanol from glucose is derived from the biosynthesis of the branched-chain amino acids L-valine and L-leucine (see Figure 3). Essentially, two pyruvic acid molecules are combined to 2-acetolactate under the release of CO_2 via the enzyme acetolactate synthase AlsS. Next, 2-acetolactate is converted to 2,3-dihydroxyisovalerate via a ketol-acid reductoisomerase (KARI, IlvC) with NADPH as a cofactor. Subsequently, a dihydroxyacid dehydratase (DHAD, IlvD) dehydrates the intermediate to 2-ketoisovaleric acid (2-KIV) that also serves as the precursor for valine and (iso-)leucine. Finally, two more reaction steps of the Ehrlich pathway yield isobutanol through the decarboxylation of 2-KIV to isobutyraldehyde via a ketoacid decarboxylase (KDC) and subsequent conversion via an alcohol dehydrogenase (ADH) (Atsumi et al., 2008; Blombach and Eikmanns, 2011; Chen, 1978; Lan and Liao, 2013).
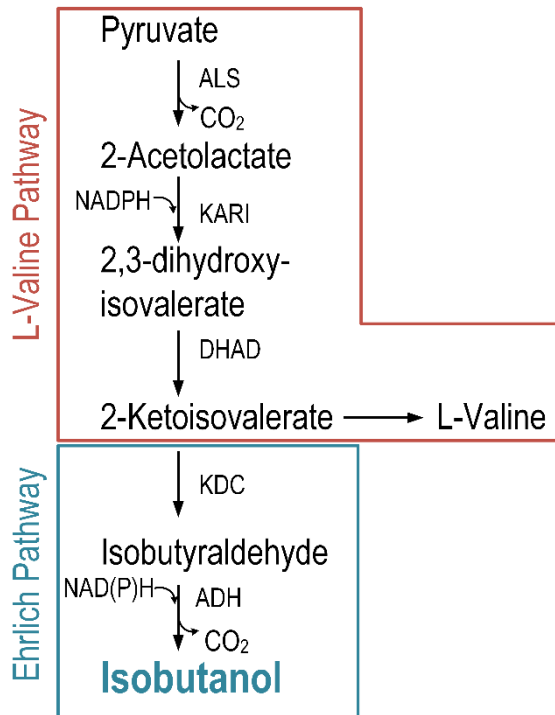
Figure 3 Metabolic pathway of isobutanol production from pyruvate via the L-valine and the Ehrlich pathway.

The common pathway for isobutanol formation in metabolically engineered strains relies on a combination of the branched-chain amino acid pathway and the Ehrlich pathway. The latter is not native in most organisms, thus must be introduced by recombinant gene expression which comprises a KDC and an ADH enzyme (Lan and Liao, 2013). The first decarboxylation step can be realized by the 2-ketoacid decarboxylase (*kivD*) from *Lactococcus lactis* whereas different alcohol dehydrogenases from *Saccharomyces cerevisiae (adh2)*, *C. glutamicum (adhA)*, *E. coli (yqhD),* or *L. lactis (adhA)* have been tested in previous studies (Atsumi et al., 2010; Atsumi et al., 2008; Blombach et al., 2011; Li et al., 2011; Smith et al., 2010).

Furthermore, for the efficient conversion of pyruvate to isobutanol, increased carbon flux and cofactor supply must be ensured in the pathway. In this regard, it was shown that overexpression of the genes coding for the enzymes in the valine pathway, that are ALS, KARI, and DHAD, is beneficial for isobutanol production (Atsumi et al., 2008; Blombach et al., 2011; Blombach and Eikmanns, 2011; Li et al., 2011). Moreover, most of the KARI enzymes used in these studies show high cofactor affinity for NADPH

(Blombach and Eikmanns, 2011; Brownstein, 2015). Additionally, the final conversion of isobutyraldehyde by ADH requires either NADH or NADPH as a cofactor. Thus, the formation of 1 mol isobutanol consumes 1 mol NADPH and 1 mol NADH or 2 mol NADPH, depending on the ADH used. Therefore, to ensure high NADPH availability for product formation, several studies (Table 4) applied micro-aerobic or anaerobic fermentation strategies in order to provide an increased reducing power, hence, shift the redox state towards the reduced forms NADH or NADPH.

In case of *E. coli* or *C. glutamicum*, two moles of NADH are generated in the glycolysis from glucose to pyruvate, thus supplying ample amounts of catabolic cofactors, even under oxygen depletion. Nevertheless, either one or two moles of the anabolic cofactor NADPH are required in the L-valine and Ehrlich pathway. The TCA cycle serves as major source for NADPH (via isocitrate dehydrogenase and malic enzyme (Spaans et al., 2015)) but is strictly downregulated or inactive under oxygen limitation in most organisms, e.g. *C. glutamicum* (Lange et al., 2018). Thus, the NADPH supply must be ensured either by exchanging NAD+ to NADP+ dependent enzymes in the glycolysis, or by increasing the pentose phosphate flux, or by using transhydrogenase enzymes that catalyze the proton transfer from NADH to NADP+. The native membrane-bound transhydrogenase in *E. coli* seems to be beneficial for cofactor balance, as a high yield of 0.86 $mol_{isobutanol}$ $mol_{glucose}^{-1}$ was achieved with *E. coli* harboring the native NADPH dependent alcohol dehydrogenase YqhD (Atsumi et al., 2010; Atsumi et al., 2008). In contrast, Bastian et al. (2011) introduced an NADH-dependent KARI enzyme that was generated by mutagenesis and an NADH-dependent ADH (from *L. lactis*) enzyme in *E. coli* to overcome the NADPH dependency which resulted in a maximal yield of 1 $mol_{isobutanol}$ $mol_{glucose}^{-1}$ in *E. coli* under anaerobic conditions. Furthermore, the authors overexpressed the native transhydrogenase PntAB in a strain with an NADPH dependent pathway which similarly yielded 100% conversion of glucose into isobutanol under anaerobic condition. Recombinant expression of *pntAB* improved isobutanol production in *C. glutamicum*, too (Blombach et al., 2011). To summarize, the cofactor supply, in particular NADPH, and the redox balance plays an important role in isobutanol-producing organisms.

Table 4 Several approaches to synthesis of isobutanol with different microorganisms and various substrates. The related maximum titers and the cultivation systems are listed.

Organism	Substrate	Titer	Bioreactor	Reference
E. coli	Glucose	13.4 g L^{-1}	Flask	(Bastian et al., 2011)
E. coli	Glucose	22 g L^{-1}	Shake flask	(Atsumi et al., 2008)
E. coli	Glucose	50 g L^{-1}	Bioreactor	(Baez et al., 2011)
C. cellulolyticum	Cellulose	0.66 g L^{-1}	Tube	(Higashide et al., 2011)
G. thermoglucosidasius	Cellobiose	0.6 g L^{-1}	Tube	(Lin et al., 2014)
C. thermocellum	Cellulose	5.4 g L^{-1}	Tube	(Lin et al., 2015)
S. cerevisiae	Glucose	1.62 g L^{-1}	Flask	(Matsuda et al., 2013)
S. elongatus PCC7942	CO_2	0.45 g L^{-1}	Bottle	(Atsumi et al., 2009)
R. eutropha	CO_2	0.846 g L^{-1}	Bioreactor	(Li et al., 2012)
B. subtilis	Amino acids	1 g L^{-1}	Flask	(Choi et al., 2014)
C. glutamicum	Glucose	13.3 g L^{-1}	Bioreactor	(Blombach et al., 2011)
Z. mobilis	Amino acids	4 g L^{-1}	Flask	(Qiu et al., 2020)
C. ljungdahlii	CO_2, CO, H_2	0.13 g L^{-1}	Bioreactor	(Hermann et al., 2021)
Pseudomonas sp. strain VLB120	Glucose	0.003 mg L^{-1}	Flask	(Lang et al., 2014)

2.2. *PSEUDOMONAS PUTIDA* KT2440 AS MICROBIAL PRODUCTION HOST

2.2.1. THE VERSATILE METABOLISM OF *P. PUTIDA*

Taken into the natural habitat of microbial producers, some microbes might be more adapted to fluctuating substrate availability than others. As such the soil-dweller *Pseudomonas putida* is well-endowed, thanks to evolution, to live a life in 'feast and famine' and shares the remarkable ability to adapt to different physicochemical and nutritional niches with other *Pseudomonas* species (Nikel et al., 2014). *Pseudomonas putida* KT2440 is a gram-negative derivative of *Pseudomonas arvilla* mt-2 that was originally found in soil samples in Japan (Nakazawa, 2002). *P. putida* benefits from an atypical central carbon metabolism. Its genome includes all the genes from the three prominent catabolic pathways: the Entner-Doudoroff (ED), the Embden-

Meyerhof-Parnas (EMP), and the pentose phosphate (PP) pathway except the enzyme 6-phospho-fructo-1-kinase (Pfk) (Chavarría et al., 2013). It was demonstrated that glucose as a carbon source is converted in a cyclical way with the contribution of all three pathways in the so-called EDEMP cycle providing the necessary building blocks for the cellular functions (Nikel et al., 2015). However, the intermediate 6-phosphogluconate is processed mainly through the ED pathway, which yields pyruvate and glyceraldehyde-3-phosphate (GA3P) (del Castillo et al., 2007; Nikel et al., 2015). Furthermore, glucose uptake in *P. putida* comprises the initial periplasmic oxidation to gluconic acid and a further small proportion is converted to 2-ketogluconic acid (del Castillo et al., 2007). Only approx. 10% of glucose is channeled directly to glucose-6-phosphate via glucokinase (Glk) (Nikel et al., 2015).

The architecture of its central carbon metabolism provides high reducing power (Ebert et al., 2011). More precisely, it was shown by in silico flux analysis that the cells exhibit a surplus of NADPH (Kohlstedt and Wittmann, 2019; Nikel et al., 2015), thus enabling this strain to endure oxidative stress and adapt its redox balance to current needs (Kim and Park, 2014; Nikel et al., 2016a). This organism is gaining increased attention from industry and research as it is genetically accessible (Bagdasarian et al., 1981; Nelson et al., 2002), certified as HV1 (Kampers et al., 2019b), and exhibits a broad range of substrate affinities among them harvest residuals such as lignocellulose and oils (Hintermayer and Weuster-Botz, 2017; Weimer et al., 2020). Moreover, *P. putida* shows a natural tolerance towards solvents and toxic compounds (Nikel and Lorenzo, 2014; Ramos et al., 2015; Simon et al., 2015). Since this bug is a natural degrader of different complex sources, it can be used for bioremediation (Dvořák et al., 2017; Lorenzo, 2008; Raghavan and Vivekanandan, 1999; Weimer et al., 2020) and biopolymer production such as poly(3-hydroxyalkanoates) (Huijberts et al., 1992; Mozejko-Ciesielska et al., 2018; Prieto et al., 2016). By metabolic engineering of *P. putida*, the biocatalytic conversion of lignin to *cis,cis*-muconic acid, that was further processed to nylon, was recently demonstrated (Kohlstedt et al., 2018).

2.2.2. THE ROLE OF PHA IN *P. PUTIDA*

Several microorganisms, among them *Ralstonia*, *Bacillus*, and *Pseudomonas* species, are known to synthesize poly(3-hydroxyalkanoates) (PHA), that can be used as

precursors for biodegradable plastics, from different carbon feedstocks, industrial byproducts, or agricultural waste. The biosynthetic pathway comprises either the synthesis from the precursor acetyl-CoA via the fatty acid *de novo* synthesis pathway or the recycling of external fatty acids via the β-oxidation. The common intermediate in both pathways are 3-hydroxyalkanoates of different carbon chain lengths that are connected to short-, or medium-chain length polymers via the PHA synthase enzyme and stored in inclusion bodies as PHAs (Anjum et al., 2016). In particular, *P. putida* is well-known for its ability to accumulate poly(3-hydroxyalkanoates). Often, nitrogen or phosphate limitations trigger the intracellular production of these polymers when an external carbon source is present in excess Thereby, surplus carbon is channeled into the fatty acid synthesis pathway (Beckers et al., 2016; Poblete-Castro et al., 2012; Prieto et al., 2016). This was found to be a crucial mechanism in *P. putida* KT2442 to conserve carbon under nitrogen limitations since a PHA deficient mutant strain squandered additional resources as CO_2 instead of generating biomass (Escapa et al., 2012). In the case of nitrogen limitation, *P. putida* KT2440 predominantly accumulates the monomers of 3-hydroxydecanoic acid (C10) and 3-hydroxydodecanoic acid (C12) from different carbon sources (Huijberts et al., 1992; Mozejko-Ciesielska et al., 2018; Sohn et al., 2010). When external carbon becomes limited, the previously stored PHAs are released from the PHA granules by PHA depolymerase PhaZ. Under ATP-dependent activation via the acyl-CoA synthetase, the hydroxyalkanoates can be oxidized through the β-oxidation cycle (Ruth et al., 2008). Each cycle releases acetyl-CoA from the carbon chain and generates $FADH_2$ and NADH (Fulco, 1983). Further energy equivalents can be generated from the oxidation of acetyl-CoA via the tricarboxylic acid cycle. To summarize, since PHA anabolism and catabolism have been shown to be simultaneous processes (Doi et al., 1990; Uchino et al., 2007), the intracellular storage of carbon polymers seems to be a crucial survival strategy in the case of substrate starvation for microorganisms able to synthesize PHAs.

2.2.3. *P. PUTIDA* AS A PROMISING HOST FOR ISOBUTANOL PRODUCTION

Regarding high titers above 10 g L^{-1} (refer to Table 4), *E. coli* looks like a promising isobutanol producer. Nevertheless, the high toxicity of this alcohol is a major drawback since concentrations above 10 g L^{-1} impair growth and viability (Brynildsen and Liao, 2009). When exposing *C. glutamicum* to different concentrations of isobutanol, cells

showed higher viability compared to *E. coli*, but the percentage of viable cells still decreased to about 65 % or lower at isobutanol concentrations of 10 - 20 g L^{-1} (Smith et al., 2010). Since *P. putida* has the natural ability to grow in the presence of toxic solvents due to special efflux pumps (Ramos et al., 2015) this promising strain could become an attractive isobutanol producer. The pioneering study of Nikel and Lorenzo (2014) already illustrated the high robustness of *P. putida* KT2440 in contrast to *E. coli* when exposed to ethanol. The *P. putida* strain engineered for ethanol production showed higher cell survival compared to the ethanol-producing *E. coli* strain (Nikel and Lorenzo, 2014). Furthermore, adapted *Pseudomonas* strains, among them *P. putida* KT2440 and *Pseudomonas* sp. strain VLB120, were able to grow in the presence of 1 – 6% (v/v) butanol (Rühl et al., 2009). The molecular response of the natural degrader *P. putida* to n-butanol was analyzed in two complementary studies by Simon et al. (2015) and Vallon et al. (2015). Several proteins were shown to participate in the metabolization of *n*-butanol. Among them, quinoprotein alcohol dehydrogenases, aldehyde dehydrogenases, and enzymes of fatty acid oxidation were identified. N-butanol is oxidized by alcohol dehydrogenases (PedE, PedH) and by aldehyde dehydrogenases (PedI), followed by entering ß-oxidation via crotonoyl-CoA resulting in two acetyl-CoA metabolites which serve as a substrate in the TCA cycle. A pathway for the metabolization of n-butanol was derived from the results which helped to create the mutant strain GN346 that showed impaired growth on the alcohol as a sole carbon source (Simon et al., 2015; Vallon et al., 2015).

However, based on the present knowledge, the resistance of *P. putida* to high isobutanol concentrations has not been tested so far. The first approach to produce isobutanol in a *Pseudomonas* strain was performed by Lang et al. (2014). The authors overexpressed the 2-ketoacid decarboxylase from *L. lactis* in *Pseudomonas* sp. strain VLB120 which produced, besides isobutyric acid and 3-methyl-1-butanol, 72 µM isobutanol. This study indicates the presence of alcohol and aldehyde dehydrogenases in *Pseudomonas* sp. strain VLB120 to convert isobutyraldehyde into its acid or alcohol derivative. Another prerequisite for effective isobutanol production with *P. putida* is the sufficient supply of redox cofactors for the NADPH extensive isobutanol biosynthesis. As recently shown by Nikel et al. (2015) and Kohlstedt and Wittmann (2019), *P. putida* KT2440 is endowed with a surplus of NADPH and ATP when grown on glucose, which allows it to adjust its energy needs to stress situations such as redox-intensive

reactions (Kohlstedt and Wittmann, 2019; Nikel et al., 2015). One mechanism to sustain the cells redox homeostasis is the existence of two different pyridine nucleotide transhydrogenases SthA and PntAB in *P. putida* KT2440 (Nikel et al., 2016b): In *E. coli*, the soluble transhydrogenase SthA primarily translocates protons from NADPH to NAD+, and the membrane-bound transhydrogenase PntAB catalyzes the reverse reaction to reduce NADP+ with protons from NADH (Fuhrer and Sauer, 2009; Sauer et al., 2004) and the same functions are anticipated for *P. putida* KT2440 (Nikel et al., 2016b). In addition, the ability to use different metabolic pathways to generate NADPH (Nikel et al., 2016a; Nikel et al., 2014), or ATP, e.g. via periplasmic glucose oxidation (del Castillo et al., 2007) renders *P. putida* as the ideal chassis for isobutanol synthesis. When exposed to oxidative stress, *P. putida* KT2440 is able to redirect the carbon flux of upper glucose metabolism for the sake of increasing NADPH formation (Chavarría et al., 2013; Nikel et al., 2021).

2.2.4. *FROM AEROBIOSIS TO MICRO-AEROBIOSIS AND ANAEROBIOSIS*

Despite bacteria that possess a fermentative pathway or that can utilize chemicals like nitrate or hydrogen as a final electron acceptor, many organisms, among them *P. putida,* are dependent on the availability of oxygen to balance their redox and energy status. Adenosine 5'triphosphate (ATP) is used for many intracellular reactions such as biosynthesis, DNA replication, and protein fabrication. Moreover, ATP plays a significant role in the stress response (Hara and Kondo, 2015). Besides substrate-level phosphorylation, one major source for intracellular ATP supply in *P. putida* KT2440 is the phosphorylation step of the ATP synthase that is bound to the electron transport in the respiratory chain (Kohlstedt and Wittmann, 2019; Nikel et al., 2015). In the case of the obligate aerobic organism *P. putida* KT2440 (Stanier et al., 1966), electrons can be transferred from the redox cofactors NADH and $FADH_2$ that are primarily reduced in the Embden-Meyerhof-Parnas pathway and the tricarboxylic acid cycle (Nikel et al., 2015). Recently, it was shown that most ATP is generated by oxidative phosphorylation through NADH and $FADH_2$ whereas only a minor part accounts for direct phosphorylation in the central carbon metabolism. However, a substantial part of ATP supply is realized by periplasmatic oxidation of glucose to gluconate and 2-ketogluconate through electron transfer onto the respiratory chain component $PQQH_2$

(Kohlstedt and Wittmann, 2019). Through the transport of electrons, a proton gradient is created. Eventually, protons drive the ATP synthase and oxygen is reduced to water.

Therefore, sufficient oxygen must be supplied during the exponential growth of *P. putida* cells. This can be achieved by aerating the medium inside the bioreactor to increase the boundary layer between the gas and liquid phase. The difference of the oxygen concentration in the in- and outflowing gas can be detected to determine the oxygen transfer rate (OTR) which describes the uptake of oxygen by the cells. Hereby, the factor f is used to correct the delay of the diffusion from the liquid phase into the head space of the bioreactor. Similarly, the carbon dioxide transfer rate (CTR) equals the gaseous carbon dioxide that is excreted by heterotrophic cells. These non-invasive measurements can help to characterize the state of a culture, especially during continuous cultivation.

$$f = \frac{100 - x_{O_2,in} - x_{CO_2,in}}{100 - x_{O_2,out} - x_{CO_2,out}}$$
Equation 1

$$OTR = \frac{\dot{V}_{in}}{V_m * V_R} * (x_{O_2,in} - f * x_{O_2,out})$$
Equation 2

$$CTR = \frac{\dot{V}_{in}}{V_m * V_R} * (x_{CO_2,out} - f * x_{CO_2,in})$$
Equation 3

$x_{O2/CO2}$: proportion of oxygen or carbon dioxide in the in- and out-flowing gas [mol %]

$\dot{V}_{in}$: Flow rate of the inflowing gas [L h^{-1}]

V_m: Molar gas volume [mol L^{-1}]

V_R: Working volume in the bioreactor [L]

In contrast to other facultative anaerobic pseudomonas species (e.g. *P. aeruginosa* (Eschbach et al., 2004) or industrially relevant bacteria like *E. coli* or *C. glutamicum*, *P. putida* KT2440 is not endowed with a fermentative pathway to control its energy and redox state under anaerobic conditions. Thus, efforts were made to enable *P. putida* for anaerobic conversion of carbon substrates by knocking in the acetate kinase of *E. coli* and the pyruvate decarboxylase together with the alcohol dehydrogenase from *Z. mobilis* (Nikel and Lorenzo, 2013; Sohn et al., 2010). Another approach aimed to introduce the nitrate or nitrite respiration mechanism from *P. aeruginosa* into *P. putida*. The mutant strains metabolized succinate and efficiently reduced nitrate or nitrite during anaerobic conditions which extended the survival of *P. putida* cells to several days (Steen et al., 2013). Another approach to realize anaerobic respiration in *P. putida* was conducted by Schmitz et al. (2015). The authors transferred phenazine and pyocyanin biosynthesis genes known from *P. aeruginosa* into *P. putida* KT2440. The recombinant expression of phenazine acted as a redox mediator that transferred electrons from the cell to an anode inside the bioreactor, thus enabling partial redox balancing under anaerobic conditions. Similarly, oxygen limited synthesis of rhamnolipids was demonstrated in a bioelectrochemical system using a phenazine producing *P. putida* strain (Askitosari et al., 2020). The metabolic activity during anoxic conditions was also shown for *P. putida* F1 that transferred electrons via different chemical redox mediators to an electrode inside the bioreactor, allowing physiological energy charges and survival for over 300 h (Lai et al., 2016; Yu et al., 2018). Noteworthy, electrons were mainly generated from the periplasmatic oxidation of glucose to 2-KG since high excretion of the latter organic acid was observed. However, all these attempts could only enable *P. putida* to survive but not to grow anaerobically. In another study, an anaerotolerant *P. putida* strain was created using in silico guided strain engineering that showed growth under micro-oxic conditions (Kampers et al., 2019a). In general, a micro-aerobic environment is often used as a physiological adaptation bridge from aerobic growth to anaerobic zero-growth phases in sophisticated bioprocesses (Lange et al., 2018; Lange et al., 2017). *P. putida* can withstand low dissolved oxygen tensions of 1.5% which results in more rapid DNA replication (Lieder et al., 2016). Nevertheless, (Kampers et al., 2021) concluded in their rational design study that 61 additional genes would be required for anaerobic

respiration and survival of *P. putida* KT2440. Therefore, complex genetic modifications might be necessary to achieve anaerobic fermentation processes with *P. putida*.

2.3. MICROBIAL CULTIVATION STRATEGIES

2.3.1. MICROBIAL GROWTH IN BATCH CULTURES

Microbial growth is reflected by the increase of biomass that happens through the proliferation of the cells. To control the growth of the cells, defined conditions concerning e.g., the temperature, medium components, and the pH value, must be considered. Most organisms exhibit a pH optimum between 6.5 and 7.5. In the case of aerophil species, oxygen must be supplied to the medium. Concerning substrate consumption, different subgroups of organisms are known. Among these, heterotrophic organisms utilize carbon compounds for biosynthesis and energy supply (Gross, 1995). If sufficient nutrients are supplied, bacterial growth follows an exponential dynamic, in which the rise of the biomass is dependent on the specific growth rate µ and the time. In a batch culture, cells grow with a specific growth rate until one critical nutrient, in most cases the carbon source, becomes limited. Afterward, cells enter a stationary phase without cell proliferation which finally leads to cell death and reduction of cells through lysis (Monod, 1949; Panikov, 1995).

The specific growth rate that is characteristic for each organism and depends on the nutrient supply can be described by the Monod kinetic (Equation 4) (Monod, 1950; Monod, 1949). The growth rate depends on the substrate concentration S, the maximal growth rate μ_{max}, and the substrate-specific saturation constant K_S. This model is derived from the Michaelis-Menten kinetic that is used to describe enzymatic reactions (Michaelis and Menten, 1913). The specific parameter K_S describes the substrate concentration at which cells exhibit half of the maximum growth rate. A low K_S value equals higher substrate affinity in contrast to a high K_S.

$$\mu = \mu_{max} * \frac{c_S}{c_S + K_S}$$

Equation 4

2.3.2. Fed-batch Cultivation as Industrial State of the Art

Since the cultivation of cells in shaking tubes or flasks is not ideal due to uncontrolled oxygen transfer or pH conditions, it is best practice to culture cells in a controlled bioreactor to achieve optimal growth. Mostly a stirred tank reactor is used that can be operated in different ways e.g., batch, fed-batch, or continuous mode. Fed-batch cultures have been widely used in the biotechnology industry for various products through the defined exponential addition of nutrients. Often, either the carbon or the nitrogen component will be supplied in limited concentration to control the organism's growth rate (Pirt, 1979, 1974; Yamanè and Shimizu, 1984). Therefore, cells face limited substrate availability during fed-batch cultivations, and even starvation zones in large-scale bioreactors due to inhomogeneous mixing. The main goal of continuously adding nutrients to the culture is to increase the cell density and thus increase the volumetric productivity of the bioreactor (Riesenberg and Guthke, 1999). Several studies applied different glucose feeding strategies to achieve high cell density cultivations with *P. putida* up to a cell dry weight (CDW) of 62 g_{CDW} L^{-1}. Due to its obligate aerobic nature, pure oxygen had to be supplied to maintain these high cell densities (Poblete-Castro et al., 2014; Poblete-Castro et al., 2013; Sun et al., 2006). The combination of an exponential, followed by a linear increasing glucose feed yielded a biomass concentration of 102 g_{CDW} L^{-1} with the need for oxygen-enriched air (Davis et al., 2015). However, the extensive oxygen demand of *P. putida* can be seen as a major drawback for the widespread industrial application of this obligate aerobic microorganism.

2.3.3. Using Continuous Cultivation to Study Diverse Cellular Responses

A continuous culture differs from the fed-batch strategy since fresh medium is constantly fed and cell broth is withdrawn concomitantly. Different modes such as nutristat, turbidostat, or chemostat are known for operating continuous cultivation. The latter is defined by equal rates of in and outgoing flows. Hereby, the volume in the bioreactor is kept constant for a long time which creates a dynamic equilibrium of flows, a "steady state". This stationarity is realized by a constant specific growth rate of the cells through limited substrate availability. Within the steady state, all process parameters are constant and time-independent (Herbert et al., 1956; Monod, 1950; Novick and Szilard, 1950). The dilution rate D equals the feed rate per reactor volume

and its reciprocal is the residence time τ. The dilution rate and therefore, the growth rate in a continuous culture can be increased until μ_{max}. Equation 5 and Equation 6 show the balances of the steady state substrate concentration $\tilde{c}_S$ and biomass concentration $\tilde{c}_X$ during the steady state of a chemostat. Figure 4 illustrates the context between the steady state concentrations of the biomass X and the substrate S in the bioreactor as a function of the dilution rate. Dilution rates above the maximum specific growth rate will lead to a wash-out of cells resulting in a constantly declining biomass concentration and increasing substrate concentration as the amount of harvested cells is higher than the amount of new cells in the bioreactor within the same time frame (Herbert et al., 1956).

$$\tilde{c}_S = \frac{K_S}{\frac{\mu_{max}}{D} - 1}$$

Equation 5

$$\tilde{c}_X = \frac{D * (c_{S,in} - \tilde{c}_S)}{\frac{1}{Y_{XS}} * D + m_S}$$

Equation 6

$c_{S,in}$:   substrate concentration in the feed

$\tilde{c}_S$:   substrate concentration in the bioreactor

$Y_{X/S}$:   biomass yield per substrate

m_S: maintenance coefficient

For *P. putida*, chemostat processes were used to study the response to single specific stimuli, for instance to alternating growth rates or low oxygen levels (Lieder et al., 2016), and exposure to *n*-butanol (Vallon et al., 2015). Furthermore, continuous cultivation was helpful in identifying the metabolization routes of different carbon sources (Sudarsan et al., 2014) and in unraveling metabolic fluxes and gene expression patterns during accumulation of PHAs as well as identifying their carbon compositions during nitrogen or carbon limitation (Beckers et al., 2016; Poblete-Castro et al., 2012). In addition, fed-batch scenarios with substrate limitation and simultaneous

starvation zones can be realized in small-scale continuous experiments (Löffler et al., 2016; Simen et al., 2017).
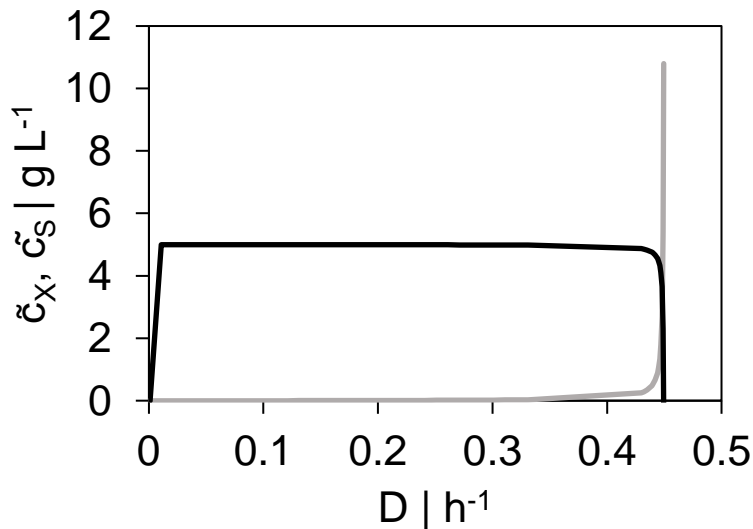
Figure 4 Example of a X-D diagram with steady state concentrations of biomass $č_X$ (black) and substrate $č_S$ (grey) as function of the dilution rate D with $K_S = 0.012$ g L^{-1}, $Y_{XS} = 0.5$ g g^{-1}, $μ_{max} = 0.45$ h^{-1}, and $c_{S,in} = 10$ g L^{-1}. The significant increase of substrate concentration and biomass reduction characterizes the wash-out point.

2.4. UNDERSTANDING LARGE-SCALE EFFECTS ON MICROORGANISMS USING LAB-SCALE METHODS

2.4.1. PROBLEMS CONCERNING SCALE-UP OF MICROBIAL PRODUCTION PROCESSES

As previously mentioned, biological, chemical, and physical impacts during the scale-up of a bioprocess (Takors, 2012), accompanied by high microbial consumption rates and insufficient homogeneous mixing lead to substrate gradients. In large-scale bioreactors (>10 m³), mixing times were determined to range from 50 s to 360 s (Junker, 2004; Lara et al., 2006a), which was also predicted by computational fluid dynamics simulations with *C. glutamicum* cells (Kuschel and Takors, 2020). Consequently, this leads to population inhomogeneities as cells inside a large-scale bioreactor will face different zones of substrate availability. The transition of cells

through different microenvironments in the bioreactor causes stress and can lead to varying growth rates for cells circulating through the bioreactor (Kuschel and Takors, 2020). Lara et al. (2006a) published a comprehensive list of negative effects on microbial growth due to large-scale stress. For example, formate accumulation and reduced biomass yield caused by zonal oxygen limitation were observed in a 22 m³ fed-batch cultivation with *E. coli* (Enfors et al., 2001). Moreover, Bylund et al. (1998) discovered a 20% lower biomass yield due to immense glucose accumulation zones in a 12 m³ reactor during a glucose-limited fed-batch process with *E. coli.*

2.4.2. SCALE-DOWN STUDIES

Since sampling in a large-scale bioreactor is quite complex and usually, research institutes are not equipped with cubic scale bioreactors, scale-down devices were invented to mimic large-scale conditions in lab-scale. Several approaches were established comprising experimental setups with combined stirred tank reactors (STR) or a plug flow reactor (PFR) connected to an STR (Buchholz et al., 2014; Delvigne et al., 2017; Lara et al., 2006b; Neubauer et al., 1995; Neubauer and Junne, 2010). By using glucose as a trigger for limited growth in such an STR-PFR environment, Löffler et al. (2016) observed *E. coli's* quick metabolic responses along with fundamental transcriptional changes to short-term starvation. Similar severe transcriptional changes in *E. coli* were observed in a subsequent study with fluctuating nitrogen supply (Simen et al., 2017). These studies also revealed reduced energy charges during starvation accompanied by several upregulated genes with high ATP costs. The authors identified several genes as targets for a streamlined chassis aiming to enhance the cell's performance under large-scale conditions (Löffler et al., 2016; Simen et al., 2017). The cell's energetic state is of utmost importance, especially in industrially engineered strains, thus emphasizing the relevance of deciphering stress-related ATP-demanding or -generating reactions. In this context, Kuschel et al. (2017) predicted the population heterogeneity of *P. putida* grown in a 54,000 L bioreactor using an *in silico* approach. Varying growth rates, resulting in increased or diminished ATP maintenance demands were demonstrated in their study.

Despite being starved of carbon or nitrogen sources, cells might also face oxygen inhomogeneities in industrial-scale bioreactors, leading to short-term micro- or

anaerobic environments. This situation was already addressed for different relevant industrial organisms. Agreeing with Enfors et al. (2001), Soini et al. (2008) discovered the accumulation of formate in *E. coli* cultivations with transient anaerobic zones but showed that side product formation could be prevented completely by the addition of the trace elements selenium, molybdenum, and nickel. Furthermore, *C. glutamicum* exhibited oscillating lactate formation and consumption (Käß et al., 2014) and shifting transcriptional as well as metabolic adaptations (Limberg et al., 2017) in non-aerated zones while growing on glucose. However, obligate aerobic organisms, such as *Yarrowia lipolytica* and *Pichia pastoris*, were investigated in only a few studies (Kar et al., 2012; Kar et al., 2010; Lorantfy et al., 2013) but similar studies for *P. putida* are currently lacking.

2.4.3. TRANSCRIPTOMICS TO INVESTIGATE THE CELL'S STRESS RESPONSE

The quantification of the transcriptome that is the total of RNA species aims to analyze and interpret transcriptional mechanisms under specific physiological circumstances (Wang et al., 2009). In particular, the abundance of mRNA species indicates changes in protein levels since these transcribed ribonucleotide strands serve as instruction plans for protein synthesis. For this purpose, RNA must be isolated and stabilized from immediately quenched cells. Next, using RNA sequencing technologies, a library of cDNA fragments is created and subsequently sequenced by performing e.g., high-throughput Illumina sequencing. The sequenced library can then be mapped to a reference genome to detect aligned reads and their abundance (Wang et al., 2009). By using bioinformatic tolls such as DESeq2 (Love et al., 2014) a comparison of the amount of reads between different conditions is performed. Consequently, by comparing differential expressed genes between one or more diverse conditions, transcriptional regulations can be identified. In general, the stress resistance phenotype derives from the interplay of transcriptional factors, specific enzymes, and metabolic pathways. One key factor for translational regulations is small non-coding RNAs (sRNA) as they seem to interfere in all kinds of stress-related functions (Gottesman and Storz, 2011). The non-coding regions within the DNA have long time been regarded as "genetic junk" since no protein function could be attributed to these base sequences. In the human genome, 98.5% of the DNA accounts for non-protein coding regions, which partially code for ribosomal and transfer RNA molecules. It is

only in recent years that more and more non-coding RNA sites have been explored in the genome of all domains of life and have contributed to a deeper understanding of post-transcriptional gene regulation (Viegas and Arraiano, 2008). These sRNA molecules are around 50 to 250 nucleotides big and act by pairing with a target mRNA sequence which leads to either the inhibition or activation of mRNA translation. Furthermore, the small RNA molecules can bind directly to the active site of proteins. Thus, sRNAs regulate gene expression and modify protein activity (Viegas and Arraiano, 2008; Waters and Storz, 2009).

In addition to ubiquitous RNA regulation factors, the general stress response of *P. putida* is regulated by the sigma factor (σ^S) expressed by the *rpoS* gene. σ^S enables cells to withstand environmental and nutritional challenges, in particular carbon starvation, and it orchestrates the stress response in different types of non-ideal conditions. Thus, rpoS-levels serve as a reporter of the stress reaction in cells and participate in the adaption mechanisms to harsh conditions (Ramos-González and Molin, 1998). During starvation, the stringent response is crucial in bacteria so they can adapt to nutritional stress by downregulating the transcription and protein synthesis and concomitantly upregulating the catabolic processes of amino acids (Chatterji and Kumar Ojha, 2001). As known from many bacteria, the accumulation of the alarmone ppGpp is assumed to initiate the stringent response under stress exposure such as carbon starvation (Hardiman et al., 2007; Hauryliuk et al., 2015; Traxler et al., 2011). The pivotal role of the stringent response is to orchestrate regulation mechanisms on protein and mRNA levels through the activity of the genes *relA* and *spoT*. Intracellular levels of ppGpp are typically regulated by RelA (ppGpp synthase) and SpoT (ppGpp hydrolase) homolog proteins (Potrykus and Cashel, 2008). The expression of the sigma factor σ^S is also regulated by ppGpp and was found to be upregulated in starving or stationary *E. coli* cells (Gentry et al., 1993; Löffler et al., 2016).

By investigating the stress response in *P. putida* KT2440, Lieder et al. (2016) showed a strong relationship between general stress and acceleration of DNA replication. The replication rate at 5% dissolved oxygen tension (DOT) rose 1.5-fold compared to standard conditions and increased 1.6-fold when exposed to decanol (5% v/v) and even lower dissolved oxygen (1.5%). Due to solvent stress, significant changes in the

expression of 540 transcripts were identified. Among them, genes correlated to DNA repair were observed. These observations lead to a two-fold strategy for cells to overcome stress: repairing errors in DNA and increasing the frequency of recombination events that may help to adapt to stress situations (Lieder et al., 2016). Since regulation of genes and thus protein synthesis is connected to ATP demand, unraveling stress-related genes in *P. putida* could contribute to streamlining the strain with regard to a reduced ATP and substrate demand.

3. PUBLICATIONS

As previously mentioned, the current knowledge regarding *Pseudomonas putida* KT2440's stress response is already quite sophisticated, however, a deeper understanding of this bacteria's behavior under industrial-scale production conditions lacks so far. The scientific publications that are part of this dissertation aim to shed light on transcriptional and metabolic patterns in *P. putida* when exposed to substrate limitations or high redox co-factor demanding conditions. Thereby, the question of whether *P. putida* is suitable for large-scale applications is addressed in this thesis. Furthermore, the suitability of this organism as an industrial isobutanol producer will be evaluated. All the results of this thesis were published in peer-reviewed journals. Each publication (**P**) is inserted in its original format within this section. A short summary of the scientific output and the declaration of the authors' contributions is provided prior to each publication in the following chapter.

Table 5 List of the five submitted publications that serve as the basis of this cumulative dissertation.

P-I Pobre, V., Graça-Lopes, G., Saramago, M., Ankenbauer, A., Takors, R., Arraiano, C. M., & Viegas, S. C. (2020). Prediction of novel non-coding RNAs relevant for the growth of *Pseudomonas putida* in a bioreactor. *Microbiology* (Reading, England), 166(2), 149–156. https://doi.org/10.1099/mic.0.000875

P-II Ankenbauer, A., Schäfer, R. A., Viegas, S. C., Pobre, V., Voß, B., Arraiano, C. M., & Takors, R. (2020). Pseudomonas putida KT2440 is naturally endowed to withstand industrial-scale stress conditions. *Microbial biotechnology*, *13*(4), 1145–1161. https://doi.org/10.1111/1751-7915.13571

P-III Demling, P., Ankenbauer, A., Klein, B., Noack, S., Tiso, T., Takors, R. and Blank, L.M. (2021), *Pseudomonas putida* KT2440 endures temporary oxygen limitations. *Biotechnology and Bioengineering*, 1-16. https://doi.org/10.1002/bit.27938

P-IV Nitschel, R., Ankenbauer, A., Welsch, I., Wirth, N. T., Massner, C., Ahmad, N., McColm, S., Borges, F., Fotheringham, I., Takors, R., & Blombach, B. (2020). Engineering *Pseudomonas putida* KT2440 for the production of isobutanol. *Engineering in life sciences*, *20*(5-6), 148–159. https://doi.org/10.1002/elsc.201900151

P-V Ankenbauer, A., Nitschel, R., Teleki, A., Müller, T., Favilli, L., Blombach, B., & Takors, R. (2021). Micro-aerobic production of isobutanol with engineered *Pseudomonas putida*. *Engineering in life sciences*, 21(7), 475–488. https://doi.org/10.1002/elsc.202000116

Further scientific contributions:

Andreas Ankenbauer, Tom Preuß, Ralf Takors: Metabolic response of *Pseudomonas putida* to large-scale stress – a scale-down approach. Poster presentation at the Dechema Himmelfahrtstagung 2018 in Magdeburg, Germany.

Andreas Ankenbauer, Richard Schäfer, Robert Nitschel, Tobias Müller, Ralf Takors: Challenges of scaling up a bioprocess with *P. putida* and its performance in large scale. Oral presentation at the second *Pseudomonas* Grassroots Meeting 2019 in Leiden, The Netherlands.

3.1. P-I: Prediction of Novel Non-coding RNAs Relevant for the Growth of Pseudomonas putida in a Bioreactor

Putative non-coding small RNAs were discovered in *Pseudomonas putida* KT2440 when cultivated under simulated large-scale conditions in a scale-down system consisting of a STR and a PFR to mimic repeated glucose starvation. The prediction of 725 novel ncRNAs contributes to understanding *P. putida's* adaptation to starvation stress and provides engineering targets for a streamlined strain.

V. Pobre is the main author of this manuscript and was supported by G. Graça-Lopes and M. Saramango with the bioinformatic analysis. A. Ankenbauer performed the bioreactor experiments and prepared the samples for RNA extraction by quenching the cells. A. Ankenbauer also wrote the chapter "Bioreactor and sampling" including Figure 1 and contributed ideas and remarks to the manuscript and assisted with proofreading. S. C. Viegas, C. M. Arraiano (corresponding author), and R. Takors supervised this study and co-authored the manuscript.

MICROBIOLOGY
SOCIETY

Prediction of novel non-coding RNAs relevant for the growth of *Pseudomonas putida* in a bioreactor

Vânia Pobre[1]†, Gil Graça-Lopes[1]†, Margarida Saramago[1], Andreas Ankenbauer[2], Ralf Takors[2,*], Cecília M. Arraiano[1,*] and Sandra C. Viegas[1]

Abstract

Pseudomonas putida is a micro-organism with great potential for industry due to its stress-endurance traits and easy manipulation of the metabolism. However, optimization is still required to improve production yields. In the last years, manipulation of bacterial small non-coding RNAs (ncRNAs) has been recognized as an effective tool to improve the production of industrial compounds. So far, very few ncRNAs are annotated in *P. putida* beyond the generally conserved. In the present study, *P. putida* was cultivated in a two-compartment scale-down bioreactor that simulates large-scale industrial bioreactors. We performed RNA-Seq of samples collected at distinct locations and time-points to predict novel and potentially important ncRNAs for the adaptation of *P. putida* to bioreactor stress conditions. Instead of using a purely genomic approach, we have rather identified regions of putative ncRNAs with high expression levels using two different programs (Artemis and sRNA detect). Only the regions identified with both approaches were considered for further analysis and, in total, 725 novel ncRNAs were predicted. We also found that their expression was not constant throughout the bioreactor, showing different patterns of expression with time and position. This is the first work focusing on the ncRNAs whose expression is triggered in a bioreactor environment. This information is of great importance for industry, since it provides possible targets to engineer more effective *P. putida* strains for large-scale production.

INTRODUCTION

Pseudomonas putida is a ubiquitous non-pathogenic Gram-negative soil bacterium widely used as a laboratory model for environmental bacteria [1]. *P. putida* has an impressive robustness towards stress and a superior tolerance to organic solvents [2, 3]. The strain *P. putida* KT2440 [4, 5] is biosafe for industrial-scale production [6], and its complete genome sequence is published [7]. This strain has been an attractive host for applications in industrial biotechnology and synthetic biology [8].

The adaptation to large-scale industrial cultivation occurs through the rapid modulation of gene expression. Small non-coding RNAs (ncRNAs) coordinate bacterial adaptation to diverse stresses since they regulate both mRNA and protein levels (reviewed in [9]).

Few transcriptional studies have been performed to detect new ncRNAs in *Pseudomonas* [10–16]. Most were studied

in *P. aeruginosa*, but ncRNA sequence conservation in *Pseudomonas* species is scarce [12, 13].

To study *P. putida* grown in a bioreactor, we have set up a continuous cultivation approach consisting of a stirred tank reactor (STR) coupled to a plug flow reactor (PFR; as described in [17]) (Fig. 1). The PFR is used to simulate substrate shortage in a large reactor. In this way, there is a steady-state reference state without glucose gradients and a subsequent period with gradients. Samples were collected at different locations and time points of the bioreactor. Using this approach, the tactical (short-term) and the strategic (long-term) response of *P. putida* to periodically changing glucose availability could be deciphered.

Under our experimental set up and with our approach, 725 new ncRNA transcripts were detected in this micro-organism. Our results increase the number of ncRNAs discovered in *P.*

Fig. 1. Setup of the scale-down system. A STR is operated in chemostat with cells growing at µset=0.2 1/h. Sample S_0 min represents a reference state. Subsequently, a PFR will be connected to the STR, to simulate a substrate gradient. Cells flowing from the STR through the PFR will face a glucose gradient resulting in starvation, which lasts for 143 s, before streaming back into the STR. Samples are withdrawn from sampling ports S, P1, P3 and P5 at distinct time points. The whole scale-down system is operated for 25 h under constant conditions.

putida KT2440 and add rich detail to the understanding of stress responses in this bacterium.

METHODS

Bioreactor and sampling

The *P. putida* strain KT2440 (DSM-6125, ATCC47054) was cultivated in a scale-down bioreactor system that consists of a 3 l STR in combination with a PFR (see Fig. 1). Mineral salts medium (M12) [18] was used for cultivations and consisted of the following components: 2.2 g l^{-1} $(NH_4)_2SO_4$, 0.4 g l^{-1} $MgSO_4 \times 7\ H_2O$, 0.04 g l^{-1} $CaCl_2 \times 2H_2O$, 0.02 g l^{-1} NaCl, 2 g l^{-1} KH_2PO_4, and trace elements (2 mg l^{-1} $ZnSO_4 \times 7\ H_2O$, 1 mg l^{-1} $MnCl_2 \times 4\ H_2O$, 15 mg l^{-1} Na_3-Citrate$\times 2\ H_2O$, 1 mg l^{-1} $CuSO_4 \times 5$ H_2O, 0.02 mg l^{-1} $NiCl_2 \times 6\ H_2O$, 0.03 mg l^{-1} $Na_2MoO_4 \times 2\ H_2O$, 0.3 mg l^{-1} H_3BO_3, 10 mg l^{-1} $FeSO_4 \times 7\ H_2O$). Prior to each cultivation a preculture in 500 ml baffled shake flask containing 50 ml M12 medium with 4 g l^{-1} glucose, 10 g l^{-1} MOPS and 0.5 g l^{-1} yeast extract (VWR International, Radnor, PA, USA) was started from a working cell bank (33% glycerol stock, stored at −70 °C). After 6–8 h of incubation (130 r.p.m., 30 °C, pH 7) a second preculture in 1000 ml shaking flask containing 100 ml M12 medium with 4 g l^{-1} glucose and 10 g l^{-1} MOPS was inoculated using exponential growing cells (OD ~3). After 14 h, the second preculture (OD ~3.5) was used to start the batch in the 3 l stirred tank reactor (Bioengineering, Wald, Switzerland) containing 1.6 l M12 medium (inoculum included) with 15 g l^{-1} glucose (30 °C, total pressure of 1.5 bar,

constant aeration of 1.5 l min^{-1}). During fermentation, pH was adjusted at 7 using 25% NH_4OH (Carl Roth, Karlsruhe, Germany) and dissolved oxygen (DO) was kept above 20% by adjusting stirrer speed. After depletion of initial glucose, the chemostat was started, setting a constant feed (M12 medium with 18 g l^{-1} glucose) at a dilution rate of 0.2 h^{-1}. Antifoam (Struktol J 647, Schill+Seilacher, Hamburg, Germany) was added at a rate of 50 µl h^{-1}. After reaching a steady state (*t*>five residence times) the PFR was connected to the STR via a pump. Accordingly, the volume ratio of about 3:1 (STR:PFR) was installed with a mean residence time of 128 s of the cells in the PFR, similar to [17]. Notably, the dilution rate of the entire system remained with *D*=0.2 h^{-1}. The heat-insulated PFR was aerated with 0.1 l min^{-1} via port 1 to prevent oxygen depletion. All experiments were performed as biological triplicates.

RNA extraction

Total RNA was extracted using Trizol (Ambion). For cell harvest, 2 ml of ice-cold stop solution (5% water-saturated phenol in ethanol) were added to 10 ml of bacterial culture and mixed, divided by six Eppendorfs and centrifuged 4000 *g*, 5 min at 4 °C. The supernatant was removed, and each pellet resuspended into 350 µl of lysis solution (0.2% lysozyme in Tris-HCl pH7.5) and incubated 5 min at 37 °C. Cells were then lysed in FastPrep homogenizer using 0.5 ml of small glass beads and 0.5 ml of acid phenol, and centrifuged at 14000 r.p.m. 10 min at 4 °C. The aqueous phase was treated

with 10U of Turbo DNase (Ambion), for 1 h at 37 °C. RNA extraction proceeded with Trizol treatment and after ethanol precipitation (with 300 mM sodium acetate) RNA was resuspended in RNase free water. RNA integrity was evaluated by agarose gel electrophoresis and its concentration estimated spectrophotometrically (NanoDrop ND-1000).

RNA–Seq and reads mapping

Total RNA was sent to StabVida (Portugal) for sequencing (Illumina, paired-end, 150 bp, 20M reads). rRNA was depleted from the samples with the RiboZero kit and sequencing libraries were constructed with the TruSeq kit (Illumina) for bacteria. The quality of the RNA-Seq data was confirmed using the fastQC program. Contaminant adapters and low quality reads were removed with cutadapt [19] and the remaining reads were mapped against *P. putida* KT2440 genome (NC_002947.4, downloaded from NCBI genome database) using Bowtie2 program [20]. Samtools [21] was used to sort the mapping files by genomic position.

Prediction of novel ncRNAs

Detection of novel putative ncRNAs was accomplished with sRNA-Detect, a python script specially developed for detecting bacterial transcripts from RNA-Seq data [22]. The sRNA-Detect script was run for each RNA-Seq data file mapped against *P. putida* KT2440 genome (triplicates were run together) with the following parameters: transcripts with a length between 50–500 nt and a minimum coverage of 500 reads per sample. A filtration step was performed with BEDTools intersect to exclude transcripts that overlapped with genome annotated regions [23]. The annotation file used was downloaded from NCBI (GCF_000007565.2) and the 67 ncRNAs already annotated were excluded from our prediction. To diminish false positives a second bioinformatics tool was applied. The mapped files were opened with the genomic browser Artemis [24]. The annotation file was also loaded and the function 'search for novel features' was run with the same parameters of sRNA-Detect script.

The output of both approaches was compared using Microsoft Excel 2013 and only ncRNAs identified by both sRNA-Detect and Artemis were selected. The expression values of each ncRNA were calculated using the reads per kilobase million (RPKM) normalization method and only those with RPKM higher than 10 were kept. Following verification to adjust the slightly different genomic positions and sizes predicted, a final list of novel putative ncRNAs was obtained.

Analysis of the predicted ncRNAs

Classification as *cis*-encoded, *trans*-encoded or undefined was performed using Artemis and the annotation file (GCF_000007565.2). Full complementarity with an annotated feature was regarded as *cis*-encoded; absence of complementarity as *trans*-encoded; partial complementarity as undefined. Quantification of reads was accomplished with featureCounts [25] and estimation of the expression levels was normalized by the RPKM method. The expression values

were plotted using HeatMapper [26]. A FASTA file containing the sequences of our predicted ncRNAs was created and submitted to the Rfam database (version 14.1) to look for sequences bearing similarity with ours [27]. A comparison between our candidates and those predicted by Bojanovic *et al.* [28] was carried out using the same Excel function used to compare sRNA-Detect and Artemis results.

Availability of supporting data

The RNA-Seq data used in this publication has been deposited in NCBI's Gene Expression Omnibus [29] and is accessible through GEO Series accession number GSE129947. Other supporting data are available as additional Table S1, available in the online version of this article.

To review GEO accession GSE129947:

Go to https://www.ncbi.nlm.nih.gov/geo/query/acc.cgi?acc= GSE129947

Enter token *adotcksqvpujnmb* into the box.

RESULTS AND DISCUSSION

Novel ncRNAs predicted from RNA–Seq expression data

In this work, we have predicted novel ncRNAs from *P. putida* grown in a lab scale bioreactor (Fig. 1) set up with a continuous cultivation approach that consists of a STR coupled to a PFR (STR-PFR two-compartment system). The steady-state in the STR, before connection to the PFR, served as a reference (S_0 min). After connection to the PFR, STR sampling (S_15 min–S_25 h) documented the long-term response of the entire culture to repeated glucose starvation. Sampling along the PFR (P1, P3 and P5) mirrored the short-term response of *P. putida*, i.e. the sudden ncRNA dynamics caused by rapid glucose starvation (similar experiments with *E. coli* in [17]). RNA was extracted from the different samples of *P. putida* cultivations collected over time at distinct locations of the bioreactor. The full transcriptome of *P. putida* was obtained by RNA-Seq. Using this data, we were able to predict novel ncRNAs. Contrary to most studies, we did not perform a prediction based on sequence homology or intrinsic features such as secondary structure, followed by confirmation with RNA-Seq expression data. Instead, we took advantage of RNA-Seq data to predict novel regions of the genome with high expression values that could potentially correspond to ncRNAs. Two different methods were used for this approach. We employed the sRNA-Detect program, which was designed specifically for the detection of bacterial small RNAs. This software was shown to surpass other computational approaches in the detection of small transcripts [22]. To increase our confidence, our analysis was complemented with Artemis, a genome browser capable of searching for novel genomic features in any organism [24]. We identified 1303 potential ncRNAs with sRNA-Detect and 1001 with Artemis (Fig. 2a). The two approaches were compared and only the regions identified by both methods, and displaying no overlap with a previously annotated gene,
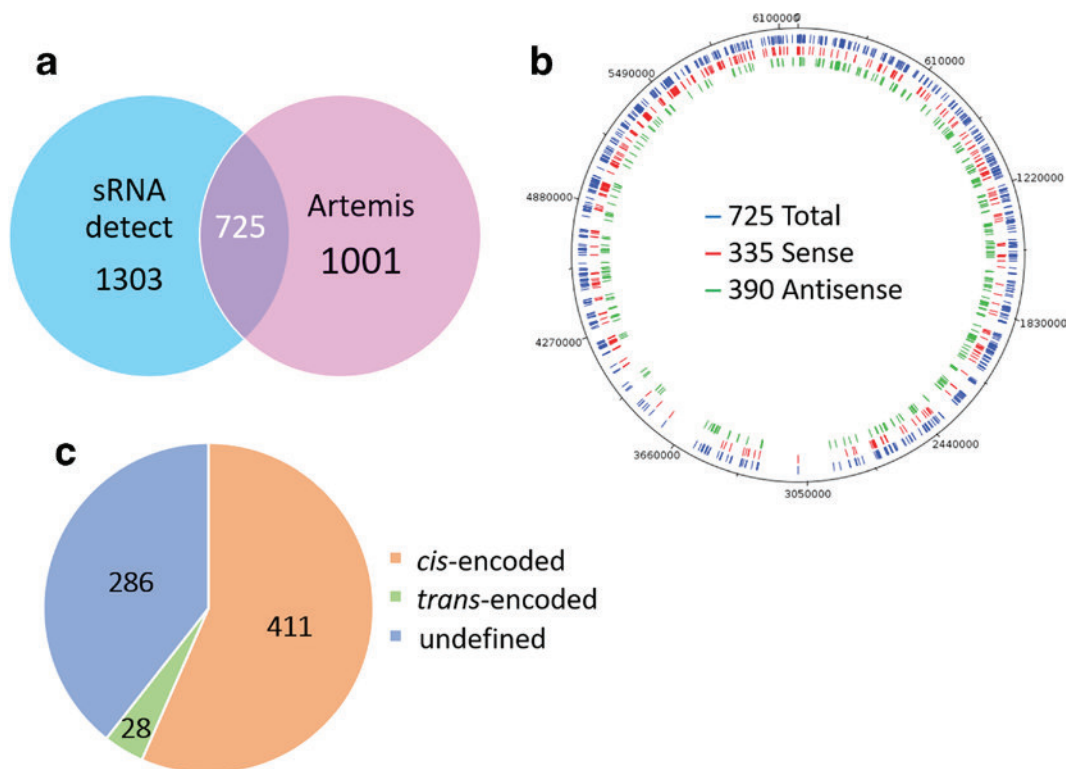
Fig. 2. Prediction of novel *P. putida* ncRNAs from RNA-Seq data and their genomic distribution. (a) Venn diagram representing the number of putative ncRNAs predicted by sRNA-Detect and Artemis tools. In the centre is the number of ncRNAs identified by both approaches. (b) Distribution of the 725 putative ncRNAs in the genome of *P. putida* is represented in blue. The ncRNAs annotated on the sense strand are marked red and those annotated on the antisense strand are marked green. (c) Classification of the 725 putative ncRNAs. Classification as *cis*-encoded is indicative of full complementarity with an annotated gene. Absence of complementarity is regarded as *trans*-encoded. Partial complementarity is categorized as undefined.

were considered for subsequent analysis. In the end, we were able to identify 725 novel ncRNAs that were distributed throughout the genome in both sense (335 ncRNAs) and antisense (390 ncRNAs) strands (Fig. 2b, Table S1). Surprisingly, we detected two regions of the genome (the first between base pairs 2926000–3275000; the second between base pairs 3583000–3875000) where only one ncRNA was predicted, PP_nc403 and PP_nc434, respectively (Fig. 2b).

There are several approaches available for the identification of novel ncRNAs. The most common is to use genome information to predict ncRNAs [30]. These tools are mostly designed for eukaryotic organisms and have very specific parameters, such as searching by secondary structure or evolutionary conservative sequences, what greatly limits the results obtained. With next-generation techniques search methods for ncRNAs have also expanded. RIP-Seq is frequently used and is based on the RNA chaperone Hfq [31] that binds to ncRNAs and promotes the interaction between the ncRNA and its mRNA target [9, 32]. However, there are several known ncRNAs that do not bind Hfq, especially the *cis*-encoded ncRNAs that have full complementarity with their targets, not requiring Hfq for the interaction. Moreover, it is now known that there are other RNA chaperones, such

as ProQ, that can also bind to ncRNAs [33]. This makes the identification of novel ncRNAs through RIP-Seq experiments much more restricted. For all these reasons, in this work we used directly the RNA-Seq data to search for highly expressed regions of the genome with the potential to correspond to putative ncRNAs.

Classification of the predicted ncRNAs

The classification of ncRNAs is becoming a very difficult task since new classes of ncRNAs are being discovered every year. In bacteria, ncRNAs are usually classified as *cis*-encoded or *trans*-encoded RNAs depending on their location in the genome [34]. In an attempt to classify the predicted ncRNAs we considered as *cis*-encoded all novel transcripts that had full complementarity with another gene, and *trans*-encoded those with no complementarity (Fig. 2c). Taking this into account we were able to classify 411 ncRNAs as *cis*-encoded, 28 as *trans*-encoded and the 286 remaining as undefined (Fig. 2c). These undefined correspond to ncRNAs that have a partial complementary to either the 5′-end or the 3′-end of a gene in the opposite strand. This is supported by the fact that of the 725 novel ncRNAs we could only definitely classify 28 as *trans*-RNAs, a very low number when compared with the
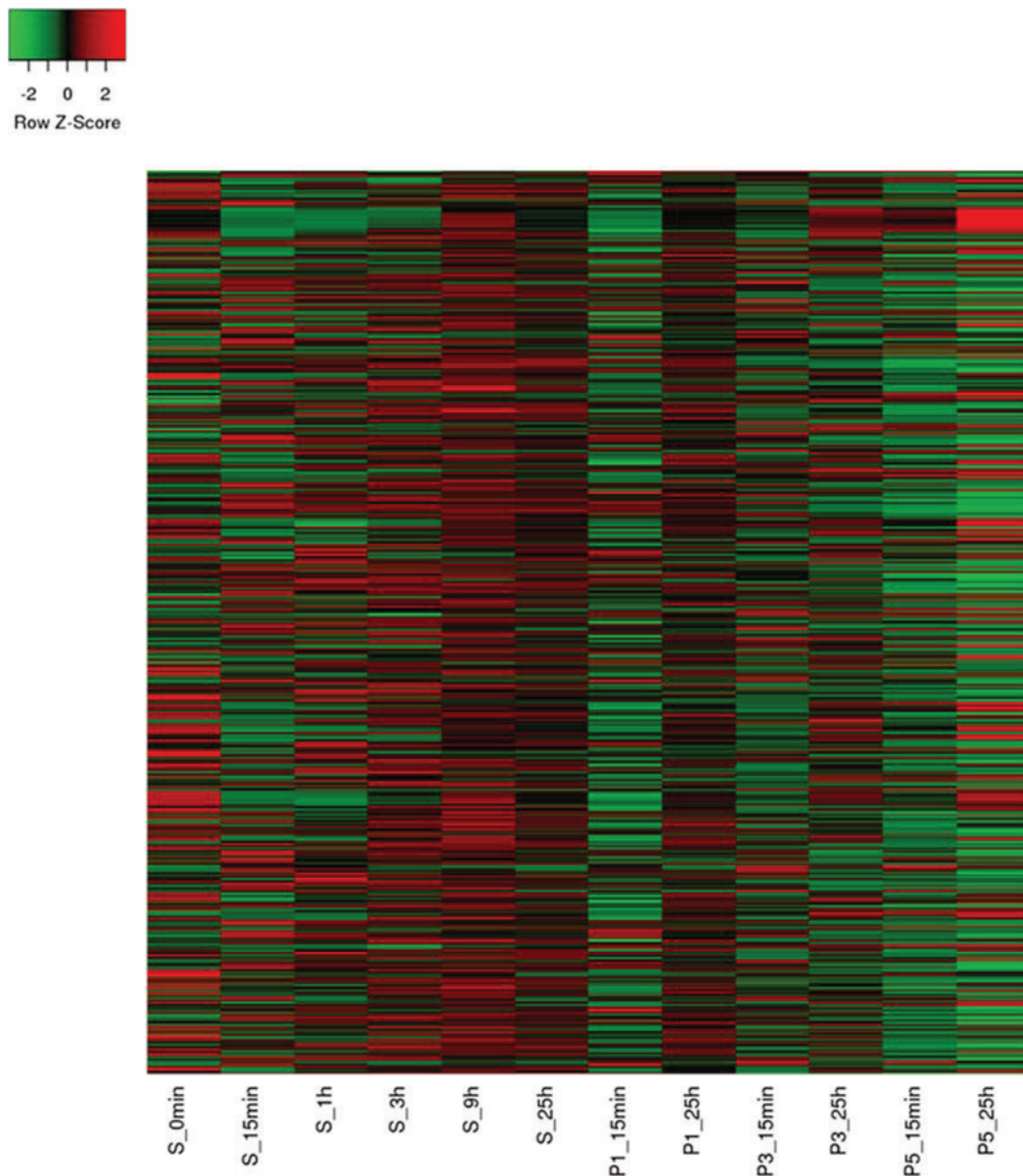
Fig. 3. Heatmap of the 725 novel ncRNAs. The heatmap shows the relative expression levels of the predicted ncRNAs and was generated using the average expression levels of the three biological replicates collected in each condition. The z-score indicates which ncRNAs have expression levels above the mean (red) and those with values below the mean (green).

predicted *cis*-encoded ncRNAs. This classification could actually be misleading since there is evidence of some *cis*-RNAs also acting as *trans*-RNAs [35–38]. It is proposed merely as a guide regarding the position of these ncRNAs in the genome rather than as a suggestion to their potential role in the cell.

With the advances of sequencing techniques, pervasive transcription has been identified as a widespread phenomenon [39]. It consists in the transcription of both sense and antisense strands, and appears to be the source of many potentially functional antisense RNAs [40]. In *E. coli* more than 300 antisense RNAs with different sizes were identified using an

approach to detect pervasive transcription [40]. Moreover, this phenomenon can produce many smaller antisense RNAs (around 22 nt) [41]. Since we removed all ncRNAs with a size<50 nt from our analysis, it is possible that the number of *cis*-encoded RNAs that exists could be even higher than what is currently thought.

Novel *P. putida* ncRNA expression

The expression levels of the novel predicted ncRNAs were estimated in all the conditions tested. To obtain expression values that could be reliably compared to each other, the read counts
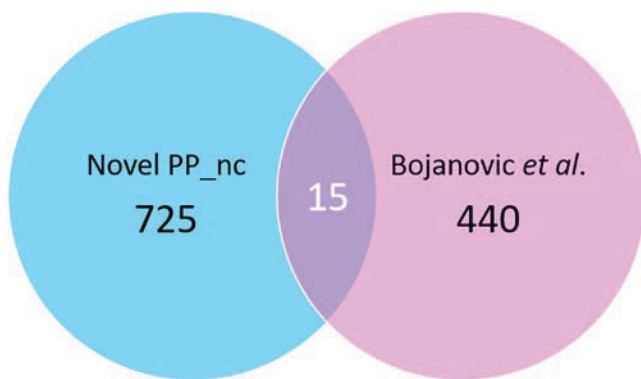
Fig. 4. Intersection with ncRNAs predicted in another study. Venn diagram displaying the number of ncRNAs predicted by the present work and those previously predicted by Bojanovic *et al.* [28]. In the centre is indicated the number of putative ncRNAs detected by both studies.

for each ncRNA were normalized using the RPKM method (Table S1). The normalized expression values for each ncRNA in all the conditions analysed were then plotted in a heatmap (Fig. 3). Not all predicted ncRNAs were expressed in all 12 conditions analysed, with the expression of these ncRNAs changing according to the location in the bioreactor. Most ncRNAs appear to be more expressed in the STR and exhibit lower expression values at the outlet of the PFR (absence of glucose) (Fig. 3). In fact, it seems that the glucose levels are in direct correlation with the ncRNA expression, with the lower glucose levels leading to a repression of most ncRNAs. Most studies involving the effect of glucose starvation on ncRNA focus on the identification of novel ncRNAs that are being expressed under glucose depletion, however a previous study found that when *Pectobacterium atrosepticum* is subjected to glucose starvation 21 of its 68 predicted ncRNAs were down-regulated [42]. There are, however, some ncRNAs that are highly expressed due to starvation at the outlet of the PFR (P5), namely PP_nc235 and PP_nc608 (Table S1). Even though these ncRNAs are very highly expressed in all samples analysed their expression peak is at P5. Another interesting observation is that PP_nc406 ncRNA has a very low expression value in the STR but a high expression after 128 s of starvation (P5), suggesting that this ncRNA might be involved in the glucose metabolism pathway.

Not only does the location in the bioreactor affect the expression of the ncRNAs, but also the time at which samples were collected. The peak of expression for most ncRNAs occurs after 9 h in the STR (S_9 h) (long-term response to repeated glucose starvation). It appears that many ncRNAs that have an above average expression at the reference state (S_0 min) will have a slightly lower expression value after 15 min (S_15 min) of repeated glucose starvation but starts to increase after 1 h (S_1 h), resulting in most ncRNAs being expressed after 3 h (S_3 h). The fact that we identified more expressed ncRNAs after 25 h than after 15 min of growth in the STR-PFR system

(S, P1, P3 and P5) might pinpoint to a long-term adaptation to repeated glucose starvation in terms of ncRNA expression.

While the main stress condition in the bioreactor was glucose starvation, other stresses may be influencing the higher or lower expression values observed, such as shearing stress and hydrostatic pressure in the PFR. Therefore, a prediction of such a high number of ncRNAs is not surprising. A detailed knowledge of the function of these ncRNAs and their regulation mechanisms will help to improve the adaptation of *P. putida* to large-scale bioreactors, promoting the production of industrially valuable compounds.

Rfam identity of the *P. putida* novel ncRNAs

To identify some of the 725 predicted ncRNAs, a search was conducted on the Rfam database for sequences bearing similarity with the sequences of our ncRNAs. PP_nc320 was the only ncRNA with Rfam identity, as a self-catalytic ribozyme (group-II-D1D4_3). PP_nc320 is 428 nt in length and has been classified as undefined, being partially antisense to rna74 (tRNA) and close to PP_1846, which encodes for a group II intron-encoding maturase. The identification of a single ncRNA through Rfam might be due to the low conservation of ncRNA sequences that exists between *Pseudomonas* species [13]. Furthermore, since the 67 annotated ncRNAs had been removed from our analysis, most conserved ncRNAs were already excluded from our list, and therefore they could not be detected with Rfam.

Intersection with previously predicted ncRNAs

A previous study in *P. putida* had already predicted some ncRNAs using genomic prediction tools, which were further validated with RNA-Seq data obtained under stress conditions [28]. This study had also a low percentage of identification using the Rfam database, and most of the ncRNAs identified were excluded from our analysis, since they were already annotated. It is striking the low intersection between the predictions of both studies. We predicted a higher number of potential ncRNAs (725 – new *versus* 440 –previously predicted), and when comparing the start and end positions of these candidates, we only had 15 ncRNAs in common (Fig. 4). It is important to highlight that the approaches and parameters used were distinct. We limited our search to ncRNAs with sizes between 50 and 500 nt, while the previous work considered ncRNAs between 21 and 1612 nt. Moreover, in the previous work, the prediction of ncRNAs was based on a genomic prediction program (Rockhopper), followed by confirmation through RNA-Seq expression data from three different stress conditions (oxidative, osmotic and imipenem). In contrast, in this work we used RNA-Seq data of 12 different conditions from a bioreactor that includes several stresses (glucose starvation, shearing stress, hydrostatic pressure, etc.) to directly infer regions of the genome based on expression values. Finally, the RNA extraction protocol and library preparation were also different in both studies. Considering all these differences the higher number of predicted ncRNAs that we have obtained and the low intersection between both studies is therefore comprehensible. This

also seems to indicate that bioreactor conditions induce the expression of many ncRNAs that do not seem to be triggered in other conditions.

Overall, this is the first work predicting ncRNAs in a bioreactor setting. Our data set is of great importance, since it will serve as a tool for the optimization of *P. putida* as a cell factory, improving the production yields of economically valuable products.

Conflicts of interest
The authors declare that there are no conflicts of interest.

References
1. **Palleroni NJ**. Genus *Pseudomonas*. In: Krieg NR, Holt JG (editors). *Bergey's Manual of Systematic Bacteriology. 1*. Baltimore, MD: USA Williams & Wilkins; 1984. pp. 141–199.
2. **Nikel PI, Martínez-García E, de Lorenzo V**. Biotechnological domestication of pseudomonads using synthetic biology. *Nat Rev Microbiol* 2014;12:368–379.
3. **Ramos J-L, Sol Cuenca M, Molina-Santiago C, Segura A, Duque E** *et al.* Mechanisms of solvent resistance mediated by interplay of cellular factors in *Pseudomonas putida*. *FEMS Microbiol Rev* 2015;39:555–566.
4. **Bagdasarian M, Lurz R, Rückert B, Franklin FC, Bagdasarian MM** *et al.* Specific-purpose plasmid cloning vectors. II. broad host range, high copy number, RSF1010-derived vectors, and a host-vector system for gene cloning in *Pseudomonas*. *Gene* 1981;16:237–247.
5. **Regenhardt D, Heuer H, Heim S, Fernandez DU, Strömpl C** *et al.* Pedigree and taxonomic credentials of *Pseudomonas putida* strain KT2440. *Environ Microbiol* 2002;4:912–915.
6. **Register F**. Appendix E, certified host-vector systems 1982;47:17197.
7. **Nelson KE, Weinel C, Paulsen IT, Dodson RJ, Hilbert H** *et al.* Complete genome sequence and comparative analysis of the metabolically versatile *Pseudomonas putida* KT2440. *Environ Microbiol* 2002;4:799–808.
8. **Loeschcke A, Thies S**. *Pseudomonas putida*-a versatile host for the production of natural products. *Appl Microbiol Biotechnol* 2015;99:6197–6214.
9. **Waters LS, Storz G**. Regulatory RNAs in bacteria. *Cell* 2009;136:615–628.
10. **Ferrara S, Brugnoli M, De Bonis A, Righetti F, Delvillani F** *et al.* Comparative profiling of *Pseudomonas aeruginosa* strains reveals differential expression of novel unique and conserved small RNAs. *PLoS One* 2012;7:e36553.
11. **Filiatrault MJ, Stodghill PV, Bronstein PA, Moll S, Lindeberg M** *et al.* Transcriptome analysis of *Pseudomonas syringae* identifies new genes, noncoding RNAs, and antisense activity. *J Bacteriol* 2010;192:2359–2372.
12. **Gómez-Lozano M, Marvig RL, Molin S, Long KS**. Genome-wide identification of novel small RNAs in *Pseudomonas aeruginosa*. *Environ Microbiol* 2012;14:2006–2016.
13. **Gómez-Lozano M, Marvig RL, Molina-Santiago C, Tribelli PM, Ramos J-L** *et al.* Diversity of small RNAs expressed in *Pseudomonas* species. *Environ Microbiol Rep* 2015;7:227–236.
14. **Wurtzel O, Sesto N, Mellin JR, Karunker I, Edelheit S** *et al.* Comparative transcriptomics of pathogenic and non-pathogenic listeria species. *Mol Syst Biol* 2012;8:583.
15. **D'Arrigo I, Bojanovič K, Yang X, Holm Rau M, Long KS**. Genome-wide mapping of transcription start sites yields novel insights into the primary transcriptome of *Pseudomonas putida*. *Environ Microbiol* 2016;18:3466–3481.
16. **Frank S, Klockgether J, Hagendorf P, Geffers R, Schöck U** *et al.* *Pseudomonas putida* KT2440 genome update by cDNA sequencing and microarray transcriptomics. *Environ Microbiol* 2011;13:1309–1326.
17. **Löffler M, Simen JD, Jäger G, Schäferhoff K, Freund A** *et al.* Engineering *E. coli* for large-scale production - Strategies considering ATP expenses and transcriptional responses. *Metab Eng* 2016;38:73–85.
18. **Vallon T, Simon O, Rendgen-Heugle B, Frana S, Mückschel B** *et al.* Applying systems biology tools to study *n*-butanol degradation in *Pseudomonas putida* KT2440. *Eng Life Sci* 2015;15:760–771.
19. **Martin M**. Cutadapt removes adapter sequences from high-throughput sequencing reads. 2011 2011;17:3.
20. **Langmead B, Salzberg SL**. Fast gapped-read alignment with Bowtie 2. *Nat Methods* 2012;9:357–359.
21. **Li H, Handsaker B, Wysoker A, Fennell T, Ruan J** *et al.* The sequence Alignment/Map format and SAMtools. *Bioinformatics* 2009;25:2078–2079.
22. **Peña-Castillo L, Grüell M, Mulligan ME, Lang AS**. Detection of bacterial small transcripts from RNA-Seq data: a comparative assessment. *Pac Symp Biocomput* 2016;21:456–467.
23. **Quinlan AR, Hall IM**. BEDTools: a flexible suite of utilities for comparing genomic features. *Bioinformatics* 2010;26:841–842.
24. **Carver T, Harris SR, Berriman M, Parkhill J, McQuillan JA**. Artemis: an integrated platform for visualization and analysis of high-throughput sequence-based experimental data. *Bioinformatics* 2012;28:464–469.
25. **Liao Y, Smyth GK, Shi W**. The Subread aligner: fast, accurate and scalable read mapping by seed-and-vote. *Nucleic Acids Res* 2013;41:e108.
26. **Babicki S, Arndt D, Marcu A, Liang Y, Grant JR** *et al.* Heatmapper: web-enabled heat mapping for all. *Nucleic Acids Res* 2016;44:W147–W153.
27. **Kalvari I, Argasinska J, Quinones-Olvera N, Nawrocki EP, Rivas E** *et al.* Rfam 13.0: shifting to a genome-centric resource for non-coding RNA families. *Nucleic Acids Res* 2018;46:D335–D342.
28. **Bojanovič K, D'Arrigo I, Long KS**. Global transcriptional responses to osmotic, oxidative, and imipenem stress conditions in *Pseudomonas putida*. *Appl Environ Microbiol* 2017;83:e03236–16.
29. **Edgar R, Domrachev M, Lash AE**. Gene expression Omnibus: NCBI gene expression and hybridization array data Repository. *Nucleic Acids Res* 2002;30:207–210.
30. **Zhang Y, Huang H, Zhang D, Qiu J, Yang J** *et al.* A review on recent computational methods for predicting noncoding RNAs. *Biomed Res Int* 2017;2017:9139504–.
31. **Chao Y, Papenfort K, Reinhardt R, Sharma CM, Vogel J**. An atlas of Hfq-bound transcripts reveals 3' UTRs as a genomic reservoir of regulatory small RNAs. *Embo J* 2012;31:4005–4019.
32. **Valentin-Hansen P, Eriksen M, Udesen C**. The bacterial Sm-like protein Hfq: a key player in RNA transactions. *Mol Microbiol* 2004;51:1525–1533.
33. **Olejniczak M, Storz G**. ProQ/FinO-domain proteins: another ubiquitous family of RNA matchmakers? *Mol Microbiol* 2017;104:905–915.
34. **Liu JM, Camilli A**. A broadening world of bacterial small RNAs. *Curr Opin Microbiol* 2010;13:18–23.
35. **Opdyke JA, Kang J-G, Storz G, GadY SG**. A small-RNA regulator of acid response genes in *Escherichia coli*. *J Bacteriol* 2004;186:6698–6705.
36. **Jäger D, Pernitzsch SR, Richter AS, Backofen R, Sharma CM** *et al.* An archaeal sRNA targeting *cis*- and *trans*-encoded mRNAs via two distinct domains. *Nucleic Acids Res* 2012;40:10964–10979.

37. **Melamed S**, **Peer A**, **Faigenbaum-Romm R**, **Gatt YE**, **Reiss N** *et al*. Global mapping of small RNA-Target interactions in bacteria. *Mol Cell* 2016;63:884–897.

38. **Sayed N**, **Jousselin A**, **Felden B**. A *cis*-antisense RNA acts in *trans* in *Staphylococcus aureus* to control translation of a human cytolytic peptide. *Nat Struct Mol Biol* 2011;19:105–112.

39. **Wade JT**, **Grainger DC**. Pervasive transcription: illuminating the dark matter of bacterial transcriptomes. *Nat Rev Microbiol* 2014;12:647–653.

40. **Lybecker M**, **Zimmermann B**, **Bilusic I**, **Tukhtubaeva N**, **Schroeder R**. The double-stranded transcriptome of *Escherichia coli*. *Proc Natl Acad Sci USA* 2014;111:3134–3139.

41. **Lasa I**, **Toledo-Arana A**, **Dobin A**, **Villanueva M**, **de los Mozos IR** *et al*. Genome-Wide antisense transcription drives mRNA processing in bacteria. *Proc Natl Acad Sci USA* 2011;108:20172–20177.

42. **Kwenda S**, **Gorshkov V**, **Ramesh AM**, **Naidoo S**, **Rubagotti E** *et al*. Discovery and profiling of small RNAs responsive to stress conditions in the plant pathogen *Pectobacterium atrosepticum*. *BMC Genomics* 2016;17:47.

3.2. P-II: *Pseudomonas putida* KT2440 is Naturally Endowed to Withstand Industrial-Scale Stress Conditions

The metabolic and transcriptional responses to large-scale stress were investigated using the STR-PFR scale-down system. *P. putida* shows stable growth performance during repeated glucose starvation. A stringent response mechanism was discovered that addresses intracellular carbon storage compounds (PHA) and amino acids to balance the cells' energy charge. Additionally, transcriptional responses consuming large amounts of energy were detected that may serve as putative engineering targets.

A. Ankenbauer is the first author of this manuscript and performed all the experiments, quantification methods, and data analysis. R. A. Schäfer is second co-author and performed the bioinformatic processing and differential expression analysis. R. A. Schäfer wrote the chapters "Data processing", Differential expression analysis", "Gene set enrichment analysis", as well as the supplementary chapters "Data processing", "Differential Expression Analysis", and "Gene Set Enrichment Analysis", and created the supplementary data file. S. C. Viegas and V. Pobre performed the RNA sequencing and wrote the chapter "RNA sequencing". C. M. Arraiano and B. Voß supervised this study and proofread the manuscript. R. Takors (corresponding author) supervised this study, contributed ideas, and edited the manuscript.

microbial biotechnology

Pseudomonas putida KT2440 is naturally endowed to withstand industrial-scale stress conditions

Andreas Ankenbauer,[1] Richard A. Schäfer,[1] Sandra C. Viegas,[2] Vânia Pobre,[2] Björn Voß,[1] Cecília M. Arraiano[2] and Ralf Takors[1]*

[1] Institute of Biochemical Engineering, University of Stuttgart, Allmandring 31, 70569, Stuttgart, Germany.
[2] ITQB, Instituto de Tecnologia Química e Biológica António Xavier, Universidade Nova de Lisboa, Av. da República, 2780-157, Oeiras, Portugal.

Summary

Pseudomonas putida is recognized as a very promising strain for industrial application due to its high redox capacity and frequently observed tolerance towards organic solvents. In this research, we studied the metabolic and transcriptional response of *P. putida* KT2440 exposed to large-scale heterogeneous mixing conditions in the form of repeated glucose shortage. Cellular responses were mimicked in an experimental setup comprising a stirred tank reactor and a connected plug flow reactor. We deciphered that a stringent response-like transcriptional regulation programme is frequently induced, which seems to be linked to the intracellular pool of 3-hydroxyalkanoates (3-HA) that are known to serve as precursors for polyhydroxyalkanoates (PHA). To be precise, *P. putida* is endowed with a survival strategy likely to access cellular PHA, amino acids and glycogen in few seconds under glucose starvation to obtain ATP from respiration, thereby replenishing the reduced ATP levels and the adenylate energy charge. Notably, cells only need 0.4% of glucose uptake to build those 3-HA-based energy buffers. Concomitantly, genes that are related to amino acid catabolism and β-oxidation are upregulated during the transient absence of glucose. Furthermore, we provide a detailed list of transcriptional short- and long-term responses that increase the cellular maintenance by about 17% under the industrial-like conditions tested.

Introduction

Pseudomonas putida is a very promising industrial host (Poblete-Castro *et al.*, 2012a; Nikel and Lorenzo, 2018). This strain is naturally endowed to adapt to different physicochemical and nutritional niches (Nikel *et al.*, 2014) and offers strong metabolic redox power (Ebert *et al.*, 2011), which enables it to endure high oxidative stress (Kim and Park, 2014; Nikel *et al.*, 2016). Accordingly, the strain is immensely attractive not only for realizing biotransformation processes but also for the production of secondary or non-native metabolites, lipids and even proteins in the industrial settings.

Often enough, the economic needs demand for industrial applications in large-scale bioreactors (> 50 000 l) to exploit the economy-of-scale benefits, thereby reducing the manufacturing costs to a minimum (Takors, 2012). Accordingly, the strain constructs and process developments designed under well-defined, appropriately controlled and homogenous laboratory-scale conditions crucially need to perform equally well under poorly mixed industrial production scenarios (Takors, 2012; Lorenzo and Couto, 2019). To be precise, large-scale substrate gradients of carbon or nitrogen sources generally reflect the physical limitations of mixing. Intentionally, aerobic industrial fed-batch processes typically comprise a carbon- or nitrogen-limited production period to keep the metabolic activity in the bioreactor within the technical limits of oxygen transfer and cooling.

Several studies have already addressed the scale-up issue (Neubauer *et al.*, 1995; Enfors *et al.*, 2001; Neubauer and Junne, 2010), typically focusing on the phenotypic performance of microorganisms. In addition, present scale-up studies are expected to exceed the conventional black box tests by understanding the subcellular responses in detail. Hence, the holistic cellular feedback on external heterogeneities should be predicted to prevent unwanted large-scale performance losses *a priori* (Delvigne and Noorman, 2017). Accordingly, metabolic and transcriptional insights that specify the cellular feedback under large-scale conditions are required to eventually derive detailed, large-scale

simulation models (Zieringer and Takors, 2018). Using an experimental set-up comprising a stirred tank reactor (STR) and a plug flow reactor (PFR), such studies were already performed by Löffler *et al.* (2016) and Simen *et al.* (2017) investigating *Escherichia coli.* Notably, the pivotal role of ppGpp-mediated stringent response was outlined orchestrating the metabolic and transcriptional regulation when cells were frequently exposed to glucose or ammonia starvation.

For *P. putida*, similar studies are missing. The same holds true for the fundamental question raised on the reaction of *P. putida* when repeatedly exposed to limiting glucose supply. Moreover, the putative existence of the stringent response and whether the alarmone ppGpp plays a similar role in *P. putida* as that in other bacteria (Hauryliuk *et al.*, 2015) needs to be addressed.

Consequently, this study focuses on gaining a holistic picture of the metabolic and transcriptional response of the promising strain *P. putida* KT2440 when it is exposed to large-scale stress conditions. For this purpose, cells were cultivated in the aforementioned STR-PFR setup to decipher the transcriptional response and quantify the cellular maintenance demands. Furthermore, we conclude with guidelines for a putative genome reduction based on stress-related energy expense. Finally, the interplay of starvation stress and medium-chain-length (*mcl*) polyhydroxyalkanoates (PHAs) will be unravelled, a particular trait of *P. putida,* which renders the strain as unique compared with the others.

Results

Cultivation in the STR-PFR system

Cells of *P. putida* KT2440 were cultivated in biological triplicates in a scale-down system combining a stirred tank reactor with a plug flow reactor (see Fig. 1). After an initial batch phase, each cultivation was operated in chemostat mode that was achieved by glucose limitation (dilution rate = growth rate of $0.19 \pm 0.01 \, h^{-1}$). Steady states in the STR before connection of the PFR served as a reference. These steady states were characterized by the glucose levels in the medium below detection limit and were approved after constant conditions of dissolved oxygen tension (DOT), oxygen uptake rate (OUR) and carbon emission rate (CER) were monitored for minimum five residence times (refer to Fig. S1). Reference samples for the analysis of biomass, transcripts, intracellular nucleotides and supernatant were collected before connecting the PFR during the steady state in the STR. Through connection of the PFR via a pump, cells circulating through the PFR repeatedly experience glucose starvation after depleting the remaining low glucose carried over from the STR. The DOT levels in the PFR were measured online at ports P1, P2 and P5 and were

maintained above 20% by aeration after port P1. On average, the cells circulating in the STR-PFR compartment remained for about 6.2 min in the STR (Löffler *et al.*, 2016) and 2.6 min in the PFR. The setup aimed to mimic the zones of different substrate availability in large-scale bioreactors, thereby allowing to investigate cellular short- and long-term responses at metabolic and transcriptional levels. The long-term responses were observed by sampling the STR (port S) during 25 h. Accordingly, the adaptation of *P. putida* to the repeated PFR stimulus was monitored. Based on the converging online signals and biomass concentrations, a new steady state was attained after 25 h, which was in accordance with the observations of Löffler *et al.* (2016) for *E. coli*.

In addition, to record the short-term response to a sudden glucose depletion, samples were withdrawn from the PFR ports P1–P5 after 15 min and 25 h. Neither glucose nor gluconate was found in STR and PFR; however, small amounts of 2-ketogluconic acid ($< 40 \, mg \, l^{-1}$) were detected in the supernatant, but they remained constant in the STR and PFR. During the course of the experiment, biomass (X) specific glucose (S) uptake rates persisted around an average value of $0.52 \pm 0.03 \, g_S \, g_X^{-1} \, h^{-1}$. Considering the biomass concentration and the glucose consumption rate, the remaining glucose in the STR was presumably depleted at P1 in the PFR. However, direct experimental evidence is missing as the detection limit of the glucose enzyme kit is above $20 \, mg \, l^{-1}$.

Short-term response to repeated glucose shortage

Metabolic response. The immediate metabolic dynamics on glucose shortage was monitored by measuring the intracellular nucleotides and metabolites of cells inside the PFR in the new steady state (25 h). Figure 2A illustrates the intracellular ATP, ADP and AMP kinetics in relation to the residence time in the PFR, revealing the quick decline of ATP and the concurrent rise of ADP and AMP levels immediately after glucose depletion (about 35 s). The nucleotide levels could have followed the expected trend of permanent decline as glucose shortage is directly linked to reduced ATP formation via glycolysis and the respiratory chain. However, the ATP levels recovered to $4.4 \, \mu mol \, g_X^{-1}$ within 27 s, thereby reinstalling the pre-shortage ATP-to-ADP ratio. Notably, the substrate limitation continued while cells remained in the PFR. The adenylate energy charge (AEC) is presented as a measure of the cellular energetic state. Figure 2B reveals that ATP and AEC courses are similar in the PFR. When the ATP pools were reduced (P1), AEC equally dropped from 0.77 (measured in the STR) to 0.7. Later, AEC recovered as fast as ATP to the pre-shortage value.
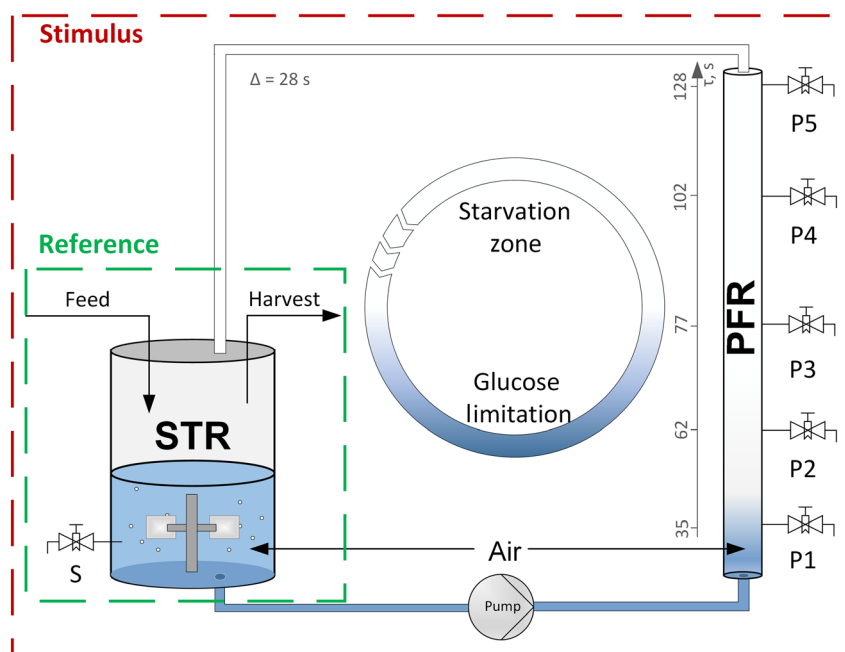
Fig. 1. Setup of the scale-down system comprising a stirred tank reactor (STR) that is operated in chemostat mode using glucose as the limiting factor (Reference condition). Via connection of the plug flow reactor (PFR), a stimulus in form of a substrate gradient is applied. The PFR was sampled at distinct time points at the ports P1, P2, P3, P4 and P5 simultaneously.

Furthermore, we analysed intracellular ppGpp levels via HPLC. This second messenger is known to trigger the activation of the stringent response in *E. coli* (Ferenci, 2001; Löffler *et al.*, 2016) and is anticipated to have the same function in *P. putida* (Liu *et al.*, 2017; Mozejko-Ciesielska *et al.*, 2017). Figure 2B depicts the immediate increase of the intracellular ppGpp pool, from 0.1 to 0.4 μmol g_X^{-1} within 77 s, after glucose depletion. Afterwards, the concentration remained constant until the end of the PFR.

In *P. putida*, the monomers of 3-hydroxydecanoic acid (C10) and 3-hydroxydodecanoic acid (C12) accumulate predominantly from different carbon sources in combination with nitrogen limitation (Huijberts *et al.* (1992), Sohn *et al.* (2010) and Mozejko-Ciesielska *et al.* (2018)). In accordance, *P. putida* KT2440 accumulated the C10 and C12 monomers to 4.0 mg_{C10} g_X^{-1} and 4.4 mg_{C12} g_X^{-1} under glucose as sole limiting factor (STR, 25 h). Even more, the amounts of C10 and C12 decreased to 3.2 mg_{C10} g_X^{-1} and to 3.1 mg_{C12} g_X^{-1} within 77 s of glucose starvation in the PFR (see Fig. 2C). However, the apparent trend of intracellular 3-HA reduction while cells suffer starvation in the PFR is statistically not significant (ANOVA *P*-value > 0.05). Raw values with statistical analysis are provided in the Data S1.

Transcriptional response. To investigate whether the repeated glucose shortage affected the transcriptional

regulation, a differential gene expression analysis was performed. Transcript profiles derived from the samples collected at the PFR (P1, P3, P5) were compared with those of the STR. Sampling was performed at 15 min and 25 h after the PFR was connected with the STR. The complete DEG analysis including log₂-fold changes and FDR-adjusted *P*-values can be found in the Data S1. In general, both the short-term transcriptional response along the PFR and the long-term culture adaptation were monitored. Figure 3A illustrates the amount of differentially expressed genes with a log₂-fold change $\geq$ 0.585 and a FDR < 0.01. By trend, the number of differentially expressed genes (DEGs) increased (i) with the duration of starvation (residence in the PFR) and (ii) with the frequency of the exposure to the glucose limitation. To be precise, first significant transcriptional changes occurred after 35 s of starvation in the PFR, both, in the 'early' (15 min) and in the 'late' (25 h) phase of running the STR-PFR experiment. After 77 s of starvation, 115 DEGs (up: 25; down: 90) were detected in the 'early' phase and 159 DEGs (up: 29; down: 130) in the 'late' phase. As aforementioned, the trend in relation to the time of starvation increased: 128 s of glucose depletion resulted in an 'early' response of 665 DEGs (up: 270; down: 395) whereas in the 'late' phase, 916 genes (up: 379; down: 537) were found as significantly differentially expressed.
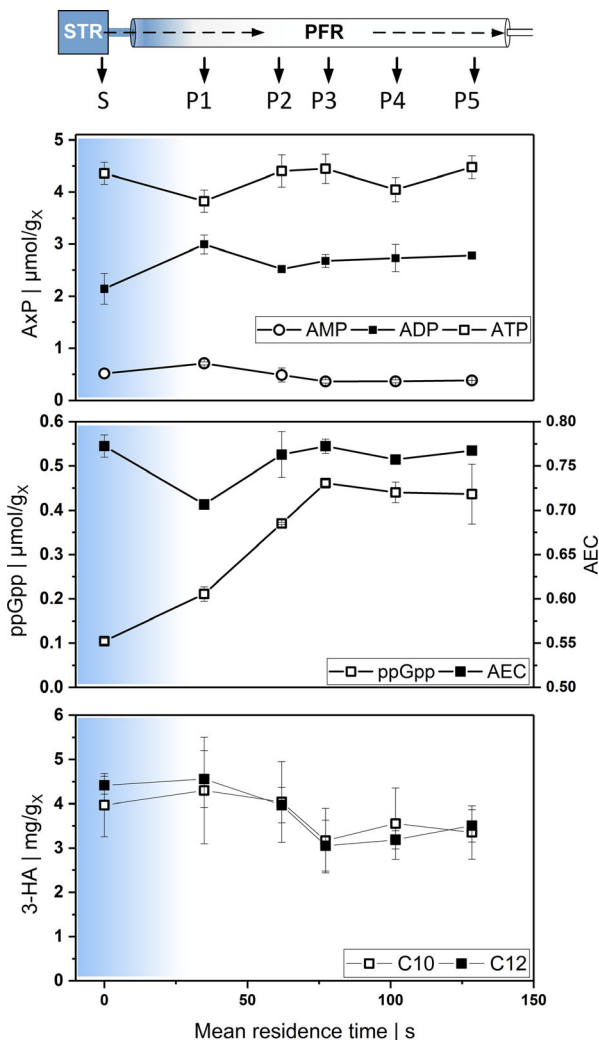
Fig. 2. Metabolic response to transition from glucose limitation in the STR (S) to depletion (symbolized by blue gradient) and starvation in the PFR (P1-P5). Samples are withdrawn after 25 h of repeated glucose starvation. X-axis indicates the mean residence time (s) in the PFR compartment **A**: intracellular nucleotides AMP, ADP and ATP per gram CDW; (B): ppGpp per gram CDW and adenylate energy charge (AEC) calculated from nucleotides; (C): intracellular concentrations of 3-hydroxydecanoic acid (C10) and 3-hydroxydodecanoic acid (C12) per gram CDW.

Furthermore, $\log_2$-fold changes (PFR-P5, 25 h) of genes related to the sigma factors were identified and plotted in Fig. 3B (FDR < 0.01). The gene *rpoS,* coding for RNA polymerase sigma S factor and *relA,* known for its ppGpp synthase activity, were upregulated at port P5 in the 'late' phase. Besides *relA, spoT* plays an important role in the stringent response, too. This gene that encodes ppGpp hydrolase was downregulated in the 'late' stage.

Regulation of central carbon metabolism. To unravel the hidden regulatory patterns of transcriptional regulation, the DEGs were grouped according to their roles in central metabolism. Figure 4 shows heatmaps of these groups according to the $\log_2$-fold change (FDR < 0.01) of the respective genes (refer to the Data S1 for $\log_2$-fold changes and *P*-values). A red or green colour represents down- or upregulation of each gene, respectively. Each heatmap is divided into long-term (STR 15 min – STR 25 h) and short-term changes (PFR P1 – P5, 25 h). In general, the most prominent dynamics is reflected by the short-term transcriptional response along the PFR, whereas the long-term transcriptional changes converged to the new steady state. The latter is elaborated in detail in the section Long-term response to repeated glucose starvation.

Within the 'glucose uptake' group, prominent short-term transcriptional changes were found for glucose oxidation via gluconate and 2-ketogluconate (2-KG). Glucose dehydrogenase (*gcd*) and the 2-KG related gene *kguT* are clearly upregulated at the exit of the PFR. In addition, upregulation was found for genes belonging to glycogen biosynthesis (*glgA, glgB*) and its degradation (*glgX, glgP, malQ*). Furthermore, glucose catabolism to pyruvate reveals only moderate transcriptional adaptation except for *tpiA* ($\log_2$-fold = −1.7), coding for triosephosphate isomerase and *pyk* ($\log_2$-fold = 0.7), coding for pyruvate kinase. In the tricarboxylic acid (TCA) cycle including the glyoxylate shunt, the transcriptional picture is more coherent. Almost all genes are repeatedly upregulated in the PFR; only succinate dehydrogenase enzymes (*sdhC, sdhD*) show the opposite trend.

Moreover, a clear transcriptional response of PHA metabolism can be observed. The short-term dynamics in the PFR reveals upregulation of 6 out of 14 genes (*fadB, fadBA, fadE, fadD-II, acd, pcaF-I*) belonging to the β-oxidation group; whereas, 6 downregulated (*accA, accD, fabD, fabF, fabZ, acpP*) and one upregulated gene (*aacS*) out of 12 genes as part of the fatty acid *de novo* synthesis are observed. Furthermore, *phaC-II*, coding for a PHA polymerase subunit, as well as the acetyl-coenzyme A synthetase genes (*acsA-I, acsA-II*) reveals upregulation.

To further identify transcriptional changes in the glucose-starved metabolism, we applied two-sample *t*-statistics for sets ($n > 3$) using GAGE. Genes were grouped ($n > 3$) according to their metabolic pathway assignment and gene ontology (GO) (see Data S1). Resulting *t*-values are illustrated in Fig. 5. In accordance with Fig. 4, the groups of β-oxidation and TCA show statistically sound upregulation whereas fatty acid *de novo* synthesis reveals downregulation. Further upregulations were found for gene sets encoding amino acid catabolism (GO:0009063), PHA metabolism (anabolism + catabolism), glycogen catabolism and glucose uptake. However, amino acid biosynthesis (GO:0008652), proteolysis (GO:0006508) and EMP + ED are characterized by low *t*-values which qualifies their transcriptional changes as low compared with the
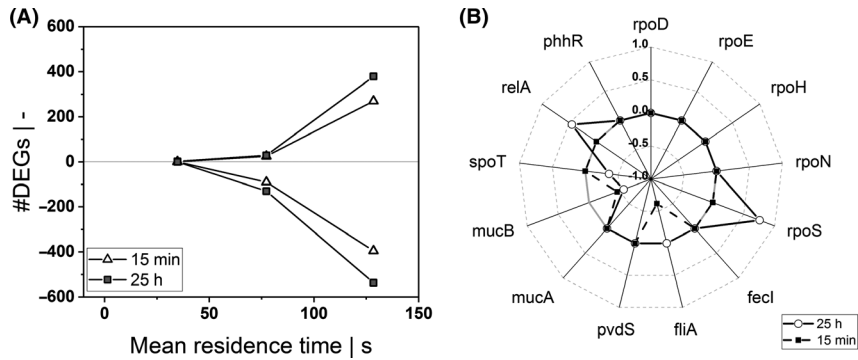
Fig. 3. A: Amount of differentially expressed genes (DEGs) that are significantly (log$_2$-fold change > 0.585, FDR < 0.01) upregulated (positive) or downregulated (negative) as a function of mean residence time in the PFR after 15 min and 25 h relative to the STR analogs. B: log$_2$-fold changes (FDR < 0.01) of genes related to sigma factors at P5 after 15 min and 25 h.

reference. Furthermore, the genes *ppk,* and *ppkB*, related to polyphosphate kinase, show significant upregulation at the outlet of the PFR (refer to Data S1).

Energetic burden of glucose starvation response. Besides transcriptional analysis, we estimated the energetic burden imposed by transcription and translation. Calculations are based on the computation of nucleotide and amino acid costs and on the estimation of ATP costs of gene expression (refer to section 'experimental procedures'). Again, we compared the state in the STR to that of the PFR outlet (P5).

In total, we calculated 23.3 $\mu mol_{ATP}\ g_X^{-1}$ as additional ATP cost for differential gene expressions in the PFR, based on the counts of DEGs within 128 s. Thereof, 19.7 $\mu mol_{ATP}\ g_X^{-1}$ accounts for translation and 3.7 $\mu mol_{ATP}\ g_X^{-1}$ for transcription. With respect to the non-growth-associated maintenance (NGAM) demand of 140.8 $\mu mol_{ATP}\ g_X^{-1}$ for *P. putida* (van Duuren *et al.*, 2013) within the time frame of 128 s, this equals an add-on of 14.0% and 2.6% due to translation and transcription, respectively. The total add-on increased NGAM to 164.1$\mu mol_{ATP}\ g_X^{-1}$.

As presented in Fig. 2C, the degradation of 3-hydroxyalkanoates (3-HA) was observed when the cells passed through the PFR. As a consequence, energy equivalents as well as C2-carbons in the form of acetyl-CoA were remobilized to serve as temporary energy and carbon sources. To balance the energy regain from degradation of 3-HA, the following equation was used (adaptation from Reddy *et al.* (2014)):

$$3\text{-OH-C}_n + ATP = \frac{n}{2} \times Acetyl - CoA + \left(\frac{n}{2} - 1\right) \times (FADH_2 + NADH) + AMP + PP_i. \quad (1)$$
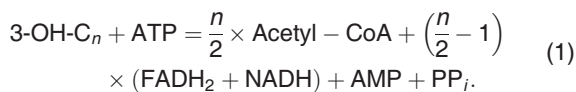
Under carbon starvation, 3-HAs are released from PHA granules by PHA depolymerase PhaZ (equals *phaB* (PP_5004)). Further activation via the ATP-dependent ACS1 leads to hydroxyacyl-CoA, which fuels the fatty acid

β-oxidation cycle (Ruth *et al.*, 2008). Each cycle yields one acetyl-CoA, reduces one FAD$^+$ to FADH$_2$ and one NAD$^+$ to NADH, and eventually leads to C$_{n-2}$ acyl-CoA. Hence, oxidation of a C10 HA costs 2 ATP but generates 4 FADH$_2$, 4 NADH and 5 acetyl-CoA (Fulco, 1983). Moreover, the remobilized acetyl-CoA is further fuelled into the TCA and oxidized to CO$_2$, thereby generating additional 3 NAD(P)H, 1 FADH$_2$ and 1 ATP (Nikel *et al.*, 2015). In total, 568.9 $\mu mol_{ATP}\ g_X^{-1}$ are recuperated from the observed degradation of 3-hydroxydecanoate (C10) and 3-hydroxydodecanoate (C12) assuming the P/O ratio of 1.33.

To sum up the energetic burden of *P. putida* in the PFR, Fig. 6 illustrates the theoretical growth (GAM) and non-growth-associated maintenance (NGAM) demands (in total 715$\mu mol_{ATP}\ g_X^{-1}$), additional ATP expenses for transcription and translation and ATP regeneration from PHA degradation in the starvation zone of the PFR. To be precise, the HA-based ATP regain can cover 79.6% of the total ATP required for cellular maintenance in the starvation zone of the PFR. Noteworthy, the amount of acetyl-CoA attained from degradation of C10 and C12 in the PFR (about 0.07 $mmol_{acetyl-CoA}\ g_X^{-1}$) equals 32% of the glucose-based acetyl-CoA production in the STR (glucose uptake in 128 s = 0.11 $mmol_S\ g_X^{-1}$).

Long-term response to repeated glucose starvation

Phenotypical adaptation. To qualify the long-term adaptation, key parameters of the reference condition, that is, non-perturbed *P. putida* growing with $\mu = 0.19\ h^{-1}$, are listed in Table 1. Additionally, new steady state values are listed, which were attained after the STR-PFR was operated for 25 h. The biomass-to-substrate yield $Y_{X/S}$ remained unchanged (*t*-test *P*-value > 0.05), whereas the AEC decreased significantly (*t*-test *P*-value < 0.05) from 0.87 to 0.79 in the STR-PFR system. Additionally, a trend of reduced PHA pools in the late phase compared with the early phase can be observed: the concentration of 3-hydroxydecanoic acid (C10) significantly (*t*-test *P*-
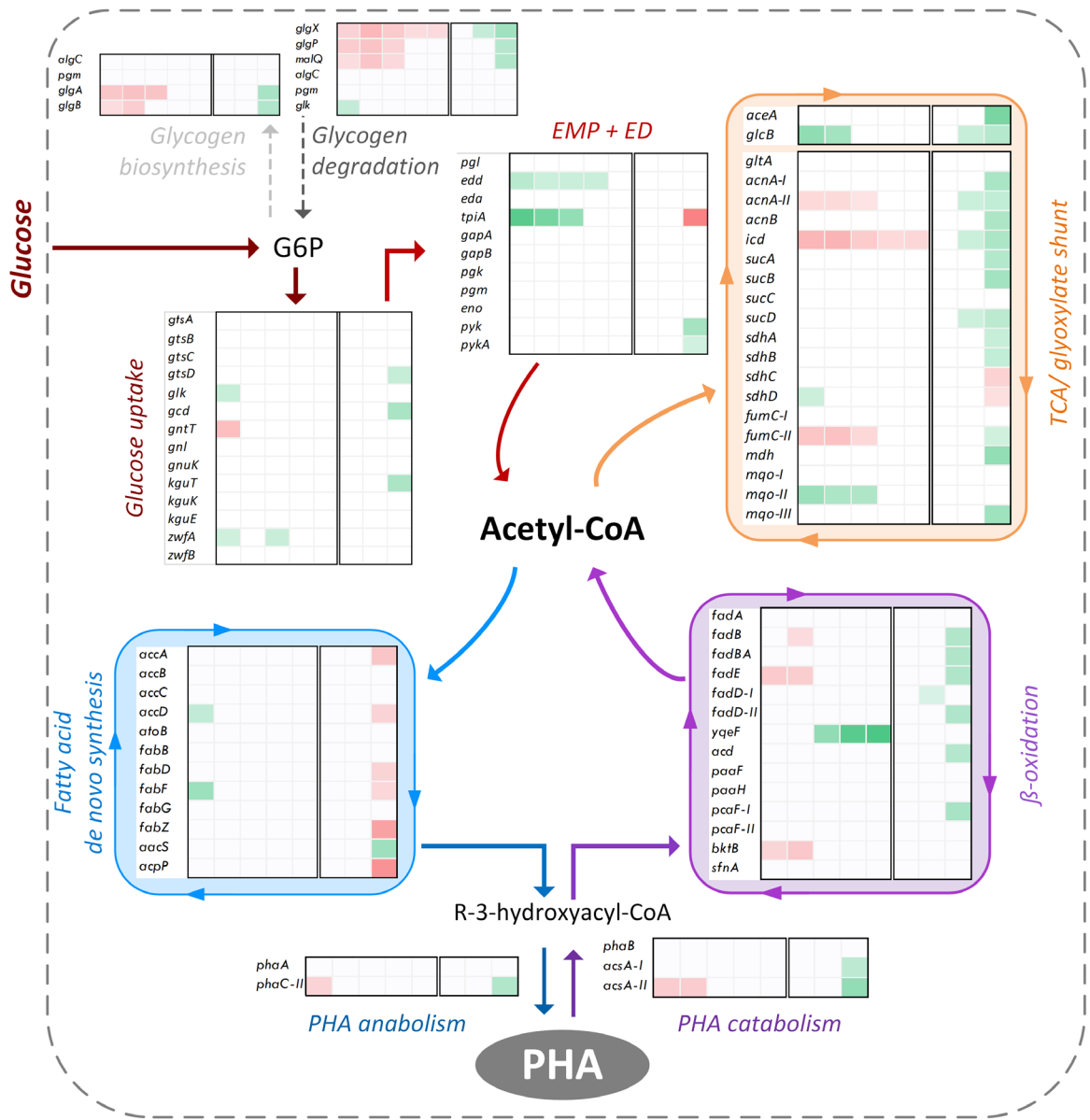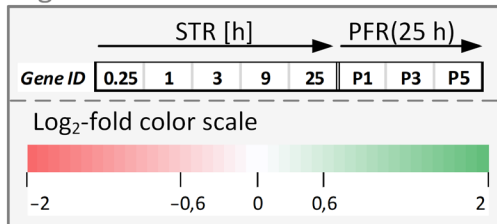
Fig. 4. Pathway-related heatmaps based on log2-fold changes of differentially expressed genes (FDR < 0.01). Genes are grouped with respect to their metabolic function. The first five columns next to the gene ID in each heatmap indicate transcriptional changes after 15 min and 1, 3, 9 and 25 h with respect to the non-perturbed reference in the STR. The last three columns depict transcript changes measured at PFR ports P1, P3 and P5 with respect to the STR analog after 25 h. The heatmap coding is presented in the legend. G6P = glucose 6-phosphate; EMP = Embden–Meyerhof–Parnas pathway from glyceraldehyde-3-phosphate to pyruvate; ED = Entner–Doudoroff pathway; PHA = polyhydroxyalkanoate.
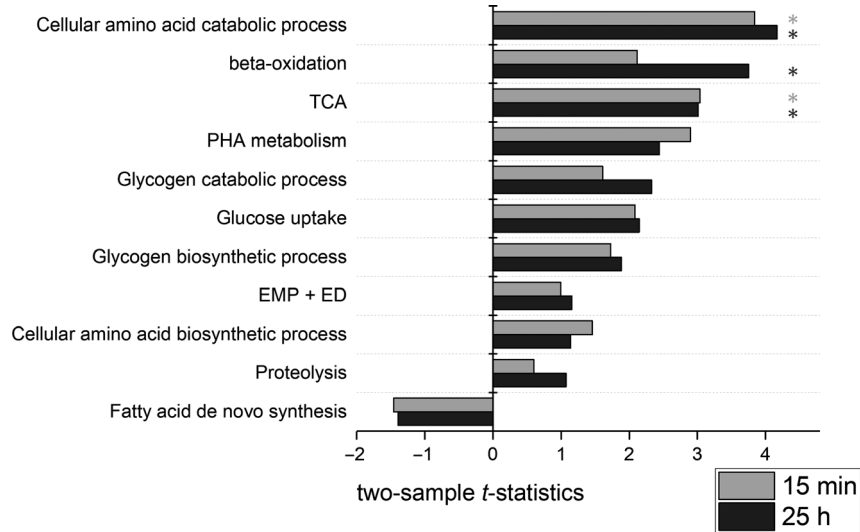
Fig. 5. Enrichment analysis of specific gene sets using GAGE. Two-sample *t*-statistics for PFR-P5 vs. STR after 15 min and 25 h of repeated glucose starvation are presented for each group. Functional groups with significant changes (FDR < 0.05) are indicated with an asterisk. The gene sets can be found in the Data S1.
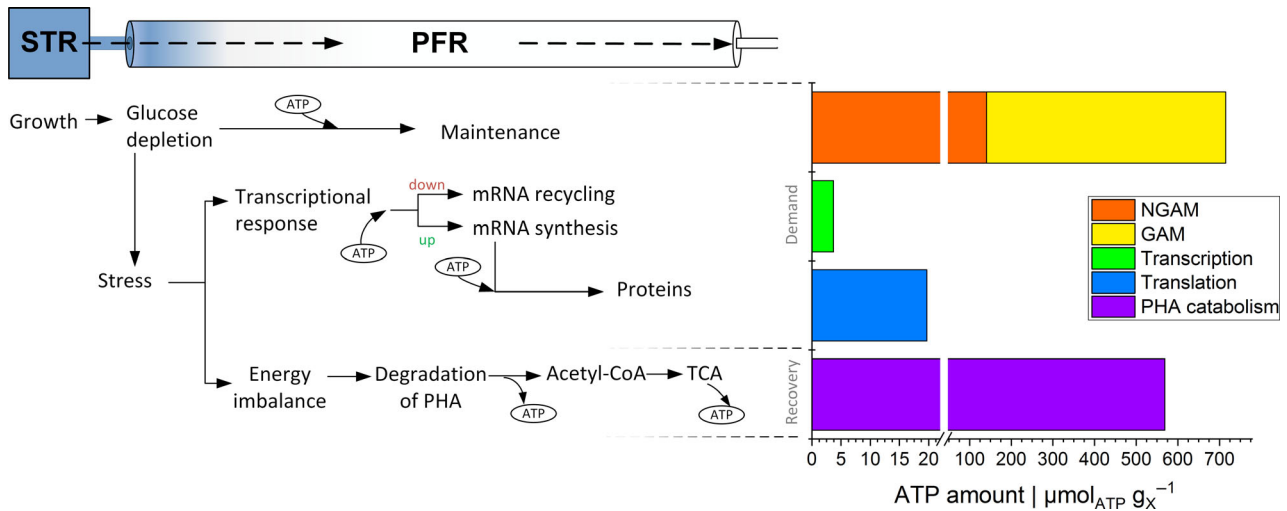
Fig. 6. Scheme of short-term response of *P. putida* to sudden glucose depletion at the transcriptional and metabolic levels. On the right side, theoretical ATP maintenance demand of cells growing at 0.19 h^{-1} and add-on of ATP costs are presented in contrast to the ATP recovery from PHA degradation within a time frame of 128 s inside the PFR.

value < 0.05) decreased by 31% from 5.86 ± 1.04 to 4.04 ± 0.43 mg g_X^{-1} and 3-hydroxydodecanoic acid (C12) from 5.0 ± 0.93 to 4.61 ± 0.29 mg g_X^{-1} (not significant). Further analysis revealed that 3-HA yields on glucose decreased in a similar manner for $Y_{C10/S}$ and $Y_{C12/S}$, respectively. Furthermore, we calculated the ATP demand for storing intracellular 3-HA (3-OH-C$_n$) using Eq. 2:

$$\frac{n}{2} \times \text{Acetyl} - \text{CoA} + \left(\frac{n}{2} - 1\right) \times \text{ATP} + (n-3) \times \text{NADPH} = 3 - \text{OH} - \text{C}_n. \quad (2)$$

In theory, acetyl-CoA is converted to malonyl-CoA via an ATP-dependent carboxyltransferase. Malonyl-CoA is then transferred to an acyl-carrier protein and incorporated with another acetyl-CoA under split-off of CO_2 into fatty acid *de novo* synthesis that yields 3-hydroxybutyrate (C$_4$). For elongation purpose, further malonyl-CoA molecules are added to form C$_{n+2}$ 3-hydroxyalkanoates. For energy costs of acetyl-CoA, refer to Table S2. If we consider similar assumptions for the degradation of 3-HA as aforementioned, the ATP demand for storing 5.86 mg$_{C10}$ g_X^{-1} at a growth rate of 0.19 h^{-1} is calculated to 0.18 mol$_{ATP}$ g_X^{-1} h^{-1} Similarly, the continuous production of 5.0 mg$_{C12}$ g_X^{-1} will cost 0.18 mol$_{ATP}$ g_X^{-1} h^{-1}. This minimal but constant production of 3-hydroxyalkanoates accounts for 1.7% of the total ATP maintenance demand

Table 1. Consequences of repeated glucose oscillation on key cultivation parameters. The 'STR' parameters (standard deviation in parenthesis) are derived in the reference steady state and the 'STR + PFR' parameters in the new steady state after 25 h.

| | $Y_{X/S}$ | AEC | $Y_{C10/X}$ | $Y_{C12/X}$ | $Y_{C10/S}$ | $Y_{C12/S}$ | ATP demand for 3-HA synthesis | |
| | | | | | | | $mmol_{ATP}\ g_X^{-1}\ h^{-1}$ | |
Condition	$g\ g^{-1}$	–	$mg\ g_X^{-1}$	$mg\ g_X^{-1}$	$mg\ g_S^{-1}$	$mg\ g_S^{-1}{}_S$	C10	C12
STR	0.38 (0.03)	0.87 (0.01)	5.86 (1.04)	5.00 (0.93)	2.57 (0.72)	2.20 (0.64)	0.18	0.18
STR + PFR	0.39 (0.03)	0.79 (0.04)	4.04 (0.43)	4.61 (0.29)	1.80 (0.34)	2.04 (0.25)	0.13	0.17

(NGAM + GAM). In the new large-scale-like steady state, the ATP costs account for only 1.4% of the maintenance.

Adaptation on transcriptional level. The transcriptional adaptation of the total culture is analysed by comparing the transcriptional patterns in the STR (sampling at port S) after 15 min and 25 h versus the reference condition without PFR link. Fig. 7 contours the relatively strong response after 15 min, indicated by 615 significant DEGs (up: 344 and down 271), which reduced to rather small changes (up: 38; down: 27) after 25 h. However, the majority of upregulated (95%) and 59% of downregulated genes of the late transcriptional responses are dominated by early transcriptional changes, which are consequently termed as 'strategic' adaptions. Among those, *icd,* coding for isocitrate dehydrogenase, *glgX* coding for the glycogen debranching enzyme, and *yqeF,* coding for acetyl-CoA acetyltransferase, which is an important enzyme in the β-oxidation cycle, were discovered. For completeness, a further differential expression analysis along with a gene set enrichment analysis can be found in the Data S1.

To further evaluate the transcriptional dynamics, ATP costs for mRNA synthesis and subsequent protein formation are estimated using the set of upregulated DEGs (FDR < 0.01) found after 25 h at port P5-PFR. Table 2 lists the top 20 genes responsible for the highest ATP expense. ATP requirements are indicated relative to the NGAM and are separated in transcriptional and translational costs. The highest impact presents the RNA polymerase sigma factor encoded by *rpoS* with an addition of 1.22%. Moreover, one gene that is particularly important for flagellum-dependent cell motility, *fliC,* accounts for over 0.85% of additional energy costs. Another ATP expensive reaction to sudden glucose shortage is the overexpression of *oprF* that is responsible for more than 0.92% of the additional energy costs. Together, these 20 genes account for 8.2% of the additional maintenance demand, which equals 55% of the total NGAM increase. The remaining 426 genes only represent 6.7% of maintenance increase, which renders Table 2, except for

essential genes, as a valid recommendation list for genome reduction to minimize additional maintenance costs.

Discussion

Dynamics of the adenylate energy charge

The well-balanced AEC of *P. putida* in the starvation compartment of the PFR is noteworthy. The AEC decreased within the first 35 s but recovered to its initial state of > 0.75 even in absence of substrate. The measured AEC values are in accordance with recent studies: Vallon *et al.* (2015) reported an AEC of approximately
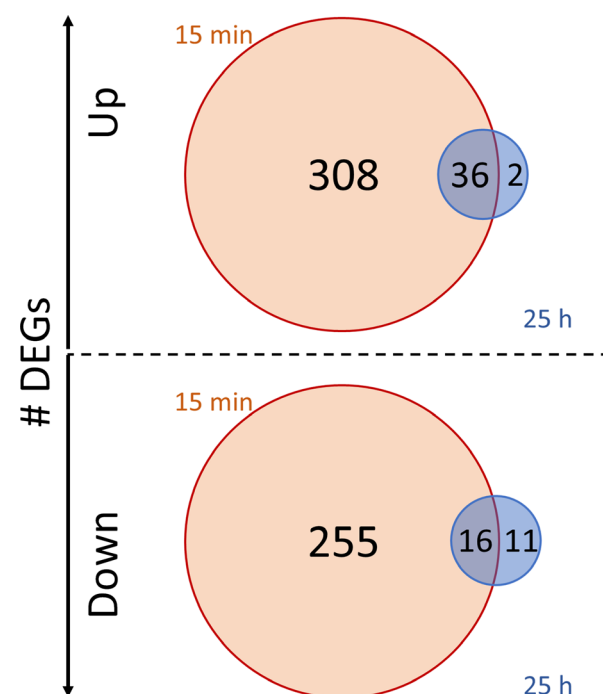
Fig. 7. Amount of differentially expressed genes (DEGs) (FDR < 0.01) as part of the long-term response to repeated glucose starvation indicated inside the circles. The gene expression profile in the STR at the late phase (25 h, blue) is compared with the analog profile measured in the early phase (after 15 min, red) in the STR. The intersection indicates the amount of common genes in both phases.

0.8 in mixed glucose/*n*-butanol-limited chemostat at growth rates between 0.1 and 0.3 h^{-1} and Martínez-García *et al.* (2014) reported an AEC > 0.75 for *P. putida* grown in shaking flasks. Chapman *et al.* (1971) concluded in their studies that growth in *E. coli* can occur only with AECs > 0.8. Accordingly, moderate AEC values between 0.5 and 0.8 ensure viability but no excessive growth. In our study, *P. putida's* energy charge was close to or > 0.8 measured in the reference state and in the new steady state. As shown in Fig. 2, the cells were affected by the transient substrate depletion, but cellular countermeasures restored the AEC to physiological levels. For comparison, the ADP levels in *E. coli* were found to increase after exposing the cells to substrate starvation, eventually leading to decreased AECs < 0.7 (Löffler *et al.*, 2016).

The stringent response in P. putida KT2440

We observed a strong correlation between glucose depletion and the intracellular amplification of ppGpp in *P. putida*. This alarmone is well known to initiate the stringent response (Traxler *et al.*, 2011; Hauryliuk *et al.*, 2015). Intracellular levels are typically regulated by RelA (ppGpp synthase) and SpoT (ppGpp hydrolase) homolog proteins (Potrykus and Cashel, 2008). As described by Gentry *et al.* (1993), the expression of sigma factor σ^S, encoded by *rpoS*, is also regulated by ppGpp, thus revealing its dominant role when *E. coli* enters the stationary phase after exponential growth.

In *P. putida*, the role of the stringent response is elucidated less compared with that in *E. coli*. Studies with *P. putida* and *P. aeruginosa* reported that ppGpp plays a crucial role in biofilm regulation (Liu *et al.*, 2017) and quorum sensing (van Delden *et al.*, 2001); however, its regulatory function during carbon starvation remains unclear. In our study, we observed the upregulation of *rpoS* at P5 in the PFR (see Fig. 3B) coinciding with increased levels of ppGpp. The trend of ppGpp dynamics was comparable to that of the *E. coli* studies (Löffler *et al.*, 2016) although the maximum value of 0.46 $\mu mol\, g_X^{-1}$ in *P. putida* was lower than that in *E. coli* (> 1 $\mu mol\, g_X^{-1}$). The *relA* gene was always upregulated at P5, suggesting that the encoded ppGpp synthase was responsible for the increase of the alarmone levels. RelA is typically activated under nitrogen and amino acid starvation; whereas, the activity of SpoT is linked to phosphate, carbon or fatty acid starvation often offering both, ppGpp-hydrolytic and synthetic activity (Hauryliuk *et al.*, 2015). In accordance, the gene expression level of *spoT* is reduced in starving *P. putida* cells (P5, 25h), thus underlining its hydrolytic function. Furthermore, ppGpp is involved in the metabolism of fatty acids in starving *E. coli* (Traxler *et al.*, 2008) and *P. putida* (Mozejko-Ciesielska *et al.*, 2017). As we observed downregulation of multiple fatty acid synthesis genes, along with upregulation of the ppGpp synthesis gene *relA* and several β-oxidation-related genes, both coinciding with rising ppGpp levels during starvation in the PFR, we conclude that ppGpp triggers regulatory programmes known from other bacteria in *P. putida*, as well. Additionally, we found strong upregulation of *aceA* and *glcB* indicating the amplification of the glyoxylate shunt activity, as it was recently revealed for *E. coli*, (Michalowski *et al.*,

Table 2. Top 20 ATP-consuming upregulated genes at the PFR outlet (P5) after 25 h. ATP costs for transcription and translation as well as log$_2$fold changes are given for individual genes.

Gene	Transcription	Translation	Σ	log$_2$-fold	Function
oprI	0.67	1.48	2.15	0.30	Major outer membrane lipoprotein
rpoS	0.48	1.04	1.52	0.70	RNA polymerase sigma S factor
rmf	0.43	0.97	1.40	0.03	Ribosome modulation factor
oprF	0.38	0.84	1.23	0.41	Porin F
fliC	0.34	0.74	1.07	0.52	Flagellin
oprB-I	0.31	0.67	0.99	0.53	Carbohydrate-selective porin
tufB	0.26	0.57	0.82	0.68	Elongation factor Tu-B
fusA	0.23	0.50	0.72	0.68	Elongation factor G 1
hpf	0.21	0.46	0.67	0.42	Ribosome hibernation promoting factor
rpsO	0.19	0.42	0.61	0.46	30S ribosomal protein S15
rplL	0.18	0.39	0.57	0.23	50S ribosomal protein L7/L12
yohC	0.17	0.37	0.54	1.50	Inner membrane protein
yeaG	0.17	0.37	0.54	1.06	Protein kinase
rplJ	0.17	0.37	0.54	0.29	50S ribosomal protein L10
rpsS	0.17	0.37	0.54	0.32	30S ribosomal protein S19
groL	0.14	0.31	0.45	0.57	Chaperonin GroEL
ygaU	0.14	0.30	0.43	0.29	Murein cross-linking regulator
proC	0.13	0.28	0.40	0.42	Pyrroline-5-carboxylate reductase
rpoA	0.12	0.26	0.37	0.51	DNA-directed RNA polymerase subunit alpha
tufA	0.11	0.25	0.37	0.40	Elongation factor Tu-A
Σ	4.98	10.96	15.94		

2017). From the aforementioned findings, we anticipate that ppGpp plays a similar role in *P. putida* than in other microbes such as in *E. coli*: ppGpp appears to be the alarmone of the stringent response. Maximum intracellular levels are slightly below the thresholds of other bacteria as reported by Lazzarini *et al.* (1971), Ryals *et al.* (1982) and Traxler *et al.* (2011). However, measurements of intracellular levels are rather error-prone and there is no rationale that equal ppGpp levels need to be present in all bacteria. Though, a high threshold saves the bacteria from erroneously expressing stationary phase genes in transient nutritional starvation.

Consequences of repeated starvation

The repeated exposure of *P. putida* to glucose-limiting conditions revealed short- and long-term responses with partially opposite trends: After 25 h in STR, the total number of differentially expressed genes diminished to only 10% of the DEGs measured after 15 min. This reduction implies that cells have adapted in the long-term to the repeated glucose shortage. In contrast, the short-term response to glucose depletion continued to amplify in the PFR comprising 974 DEGs after 25 h versus 662 genes after 15 min. This phenomenon is in contrast to the findings of Löffler *et al.* (2016) who found reducing numbers of DEGs in *E. coli* after repeated PFR exposure. Indeed, the technical impacts such as 18 s extended exposure time in PFR or the application of different analytical tools (DESeq2 vs. edgeR) might cause some bias, but they may not explain the fundamental trend. However, one key feature of *P. putida* needs to be considered: the existence of the intracellular PHA buffer which, interestingly enough, was reduced by > 30% in case of the C10 3-HA after repeated glucose starvation compared with the initial state. Hence, we anticipate that intracellular levels of the buffer additionally interact with the stringent response, which is apparently a unique link in *P. putida*.

The crucial role of 3-HAs in Pseudomonas putida as a survival strategy

As aforementioned, 3-hydroxyalkanoates can be polymerized to mcl-PHA serving as intracellular carbon and energy depot to counteract sudden starvation conditions. This requires (i) the existence of said PHA pools and (ii) cellular ability to quickly access the storage.

Referring to (i) PHA formation is predominately described as a consequence of nitrogen limitation or use of fatty acids as sole carbon and energy source. Strictly speaking, we cannot show the existence of PHAs in *P. putida* KT2440 under glucose-limited growth conditions but we give evidence to accumulated 3-HAs with

relatively low intracellular levels of 1.1% biomass weight (STR, 25 h). This content is slightly lower than the 2.7% found in steadily growing *P. putida* KT2440 on glycerol with a dilution rate of 0.12 h⁻¹ (Beckers *et al.*, 2016). Noteworthy, the overall reduction of the 3-HA content due to the repeated starvation could be part of the adaptation mechanism in *P. putida*. This would result in a reduction of 17% of ATP needs for 3-HA *de novo* synthesis.

Considering (ii), the trend of a reduction of intracellular 3-HAs as countermeasure to a decreased energy charge as well as significant expression of PHA-related genes illustrates the high dynamics of PHA catabolism initiated under glucose starvation condition. The basic role of PHA synthesis as a storage of energetic building blocks has already been anticipated by Escapa *et al.* (2012) for *P. putida* KT2442 and by James *et al.* (1999) for *Legionella pneumophila*. Escapa *et al.* (2012) reported that wild-type *P. putida* KT2442 formed more biomass than *phaC1* (Poly (3-hydroxyalkanoate) polymerase)-deficient mutants when growing on octanoic acid. Thus, our findings are in accordance with those studies and further highlight the quick response that presumably starts with PHA depolymerization followed by immediate oxidation of the prevalent C10 and C12 monomers via β-oxidation, and eventually, the oxidation of acetyl-CoA to CO_2 in the TCA, all in a matter of seconds. As depicted in Fig. 6, the theoretical 3-HA-based recovery of ATP can account for 79.6% of the cell's ATP maintenance demand under glucose starvation assuming steady growth and applying the rather conservative P/O ratio of 1.33 (van Duuren *et al.*, 2013; Hintermayer and Weuster-Botz, 2017). However, if higher P/O ratios are considered, such as 1.75 (Nogales *et al.*, 2008; Lieder *et al.*, 2015; Beckers *et al.*, 2016) or 1.85 (Hardy *et al.*, 1993; Oberhardt *et al.*, 2011), the total 3-HA-based recuperation of ATP would cover approximately 100% of ATP maintenance demand. Noteworthy, C10 and C12 pools are found to be low and almost equal under the carbon-limiting conditions applied in this study. The observation contrasts usually measured high C10 to low C12 proportions of PHA (Beckers *et al.*, 2016; Mozejko-Ciesielska *et al.*, 2018). However, the latter reflect the scenario of high external glucose levels which differs from the low external glucose conditions and the limited uptake rates of this study. For such a scenario, no reference compositions have been published so far. Considering equal levels of C10 and C12 pools under glucose-limited conditions fragments of cellular phospholipids with similar chain length might have impaired the GC-based detection of C12 3-HAs additionally.

We further assume that NADPH, that is essential for growth, is partly regenerated by the oxidation of acetyl-CoA derived from 3-HAs under glucose starvation. Besides, a significant upregulation of transhydrogenase-related genes (*pntAB* and *pntB*) in cells leaving the PFR

(128 s) might result in an increased conversion from NADH to NADPH. Consequently, the catabolism of intracellular-stored PHAs can be qualified as a very powerful and fast tactical measure to shift between 'feast and famine' lifestyles.

Transient carbon starvation intensifies catabolic reactions

The basic trend is as follows: key genes of *de novo* synthesis of fatty acids (Mozejko-Ciesielska *et al.*, 2018) are down-regulated whereas β-oxidation-related genes are clearly amplified along the PFR. This observation underlines the shift from an anabolic to a catabolic fatty acid metabolism due to the sudden starvation stress. Noteworthy, *phaC-II* (PP_5005) is exceptionally upregulated and encodes the integration of activated 3-HA building blocks (R-3-hydroxya-cyl-CoA) into PHAs. These monomers are also the hydroxylated products of 3-HA released from PHA granules via PHA depolymerase (*phaB*) and activated via acyl-CoA synthetase (*acsA-I, acsA-II*) (Ruth *et al.*, 2008), which was found to be amplified under the said starvation conditions. Accordingly, transient surplus of hydroxyacyl-CoAs may have initiated the back integration which reflects the dual role of anabolism and catabolism in the PHA cycle (Doi *et al.*, 1990; Uchino *et al.*, 2007; Ren *et al.*, 2009). Interestingly, the acetyl-CoA fuelling into the TCA cycle is accompanied by the downregulation of succinate dehydrogenase and the upregulation of the glyoxylate shunt (*aceA, aceK, glcB*), which can be qualified as a measure to prevent further carbon loss via nonessential decarboxylation.

Besides oxidation of 3-hydroxyalkanoates, further catabolic activity can be anticipated from transcriptomic data (see Fig. 5) such as the upregulation of the majority of TCA genes, which can only partly be explained by the short-term-boosted acetyl-CoA flux caused by the breakdown of 3-HAs. Most likely, the transcriptional pattern reflects the already initiated next step of starvation response, namely to access additional carbon sources such as intracellular amino acids. Indeed, there is a significant upregulation of genes coding for amino acid catabolism somehow reminding on the well-known autophagy processes in eukaryotic cells (Hamasaki *et al.*, 2003). In accordance, amino acid transport and metabolism were also found to be increased in transiently starving *E. coli* cells (Löffler *et al.*, 2016). Additionally, glycogen might serve as carbon buffer in glucose grown *P. putida* cells as upregulation was found for both, glycogen degrading and synthesizing genes (refer to Fig. 4). Poblete-Castro *et al.* (2012b) reported similar transcript changes in glycogen metabolism for decanoate-grown *P. putida* KT2442 under nitrogen and carbon–nitrogen limitation. In summary, the coincidence of glucose starvation, ongoing maintenance demands,

rapid restoration of adenylate energy levels, 3-HA degradation and upregulation of gene sets with catabolic function build the basis for the hypothesis that *P. putida* actively degrades intracellular carbon buffers to deal with short-term carbon (and ATP) shortage. ATP balancing further supports this hypothesis. Noteworthy, significant upregulation of polyphosphate kinase-related genes indicates a further strategy to balance dropping ATP levels. Accordingly, we qualify the 3-HA degradation programme as one of the short-term responses only affecting cellular metabolism to a minor extent. As indicated by transcript analysis, 3-HA degradation coincides with the degradation of intracellular amino acid pools and the access to glycogen pools as an apparent complementary measure to manage threatening starvation conditions. Therefore, the transcriptional regulation may be part of the stringent response programme in *P. putida*.

Engineering a streamlined P. putida strain for large-scale application

Table 2 lists those genes, which were repeatedly upregulated, thereby utilizing ATP unnecessarily for transcription and translation. Noteworthy, the respective upregulated genes most likely mimic long-term strategic cellular programmes that are redundant in large-scale bioreactors when cells simply fluctuate between different zones. Transcriptional dynamics occur despite *P. putida*'s countermeasures of 3-HA degradation, which only serve to prevent the precursor and ATP shortage.

In essence, Table 2 may serve as a guideline to genetically streamline *P. putida* for better performance in large-scale as less ATP is wasted but possible deletion targets require careful consideration regarding metabolic consequences. For instance, the deletion of the flagellar system (*fliC*) may be an obvious target accounting for 0.85 % of additional energy costs. Recently, Martínez-García *et al.* (2014) showed that the deletion of the major motility apparatus resulted in physiological advantages such as increased energy charge and improved tolerance to oxidative stress which was reflected by improved NAD(P)H supply. Moreover, Lieder *et al.* (2015) demonstrated improved recombinant protein production and energy status using the streamlined *P. putida* strains EM329, lacking flagellar genes and EM383, with additional elimination of the proviral DNA. Other promising deletions may comprise the knock-out of non-necessary carbon uptake and processing pathway which are numerously present in the degrading microbe *P. putida* and which are not necessary when the cell is growing in well-defined synthetic media. Moreover, the knowledge of numerous non-coding RNAs that were recently discovered in repeatedly starving *P. putida* KT2440 (Pobre *et al.*, 2020) could complement the data obtained in this study regarding putative deletion

targets to genetically optimize this strain for large-scale application.

Conclusion

Despite being glucose-limited, *P. putida* KT2440 accumulated PHA-precursors 3-hydroxyalkanoates to 1.1% of biomass, which already indicates the prominent role of the storage compound. We conclude that *P. putida* is able to access 3-HAs, most presumably released from PHA granules, within seconds, and further oxidizes the intermediates to acetyl-CoA, which is fuelled into TCA eventually to gain ATP via respiration. Noteworthy, *P. putida* may buffer the carbon shortage for approximately 5 min following this strategy. Consequently, the intracellular ATP pools and AECs are quickly restored, thereby resulting in a highly robust metabolism and energy status, a trait that is most welcome in large-scale heterogeneously mixed bioreactors. To be precise, *P. putida* is already endowed with a gift other industrial hosts such as *E. coli* cannot offer. Under the conditions tested, *P. putida* only needs 0.4% of the consumed sugar to refill 3-HA stores, which is considered as a minor expense given that *P. putida* continues to grow and to keep high energy status even when it is strictly glucose starved. Nevertheless, *P. putida* already initiates next steps of the carbon starvation programme as soon as 3-HA levels start degrading. In particular, intracellular sources of amino acids, glycogen and polyphosphates seem to be addressed as part of the stringent response. Concomitantly, the transcriptional response even increases with lowering 3-HA pools. These phenomena deserve further investigation to render *P. putida* as the optimum host for large-scale application.

Experimental procedures

Strain and medium

The *Pseudomonas putida* strain KT2440 (Bagdasarian *et al.*, 1981) (DSM-6125, ATCC47054) was used in all experiments. Mineral salts medium (M12) (Vallon *et al.*, 2013) was applied for the cultivations consisting of (per litre): 2.2 g $(NH_4)_2SO_4$, 0.4 g $MgSO_4 \times 7 H_2O$, 0.04 g $CaCl_2 \times 2 H_2O$, 0.02 g NaCl, 2 g KH_2PO_4; and trace elements: 2 mg $ZnSO_4 \times 7 H_2O$, 1 mg $MnCl_2 \times 4 H_2O$, 15 mg $Na_3C_6H_5O_7 \times 2 H_2O$, 1 mg $CuSO_4 \times 5 H_2O$, 0.02 mg $NiCl_2 \times 6 H_2O$, 0.03 mg $Na_2MoO_4 \times 2 H_2O$, 0.3 mg H_3BO_3, 10 mg $FeSO_4 \times 7 H_2O$ (Merck, Darmstadt, Germany).

Cultivation

Prior to each bioreactor fermentation, a preculture was inoculated from the working cell bank (33% glycerol stock, stored at $- 70$ °C) and cultivated in a 500 ml baffled shake flask containing 50 ml M12 medium with 4 g l^{-1} glucose, 10 g l^{-1} 3-morpholino-propanesulphonic acid (MOPS), and 0.5 g l^{-1} yeast extract (VWR International, Radnor, Pennsylvania). After 6–8 h of incubation (130 rpm, 30 °C, pH 7), the second preculture was performed in 1000 ml shaking flask containing 100 ml M12 medium with 4 g l^{-1} glucose and 10 g l^{-1} MOPS. For inoculation, the exponentially growing cells (about 0.9 g_X l^{-1}) from the first preculture were applied. After incubation for 14 h, the total volume of the second preculture (about 1.0 g_X l^{-1}) was used to start batch cultivation. The batch process was carried out in a 3 l stirred tank reactor (STR) (Bioengineering, Wald, Switzerland) containing 1.6 l M12 medium (inoculum included) with 15 g l^{-1} glucose, at 30 °C with total pressure of 1.5 bar and constant aeration of 1.5 l min^{-1}. During fermentation, the pH was adjusted at 7 using 25% NH_4OH (Carl Roth, Karlsruhe, Germany). Dissolved oxygen was maintained above 20% by controlling the stirrer speed. After depletion of initial glucose, the chemostat was started, thereby setting the constant feed (M12 medium with 18 g l^{-1} glucose) at 0.2 h^{-1} dilution rate. Antifoam (Struktol J 647, Schill + Seilacher, Hamburg, Germany) was added with 50 µl h^{-1}. After attaining a steady state (t > five residence times), the plug flow reactor (PFR) was connected to the STR via a diaphragm metering pump (Sigma/1, ProMinent, Heidelberg, Germany), which continuously drained approx. 25% of the biosuspension through the PFR and back into the STR (see Fig. 1). The scale-down setup was identical to that of Löffler *et al.* (2016) except for the different diaphragm metering pump (Sigma/1, ProMinent, Heidelberg, Germany) leading to slightly modified mean residence times in the PFR (see Table S5). Moreover, the aeration after port 1 of the PFR was 0.1 l min^{-1} leading to the total aeration of 1 vvm. PFR was heated to maintain a temperature of 30 °C.

Determination of biomass and organic acids

To quantify the cell dry weight (CDW) concentration, 4×1 ml of biosuspension was centrifuged with 14,000 rpm for 5 min at 4 °C, washed twice with demineralized water, transferred into pre-weighed glass vials (1.5 ml, VWR International, Radnor, Pennsylvania) and eventually dried at 105 °C for 24 h. The weight was determined using a micro balance (XP26 Delta Range®, Mettler Toledo, Gießen, Germany). Enzyme kits (r-biopharm AG, Darmstadt, Germany) were applied to quantify the organic acids, D-glucose and D-gluconic acid in the supernatant. 2-ketogluconic acid was measured using isocratic HPLC equipped with the RI detector (1200Series, Agilent, Santa Clara, CA, USA) and a Rezex ROA-Organic Acid H$^+$ (300 × 7.8 mm) column (Phenomenex,

Aschaffenburg, Germany) at 50 °C. 5 mM H_3SO_4 was used as a mobile phase at a rate of 0.4 ml min^{-1}.

Nucleotide analysis

Two millilitre of biosuspension was quenched using pre-cooled (-22 °C) perchloric acid (35% v/v) containing 80 μM EDTA and was incubated for 15 min at 6 °C while shaking (Cserjan-Puschmann *et al.*, 1999). Samples were processed and analysed with HPLC, as described by Löffler *et al.* (2016). Concentrations of AMP, ADP, ATP and ppGpp were normalized by dry biomass, and the adenylate energy charge (AEC) was calculated using the following approach (Atkinson, 1968):

$$AEC = \frac{[ATP] + 0.5[ADP]}{[AMP] + [ADP] + [ATP]}$$

Computation of nucleotide and amino acid energy costs

ATP costs of transcription and translation were estimated following the *E. coli* approach of Löffler *et al.* (2016). As *P. putida*'s central carbon metabolism differs from that of *E. coli,* several changes were applied. First, the phosphate/oxygen ratio (P/O) of 1.33 (van Duuren *et al.*, 2013), as conversion factor of ATP gain from respiratory oxidation of NADH (and FADH), was used instead of 1.49. ATP costs for forming metabolic precursors are presented in Table S1. These energy costs were considered to calculate the ATP requirements for synthesizing nucleotide triphosphates (NTPs), listed in Table S2. In addition, Table S3 reveals ATP requirements for producing amino acids from the respective precursors. The stoichiometry of enzymatic reactions was derived from the *Pseudomonas* Genome Database (Winsor *et al.*, 2016) collectively with the recently published metabolic flux balances of glucose grown *P. putida* KT2440 (Kohlstedt and Wittmann, 2019).

Analysis and quantification of 3-HA

Intracellular 3-hydroxyalkanoate monomers were methanolized prior to determination by GC-FID. 8 ml of biosuspension was sampled into the precooled centrifuge tubes and immediately centrifuged with 7197 $\times$ g for 5 min at 4 °C. After one washing step with 9 ml demineralized H_2O and a second centrifugation step, the cell pellet was deep-frozen at $-$ 70 °C. The frozen biomass was then subsequently lyophilized. For derivatization, 10–20 mg of lyophilized biomass was resuspended in 2 ml chloroform containing 0.05 g l^{-1} 3-methylbenzoic acid as the internal standard and 2 ml acid methanol (15% v/v sulphuric acid). After incubation at 97 °C ($\pm$ 3 °C) for 5 h, the samples were cooled, 1 ml of demineralized water was added, and the samples were then centrifuged for phase separation. For quantification, standards of 3-hydroxydecanoate and

3-hydroxydodecanoate were derivatized in the same manner (see Fig. S2). The organic phase was analysed via GC-FID. The GC system comprised an HP 5890 series II equipped with a Zebron ZB-5MS column (30 m, 0.25 mm ID, 0.25 μm df). Therefore, 1 μl of the sample was injected with a split ratio of 20:1 at an inlet temperature of 280 °C. Initial oven temperature was maintained at 100 °C for 2 min, followed by a gradient of 8 °C/min until 280 °C and was maintained for 5 min. Sample preparation procedure was adopted from Eugenio *et al.* (2010). To compensate for the expected low intracellular 3-HA pool sizes, the relatively large sampling volume of 8 ml biosuspension was used ensuring 3-HA titres of 25 to 50 $mg_{3\text{-}HA}$ l^{-1} in the extracted samples. For quantitative analysis, the peak areas of analytes in the derived chromatograms were normalized by the respective peak area of the internal standard and correlated to the linear fit of the calibration. The resulting concentrations were normalized by the dry biomass weight used for extraction to obtain biomass-specific intracellular concentrations.

RNA sequencing

Total RNA was extracted using the Trizol reagent (Ambion), following the protocol of the supplier, except for few modifications: For cell harvest, 2 ml of ice-cold stop solution (5% water-saturated phenol in ethanol) was added to 10 ml of bacterial culture, well mixed and centrifuged at 4000 $\times$ *g*, for 5 min at 4 °C. The supernatant was carefully removed, and the pellet was resuspended in 350 μl of lysis solution (0.2% lysozyme in Tris-HCl, pH 7.5) and was then incubated for 5 min at 37 °C. Next, the cells were lysed in a FastPrep homogenizer using 0.5 ml of small glass beads and 0.5 ml of acid phenol, and were centrifuged at a maximum speed for 10 min at 4 °C. The aqueous phase was collected and treated with 10 U of Turbo DNase (Ambion), for 1 h at 37 °C. RNA extraction proceeded with Trizol treatment, and after precipitation in ethanol (with 300 mM sodium acetate), the RNA was resuspended in RNase-free water. RNA integrity was evaluated by agarose gel electrophoresis, and its concentration was estimated spectrophotometrically (NanoDrop ND-1000). Total RNA was sequenced (Illumina, paired-end, 150 bp, 20M reads) by StabVida (Portugal). The rRNA was depleted from the samples with the RiboZero kit, and the sequencing libraries were constructed with the TruSeq kit (Illumina) for bacteria. The sequencing raw files are available at the Gene Expression Omnibus under the accession number GSE129947.

Data processing

Initially, we utilized FastQC v0.11.8 (Andrews, 2010) to perform quality control on the paired-end raw

sequencing reads before and after the data preprocessing. Trimmomatic v0.39 (Bolger *et al.*, 2014) was used to remove the technical sequences within the reads. Furthermore, we discarded the reads with an average Phred quality score below 20 units, and we expected a read length of 35 bases to reduce the mapping ambiguity. As a result, roughly 84.4% of the raw reads were left after the preprocessing procedure. Subsequently, the surviving paired-end reads were aligned against the reference genome of *P. putida* KT2440 (NC_002947.4) obtained from the NCBI reference sequence database (O'Leary *et al.*, 2016) using Segemehl v0.3.4 (Hoffmann *et al.*, 2009; Otto *et al.*, 2014). Therefore, we require the reads to match to the reference sequence at least by 90% resulting in 83.9% of all the (preprocessed) sequencing reads that could be aligned against the reference genome (Fig. S3). Later, featureCounts v1.6.4 (Liao *et al.*, 2014) was applied using the respective annotations for the selected reference sequence to enumerate the number of reads overlapping the transcripts of interest. We selected features characterized as 'CDS' and report the attribute 'Name' that corresponds to the RefSeq accession identifiers in order to ensure the further use of only protein-coding transcripts in the downstream analysis. In total, 72.6% of the preprocessed reads could be assigned uniquely to the annotated features thus making up between 4.8 and 12 million counts per sample (see Supplementary Data, sheet 'statistics', Fig. S5).

Differential expression analysis

Initially, we assessed the data quality using the regularized log-transformed count data, wherein we performed a principal component analysis (PCA) using a subset of 1000 genes with the highest standard deviation between samples (Fig. S5B–D). The DESeq2 R-package v3.8 (Love *et al.*, 2014), available from Bioconductor (http://www.bioconductor.org), was used to perform the differential gene expression analyses. The resulting *P*-values were adjusted for multiple testing according to Benjamini and Hochberg (1995) in order to control the false discovery rate (FDR). We identified genes as significantly differentially expressed by applying the FDR-adjusted *P*-values < 0.01 and of a fold change > 1.5 and < -1.5 (equals $\log_2$-fold > 0.585 and < -0.585). Subsequently, we assigned gene information to the initial RefSeq accession identifiers by combing information from the NCBI RefSeq, UniProt (The UniProt Consortium, 2019) and the Pseudomonas genome database (Winsor *et al.*, 2016). In addition, we used this database to categorize the genes into separate pathways and metabolic functions.

Gene set enrichment analysis

Similar to Löffler *et al.* (2016) and Simen *et al.* (2017), we performed functional enrichment tests using Bioconductor's R package Gage v3.5.2 (Luo *et al.*, 2009) to identify significant up- or downregulated sets of genes. We used the Gene Ontology term annotations for *P. putida* obtained from the Pseudomonas genome database or grouped genes according to pathways/ metabolic function and applied the rlog-transformed raw count data (see Data S1). We configured Gage to conduct group-on-group comparisons (compare="as.group") between the reference and target condition equal to the differential expression analysis using two-sample t-test statistics (use.fold=F). The gene sets were considered to be significantly different with an FDR *q*-value < 0.05 corrected after Benjamini and Hochberg (1995). The underlying data are provided in the Data S1 (see tab 'GSEA').

Conflict of interest

None declared.

References

Andrews, S. (2010) *Babraham Bioinformatics – FastQC A Quality Control tool for High Throughput Sequence Data.* URL https://www.bioinformatics.babraham.ac.uk/projects/fastqc/.

Atkinson, D.E. (1968) The energy charge of the adenylate pool as a regulatory parameter. Interaction with feedback modifiers. *Biochemistry* **7:** 4030–4034.

Bagdasarian, M., Lurz, R., Rückert, B., Franklin, F.C.H., Bagdasarian, M.M., Frey, J., and Timmis, K.N. (1981) Specific-purpose plasmid cloning vectors II. Broad host

range, high copy number, RSF 1010-derived vectors, and a host-vector system for gene cloning in Pseudomonas. *Gene* **16:** 237–247.

Beckers, V., Poblete-Castro, I., Tomasch, J., and Wittmann, C. (2016) Integrated analysis of gene expression and metabolic fluxes in PHA-producing *Pseudomonas putida* grown on glycerol. *Microb Cell Fact* **15:** 73.

Benjamini, Y., and Hochberg, Y. (1995) Controlling the false discovery rate: a practical and powerful approach to multiple testing. *J Roy Stat Soc: Series B (Methodological)* **57:** 289–300.

Bolger, A.M., Lohse, M., and Usadel, B. (2014) Trimmomatic: a flexible trimmer for Illumina sequence data. *Bioinformatics* **30:** 2114–2120.

Chapman, A.G., Fall, L., and Atkinson, D.E. (1971) Adenylate energy charge in *Escherichia coli* during growth and starvation. *J Bacteriol* **108:** 1072–1086.

Cserjan-Puschmann, M., Kramer, W., Duerrschmid, E., Striedner, G., and Bayer, K. (1999) Metabolic approaches for the optimisation of recombinant fermentation processes. *Appl Microbiol Biotechnol* **53:** 43–50.

van Delden, C., Comte, R., and Bally, A.M. (2001) Stringent response activates quorum sensing and modulates cell density-dependent gene expression in *Pseudomonas aeruginosa*. *J Bacteriol* **183:** 5376–5384.

van Duuren, J.B.J.H., Puchalka, J., Mars, A.E., Bucker, R., Eggink, G., Wittmann, C., *et al.* (2013) Reconciling in vivo and in silico key biological parameters of *Pseudomonas putida* KT2440 during growth on glucose under carbon-limited condition. *BMC Biotechnol* **13:** 93.

Delvigne, F., and Noorman, H. (2017) Scale-up/Scale-down of microbial bioprocesses: a modern light on an old issue. *Microb Biotechnol* **10:** 685–687.

Doi, Y., Segawa, A., Kawaguchi, Y., and Kunioka, M. (1990) Cyclic nature of poly(3-hydroxyalkanoate) metabolism in *Alcaligenes eutrophus*. *FEMS Microbiol Lett* **55:** 165–169.

Ebert, B.E., Kurth, F., Grund, M., Blank, L.M., and Schmid, A. (2011) Response of *Pseudomonas putida* KT2440 to increased NADH and ATP demand. *Appl Environ Microbiol* **77:** 6597–6605.

Enfors, S.-O., Jahic, M., Rozkov, A., Xu, B., Hecker, M., Jürgen, B., *et al.* (2001) Physiological responses to mixing in large scale bioreactors. *J Biotechnol* **85:** 175–185.

Escapa, I.F., García, J.L., Bühler, B., Blank, L.M., and Prieto, M.A. (2012) The polyhydroxyalkanoate metabolism controls carbon and energy spillage in *Pseudomonas putida*. *Environ Microbiol* **14:** 1049–1063.

de Lorenzo, V., and Couto, J. (2019) The important versus the exciting: reining contradictions in contemporary biotechnology. *Microb Biotechnol* **12:** 32–34.

de Eugenio, L.I., Escapa, I.F., Morales, V., Dinjaski, N., Galán, B., García, J.L., and Prieto, M.A. (2010) The turnover of medium-chain-length polyhydroxyalkanoates in *Pseudomonas putida* KT2442 and the fundamental role of PhaZ depolymerase for the metabolic balance. *Environ Microbiol* **12:** 207–221.

Ferenci, T. (2001) Hungry bacteria – definition and properties of a nutritional state. *Environ Microbiol* **3:** 605–611.

Fulco, A.J. (1983) Fatty acid metabolism in bacteria. *Prog Lipid Res* **22:** 133–160.

Gentry, D.R., Hernandez, V.J., Nguyen, L.H., Jensen, D.B., and Cashel, M. (1993) Synthesis of the stationary-phase sigma factor sigma s is positively regulated by ppGpp. *J Bacteriol* **175:** 7982–7989.

Hamasaki, M., Noda, T., and Ohsumi, Y. (2003) The early secretory pathway contributes to autophagy in yeast. *Cell Struct Funct* **28:** 49–54.

Hardy, G.P.M.A., Joost Teixeira de Mattos, M., and Neijssel, O.M. (1993) Energy conservation by pyrroloquinoline quinol-linked xylose oxidation in *Pseudomonas putida* NCTC 10936 during carbon-limited growth in chemostat culture. *FEMS Microbiol Lett* **107:** 107–110.

Hauryliuk, V., Atkinson, G.C., Murakami, K.S., Tenson, T., and Gerdes, K. (2015) Recent functional insights into the role of (p)ppGpp in bacterial physiology. *Nat Rev Microbiol* **13:** 298–309.

Hintermayer, S.B., and Weuster-Botz, D. (2017) Experimental validation of in silico estimated biomass yields of *Pseudomonas putida* KT2440. *Biotechnol J* **12:** 1600720.

Hoffmann, S., Otto, C., Kurtz, S., Sharma, C.M., Khaitovich, P., Vogel, J., *et al.* (2009) Fast mapping of short sequences with mismatches, insertions and deletions using index structures. *PLoS Comput Biol* **5:** e1000502.

Huijberts, G. N., Eggink, G., and Waard, P.d., Huisman, G.W., and Witholt, B., (1992) *Pseudomonas putida* KT2442 cultivated on glucose accumulates poly(3-hydroxyalkanoates) consisting of saturated and unsaturated monomers. *Appl Environ Microbiol* **58:** 536–544.

James, B.W., Mauchline, W.S., Dennis, P.J., Keevil, C. W., and Wait, R. (1999) Poly-3-hydroxybutyrate in *Legionella pneumophila*, an energy source for survival in low-nutrient environments. *Appl Environ Microbiol* **65:** 822–827.

Kim, J., and Park, W. (2014) Oxidative stress response in *Pseudomonas putida*. *Appl Microbiol Biotechnol* **98:** 6933–6946.

Kohlstedt, M., and Wittmann, C. (2019) GC-MS-based 13C metabolic flux analysis resolves the parallel and cyclic glucose metabolism of *Pseudomonas putida* KT2440 and *Pseudomonas aeruginosa* PAO1. *Metab Eng* **54:** 35–53.

Lazzarini, R.A., Cashel, M., and Gallant, J. (1971) On the regulation of guanosine tetraphosphate levels in stringent and relaxed strains of *Escherichia coli*. *J Biol Chem* **246:** 4381–4385.

Liao, Y., Smyth, G. K., and Shi, W. (2014) featureCounts: an efficient general purpose program for assigning sequence reads to genomic features. *Bioinformatics* **30:** 923–930.

Lieder, S., Nikel, P. I., de Lorenzo, V., and Takors, R. (2015) Genome reduction boosts heterologous gene expression in *Pseudomonas putida*. *Microb Cell Fact* **14:** 23.

Liu, H., Xiao, Y., Nie, H., Huang, Q., and Chen, W. (2017) Influence of (p)ppGpp on biofilm regulation in *Pseudomonas putida* KT2440. *Microbiol Res* **204:** 1–8.

Löffler, M., Simen, J.D., Jager, G., Schaferhoff, K., Freund, A., and Takors, R. (2016) Engineering *E. coli* for large-scale production – Strategies considering ATP expenses and transcriptional responses. *Metab Eng* **38:** 73–85.

Love, M.I., Huber, W., and Anders, S. (2014) Moderated estimation of fold change and dispersion for RNA-seq data with DESeq2. *Genome Biol* **15:** 550.

Luo, W., Friedman, M.S., Shedden, K., Hankenson, K.D., and Woolf, P.J. (2009) GAGE: generally applicable gene set enrichment for pathway analysis. *BMC Bioinform* **10:** 1–17.

Martínez-García, E., Nikel, P.I., Aparicio, T., and de Lorenzo, V. (2014) Pseudomonas 2.0: Genetic upgrading of *P. putida* KT2440 as an enhanced host for heterologous gene expression. *Microb Cell Fact* **13:** 159.

Michalowski, A., Siemann-Herzberg, M., and Takors, R. (2017) *Escherichia coli* HGT: Engineered for high glucose throughput even under slowly growing or resting conditions. *Metab Eng* **40:** 93–103.

Mozejko-Ciesielska, J., Dabrowska, D., Szalewska-Palasz, A., and Ciesielski, S. (2017) Medium-chain-length polyhydroxyalkanoates synthesis by Pseudomonas putida KT2440 relA/spoT mutant: Bioprocess characterization and transcriptome analysis. *AMB Express* **7(1):** 92.

Mozejko-Ciesielska, J., Pokoj, T., and Ciesielski, S. (2018) Transcriptome remodeling of *Pseudomonas putida* KT2440 during mcl-PHAs synthesis: effect of different carbon sources and response to nitrogen stress. *J Ind Microbiol Biotechnol* **45:** 433–446.

Neubauer, P., and Junne, S. (2010) Scale-down simulators for metabolic analysis of large-scale bioprocesses. *Curr Opin Biotechnol* **21:** 114–121.

Neubauer, P., Haggstrom, L., and Enfors, S.O. (1995) Influence of substrate oscillations on acetate formation and growth yield in *Escherichia coli* glucose limited fed-batch cultivations. *Biotechnol Bioeng* **47:** 139–146.

Nikel, P.I., and de Lorenzo, V. (2018) *Pseudomonas putida* as a functional chassis for industrial biocatalysis: from native biochemistry to trans-metabolism. *Metab Eng* **50:** 142–155.

Nikel, P.I., Martinez-Garcia, E., and de Lorenzo, V. (2014) Biotechnological domestication of pseudomonads using synthetic biology. *Nat Rev Microbiol* **12:** 368–379.

Nikel, P.I., Chavarria, M., Fuhrer, T., Sauer, U., and de Lorenzo, V. (2015) *Pseudomonas putida* KT2440 strain metabolizes glucose through a cycle formed by enzymes of the entner-doudoroff, Embden-Meyerhof-Parnas, and pentose phosphate pathways. *J Biol Chem* **290:** 25920–25932.

Nikel, P.I., Chavarria, M., Danchin, A., and de Lorenzo, V. (2016) From dirt to industrial applications: *Pseudomonas putida* as a Synthetic Biology chassis for hosting harsh biochemical reactions. *Curr Opin Chem Biol* **34:** 20–29.

Nogales, J., Palsson, B.Ø., and Thiele, I. (2008) A genome-scale metabolic reconstruction of *Pseudomonas putida* KT2440: i JN746 as a cell factory. *BMC Syst Biol* **2:** 79.

Oberhardt, M.A., Puchałka, J., Martins dos Santos, V.A.P., and Papin, J.A. (2011) Reconciliation of genome-scale metabolic reconstructions for comparative systems analysis. *PLoS Comput Biol* **7:** e1001116.

O'Leary, N.A., Wright, M.W., Brister, J.R., Ciufo, S., Haddad, D., McVeigh, R., *et al.* (2016) Reference sequence (RefSeq) database at NCBI: current status, taxonomic expansion, and functional annotation. *Nucleic Acids Res* **44:** D733–D745.

Otto, C., Stadler, P.F., and Hoffmann, S. (2014) Lacking alignments? The next-generation sequencing mapper segemehl revisited. *Bioinformatics* **30:** 1837–1843.

Poblete-Castro, I., Becker, J., Dohnt, K., dos Santos, V.M., and Wittmann, C. (2012a) Industrial biotechnology of *Pseudomonas putida* and related species. *Appl Microbiol Biotechnol* **93:** 2279–2290.

Poblete-Castro, I., Escapa, I.F., Jäger, C., Puchalka, J., Lam, C.M.C., Schomburg, D., *et al.* (2012b) The metabolic response of *P. putida* KT2442 producing high levels of polyhydroxyalkanoate under single- and multiple-nutrient-limited growth: highlights from a multi-level omics approach. *Microb Cell Fact* **11:** 34.

Pobre, V., Graça-Lopes, G., Saramago, M., Ankenbauer, A., Takors, R., Arraiano, C.M., and Viegas, S.C. (2020) Prediction of novel non-coding RNAs relevant for the growth of *Pseudomonas putida* in a bioreactor. *Microbiology (Reading, England)* **166:** 149–156.

Potrykus, K., and Cashel, M. (2008) (p)ppGpp: Still magical? *Annu Rev Microbiol* **62:** 35–51.

Reddy, B.V., Prasad, B.R., Sinha, S.N., and Ahmed, N. (2014) New mathematical derivations for calculation of ATP yield due to the complete oxidation of different types of fatty acids. *Ind J Biochem Biophys* **51:** 52–57.

Ren, Q., de Roo, G., Ruth, K., Witholt, B., Zinn, M., and Thöny-Meyer, L. (2009) Simultaneous accumulation and degradation of polyhydroxyalkanoates: futile cycle or clever regulation? *Biomacromol* **10:** 916–922.

Ruth, K., de Roo, G., Egli, T., and Ren, Q. (2008) Identification of two acyl-CoA synthetases from *Pseudomonas putida* GPo1: one is located at the surface of polyhydroxyalkanoates granules. *Biomacromol* **9:** 1652–1659.

Ryals, J., Little, R., and Bremer, H. (1982) Control of rRNA and tRNA syntheses in *Escherichia coli* by guanosine tetraphosphate. *J Bacteriol* **151:** 1261–1268.

Simen, J.D., Löffler, M., Jager, G., Schaferhoff, K., Freund, A., Matthes, J., *et al.* (2017) Transcriptional response of *Escherichia coli* to ammonia and glucose fluctuations. *Microb Biotechnol* **10:** 858–872.

Sohn, S.B., Kim, T.Y., Park, J.M., and Lee, S.Y. (2010) In silico genome-scale metabolic analysis of *Pseudomonas putida* KT2440 for polyhydroxyalkanoate synthesis, degradation of aromatics and anaerobic survival. *Biotechnol J* **5:** 739–750.

Takors, R. (2012) Scale-up of microbial processes: impacts, tools and open questions. *J Biotechnol* **160:** 3–9.

The UniProt Consortium (2019) UniProt: a worldwide hub of protein knowledge. *Nucleic Acids Res* **47:** D506–D515.

Traxler, M.F., Summers, S.M., Nguyen, H.-T., Zacharia, V.M., Hightower, G.A., Smith, J.T., and Conway, T. (2008) The global, ppGpp-mediated stringent response to amino acid starvation in *Escherichia coli*. *Mol Microbiol* **68:** 1128–1148.

Traxler, M.F., Zacharia, V.M., Marquardt, S., Summers, S.M., Nguyen, H.-T., Stark, S.E., and Conway, T. (2011) Discretely calibrated regulatory loops controlled by ppGpp partition gene induction across the 'feast to famine' gradient in *Escherichia coli*. *Mol Microbiol* **79:** 830–845.

Uchino, K., Saito, T., Gebauer, B., and Jendrossek, D. (2007) Isolated poly(3-hydroxybutyrate) (PHB) granules are complex bacterial organelles catalyzing formation of PHB from acetyl coenzyme A (CoA) and degradation of PHB to acetyl-CoA. *J Bacteriol* **189:** 8250–8256.

Vallon, T., Glemser, M., Malca, S.H., Scheps, D., Schmid, J., Siemann-Herzberg, M., *et al.* (2013) Production of 1-Octanol from n -Octane by *Pseudomonas putida* KT2440. *Chem Ing Tec* **85:** 841–848.

Vallon, T., Simon, O., Rendgen-Heugle, B., Frana, S., Mückschel, B., Broicher, A., *et al.* (2015) Applying systems biology tools to study n-butanol degradation in *Pseudomonas putida* KT2440. *Eng Life Sci* **15:** 760–771.

Winsor, G.L., Griffiths, E.J., Lo, R., Dhillon, B.K., Shay, J.A., and Brinkman, F.S.L. (2016) Enhanced annotations and features for comparing thousands of Pseudomonas genomes in the Pseudomonas genome database. *Nucleic Acids Res* **44:** D646–53.

Zieringer, J., and Takors, R. (2018) In silico prediction of large-scale microbial production performance: constraints for getting proper data-driven models. *Comput Struct Biotechnol J* **16:** 246–256.

Supporting information

Additional supporting information may be found online in the Supporting Information section at the end of the article.

Fig. S1. Physiological kinetics of *P. putida* KT2440 cultivated in a glucose-limited chemostat before and after the connection of the PFR (time point 0 h). Error bars represent the standard deviation of three biological replicates.

Fig. S2. Calibration fit for GC standards. Derivatized 3-hydroxydecanoate and 3-hydroxydodecanoate were measured via GC FID. For normalization purpose, each area was normalized by the respective area of the internal standard (IS). This calibration range was suitable to determine the 3-HA concentrations in the extracted cultivation samples.

Fig. S3. Read distribution of the samples withdrawn from the PFR (A) and the STR (B). The bars correspond to the read number before (raw) and after preprocessing (trimmed) as well as after the sequence alignment (aligned).

Fig. S4. Portion of assigned features to the total number of aligned reads for samples withdrawn from the PFR (A) and STR (B).

Fig. S5. (A) Scatterplot of the standard deviation across samples against the mean (calculated gene-wise) using the regularized log transformation. The red line depicts the running median estimator (window-width 10%). If there is no variance-mean dependence, then the line should be approximately horizontal. (B) Individuals (samples) of 12 process time points plotted on principal component 1 (PC1) and 2 (PC2). Circles and squares correspond to the location of the sampling in the PFR and STR, respectively. Arrows follow the adaptation trajectories within the PFR. A potential steady state is indicated by the green ellipse. (C) Scree plot of the PCA illustrating the contribution of each principal component to the variance. (D) Barplot of the top 20 variables (genes) contributing to the variability of PC1 and PC2. The red reference line corresponds to the expected value if the contribution where uniform and is considered as important in contributing to the dimension.

Fig. S6. Boxplot of the Cook's distances to see if one sample is consistently higher than the others (this is not the case).

Fig. S7. Results of the gene set enrichment analysis of both the short-term and long-term response. For that, samples (rows) withdrawn from the PFR (P1, P3, P5) were compared with the samples of the STR at the corresponding time points and samples withdrawn from the STR were compared to the reference condition in the STR. Gene sets were considered as significantly different with an FDR *q*-value < 0.05, shown as cells with the value of the t-statistic (indicated by the color scale) from GAGE indicating the magnitude of gene set level changes. Numbers at the bottom correspond to the size of the gene sets.

Table. S1. Energy balance for central metabolic precursors. 'Energy produced' is calculated from glucose until precursor. 'ATP produced' summarizes the energy produced based on the P/O ratio of 1.33. Negative values indicate consumption

Table. S2. Energy costs for de novo synthesis of nucleotide triphosphates (NTP). Calculation is based on the P/O ratio of 1.33.

Table. S3. Energy costs for amino acids (AA) based on their respective precursors. Total ATP costs summarize energy produced from glucose to precursor (see Table S1) and from precursor to AA. Amino acid composition for *P. putida* KT2440 is derived from Sohn et al. (2010).

Table. S4. Carbon share of biomass, PHA and CO_2 ($\pm$ standard deviation from three biological replicates) based on glucose uptake rate at $\mu = 0.194 \pm 0.01$ h^{-1}. Carbon composition of biomass was taken from van Duuren, Jozef et al. (2013).

Table. S5. Parameters for characterizing the plug flow reactor.

Table. S6. Measured values of intracellular 3-HA concentrations in experiment 1 (Exp. 1) and experiment 2 (Exp. 2), mean values and standard deviation (SD) in relation to the residence time in the PFR.

Data S1. The supplementary data file provides the underlying data of differential expression and gene set enrichment analysis.

3.3. P-III: *PSEUDOMONAS PUTIDA* KT2440

ENDURES TEMPORARY OXYGEN LIMITATIONS

The suitability of *P. putida* KT2440 in bi-phasic cultivation systems with aerobic and anaerobic zones was investigated. The wild-type strain shows stable growth performance during repeated oxygen oscillation despite transient reduced energy charges under oxygen limitation. This study paves the way for its application in solvent mixed medium to produce e.g., rhamnolipids.

ARTICLE

Pseudomonas putida KT2440 endures temporary oxygen limitations

Philipp Demling[1] [iD] | Andreas Ankenbauer[2] [iD] | Bianca Klein[3] |
Stephan Noack[3] [iD] | Till Tiso[1] [iD] | Ralf Takors[2] [iD] | Lars M. Blank[1] [iD]

[1]Institute of Applied Microbiology (iAMB), Aachen Biology and Biotechnology (ABBt), RWTH Aachen University, Aachen, Germany

[2]Institute of Biochemical Engineering, University of Stuttgart, Stuttgart, Germany

[3]Institute of Bio- and Geosciences (IBG-1): Biotechnology, Forschungszentrum Jülich GmbH, Jülich, Germany

Correspondence
Till Tiso and Lars M. Blank, Institute of Applied Microbiology, Aachen Biology and Biotechnology, RWTH Aachen University, Worringer Weg 1, 52074 Aachen, Germany.
Email: till.tiso@rwth-aachen.de and lars.blank@rwth-aachen.de

Funding information
Deutsche Forschungsgemeinschaft, Grant/Award Number: FSC 2186; H2020 Industrial Leadership, Grant/Award Number: 635536; Bundesministerium für Bildung und Forschung, Grant/Award Number: 031B0350B

Abstract

The obligate aerobic nature of *Pseudomonas putida*, one of the most prominent whole-cell biocatalysts emerging for industrial bioprocesses, questions its ability to be cultivated in large-scale bioreactors, which exhibit zones of low dissolved oxygen tension. *P. putida* KT2440 was repeatedly subjected to temporary oxygen limitations in scale-down approaches to assess the effect on growth and an exemplary production of rhamnolipids. At those conditions, the growth and production of *P. putida* KT2440 were decelerated compared to well-aerated reference cultivations, but remarkably, final biomass and rhamnolipid titers were similar. The robust growth behavior was confirmed across different cultivation systems, media compositions, and laboratories, even when *P. putida* KT2440 was repeatedly exposed to dual carbon and oxygen starvation. Quantification of the nucleotides ATP, ADP, and AMP revealed a decrease of intracellular ATP concentrations with increasing duration of oxygen starvation, which can, however, be restored when re-supplied with oxygen. Only small changes in the proteome were detected when cells encountered oscillations in dissolved oxygen tensions. Concluding, *P. putida* KT2440 appears to be able to cope with repeated oxygen limitations as they occur in large-scale bioreactors, affirming its outstanding suitability as a whole-cell biocatalyst for industrial-scale bioprocesses.

KEYWORDS
metabolic engineering, plug flow reactor, *Pseudomonas putida*, rhamnolipids, scale-down, temporary oxygen limitation

1 | INTRODUCTION

Recently, *Pseudomonas putida* has emerged as a promising host for industrial bioprocesses (Ankenbauer et al., 2020; Nikel & de Lorenzo, 2018; Tiso et al., 2014; Weimer et al., 2020). Its versatile carbon metabolism allows the usage of different carbon sources (Blank et al.,

2020; Hintermayer & Weuster-Botz, 2017; Weimer et al., 2020), potentially contributing to valorize waste streams for the production of value-added compounds in the scope of an envisioned circular bioeconomy. Prominent examples are the production of rhamnolipids from xylose (Bator, Wittgens, et al., 2020) and the upcycling of plastic waste (Tiso et al., 2021) using recombinant *P. putida* as a whole-cell

biocatalyst. Further, *P. putida* has been shown to flexibly respond to several environmental perturbations like oxidative stress (Nikel et al., 2020) and, most prominently, tolerating high concentrations of toxic substances such as organic solvents (Nikel & de Lorenzo, 2014; Ramos et al., 2015; Simon et al., 2015). This ability allows the application of an organic solvent phase, for example, in process intensification by in situ extractions (Demling et al., 2020; Wierckx et al., 2005).

P. putida KT2440 is considered the most suitable candidate among pseudomonads for industrial applications due to its host-vector (HV) system safety level 1 status (Kampers, Volkers, et al., 2019), facilitating accreditations for production processes. Further, the ability of *P. putida* KT2440 to withstand industrial-scale stress conditions in terms of fluctuations in carbon availability has recently been demonstrated (Ankenbauer et al., 2020), indicating its potential to cope with nutrient gradients and local limitations due to nonideal mixing, typically occurring in large-scale fermenters (Enfors et al., 2001; Lara et al., 2006). In this regard, recent computational fluid dynamic simulations predict mean residence times up to 76 s for bacterial cells in low glucose or low oxygen regimes inside a 300 L pilot-scale bioreactor (Kuschel & Takors, 2020). Therefore, zones within the fermenter exhibiting low oxygen concentrations pose a potential drawback to establish industrial-scale fermentations, particularly with obligate aerobic organisms such as *P. putida* KT2440. Further, in the scope of recent advances in bioreactor design, specialized apparatuses have emerged, which exhibit intentionally non-aerated compartments, leading to reactor zones with low oxygen availability (Bednarz et al., 2017; Weber et al., 2019). As inhomogeneous mixing hardly occurs in laboratory-scale fermentations, specialized scale-down reactors have been developed to intentionally induce ambient perturbations (Enfors et al., 2001; Neubauer & Junne, 2010; Neubauer et al., 1995). Considering oxygen, many studies have focused on mimicking gradients and transitions using model organisms (Nadal-Rey et al., 2020; Olughu et al., 2019) like *Escherichia coli* (Soini et al., 2008) or other industrially relevant microorganisms like *Corynebacterium glutamicum* (Käß et al., 2014; Lange et al., 2018; Limberg et al., 2017) in scale-down reactors. However, the yeasts *Pichia pastoris* (Lorantfy et al., 2013) and *Yarrowia lipolytica* (Bellou et al., 2014; Kar et al., 2012; Timoumi et al., 2017) have been the only studied microorganisms regarded as being obligate aerobic.

Several efforts have been made to engineer *P. putida* KT2440 to be capable of either anaerobic fermentation or anaerobic respiration (Nikel & de Lorenzo, 2013; Sohn et al., 2010; Steen et al., 2013). While survival of the engineered strains was successfully demonstrated, growth or the production of value-added compounds could not be sustained. However, with oxygen levels below detection limit, an isobutanol producing *P. putida* derivative revealed minimal metabolic activity for several hours (Ankenbauer et al., 2021; Nitschel et al., 2020). Further, in the absence of oxygen, bioelectrochemical systems (BES) could be employed to enable the synthesis of different products (Lai et al., 2016; Schmitz et al., 2015; Yu et al., 2018). Recently, a proof of concept for rhamnolipid production in an oxygen-limited BES was reported (Askitosari et al., 2020). Applying in

silico approaches, Kampers, van Heck, et al. (2019) identified several limitations for establishing anaerobic metabolism and a derived strategy for rational strain engineering enabled *P. putida* KT2440 to grow under micro-oxic conditions. However, for a fully anaerobic metabolism, further extensive strain engineering has been predicted (Kampers et al., 2021).

As oxygen concentrations in industrial-scale fermenters are typically fluctuating and subject to gradients, we propose that introducing a fully anaerobic metabolism into *P. putida* KT2440 is not stringently required, but rather its ability to cope with altering conditions needs to be evaluated and potentially enhanced. Thus, in this study, we assess the ability of *P. putida* KT2440 to endure temporary oxygen limitations. Different scale-down approaches, ranging from disturbed cultivations in microtiter plates (MTPs) to cultivations in stirred-tank reactors (STRs) and a defined compartmented reactor, are used to mimic industrial-scale reactor inhomogeneities in terms of oxygen availability to evaluate its effect on the growth of *P. putida* KT2440. Here, cultivations in different laboratories and operational conditions were performed to assess the robustness of *P. putida* KT2440 in varying settings. Additionally, the influence of repeated oxygen limitations on the production of secondary metabolites, here for the example of rhamnolipids, by a recombinant *P. putida* KT2440 is assessed.

2 | MATERIALS AND METHODS

2.1 | Strains, products, and media

P. putida KT2440 (DSMZ: 6125; Bagdasarian et al., 1981; Nakazawa, 2002) was used for cultivations performed to assess the growth behavior at temporary oxygen starvation. A recombinant *P. putida* KT2440 strain constitutively producing mono-rhamnolipids (mono-RLs) and their precursors 3-(hydroxyalkanoyloxy)alkanoic acids (HAAs), collectively referred to as RLs hereafter, was cultivated. The strain was previously engineered by integrating *rhlA* and *rhlB* from *Pseudomonas aeruginosa* into the genome of *P. putida* KT2440 at the *att*Tn7 site. The resulting strain *P. putida* KT2440 *att*Tn7::*Pffg-rhlAB* is further referred to as *P. putida* KT2440 SK4 (Tiso et al., 2020).

For secondary seed cultivations and MTP cultivations, mineral salts medium modified from Hartmans et al. (1989) was used (10 g L^{-1} glucose, 11.64 g L^{-1} K$_2$HPO$_4$, 4.89 g L^{-1} NaH$_2$PO$_4$, 2 g L^{-1} (NH$_4$)$_2$SO$_4$, 0.1 g L^{-1} MgCl$_2$·6H$_2$O, 10 mg L^{-1} EDTA, 2 mg L^{-1} ZnSO$_4$·7H$_2$O, 1 mg L^{-1} CaCl$_2$·2H$_2$O, 5 mg L^{-1} FeSO$_4$·7H$_2$O, 0.2 mg L^{-1} Na$_2$MoO$_4$·2 H$_2$O, 0.2 mg L^{-1} CuSO$_4$·5H$_2$O, 0.4 mg L^{-1} CoCl$_2$·6H$_2$O, and 1 mg L^{-1} MnCl$_2$·2 H$_2$O). The mineral salts medium was highly buffered to counteract the pH-decrease due to the production of gluconate and 2-ketogluconate.

For continuous cultivations in the STR-PFR setup, M12 mineral salts medium (Vallon et al., 2013) was used (17 g L^{-1} glucose, 2.2 g L^{-1} (NH$_4$)$_2$SO$_4$, 0.4 g L^{-1} MgSO$_4$·7H$_2$O, 0.04 g L^{-1} CaCl$_2$·2H$_2$O, 0.02 g L^{-1} NaCl, 2 g L^{-1} KH$_2$PO$_4$, 2 mg L^{-1} ZnSO$_4$·7H$_2$O, 1 mg L^{-1} MnCl$_2$·4H$_2$O, 15 mg L^{-1} Na$_3$C$_6$H$_5$O$_7$·2H$_2$O, 1 mg L^{-1} CuSO$_4$·5H$_2$O, 0.02 mg L^{-1} NiCl$_2$·6 H$_2$O, 0.03 mg L^{-1} Na$_2$MoO$_4$·2H$_2$O, 0.3 mg L^{-1} H$_3$BO$_3$, and

10 mg L^{-1} FeSO$_4$·7H$_2$O). A different medium compared to all other cultivations was used as the STR-PFR cultivations were performed in a different laboratory and the phenotype of *P. putida* KT2440 was to be evaluated in different operational settings.

2.2 | Strain propagation

For MTP and STR batch cultivations, cryopreserved *P. putida* KT2440 or *P. putida* KT2440 SK4 was streaked onto agar plates and incubated at 30°C for 24 h. Single colonies were used to inoculate 5 ml LB medium incubated at 30°C and 300 rpm in an orbital shaker (shaking diameter: 50 mm) for initial liquid seed cultures. Cells were transferred to a second seed culture at mid-exponential growth phase, consisting of 50 ml Hartmans mineral salts medium. The second seed culture was incubated at the same conditions as stated above and harvested for transfer into main cultures during mid-exponential growth. The initial seed train for the continuous STR-PFR cultivations was performed as described in Ankenbauer et al. (2020).

2.3 | Microtiter plate cultivations

MTP cultivations were performed in Round Well Plates (MTP-R48-B, m2p-labs; sealing: Breathseal Sealer, Greiner Bio-One) and were controlled by the BioLector I (m2p-labs). The filling volume of the wells was set to 1 ml Hartmans mineral salts medium, inoculated with wild-type *P. putida* KT2440 at an initial optical density of 0.05. The cultivation temperature was kept constant at 30°C, and humidity control was activated to limit evaporation. The oxygen transfer capacity (OTR$_{max}$) is dependent on the shaking frequency (Kensy et al., 2005). Therefore, to achieve temporary but repetitive low dissolved oxygen tensions (DOTs), a profile oscillating between 1200 rpm and 200 rpm for specific time intervals was established by developing a script implemented in the

respective backend setups of each run (Figure 1a). According to the equation published by Lattermann et al. (2014) to estimate the OTR$_{max}$ at different cultivation conditions, approximate OTR$_{max}$ of 1.2 and 60.0 mmol L^{-1} h^{-1} have been calculated for low and high shaking frequencies, respectively, thereby validating intended oscillations. Time intervals of high and low shaking frequencies were identical within one cultivation, that is, the duration of vigorously shaking was equal to the duration of restricted shaking. Time intervals of 2 min, 4 min, and 6 min were compared to a control cultivation constantly shaking at 1200 rpm. Measurement intervals were synchronized with shaking intervals to record the backscatter signal (which correlates to biomass content) at a shaking frequency of 1200 rpm. Thereby, an erroneous signal caused by sedimented cells was avoided. Cultivations were performed in five biological replicates.

2.4 | Cultivations in stirred-tank reactors

Batch cultivations were performed in 3 L stirred-tank bioreactors fully controlled by BioFlo120 units and DASware Control Software 5.5.0 (all Eppendorf AG). The working volume was set to 2 L Hartmans minimal salts medium, which was inoculated to an initial optical density of 0.2 using the second seed culture. The buffer concentration was reduced threefold compared to the medium composition stated above due to active pH control. The pH initially set to a value of 7 was monitored with online pH probes (phferm, Hamilton Company) and kept constant by the automated addition of 4 M H$_2$SO$_4$ and 4 M KOH. The temperature was set to 30°C, and the DOT was monitored with invasive probes (VisiFerm, Hamilton Company). Agitation and aeration were periodically altered between low (25 rpm, 0 vvm) and high (800 rpm, 1 vvm) setpoints to induce an oscillating DOT throughout the cultivations (Figure 1b). Intervals of high and low DOT were set to equal durations of 2 min or 4 min. Control cultivations were aerated and agitated constantly at high setpoints. Oxygen and carbon dioxide concentrations in the exhaust gas
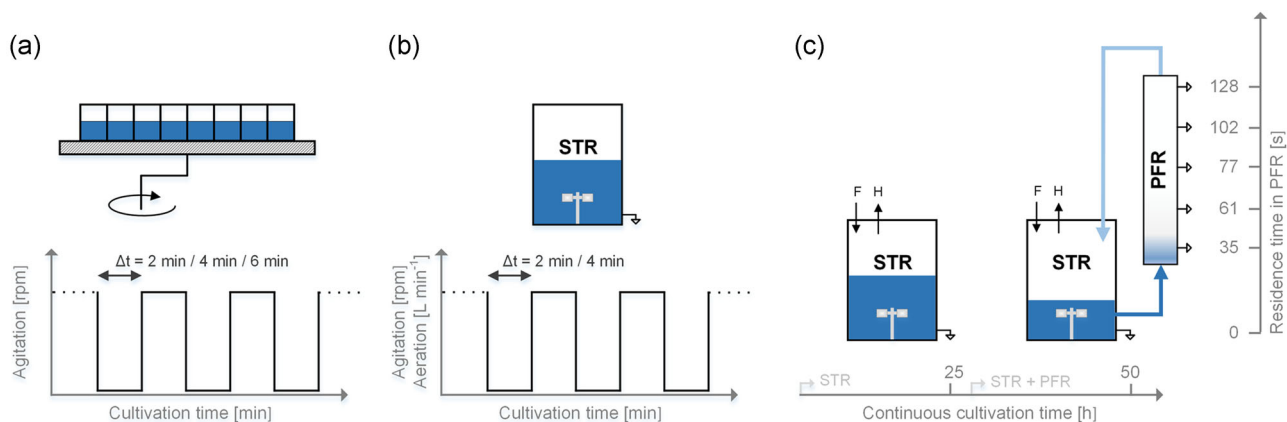
FIGURE 1 Schematic illustrations of different scale-down cultivation setups to mimic large-scale inhomogeneities in lab-scale. (a) MTP cultivations with oscillating shaking intervals. (b) STR cultivations with oscillating agitation and aeration. (c) An STR operated as glucose-limited chemostat with continuous medium feed [F] and harvest [H] served as reference conditions after reaching steady-state after five residence times. By connecting the PFR with the STR, dual substrate starvation by glucose and oxygen was applied. The STR and the five ports of the PFR were sampled simultaneously after further five residence times. MTP, microtiter plate; STR, stirred-tank reactor; PFR, plug flow reactor

were measured by BlueInOne Ferm Gas analyzers and monitored with BlueVis (both BlueSens GmbH).

Cultivations for assessing the influence of oscillating DOT on rhamnolipid production by *P. putida* KT2440 SK4 were performed at slightly modified conditions. To avoid foaming, 250 ml ethyl decanoate was added to the bioreactor for an in situ extraction of rhamnolipids. The pH was set to 6 to increase the partition coefficient and thus enhance the extraction efficiency, which has been described previously (Demling et al., 2020). The oscillating interval was set to 2 min. All STR cultivations were performed as biological duplicates.

2.5 | STR-PFR cultivation

First, steady-state growth was installed by operating a glucose-limited chemostat with a dilution rate of $0.2\,h^{-1}$ in the STR. The scale-down setup was identical to Ankenbauer et al. (2020). The DOT was controlled at 5%, pH at 6.9, and temperature at 30°C. The culture was sampled after five residence times (≥25 h) in the STR to monitor the reference status under optimal growth conditions. Next, the PFR was connected to the STR for circulating cells without feeding glucose and oxygen in the PFR (Figure 1c). Through this combinatorial setting, cells repeatedly faced glucose and oxygen starvation for 2.6 min, after staying in the well-defined limitation zone in the STR for 6.2 min. Further, five residence times later, the culture was sampled from STR and five PFR ports simultaneously. DOT was monitored continuously in the STR, at the bottom, and at the top of the PFR using oxygen probes (PreSens). STR-PFR scale-down experiments were performed as biological duplicates.

2.6 | Metabolite quantification

Concentrations of glucose, gluconate, and 2-ketogluconate in culture supernatants were determined using a DIONEX UltiMate 3000 High-Performance Liquid Chromatography System (Thermo Fisher Scientific) with an ISERA Metab AAC column $300 \times 7.8\,mm^2$ separation column (particle size: 10 μm, ISERA GmbH). Elution was performed with 5 mM H_2SO_4 at a flow rate of $0.6\,ml\,min^{-1}$ at 40°C.

For the analysis of samples from STR-PFR cultivations, gluconate and 2-ketogluconate were quantified using isocratic HPLC equipped with a RI detector (1200 Series, Agilent) and a Rezex ROA-Organic Acid H$^+$ $(300 \times 7.8\,mm^2)$ column (Phenomenex) at 50°C with a flow of $0.4\,ml\,min^{-1}$ 5 mM H_2SO_4. Furthermore, glucose concentration was detected separately using an enzymatic assay (r-biopharm AG).

2.7 | Quantification of rhamnolipids

RLs were quantified using reversed-phase HPLC-CAD (Ultimate 3000 with a Corona Veo Charged Aerosol Detector, Thermo Fisher Scientific; NUCLEODUR C18 Gravity $150 \times 4.6\,mm^2$ column, particle size: 3 μm, Macherey-Nagel GmbH & Co. KG). The applied method has been described previously (Bator, Wittgens, et al., 2020). Aqueous samples were

adjusted to pH 7 with 1 M KOH, if necessary, to avoid quantification bias. For sample preparation, acetonitrile was added in volumes equal to the aqueous samples for protein precipitation. After mixing and incubation at 4°C for more than 4 h, the samples were centrifuged (21,000g, 3 min) and filtered (Phenex RC syringe filters, 0.2 μm, d = 4 mm, Phenomenex). For samples drawn from organic phases, the ethyl decanoate was evaporated at 20 mbar, 60°C, and 1400 rpm (ScanSpeed 40 attached to ScanVac Coolsafe 110-4, both Labogene ApS, and Chemistry Hybrid Pump RC 6, vacuubrand GmbH & Co. KG). Appropriate volumes of a 50% acetonitrile – double distilled water solution were applied to resolve dry residuals and filtered subsequently (Phenomenex).

2.8 | Nucleotide analysis

A volume of 2 ml biosuspension was added to 0.5 ml precooled (−22°C) perchloric acid (35% v/v) containing 80 μM EDTA and incubated for 15 min at 6°C while shaking (Cserjan-Puschmann et al., 1999). The sample preparation and analysis were performed according to Löffler et al. (2016). After neutralization, the samples were centrifuged (15 min, 4°C, 7000g), and the supernatant was analyzed via HPLC (1200 Series, Agilent) using an RP-C18 phases column (Supercosil™ LC-18-T, 3 μm, $150 \times 4.6\,mm^2$) and a diode array detector. Concentrations of AMP, ADP, ATP, and ppGpp were normalized by dry biomass, and the adenylate energy charge (AEC) was calculated using the approach of Atkinson (1968), Equation (1). Statistical significance was evaluated by ANOVA or two-sided t-test.

$$AEC = \frac{ATP + 0.5 \cdot ADP}{AMP + ADP + ATP} \tag{1}$$

2.9 | Biomass quantification

Cell dry weight was quantified by centrifuging 1 ml of sampled fermentation broth at 21,300g and 4°C for 5 min (Centrifuge 5430R, Eppendorf AG). The supernatant was discarded, and the cells were washed by resuspending the pellet in 1 ml deionized water. After another centrifugation, the cell suspension was transferred to pre-dried and pre-weighed glass vials and incubated at 80°C. Dried samples were weighed to determine the cell dry weight. For weighing, precise micro balances were used (for STR cultivations: NewClassic MF MS105DU, Mettler Toledo; error: 0.015 mg; for STR-PFR cultivations: XP26 DeltaRange, Mettler Toledo; error: 0.008 mg). Per point of time and per biological replicate, four technical replicates were measured. Evaluation of this method revealed an error of approximately 15% for biomass titers <$0.2\,g\,L^{-1}$, which is reduced to <5% for biomass titers of >$0.5\,g\,L^{-1}$, considering biological and technical replicates.

2.10 | Untargeted proteomics

Samples were drawn as technical duplicates from each STR cultivations of *P. putida* KT2440 SK4 at the different applied conditions
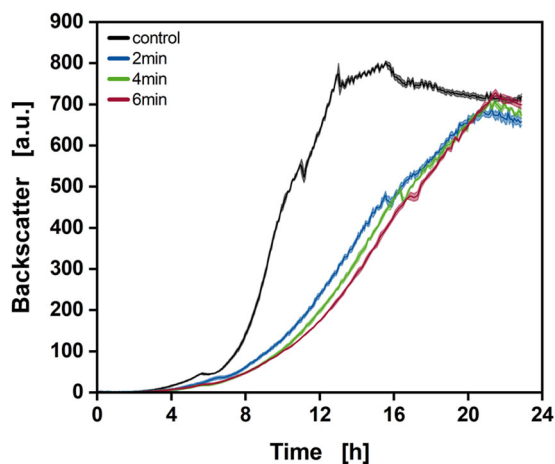
FIGURE 2 Backscatter signal throughout cultivations of *Pseudomonas putida* KT2440 in microtiter plates. A control cultivation, which was continuously shaken at 1200 rpm (black), is compared to alternating shaking frequencies of 1200 rpm and 200 rpm at intervals of 2 min (blue), 4 min (green), and 6 min (red). a.u. = arbitrary units. Shaded areas represent the standard deviation of measurements from five independent experiments

performed in biological duplicates. The control cultures were sampled at $t_1 = 7.6$ h, whereas the cultures subjected to 2 min oscillations were sampled at $t_1 = 7.6$ h and again at $t_2 = 11.9$ h, shortly before glucose depletion. About 10 ml of cultivation broth were sampled in pre-chilled (−20°C) reaction tubes, subsequently centrifuged (5000g, 10 min, 4°C), and washed with 0.9% NaCl (4°C). Cell pellets were rapidly cooled in liquid nitrogen and stored at −20°C until further analysis.

The cell pellets were suspended in lysis buffer containing 50 mM potassium phosphate buffer (pH 8.0), 2 mM EDTA, 2 mM 1,4-dithiothreitol (DTT), and supplemented with cOmplete protease inhibitor cocktail (1697 498, Roche Applied Science). Cell suspensions were disrupted in a Precellys System (Bertin Technologies SAS) using 0.1–0.2 mm glass beads plus two glass beads with 5 mm diameter for 30 s at maximum frequency was repeated two more times. The supernatant containing protein fractions was collected and frozen at −20°C until further analysis. Concentrations of proteins in crude extracts were measured using a Bradford assay (B6916, Sigma-Aldrich) with BSA as standard. According to previously described methods (Voges & Noack, 2012), the resulting crude extracts were then applied for untargeted LC-MS/MS measurement. Briefly, a maximum of 50 µl of the crude extracts (up to 100 µg total protein) were used for tryptic digestion. Crude extracts were digested with 1 µg trypsin in a total volume of 100 µl for 5 h at 42°C as recommended by the supplier (T7575, Sigma-Aldrich). Peptide solutions were diluted 1:2 with MilliQ H_2O (Millipore, Merck KGaA) before LC-MS measurements. With injected sample volumes of 10 µl, protein amounts of up to 5.0 µg were applied. Peptide mixtures were separated by reversed-phase HPLC (Infinity 1260 HPLC, Agilent Technologies; column at 21°C: 150 × 2.1 mm² Ascentis Express® Peptide ES-C18 2.7 µm (53307-U, Sigma-Aldrich); equilibration: 3% B (12 min); gradient B: 3%–40% (70 min), 40% (8 min), 40%–60% (1 min), 60% (10 min); flow:

0.2 ml min⁻¹; A: 0.1% (v/v) formic acid, B: acetonitrile+0.1% (v/v) formic acid) before ESI-MS-TOF (Q-ToF 6600 mass spectrometer, Sciex) measurements. The TripleTOF6600 was operated with CUR: 35, GS1: 50, GS2: 50, IS: 5500, TEM: 450, and DP: 120. The variable width Q1 windows were monitored in a non-scheduled manner during the elution under the above-specified parameters. SWATH window width was calculated with SWATH Variable Window Calculator_V1.0. The autosampler was set to ±6°C. Data acquisition and peak integration were performed using the software PeakView 2.1 (Sciex), while proteins were identified with the software ProteinPilot 5.1 (Sciex). Marker View software (Sciex) was used for t-test analysis.

3 | RESULTS

3.1 | Periodic oxygen starvation leads to reduced growth rates in microtiter plate cultivations

MTP cultivations were performed to assess the influence of alternating shaking frequencies and a resulting oscillation of the OTR on the growth behavior of wild-type *P. putida* KT2440. Shaking intervals of 2 min, 4 min, and 6 min at 200 rpm and 1200 rpm were compared to a culture continuously shaken at 1200 rpm.

Online backscatter signals revealed prolongations of the cultivation time until the stationary phase was reached when the culture was subjected to oscillation (Figure 2). While the continuously shaken culture entered the stationary phase after 13 h, the cultivation time of the oscillating cultures was extended to 20.8, 21.2, and 21.5 h for the intervals of 2 min, 4 min, and 6 min, respectively. Although all durations of cultivations differ significantly (all p-values < 0.05), the growth retardation was only minorly influenced by increased durations of shaking intervals, but primarily by the presence of oscillation itself. This is also reflected in the calculated growth rates during exponential phases of each set of cultivations. The maximal growth rates were determined in the latter part of the cultivations at backscatter signals (BS) > 100 to avoid technical bias (Figure a1). Obtained maximal growth rates for the control cultivations ($\mu_{ctrl} = 0.70 \pm 0.01$ h⁻¹) were approximately 2.6-fold higher compared to growth rates of all cultures subjected to oscillation ($\mu_{osc} = 0.27 \pm 0.03$ h⁻¹). Only transient phases of exponential growth could be determined, especially for the oscillating cultures, potentially indicating an oxygen limitation. However, although maximal backscatter signals of all cultivation conditions differed significantly (p-values < 0.05), generally similar values for all oscillations ($BS_{max,2min} = 683 \pm 12$ a.u., $BS_{max, 4min} = 707 \pm 7$ a.u., $BS_{max, 6min} = 728 \pm 14$ a.u.) were reached, being only slightly lower than the maximal backscatter signal of the continuously shaken control cultivations ($BS_{max,ctrl} = 770 \pm 25$ a.u.). Therefore, a decelerated growth but similar final biomass titers were concluded when *P. putida* KT2440 was subjected to oscillating OTRs.

The cultivations in the microtiter scale were influenced when subjected to oscillations in shaking frequencies leading to alternating OTR_{max}. In the described cultivations, only the online backscatter signal was accessible, thus there was no information about the DOTs

at different shaking frequencies. MTPs with integrated DOT optodes (John et al., 2003) could have given estimates. However, DOT signals respond to the oscillation in a delayed manner, and measurements could not have been synchronized to the shaking intervals. In addition, a shaken culture in microtiter scale needs validation to be comparable to cultivations in STRs (Marques et al., 2010). To gain more detailed information on the performance of *P. putida* KT2440 at oscillating oxygen availability, STR cultivations allowing to access several on- and offline signals were performed. Here, potential metabolic shifts indicated by stagnating increase in backscatter signal during the cultivations in MTPs can be elucidated by performing sampling and metabolite quantification during STR cultivations.

3.2 │ Oscillation of dissolved oxygen tension decelerates growth in STRs

For a more detailed characterization of the effects a temporary and repeated shortage of oxygen availability has on *P. putida* KT2440, STR cultivations were performed. Repeated oxygen limitation during

STR cultivations was induced by oscillating aeration and agitation between high and low setpoints. Here, intervals of 2 min and 4 min were investigated.

The duration until carbon source depletion was prolonged for both oscillating cultures compared to the control as indicated by a steep increase of the DOT signals and the measured substrate concentrations at sampling points (Figure 3a–c). All carbon in the control culture was consumed within 8.7 h, whereas carbon source in the oscillating cultures with 2 min and 4 min of oscillation was depleted after 12.8 h and 13.6 h, respectively. The prolonged duration is reflected in the specific carbon uptake rates q_S (Table 1). While the difference in cultivation time between well-aerated and oscillating conditions was significant (4.1 h and 4.9 h), increasing the interval of oscillations from 2 min to 4 min prolonged the duration of the cultivations only minorly by 0.8 h. Dissolved oxygen was temporally depleted in either oscillation interval as indicated by the DOT values at low setpoints approaching 0%. However, the culture subjected to 4 min of oscillation experienced temporal oxygen depletion earlier and over a more extended period. For comprehension, Figure 3a–c shows the minimal and maximal values of the DOT and a shaded
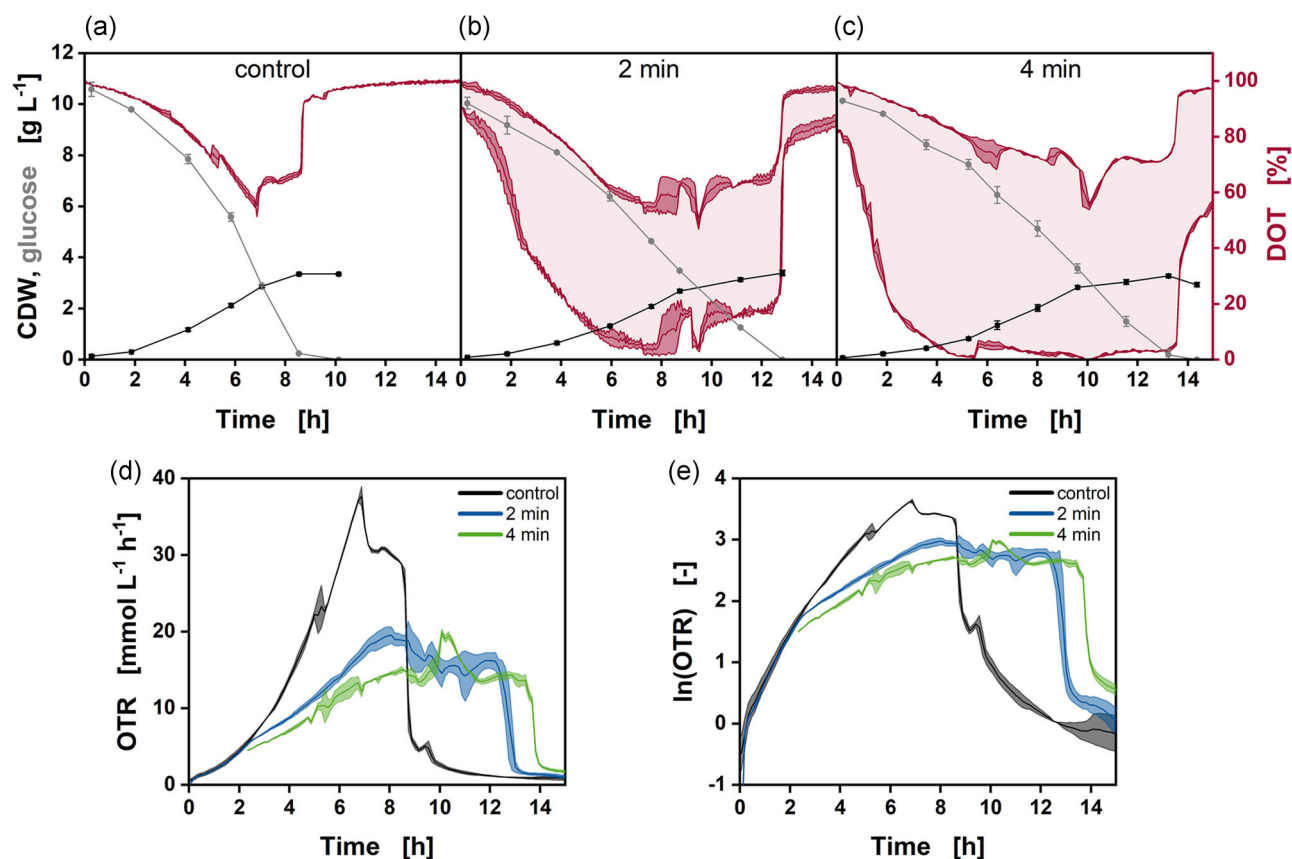
FIGURE 3 Cultivations of *Pseudomonas putida* KT2440 at different intervals of oscillating aeration and agitation. (a–c) CDW (black squares), glucose (gray dots), and DOT (red line) over the cultivation time for (a) well-aerated control cultivations, (b) 2 min intervals of oscillation, and (c) 4 min intervals of oscillation. The solid red lines represent minima and maxima of DOT values, the light red shaded area represents the range of DOT values induced by oscillation. (d, e) OTRs and the respective half-logarithmic plot for the control cultivations (black line), 2 min intervals of oscillation (blue line), and 4 min intervals of oscillation (green line). Error bars and darkly shaded areas represent errors derived from two independent experiments. CDW, cell dry weight; DOT, dissolved oxygen tension; OTR, oxygen transfer rate

TABLE 1 Performance indicators for cultivations of wild-type *Pseudomonas putida* KT2440 in STRs at different conditions

Condition[a]	m(lnOTR)[b] [h^{-1}]	q_S[c] [g g$_X^{-1}$ h^{-1}]	$Y_{X/S}$[d] [g$_X$ g^{-1}]	Gluconate[e] [g L^{-1}]	2-Ketogluconate[e] [g L^{-1}]
Control	0.50 ± 0.02	0.65 ± 0.01	0.32 ± 0.01	0.39 ± 0.00	0.50 ± 0.07
2 min	0.27 ± 0.01	0.49 ± 0.02	0.33 ± 0.02	0.45 ± 0.01	0.67 ± 0.02
4 min	0.26 ± 0.01	0.45 ± 0.01	0.30 ± 0.00	0.40 ± 0.03	0.89 ± 0.12

[a]Control represents the well-aerated culture, 2 min and 4 min the respective intervals of aeration and non-aeration.
[b]Slopes were derived via linear regression from OTR signals from 2.3 h to 5.1 h and reflect growth rates.
[c]Specific glucose uptake rates were calculated via linear regression over the first 8 h of cultivation.
[d]Biomass yields were calculated from the maximal cell dry weight and the used substrate.
[e]Data represents maximal values occurring over the entire cultivation.

range, in which DOT values oscillated. Additionally, Figure a2 depicts a close view of a section of Figure 3b to exemplarily illustrate obtained oscillations of the DOT. The biomass signals reflected the differences in time of cultivations between undisturbed and oscillating cultures. Maximal biomass titers are similar, independent of cultivation conditions ($cx_{max,ctrl}$ = 3.36 ± 0.02 g L^{-1}, $cx_{max,2min}$ = 3.39 ± 0.09 g L^{-1}, $cx_{max,4min}$ = 3.29 ± 0.02 g L^{-1}), but were reached after different durations of cultivation, coinciding with the depletion of carbon source.

Assuming an equal demand of oxygen for each cell, thus a linear correlation between growth and OTR, the OTR signals (Figure 3d) indicated a more complex growth behavior than could be derived from the sampled biomass, especially when oscillation was induced. As measurement intervals of the exhaust gas sensors and their response times did not match oscillation intervals, a moving average of the OTR is depicted, causing the signals to not appear oscillating. While the OTR of the well-aerated control cultivation and the oscillation at an interval of 2 min proceeded similarly up to a cultivation time of 2.3 h (data for the 4 min oscillation not available up to a cultivation time of 2.2 h), the signals diverged afterward as the increase in OTR of oscillating cultures decelerated. Linear regression of the OTR signals (Figure 3e) between 2.3 h and 5.1 h revealed the slope of OTR approximately to be reduced by twofold at either oscillation (Table 1), correlating with decreased growth rates of the respective cultures. Peaks and plateaus in the OTR indicate the co-metabolization of gluconate and 2-ketogluconate formed from glucose. The short stagnation of the OTR at 5 h of the control cultivation, which could also be observed in online backscatter signal of the previous cultivation in MTPs, coincided with a co-metabolization of 2-ketogluconate (refer to Figure a3). Notably, while maximal concentrations of gluconate are similar across all cultivations, the maximal concentrations of 2-ketogluconate increased with extended intervals of oscillation (Table 1 and Figure a1). The latter indicates limitations in providing NADH as the cells can circumvent the NADH-dependent ATP synthesis by generating electrons from the oxidation of gluconate to 2-ketogluconate. Integration of the OTR, starting from 2.3 h until carbon was depleted, revealed a comparable demand for oxygen, independent of disturbance (O$_2$ consumed, control = 140.4 ± 1.0 mmol L^{-1}, O$_2$ consumed, 2min = 143.6 ± 2.8 mmol L^{-1}, O$_2$ consumed, 4min = 139.1 ± 3.9 mmol L^{-1}).

In general, the results obtained from MTP cultivations could be confirmed. *P. putida* KT2440 grows at a reduced rate at oscillating oxygen availability, but final biomass titers at complete carbon depletion remain unaltered.

3.3 | *Pseudomonas putida* withstands repeated short-term oxygen starvation

Cultivations of *P. putida* KT2440 in the STR-PFR intended to unravel long- and short-term physiological responses. For the prior, the phenotypical adaptation to inhomogeneities that are likely to occur in industrial-scale bioreactors was studied. For the latter, metabolic short-term responses to sudden oxygen deprivation were monitored. In contrast to the DOT oscillations in the batch STR cultivations, only a fraction of the entire cell population is simultaneously subjected to oxygen and glucose starvation in the STR-PFR, thus rather resembling the conditions inside industrial-scale bioreactors. STR-PFR tests started with installing a steady-state glucose-limited reference (dilution rate: 0.2 h^{-1}, DOT: 5%) characterized as follows: cell dry weight concentration (c_X = 7.3 ± 0.1 g L^{-1}), adenylate energy charge (AEC = 0.84 ± 0.05), glucose uptake rate (q_S = 0.46 ± 0.01 g g$_X^{-1}$ h^{-1}), oxygen transfer rate (OTR = 58.4 ± 1.7 mmol L^{-1} h^{-1}), carbon dioxide transfer rate (CTR = 58.8 ± 1.9 mmol L^{-1} h^{-1}), see Figure 4a–c. Even though DOT was kept relatively low at 5% in the STR, the growth characteristics resemble the physiological state of the culture when DOT was kept above 20% in a previous study (Ankenbauer et al., 2020). After connection of the PFR to the STR, the low dissolved oxygen and the limited supply of glucose in the STR resulted in complete depletion of oxygen (DOT = 0%) and carbon (glucose, gluconate, and 2-ketogluconate below detection limit) at the entrance and the exit of the PFR, thus creating a transient anaerobic regime under the absence of external carbon (residence time of cells in the PFR τ_{PFR} = 2.6 min).

After additional five residence times under transient dual limitation, cells were sampled to compare physiological parameters with the reference state. *P. putida* showed stable long-term growth performance since phenotypical steady-state parameters were similar to the reference condition despite repeatedly facing starvation zones (Figure 4a–c). Only the energy charge of the cells dropped, however
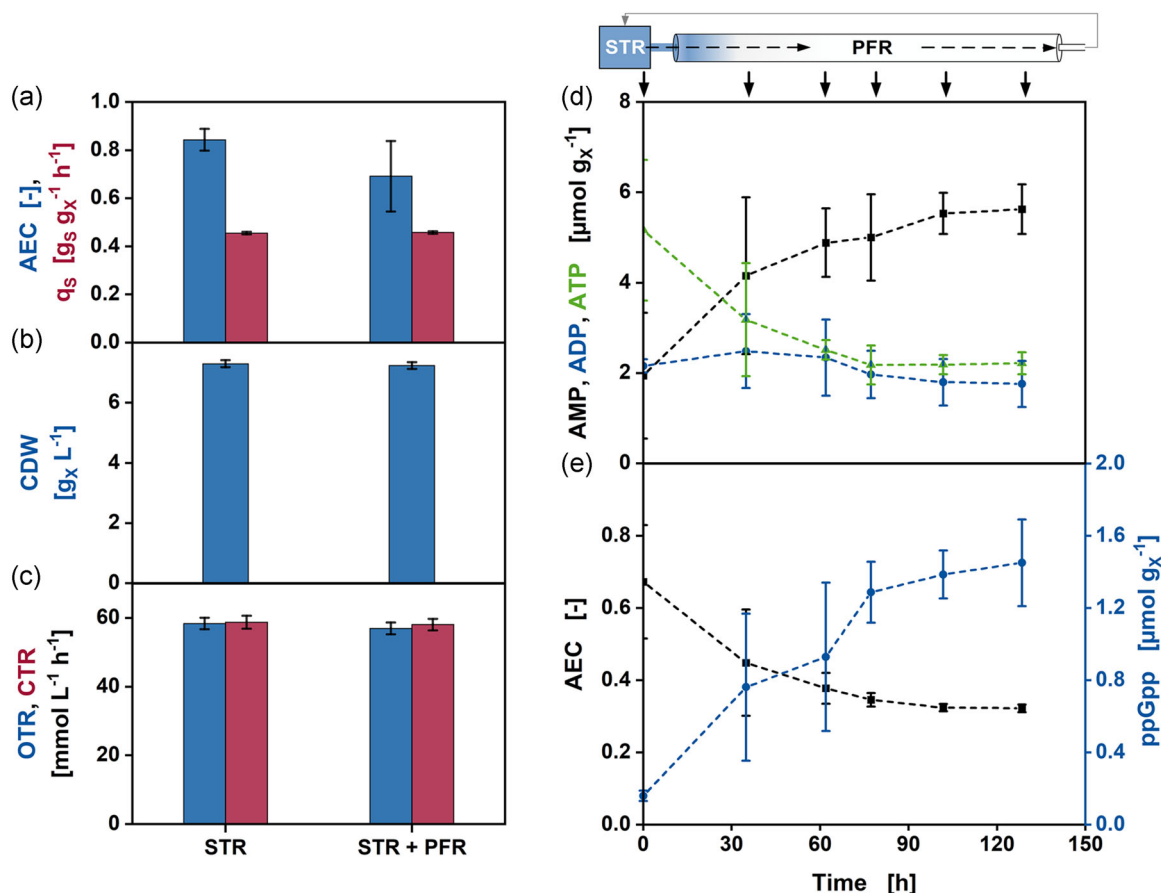
FIGURE 4 (a–c) Long-term response of *Pseudomonas putida* KT2440 to repeated transient oxygen and glucose starvation. (a) Adenylate energy charge (AEC, blue) and glucose uptake rate (qS, red), (b) cell dry weight concentration (CDW, blue), (c) oxygen transfer rates (OTRs, blue), and carbon dioxide transfer rates (CTRs, red). (d, e) Short-term response of *P. putida* KT2440 to transient oxygen and glucose starvation inside the PFR with (e) intracellular AMP (black squares), ADP (blue circles), and ATP (green triangles) concentrations; (f) AEC (black squares) and intracellular ppGpp concentration (blue circles). Error bars represent maximum and minimum values from biological duplicates

not significantly (*t*-test *p*-value > 0.05), from the reference value of 0.84 ± 0.05 to 0.69 ± 0.15.

The short-term response to the dual starvation was monitored by simultaneously sampling via the five PFR ports and the STR port at the second steady-state. The energetic condition of the cells was affected severely due to oxygen and glucose starvation. The AMP level almost doubled from 1.94 ± 1.39 to 5.63 ± 0.55 μmol g_X^{-1}, (*p*-value < 0.05) whereas the ATP level nearly halved from 5.16 ± 1.56 to 2.21 ± 0.24 μmol g_X^{-1} (*p*-value < 0.05) at the exit of the PFR in contrast to the undisturbed cells in the STR (Figure 4d). This resulted in a significant (*p*-value < 0.05) drop of the energy charge (AEC) of the cells from 0.69 ± 0.15 to a critically low level of 0.32 ± 0.01 at the exit of the PFR (Figure 4e). Concomitantly, the intracellular concentration of the stringent response alarmone ppGpp increased significantly from 0.16 ± 0.03 to 1.45 ± 0.24 μmol g_X^{-1} with progressing exposure to dual limitation. However, no significant change of intracellular ADP levels (*p*-value > 0.05) was observed. Even though *P. putida* cells showed severe metabolic reactions to short-term starvation of oxygen and glucose, their overall growth performance was not negatively affected.

3.4 | Exemplary production of rhamnolipids results in unaltered final titers at oscillating DOTs

The effect of oxygen limitation on the production capacity of *P. putida* KT2440 was also assessed, with rhamnolipids serving as an exemplary product. For this, *P. putida* KT2440 SK4, previously engineered to enable rhamnolipid synthesis (Tiso et al., 2020), was cultivated in STRs, again subjected to oscillating aeration and agitation. In addition, ethyl decanoate was added to the cultivation broth as an *in situ* extractant, and the pH was set to 6 to avoid severe foaming. Both the effect of ethyl decanoate and the lowered pH on growth and production have been described previously (Demling et al., 2020).

Similar to the STR cultivations performed with wild-type *P. putida* KT2440, the duration of the cultivation until depletion of the carbon source was prolonged at oscillating oxygen availability as indicated by the sudden increase of the DOT and the offline measurements of glucose (Figure 5a,b). However, the prolongation of cultivations was lowered to 1.5 h compared to cultivations of the wild-type *P. putida* KT2440 (4.1 h prolongation at 2 min

oscillation intervals), where no organic solvent as a second liquid phase was present. The DOT signal of the cultivation at oscillating conditions did not reach values as low as the culture of wild-type *P. putida* KT2440. As the addition of organic solvents has been proven beneficial for enhancing the mass transfer coefficient of oxygen in emulsified two-liquid phase fermentations (van Sonsbeek et al., 1993), the added ethyl decanoate might have resulted in increased oxygen availability and an attenuated oscillation. Here, with increasing RLs and biomass concentrations throughout the cultivation, the extent of this effect would be highly dynamic, depending on different proposed mechanisms. In addition, the presence of surfactants itself has an effect on the mass transfer, which is highly dependent on the type of surfactant and its concentration (Lebrun et al., 2021). Further, the lowered pH was shown to reduce growth rates of *P. putida* KT2440 (Demling et al., 2020), thus the oxygen demand of the cells is lower over time compared to the wild-type, in turn potentially resulting in a higher DOT. In addition, it is questionable how much of the measured oxygen is accessible for the microorganisms as oxygen dissolved in ethyl decanoate might be inaccessible, but the average of DOTs in both phases was measured by the optical probe.

While gluconate accumulated similarly at both cultivation conditions, nearly no 2-ketogluconate was detected (Table 2 and Figure a2). This might be due to a higher demand of glucose-6-phosphate (G6P) required to produce activated dTDP-L-rhamnose, which is transferred to HAAs by the rhamnosyltransferase RhlB to form mono-RLs. Previously, the carbon flux via the rhamnose pathway was revealed to be increased by 300% in a rhamnolipid producing *P. putida* KT2440, thus creating the mentioned demand (Tiso et al., 2016). The presence of ethyl decanoate severely impeded the determination of biomass concentration via gravimetry or spectroscopy. Therefore, exhaust gas measurements were used to calculate the moving average of OTRs as it is dependent on biomass and thus growth. Whereas the OTR of the non-oscillating cultivation generally revealed an exponential incline between approximately 1.7 h and 8 h (Table 2), a two-staged growth behavior was observed for *P. putida* KT2440 SK4 subjected to oscillations. Between cultivation times of approximately 1.7 h and 5.1 h, the OTR of the cultures exhibited an exponential incline, however, growth appears to be linear thereafter (Figure 5c,d), indicating a limitation. Similar to the cultivation of the wild-type *P. putida* KT2440, integration of the OTR lead to comparable demand of oxygen until the carbon source was depleted
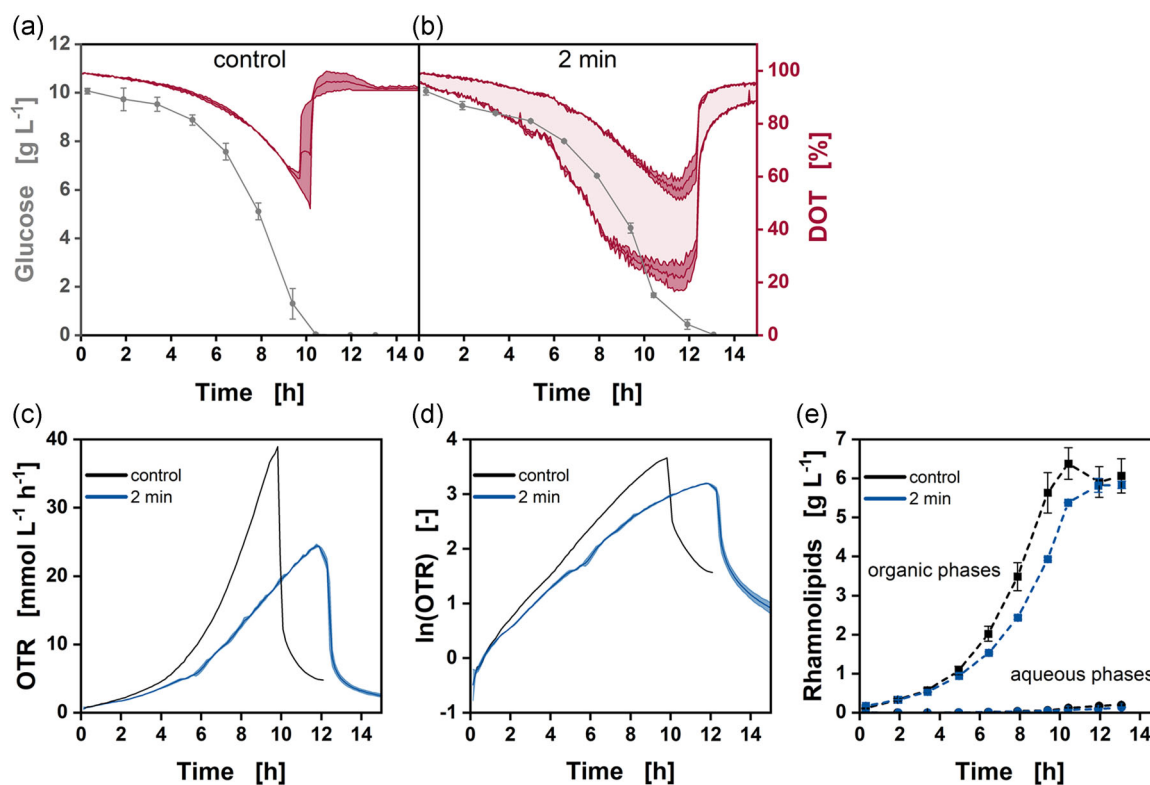
FIGURE 5 Comparison of cultivations of *Pseudomonas putida* KT2440 SK4 at different intervals of oscillating aeration and agitation. (a, b) Glucose (gray dots) and DOT (red line) over the cultivation time for (a) well-aerated control cultivations and (b) 2 min intervals of oscillation. The solid red lines represent averages of minima and maxima of DOT values. The light red shaded area represents the range of DOT values induced by oscillation. (c, d) OTRs and the respective half-logarithmic plot for the control cultivations (black line) and 2 min intervals of oscillation (blue line). (e) Average rhamnolipid titers in aqueous and organic phases for the control (black dashed lines) and 2 min intervals of oscillation (blue dashed lines). Error bars and darkly shaded areas represent errors derived from two independent experiments. For the control cultivation, only one exhaust gas measurement was recorded. DOT, dissolved oxygen tension; OTR, oxygen transfer rate

TABLE 2 Performance indicators for cultivations of *Pseudomonas putida* KT2440 SK4 in STRs at different conditions

Condition[a]	m(lnOTR)[b] [h^{-1}]	$Y_{P/S}$[c] [g$_{RL}$ g^{-1}]	STY[d] [g$_{RL}$ L^{-1} h^{-1}]	Gluconate[e] [g L^{-1}]	2-Ketogluconate[e] [g L^{-1}]
Control	0.42	0.12 ± 0.01	0.11 ± 0.01	0.85 ± 0.01	0.01 ± 0.00
2 min	0.35 ± 0.01	0.11 ± 0.00	0.09 ± 0.00	0.79 ± 0.01	0.02 ± 0.00

[a]Control represents the continuously aerated culture, 2 min intervals of aeration and non-aeration.

[b]Slopes were derived via linear regression from OTR signals from 1 to 5.1 h and reflect growth rates.

[c]Product yields were calculated from the maximal RL concentrations in the organic phase and the aqueous phase normalized by their respective volumes and the used substrate.

[d]Space-time yields were calculated from the maximal RL concentrations in the organic phase and in the aqueous phase normalized by their respective volumes and the time.

[e]Data represents maximal values occurring over the entire cultivation.
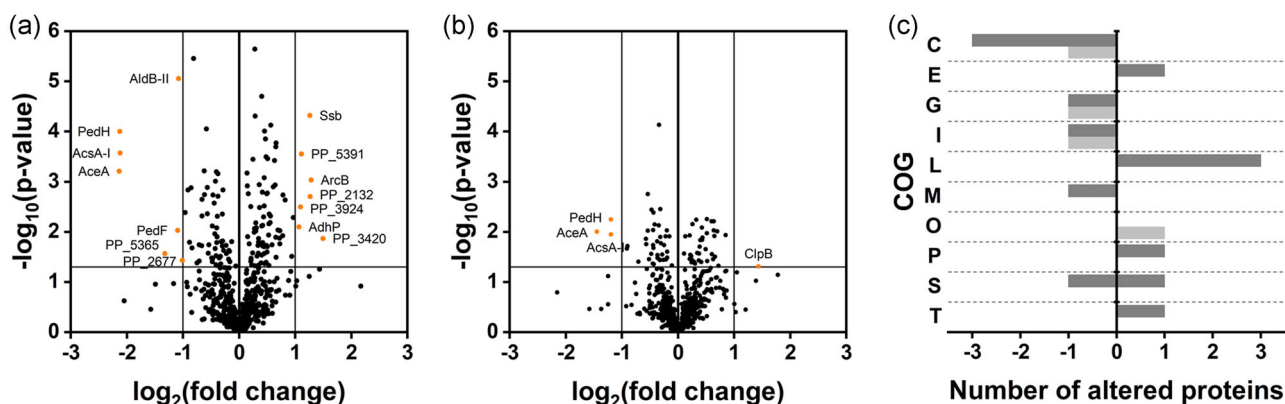
FIGURE 6 Relative differences in abundances of detected proteins in *Pseudomonas putida* KT2440 SK4 subjected to oscillating DOT compared to undistributed control cultivations. (a) Volcano plot to determine significantly altered proteins at t_1. Cutoff values were set to a log$_2$ fold change of 1 and a *p*-value of 0.05. Orange data points represent proteins of significantly altered abundance. (b) Analog to (a) for t_2. (c) Grouping of altered proteins according to COGs, which were retrieved via eggnog 5.0.0, for t_1 (dark gray bars) and t_2 (light gray bars). Positive *x*-values represent the number of proteins with increased abundance, while negative numbers represent the number of proteins with reduced abundance. COGs: C – Energy production and conversion, E – Amino acid transport and metabolism, G – Carbohydrate transport and metabolism, I – Lipid transport and metabolism, L – Replication, recombination, and repair, M – Cell wall/membrane/envelope biogenesis, O – Posttranslational modification, protein turnover, and chaperones, P – Inorganic ion transport and metabolism, S – Unknown function, T – Signal transduction mechanism. Proteins and according information are listed in Table a1. COG; cluster of orthologous groups; DOT, dissolved oxygen tension

(O$_2$ $_{consumed,control}$ = 120.7 mmol L^{-1}, O$_2$ $_{consumed,2min}$ = 123.4 ± 0.6 mmol L^{-1}).

The bulk of produced rhamnolipids was extracted from the organic phases (Figure 5e). Comparing titers of the two cultivation conditions, the same temporal offset recorded in the exhaust gas data was observed. Despite slower production in the cultivation subjected to oscillations, maximum titers were comparable, thus indicating no significant adverse effects of repeated oxygen limitations on the carbon yield, but rather on the space-time yield (Table 2), thus agreeing with the prolonged cultivation time until depletion of the carbon source.

Concluding, the cultivations of *P. putida* KT2440 SK4 in STRs showed that oscillating DOTs do not influence the strain's capacity to produce rhamnolipids, but are similar to the effect on growth results in reduced rates. While this was explicitly studied for the production of rhamnolipids, it remains unclear if it can be generalized for any

production of secondary metabolites with recombinant *P. putida* KT2440.

3.5 | *Pseudomonas putida* KT2440 subjected to oscillations alters proteome only minorly

Untargeted proteomics was used to compare samples from the STR cultivations of *P. putida* KT2440 SK4 at the different applied conditions to gain information about intracellular responses to oscillating DOTs. The continuously aerated cultures were sampled once at $t_1 = 7.6$ h, whereas the cultures subjected to oscillations were sampled at $t_1 = 7.6$ h and again at $t_2 = 11.9$ h, shortly before glucose depletion. Only proteins whose abundances were significantly altered at least twofold (*p*-value < 0.05) when subjected to oscillations were considered.

The synthesis of only a minor number of proteins was upregulated or downregulated in cells cultivated at oscillating conditions (Figure 6a,b and Table a1). Seven proteins were at least twofold more abundant, and seven proteins were reduced at least twofold compared to the control. In total, this accounts for only about 2% of all 691 detected proteins. At t_2, this ratio was even further reduced to 0.6% (one upregulated and three downregulated). The relatively low overall alteration indicates that *P. putida* KT2440 does not majorly alter its proteome but can cope with oscillating oxygen availability using its existing set of proteins. When grouping the proteins of changed abundance according to the clusters of orthologous groups (COGs) database (Tatusov et al., 1997) retrieved using eggnog 5.0.0, predominantly proteins of the COG C "Energy production and conversion" were less abundant, whereas mainly proteins associated with COG L "Replication, recombination, and repair" were synthesized at least twofold higher than in the control (Figure 6c).

The protein exhibiting the most severe downregulated synthesis at t_1 and t_2 was the isocitrate lyase (AceA, PP_4116), indicating downregulation of the glyoxylate shunt and lower carbon flux through the TCA cycle. The upregulated synthesis of proteins related to replication, recombination, and repair, chaperones, or stress response (PP_0625, chaperone protein ClpB (t_2 only); PP_0485, single-stranded DNA-binding protein; PP_2132, universal stress protein; PP_3420, sensor histidine kinase (all t_1 only)) indicates *P. putida* KT2440 to be stressed by oscillation.

Further, proteomics data showed a downregulated synthesis of the acetyl-CoA synthase AcsA-I (PP_4487) and several proteins from the *ped* cluster (PP_2675, cytochrome *c* oxidase PedF; PP_2677, hypothetical protein; PP_2679, PQQ-dependent alcohol dehydrogenase PedH; and PP_2680, aldehyde dehydrogenase AldB-II) as well as an upregulated synthesis of the alcohol dehydrogenase AdhP (PP_3839). A change in levels of alcohol dehydrogenases indicates the presence of alcohols, which could potentially be attributed to impurities of the applied ethyl decanoate (≥98% purity) or its de-esterification by *P. putida* KT2440 resulting in ethanol and decanoate. However, in both the control and the oscillating cultivation, ethyl decanoate from the same stock was used. We previously showed that *P. putida* KT2440 could not use ethyl decanoate as a carbon source in the presence of glucose or directly after glucose depletion (Demling et al., 2020). Further, metabolization of ethanol would require the activity of the acetyl-CoA synthase to generate acetyl-CoA from acetate. However, we observed the expression of *acsA-I* to be downregulated, which would result in an accumulation of acetate. Neither acetate nor ethanol was detected in the supernatant.

4 | DISCUSSION

4.1 | *Pseudomonas putida* KT2440 endures temporary oxygen starvation

We studied the influence of temporary oxygen deprivation on the growth of the obligate aerobic *P. putida* KT2440 across different cultivation systems and scales ranging from microtiter to lab-scale reactors simulating large-scale fermenters. In batch cultivations at all scales, the growth behavior appears to follow a similar pattern. When oxygen is temporarily limited, the growth rate of the cells decreases and transitions into linear growth, leading to prolonged cultivation times until carbon source depletion in contrast to well-aerated cultures. However, final biomass titers are comparable. As this phenotype is consistent throughout MTP and STR cultivations, the presented approach of implementing oscillating shaking frequencies to cause repeated oxygen shortage could be applied in similar future studies for estimations on growth behavior before running scale-down experiments in more complex setups. Strikingly, the length of oscillating intervals does not seem to impact the length of cultivation substantially as studied for MTP and STR cultivations for the wild-type *P. putida* KT2440, but rather the occurrence of oscillation causes the observed effect. This might be due to the equal durations of aeration and non-aeration within each periodic cycle. However, preliminary results from STR cultivations with unequal durations of each condition showed similar effects. Randomized durations might give different results and could be more accurate in simulating the transient conditions cells encounter due to their trajectory through large-scale reactors (Haringa et al., 2016; Kuschel et al., 2017). In the STR-PFR scale-down experiments, the overall growth performance of *P. putida* KT2440 was not impaired by repeated exposure to dual substrate starvation as the cells can reach the set growth rate of $0.2\,h^{-1}$. Recent CFD simulations revealed several transitions through oxygen and glucose starvation zones during 200 s of a bacterial lifeline circulating through a large-scale bioreactor operated as fed-batch (Kuschel & Takors, 2020). Since their study predicted glucose levels mainly below $32\,mg\,L^{-1}$ even in oxygen restricted zones, our STR-PFR setup, in which cells repeatedly traversed glucose limitation and dual starvation zones mimics large-scale inhomogeneities well enough. In accordance with our results, it was observed that *P. putida* cells achieved similar biomass yields and even accelerated the DNA replication when exposed to a critical low DOT at 1.5% compared to optimal conditions in a chemostat culture (Lieder et al., 2016). Contrarily, it was previously shown that final biomass titers of *P. putida* strains were reduced when subjected to a strict oxygen limitation induced by low but constant agitation (Escobar et al., 2016; Rodriguez et al., 2018). As we observed similar final biomass titers in this study, we infer that *P. putida* KT2440 can rapidly recover from oxygen starvation when resupplied with oxygen. This phenotype emphasizes *P. putida*'s outstanding trait to cope with different stress situations due to its versatile metabolism (Chavarría et al., 2013). Further, the RL titers produced at oscillating conditions were comparable to those of well-aerated control cultivations, but space-time yields were decreased. Therefore, we conclude that *P. putida* KT2440 is well suited for large-scale production processes exhibiting gradients in oxygen concentrations, however, at reduced productivity. Advantageously, in contrast to whole-cell biocatalysts capable of fermenting, no undesired byproducts are produced, except for gluconate and 2-ketogluconate, which are in turn metabolized and re-used as a carbon source by *P. putida* KT2440. Thereby, carbon

efficiency might be enhanced, and downstream processing might be facilitated. It needs to be validated if these conclusions can be transferred to production processes for products other than RLs.

4.2 | Intracellular mechanisms for coping with repeated oxygen starvation remain ambiguous

While growth and production appear to be robust, the distinct intracellular mechanisms for coping with repeated oxygen starvation have to be discussed further. The results from the STR-PFR scale-down experiments show that *P. putida* cells are unable to quickly recover their energy charge when facing sudden glucose and oxygen starvation. This contrasts with cells facing only glucose deprivation. It was recently observed that *P. putida* could generate energy equivalents from intracellularly accumulated 3-hydroxyalkanoates (3-HA) once external glucose is exhausted (Ankenbauer et al., 2020). Furthermore, the authors detected significant transcriptomic upregulation of genes encoding for amino acid and glycogen catabolic enzymes in glucose starving cells inside the PFR. Thus, *P. putida* is well equipped with different metabolic strategies to counteract sudden carbon starvation and, consequently, can sustain its energy charge. However, when facing dual starvation of glucose and oxygen, cells cannot properly balance their energy demand as the energy charge drops significantly from 0.7 below 0.4. Notably, energy charges above 0.7 are reported for growing *P. putida* cells (Chapman et al., 1971; Vallon et al., 2015). We assume that the lack of oxygen disrupts the electron transport in the respiratory chain that is crucial to oxidize the energy equivalents NADH and $FADH_2$ and create a proton gradient to drive the ATP synthase. In accordance with this hypothesis, the intracellular ATP level decreased, whereas AMP accumulated in the cells during transient oxygen and glucose starvation. Furthermore, increased pools of ppGpp were also found in glucose starving *E. coli* (Löffler et al., 2016) and *P. putida* cells (Ankenbauer et al., 2020). This alarmone is tightly linked to the stringent response machinery and serves as a crucial signaling molecule during starvation stress (Hauryliuk et al., 2015; Traxler et al., 2011). However, additional analytical methods such as transcriptomics and intracellular 3-HA quantification need to be applied to unveil transcriptional and metabolic responses to the installed anaerobic conditions.

In our proteome data, we detected an altered abundance of only a minor number of proteins. This contrasts with previous comparative proteomic studies of *P. putida* KT2440 subjected to stressors, like organic solvents and heavy metals (Miller et al., 2009; Santos et al., 2004), and dual limitations in carbon and phosphorus (Możejko-Ciesielska & Serafim, 2019) or iron deprivation (Heim et al., 2003), all showing a higher number of proteins with altered abundance. Our data indicates that the synthesis of the isocitrate lyase was downregulated when *P. putida* KT2440 encountered oscillating DOTs. Previously, it has been shown that a deletion of the isocitrate lyase resulted in an increased polyhydroxyalkanoates (PHA) production, assumed to cause a lower carbon flux through the tricarboxylic acid cycle, thus increasing the pool of acetyl-CoA potentially used for

PHA synthesis (Klinke et al., 2000). *P. putida* KT2440 is known to produce PHA when encountering stress caused by changing environmental conditions, for example, repeated carbon starvation or transition to nitrogen starvation (Ankenbauer et al., 2020; Obruca et al., 2018). We detected a higher abundance of proteins associated with stress response, but it is unknown if stress caused by oxygen limitation or oscillating oxygen availability induces PHA production, which was not quantified in this study. In this case, a likewise increase of RL titers could be expected as 3-hydroxyalkanoate (3-HA) is the precursor for both PHA and RLs, however, our data show no change in RL titer when cells were subjected to oscillations.

Moreover, the proteomics studies revealed a downregulated synthesis of several proteins encoded within the *ped* cluster. Recently, proteins of the *ped* cluster have been shown to be involved in the oxidation of alcohols by *P. putida* KT2440 (Bator, Karmainski, et al., 2020; Li et al., 2020; Thompson et al., 2020). Subsequently, using cytochrome *c*, electrons are transferred to the cytochrome *c* oxidase (PP_2675, PedF), which was also less abundant here, in turn reducing O_2 as part of the respiratory electron transfer chain (García-Horsman et al., 1994; Wehrmann et al., 2020). The downregulation of the *ped* can thus be reasoned with the temporary low abundance of molecular O_2, impeding the functionality of PedF and potentially the PQQ biosynthesis pathway, which requires molecular O_2 itself. As the regulation of the whole cluster seems to be multi-leveled and interconnected (Bator, Karmainski, et al., 2020; Thompson et al., 2020), similar expression levels of individual genes of the cluster might be caused by the same trigger such as limited availability of molecular O_2. The higher abundance of NAD^+-dependent AdhP indicates its function as a complementary alcohol dehydrogenase, which might be favored over PedH at shortage of NADH, which is suggested by the increasing 2-ketogluconate concentrations in the wild-type cultivations. In fact, deletion of both *pedH* and *adhP* caused *P. putida* KT2440 to lose its ability to metabolize short-chain alcohols, while single deletion strains retained functionality (Thompson et al., 2020). However, if altered abundances of proteins of the *ped* cluster and AdhP are solely due to oscillating DOTs or if the presence of an organic solvent triggers their synthesis in the first place, remains unclear.

In general, the presented data suggests that *P. putida* KT2440 can cope with repeated oxygen starvation at the cost of its energy charge but can partially restore it when oxygen becomes available again without majorly altering its proteome. Further studies on the transcriptome and proteome in combination with the quantification of PHAs need to be conducted to elucidate the intracellular coping mechanisms in more detail.

5 | CONCLUSION

Oxygen starvation zones accompanied by other substrate gradients caused by mixing inhomogeneities are likely to occur in industrial-scale bioreactors. In this study, we demonstrate the ability of *P. putida* KT2440 classified as an obligate aerobic microorganism to

withstand temporary oxygen limitations, even with simultaneous carbon starvation. The growth performance of the wild-type strain is not affected significantly by repeated exposure to oxygen starvation. Remarkably, this was confirmed in different scales and cultivation systems, different cultivation media, as well as different laboratories. Moreover, the rhamnolipid production strain accumulated similar product titers during oxygen oscillation compared to the well-aerated reference process. As we showed that both, growth and production are robust when cells are subjected to temporary oxygen starvation, the suitability of *P. putida* KT2440 for industrial-scale production processes was affirmed.

CONFLICT OF INTERESTS

LMB and TT declare that they are inventors of three related patents. (1) L. M. Blank, F. Rosenau, S. Wilhelm, A. Wittgens, T. Tiso, "Means and methods for rhamnolipid production," HHU Düsseldorf University, TU Dortmund University, 2013 (WO 2013/041670 A1), (2) L. M. Blank, B. Küpper, E. M. del Amor Villa, R. Wichmann, C. Nowacki, "Foam adsorption," TU Dortmund University, 2013 (WO 2013/087674 A1), and (3) L. M. Blank, T. Tiso, A. Germer, "Extracellular production of designer hydroxyalkanoyloxy alkanoic acids with recombinant bacteria," RWTH Aachen University, 2015 (WO2017006252A1). Apart from that, the authors declare that the research was conducted in the absence of any commercial or financial relationships that could be construed as a potential conflict of interest.

AUTHOR CONTRIBUTIONS

MTP and STR batch cultivations, analytics STR cultivations, secondary processing of proteomics data: Philipp Demling. *STR-PFR cultivation*: Andreas Ankenbauer and Philipp Demling. *Analytics STR-PFR cultivations*: Andreas Ankenbauer. *Proteomics measurements and primary processing*: Bianca Klein. *Interpreted results*: Philipp Demling, Andreas Ankenbauer, Bianca Klein, Stephan Noack, Till Tiso, Ralf Takors, and Lars M. Blank. *Drafted the manuscript*: Philipp Demling (all parts despite STR-PFR sections), Andreas Ankenbauer (STR-PFR sections). *Revised and edited the manuscript*: Stephan Noack, Till Tiso, Ralf

Takors, and Lars M. Blank. All authors read, corrected, and commented on the manuscript before publication. All authors approved the final manuscript.

DATA AVAILABILITY STATEMENT

The data that support the findings of this study are available from the corresponding author upon reasonable request.

ORCID

Philipp Demling https://orcid.org/0000-0002-0351-1119
Andreas Ankenbauer https://orcid.org/0000-0002-2843-683X
Stephan Noack http://orcid.org/0000-0001-9784-3626
Till Tiso https://orcid.org/0000-0003-4420-5609
Ralf Takors http://orcid.org/0000-0001-5837-6906
Lars M. Blank https://orcid.org/0000-0003-0961-4976

REFERENCES

Ankenbauer, A., Nitschel, R., Teleki, A., Müller, T., Favilli, L., Blombach, B., & Takors, R. (2021). Micro-aerobic production of isobutanol with engineered *Pseudomonas putida*. *Engineering in Life Sciences*, 21, 1–14. https://doi.org/10.1002/elsc.202000116

Ankenbauer, A., Schäfer, R. A., Viegas, S. C., Pobre, V., Voß, B., Arraiano, C. M., & Takors, R. (2020). *Pseudomonas putida* KT2440 is naturally endowed to withstand industrial-scale stress conditions. *Microbial Biotechnology*, 13(4), 1145–1161. https://doi.org/10.1111/1751-7915.13571

Askitosari, T. D., Berger, C., Tiso, T., Harnisch, F., Blank, L. M., & Rosenbaum, M. A. (2020). Coupling an electroactive *Pseudomonas putida* KT2440 with bioelectrochemical rhamnolipid production. *Microorganisms*, 8(12):1959. https://doi.org/10.3390/microorganisms8121959

Atkinson, D. E. (1968). Energy charge of the adenylate pool as a regulatory parameter. Interaction with feedback modifiers. *Biochemistry*, 7(11), 4030–4034. https://doi.org/10.1021/bi00851a033

Bagdasarian, M., Lurz, R., Rückert, B., Franklin, F., Bagdasarian, M. M., Frey, J., & Timmis, K. N. (1981). Specific-purpose plasmid cloning vectors II. Broad host range, high copy number, RSF 1010-derived vectors, and a host-vector system for gene cloning in *Pseudomonas*. *Gene*, 16(1), 237–247. https://doi.org/10.1016/0378-1119(81)90080-9

Bator, I., Karmainski, T., Tiso, T., & Blank, L. M. (2020). Killing two birds with one stone – Strain engineering facilitates the development of a unique rhamnolipid production process. *Frontiers in Bioengineering and Biotechnology*, 8, 899. https://doi.org/10.3389/fbioe.2020.00899

Bator, I., Wittgens, A., Rosenau, F., Tiso, T., & Blank, L. M. (2020). Comparison of three xylose pathways in *Pseudomonas putida* KT2440 for the synthesis of valuable products. *Frontiers in Bioengineering and Biotechnology*, 7, 480. https://doi.org/10.3389/fbioe.2019.00480

Bednarz, A., Weber, B., & Jupke, A. (2017). Development of a CFD model for the simulation of a novel multiphase counter-current loop reactor. *Chemical Engineering Science*, 161, 350–359. https://doi.org/10.1016/j.ces.2016.12.048

Bellou, S., Makri, A., Triantaphyllidou, I.-E., Papanikolaou, S., & Aggelis, G. (2014). Morphological and metabolic shifts of induced *Yarrowia lipolytica* by alteration of the dissolved oxygen concentration in the growth environment. *Microbiology*, 160(4), 807–817. https://doi.org/10.1099/mic.0.074302-0

Blank, L. M., Narancic, T., Mampel, J., Tiso, T., & O'Connor, K. (2020). Biotechnological upcycling of plastic waste and other

non-conventional feedstocks in a circular economy. *Current Opinion in Biotechnology*, *62*, 212–219. https://doi.org/10.1016/j.copbio.2019.11.011

Chapman, A. G., Fall, L., & Atkinson, D. E. (1971). Adenylate energy charge in *Escherichia coli* during growth and starvation. *Journal of Bacteriology*, *108*, 1072–1086.

Chavarría, M., Nikel, P. I., Pérez-Pantoja, D., & de Lorenzo, V. (2013). The Entner–Doudoroff pathway empowers *Pseudomonas putida* KT2440 with a high tolerance to oxidative stress. *Environmental Microbiology*, *15*(6), 1772–1785. https://doi.org/10.1111/1462-2920.12069

Cserjan-Puschmann, M., Kramer, W., Duerrschmid, E., Striedner, G., & Bayer, K. (1999). Metabolic approaches for the optimisation of recombinant fermentation processes. *Applied Microbiology and Biotechnology*, *53*(1), 43–50. https://doi.org/10.1007/s002530051612

Demling, P., Campenhausen, M., von, Grütering, C., Tiso, T., Jupke, A., & Blank, L. M. (2020). Selection of a recyclable *in situ* liquid-liquid extraction solvent for foam-free synthesis of rhamnolipids in a two-phase fermentation. *Green Chemistry*, *22*, 8495–8510. https://doi.org/10.1039/D0GC02885A

Enfors, S.-O., Jahic, M., Rozkov, A., Xu, B., Hecker, M., Jürgen, B., Krüger, E., Schweder, T., Hamer, G., O'Beirne, D., Noisommit-Rizzi, N., Reuss, M., Boone, L., Hewitt, C., McFarlane, C., Nienow, A., Kovacs, T., Trägårdh, C., Fuchs, L., … Manelius, Å. (2001). Physiological responses to mixing in large scale bioreactors. *Journal of Biotechnology*, *85*(2), 175–185. https://doi.org/10.1016/S0168-1656(00)00365-5

Escobar, S., Rodriguez, A., Gomez, E., Alcon, A., Santos, V. E., & Garcia-Ochoa, F. (2016). Influence of oxygen transfer on *Pseudomonas putida* effects on growth rate and biodesulfurization capacity. *Bioprocess and Biosystems Engineering*, *39*(4), 545–554. https://doi.org/10.1007/s00449-016-1536-6

García-Horsman, J. A., Barquera, B., Rumbley, J., Ma, J., & Gennis, R. B. (1994). The superfamily of heme-copper respiratory oxidases. *Journal of Bacteriology*, *176*(18), 5587–5600. https://doi.org/10.1128/jb.176.18.5587-5600.1994

Haringa, C., Tang, W., Deshmukh, A. T., Xia, J., Reuss, M., Heijnen, J. J., Mudde, R. F., & Noorman, H. J. (2016). Euler-Lagrange computational fluid dynamics for (bio)reactor scale down: An analysis of organism lifelines. *Engineering in Life Sciences*, *16*(7), 652–663. https://doi.org/10.1002/elsc.201600061

Hartmans, S., Smits, J. P., van der Werf, M. J., Volkering, F., & de Bont, J. A. M. (1989). Metabolism of styrene oxide and 2-phenylethanol in the styrene-degrading *Xanthobacter* strain 124X. *Applied and Environmental Microbiology*, *55*(11), 2850–2855.

Hauryliuk Vasili, Atkinson Gemma C., Murakami Katsuhiko S., Tenson Tanel, Gerdes Kenn (2015). Recent functional insights into the role of (p)ppGpp in bacterial physiology. *Nature Reviews Microbiology*, *13*(5), 298–309. http://dx.doi.org/10.1038/nrmicro3448

Heim, S., Ferrer, M., Heuer, H., Regenhardt, D., Nimtz, M., & Timmis, K. N. (2003). Proteome reference map of *Pseudomonas putida* strain KT2440 for genome expression profiling: Distinct responses of KT2440 and *Pseudomonas aeruginosa* strain PAO1 to iron deprivation and a new form of superoxide dismutase. *Environmental Microbiology*, *5*(12), 1257–1269. https://doi.org/10.1111/j.1462-2920.2003.00465.x

Hintermayer, S. B., & Weuster-Botz, D. (2017). Experimental validation of in silico estimated biomass yields of *Pseudomonas putida* KT2440. *Biotechnology Journal*, *12*(6), https://doi.org/10.1002/biot.201600720

John, G. T., Klimant, I., Wittmann, C., & Heinzle, E. (2003). Integrated optical sensing of dissolved oxygen in microtiter plates: A novel tool for microbial cultivation. *Biotechnology and Bioengineering*, *81*(7), 829–836. https://doi.org/10.1002/bit.10534

Kampers, L. F. C., van Heck, R. G. A., Donati, S., Saccenti, E., Volkers, R. J. M., Schaap, P. J., Suarez-Diez, M., Nikel, P. I., & Martins dos Santos, Vitor, A. P. (2019). *In silico*-guided engineering of *Pseudomonas putida* towards growth under micro-oxic conditions. *Microbial Cell Factories*, *18*(1), 179. https://doi.org/10.1186/s12934-019-1227-5

Kampers, L. F. C., Koehorst, J. J., van Heck, R. J. A., Suarez-Diez, M., Stams, A. J. M., & Schaap, P. J. (2021). A metabolic and physiological design study of *Pseudomonas putida* KT2440 capable of anaerobic respiration. *BMC Microbiology*, *21*(1), 9. https://doi.org/10.1186/s12866-020-02058-1

Kampers, L. F. C., Volkers, R. J. M., & Martins dos Santos, V. A. P. (2019). *Pseudomonas putida* KT2440 is HV1 certified, not GRAS. *Microbial Biotechnology*, *12*(5), 845–848. https://doi.org/10.1111/1751-7915.13443

Kar, T., Destain, J., Thonart, P., & Delvigne, F. (2012). Scale-down assessment of the sensitivity of *Yarrowia lipolytica* to oxygen transfer and foam management in bioreactors: Investigation of the underlying physiological mechanisms. *Journal of Industrial Microbiology & Biotechnology*, *39*(2), 337–346. https://doi.org/10.1007/s10295-011-1030-8

Käß, F., Junne, S., Neubauer, P., Wiechert, W., & Oldiges, M. (2014). Process inhomogeneity leads to rapid side product turnover in cultivation of *Corynebacterium glutamicum*. *Microbial Cell Factories*, *13*(1):6. https://doi.org/10.1186/1475-2859-13-6

Kensy, F., Zimmermann, H. F., Knabben, I., Anderlei, T., Trauthwein, H., Dingerdissen, U., & Büchs, J. (2005). Oxygen transfer phenomena in 48-well microtiter plates: Determination by optical monitoring of sulfite oxidation and verification by real-time measurement during microbial growth. *Biotechnology and Bioengineering*, *89*(6), 698–708. https://doi.org/10.1002/bit.20373

Klinke, S., Dauner, M., Scott, G., Kessler, B., & Witholt, B. (2000). Inactivation of isocitrate lyase leads to increased production of medium-chain-length poly(3-hydroxyalkanoates) in *Pseudomonas putida*. *Applied and Environmental Microbiology*, *66*(3), 909–913. https://doi.org/10.1128/aem.66.3.909-913.2000

Kuschel, M., Siebler, F., & Takors, R. (2017). Lagrangian trajectories to predict the formation of population heterogeneity in large-scale bioreactors. *Bioengineering*, *4*(2):27. https://doi.org/10.3390/bioengineering4020027

Kuschel, M., & Takors, R. (2020). Simulated oxygen and glucose gradients as a prerequisite for predicting industrial scale performance *a priori*. *Biotechnology and Bioengineering*, *117*(9), 2760–2770. https://doi.org/10.1002/bit.27457

Lai, B., Yu, S., Bernhardt, P. V., Rabaey, K., Virdis, B., & Krömer, J. O. (2016). Anoxic metabolism and biochemical production in *Pseudomonas putida* F1 driven by a bioelectrochemical system. *Biotechnology for Biofuels*, *9*(1), 39. https://doi.org/10.1186/s13068-016-0452-y

Lange, J., Münch, E., Müller, J., Busche, T., Kalinowski, J., Takors, R., & Blombach, B. (2018). Deciphering the adaptation of *Corynebacterium glutamicum* in transition from aerobiosis via microaerobiosis to anaerobiosis. *Genes*, *9*(6):297. https://doi.org/10.3390/genes9060297

Lara, A. R., Galindo, E., Ramírez, O. T., & Palomares, L. A. (2006). Living with heterogeneities in bioreactors. *Molecular Biotechnology*, *34*(3), 355–381. https://doi.org/10.1385/MB:34:3:355

Lattermann, C., Funke, M., Hansen, S., Diederichs, S., & Büchs, J. (2014). Cross-section perimeter is a suitable parameter to describe the effects of different baffle geometries in shaken microtiter plates. *Journal of Biological Engineering*, *8*(1):18. https://doi.org/10.1186/1754-1611-8-18

Lebrun, G., Xu, F., Le Men, C., Hébrard, G., & Dietrich, N. (2021). Gas–liquid mass transfer around a rising bubble: Combined effect of rheology and surfactant. *Fluids*, *6*(2) https://doi.org/10.3390/fluids6020084

Li, W.-J., Narancic, T., Kenny, S. T., Niehoff, P.-J., O'Connor, K., Blank, L. M., & Wierckx, N. (2020). Unraveling 1,4-butanediol metabolism in Pseudomonas putida KT2440. Frontiers in Microbiology, 11, 382. https://doi.org/10.3389/fmicb.2020.00382

Lieder, S., Jahn, M., Koepff, J., Muller, S., & Takors, R. (2016). Environmental stress speeds up DNA replication in Pseudomonas putida in chemostat cultivations. Biotechnology Journal, 11(1), 155–163. https://doi.org/10.1002/biot.201500059

Limberg, M. H., Joachim, M., Klein, B., Wiechert, W., & Oldiges, M. (2017). pH fluctuations imperil the robustness of C. glutamicum to short term oxygen limitation. Journal of Biotechnology, 259, 248–260. https://doi.org/10.1016/j.jbiotec.2017.08.018

Löffler, M., Simen, J. D., Jäger, G., Schäferhoff, K., Freund, A., & Takors, R. (2016). Engineering E. coli for large-scale production – Strategies considering ATP expenses and transcriptional responses. Metabolic Engineering, 38, 73–85. https://doi.org/10.1016/j.ymben.2016.06.008

Lorantfy, B., Jazini, M., & Herwig, C. (2013). Investigation of the physiological response to oxygen limited process conditions of Pichia pastoris Mut+ strain using a two-compartment scale-down system. Journal of Bioscience and Bioengineering, 116(3), 371–379. https://doi.org/10.1016/j.jbiosc.2013.03.021

Marques, M. P. C., Cabral, J. M. S., & Fernandes, P. (2010). Bioprocess scale-up: Quest for the parameters to be used as criterion to move from microreactors to lab-scale. Journal of Chemical Technology & Biotechnology, 85(9), 1184–1198. https://doi.org/10.1002/jctb.2387

Miller, C. D., Pettee, B., Zhang, C., Pabst, M., McLean, J. E., & Anderson, A. J. (2009). Copper and cadmium: Responses in Pseudomonas putida KT2440. Letters in Applied Microbiology, 49(6), 775–783. https://doi.org/10.1111/j.1472-765X.2009.02741.x

Możejko-Ciesielska, J., & Serafim, L. S. (2019). Proteomic response of Pseudomonas putida KT2440 to dual carbon-phosphorus limitation during mcl-PHAs synthesis. Biomolecules, 9(12), https://doi.org/10.3390/biom9120796

Nadal-Rey, G., McClure, D. D., Kavanagh, J. M., Cornelissen, S., Fletcher, D. F., & Gernaey, K. V. (2020). Understanding gradients in industrial bioreactors. Biotechnology Advances, 46, 107660. https://doi.org/10.1016/j.biotechadv.2020.107660

Nakazawa, T. (2002). Travels of a Pseudomonas, from Japan around the world. Environmental Microbiology, 4(12), 782–786. https://doi.org/10.1046/j.1462-2920.2002.00310.x

Neubauer, P., Haggstrom, L., & Enfors, S. O. (1995). Influence of substrate oscillations on acetate formation and growth yield in Escherichia coli glucose limited fed-batch cultivations. Biotechnology and Bioengineering, 47(2), 139–146. https://doi.org/10.1002/bit.260470204

Neubauer, P., & Junne, S. (2010). Scale-down simulators for metabolic analysis of large-scale bioprocesses. Current Opinion in Biotechnology, 21(1), 114–121. https://doi.org/10.1016/j.copbio.2010.02.001

Nikel, P. I., Fuhrer, T., Chavarría, M., Sánchez-Pascuala, A., Sauer, U., & de Lorenzo, V. (2020). Redox stress reshapes carbon fluxes of Pseudomonas putida for cytosolic glucose oxidation and NADPH generation. bioRxiv, https://doi.org/10.1101/2020.06.13.149542

Nikel, P. I., & de Lorenzo, V. (2013). Engineering an anaerobic metabolic regime in Pseudomonas putida KT2440 for the anoxic biodegradation of 1,3-dichloroprop-1-ene. Metabolic Engineering, 15, 98–112. https://doi.org/10.1016/j.ymben.2012.09.006

Nikel, P. I., & de Lorenzo, V. (2014). Robustness of Pseudomonas putida KT2440 as a host for ethanol biosynthesis. New Biotechnology, 31(6), 562–571. https://doi.org/10.1016/j.nbt.2014.02.006

Nikel, P. I., & de Lorenzo, V. (2018). Pseudomonas putida as a functional chassis for industrial biocatalysis: From native biochemistry to trans-metabolism. Metabolic Engineering, 50, 50142–155. https://doi.org/10.1016/j.ymben.2018.05.005

Nitschel, R., Ankenbauer, A., Welsch, I., Wirth, N. T., Massner, C., Ahmad, N., McColm, S., Borges, F., Fotheringham, I., Takors, R., & Blombach, B. (2020). Engineering Pseudomonas putida KT2440 for the production of isobutanol. Engineering in Life Sciences, 20(5–6), 148–159. https://doi.org/10.1002/elsc.201900151

Obruca, S., Sedlacek, P., Koller, M., Kucera, D., & Pernicova, I. (2018). Involvement of polyhydroxyalkanoates in stress resistance of microbial cells: Biotechnological consequences and applications. Biotechnology Advances, 36(3), 856–870. https://doi.org/10.1016/j.biotechadv.2017.12.006

Olughu, W., Deepika, G., Hewitt, C., & Rielly, C. (2019). Insight into the large-scale upstream fermentation environment using scaled-down models. Journal of Chemical Technology & Biotechnology, 94(3), 647–657. https://doi.org/10.1002/jctb.5804

Ramos, J.-L., Sol Cuenca, M., Molina-Santiago, C., Segura, A., Duque, E., Gomez-Garcia, M. R., Udaondo, Z., & Roca, A. (2015). Mechanisms of solvent resistance mediated by interplay of cellular factors in Pseudomonas putida. FEMS Microbiology Reviews, 39(4), 555–566. https://doi.org/10.1093/femsre/fuv006

Rodriguez, A., Escobar, S., Gomez, E., Santos, V. E., & Garcia-Ochoa, F. (2018). Behavior of several Pseudomonas putida strains growth under different agitation and oxygen supply conditions. Biotechnology Progress, 34(4), 900–909. https://doi.org/10.1002/btpr.2634

Santos, P. M., Benndorf, D., & Sá-Correia, I. (2004). Insights into Pseudomonas putida KT2440 response to phenol-induced stress by quantitative proteomics. Proteomics, 4(9), 2640–2652. https://doi.org/10.1002/pmic.200300793

Schmitz, S., Nies, S., Wierckx, N., Blank, L. M., & Rosenbaum, M. A. (2015). Engineering mediator-based electroactivity in the obligate aerobic bacterium Pseudomonas putida KT2440. Frontiers in Microbiology, 6, 284. https://doi.org/10.3389/fmicb.2015.00284

Simon, O., Klebensberger, J., Mukschel, B., Klaiber, I., Graf, N., Altenbuchner, J., Huber, A., Hauer, B., & Pfannstiel, J. (2015). Analysis of the molecular response of Pseudomonas putida KT2440 to the next-generation biofuel n-butanol. Journal of Proteomics, 122, 11–25. https://doi.org/10.1016/j.jprot.2015.03.022

Sohn, S. B., Kim, T. Y., Park, J. M., & Lee, S. Y. (2010). In silico genome-scale metabolic analysis of Pseudomonas putida KT2440 for polyhydroxyalkanoate synthesis, degradation of aromatics and anaerobic survival. Biotechnology Journal, 5(7), 739–750. https://doi.org/10.1002/biot.201000124

Soini, J., Ukkonen, K., & Neubauer, P. (2008). High cell density media for Escherichia coli are generally designed for aerobic cultivations – Consequences for large-scale bioprocesses and shake flask cultures. Microbial Cell Factories, 7(1):26. https://doi.org/10.1186/1475-2859-7-26

van Sonsbeek, H. M., Beeftink, H. H., & Tramper, J. (1993). Two-liquid-phase bioreactors. Enzyme and Microbial Technology, 15(9), 722–729. https://doi.org/10.1016/0141-0229(93)90001-I

Steen, A., Ütkür, F. Ö., Borrero-de Acuña, J. M., Bunk, B., Roselius, L., Bühler, B., Jahn, D., & Schobert, M. (2013). Construction and characterization of nitrate and nitrite respiring Pseudomonas putida KT2440 strains for anoxic biotechnical applications. Journal of Biotechnology, 163(2), 155–165. https://doi.org/10.1016/j.jbiotec.2012.09.015

Tatusov, R. L., Koonin, E. V., & Lipman, D. J. (1997). A genomic perspective on protein families. Science, 278(5338), 631–637. https://doi.org/10.1126/science.278.5338.631

Thompson, M. G., Incha, M. R., Pearson, A. N., Schmidt, M., Sharpless, W. A., Eiben, C. B., Cruz-Morales, P., Blake-Hedges, J. M., Liu, Y., Adams, C. A., Haushalter, R. W., Krishna, R. N., Lichtner, P., Blank, L. M., Mukhopadhyay, A., Deutschbauer, A. M., Shih, P. M., Keasling, J. D., & Zhou, N. Y. (2020). Fatty acid and alcohol metabolism in Pseudomonas putida: Functional analysis using random barcode transposon sequencing. Applied and Environmental

Microbiology, 86(21):e01665-20. https://doi.org/10.1128/AEM.01665-20

Timoumi, A., Bideaux, C., Guillouet, S. E., Allouche, Y., Molina-Jouve, C., Fillaudeau, L., & Gorret, N. (2017). Influence of oxygen availability on the metabolism and morphology of *Yarrowia lipolytica*: Insights into the impact of glucose levels on dimorphism. *Applied Microbiology and Biotechnology*, 101(19), 7317–7333. https://doi.org/10.1007/s00253-017-8446-7

Tiso, T., Ihling, N., Kubicki, S., Biselli, A., Schonhoff, A., Bator, I., Thies, S., Karmainski, T., Kruth, S., Willenbrink, A.-L., Loeschcke, A., Zapp, P., Jupke, A., Jaeger, K.-E., Büchs, J., & Blank, L. M. (2020). Integration of genetic and process engineering for optimized rhamnolipid production using *Pseudomonas putida*. *Frontiers in Bioengineering and Biotechnology*, 8, 976. https://doi.org/10.3389/fbioe.2020.00976

Tiso, T., Narancic, T., Wei, R., Pollet, E., Beagan, N., Schröder, K., Honak, A., Jiang, M., Kenny, S. T., Wierckx, N., Perrin, R., Avérous, L., Zimmermann, W., O'Connor, K., & Blank, L. M. (2021). Towards bio-upcycling of polyethylene terephthalate. *Metabolic Engineering*, 66, 167–178. https://doi.org/10.1016/j.ymben.2021.03.011

Tiso, T., Sabelhaus, P., Behrens, B., Wittgens, A., Rosenau, F., Hayen, H., & Blank, L. M. (2016). Creating metabolic demand as an engineering strategy in *Pseudomonas putida* – Rhamnolipid synthesis as an example. *Metabolic Engineering Communications*, 3, 234–244. https://doi.org/10.1016/j.meteno.2016.08.002

Tiso, T., Wierckx, N., & Blank, L. M. (2014). Non-pathogenic *Pseudomonas* as platform for industrial biocatalysis. In P. Grunwald (Ed.), *Industrial biocatalysis* (Vol. 1). Jenny Stanford Publishing.

Traxler M. F., Zacharia V. M., Marquardt S., Summers S. M., Nguyen H.-T., Stark S. E., Conway T. (2011). Discretely calibrated regulatory loops controlled by ppGpp partition gene induction across the 'feast to famine' gradient in Escherichia coli. *Molecular Microbiology*, 79(4), 830–845. http://dx.doi.org/10.1111/j.1365-2958.2010.07498.x

Vallon, T., Glemser, M., Malca, S. H., Scheps, D., Schmid, J., Siemann-Herzberg, M., Hauer, B., & Takors, R. (2013). Production of 1-octanol from n-octane by *Pseudomonas putida* KT2440. *Chemie Ingenieur Technik*, 85(6), 841–848. https://doi.org/10.1002/cite.201200178

Vallon, T., Simon, O., Rendgen-Heugle, B., Frana, S., Mückschel, B., Broicher, A., Siemann-Herzberg, M., Pfannenstiel, J., Hauer, B., Huber, A., Breuer, M., & Takors, R. (2015). Applying systems biology tools to study n-butanol degradation in *Pseudomonas putida* KT2440. *Engineering in Life Sciences*, 15(8), 760–771. https://doi.org/10.1002/elsc.201400051

Voges, R., & Noack, S. (2012). Quantification of proteome dynamics in *Corynebacterium glutamicum* by (15)N-labeling and selected reaction monitoring. *Journal of Proteomics*, 75(9), 2660–2669. https://doi.org/10.1016/j.jprot.2012.03.020

Weber, B., Campenhausen, M., von, Maßmann, T., Bednarz, A., & Jupke, A. (2019). CFD based compartment-model for a multiphase loop-reactor. *Chemical Engineering Science: X*, 2, 100010. https://doi.org/10.1016/j.cesx.2019.100010

Wehrmann, M., Elsayed, E. M., Köbbing, S., Bendz, L., Lepak, A., Schwabe, J., Wierckx, N., Bange, G., & Klebensberger, J. (2020). Engineered PQQ-dependent alcohol dehydrogenase for the oxidation of 5-(hydroxymethyl)furoic acid. *ACS Catalysis*, 10(14), 7836–7842. https://doi.org/10.1021/acscatal.0c01789

Weimer, A., Kohlstedt, M., Volke, D. C., Nikel, P. I., & Wittmann, C. (2020). Industrial biotechnology of *Pseudomonas putida*: Advances and prospects. *Applied Microbiology and Biotechnology*, 104(18), 7745–7766. https://doi.org/10.1007/s00253-020-10811-9

Wierckx, N. J. P., Ballerstedt, H., Bont, J. A. M., & de, Wery, J. (2005). Engineering of solvent-tolerant *Pseudomonas putida* S12 for bioproduction of phenol from glucose. *Applied and Environmental Microbiology*, 71(12), 8221–8227. https://doi.org/10.1128/AEM.71.12.8221-8227.2005

Yu, S., Lai, B., Plan, M. R., Hodson, M. P., Lestari, E. A., Song, H., & Krömer, J. O. (2018). Improved performance of *Pseudomonas putida* in a bioelectrochemical system through overexpression of periplasmic glucose dehydrogenase. *Biotechnology and Bioengineering*, 115(1), 145–155. https://doi.org/10.1002/bit.26433

SUPPORTING INFORMATION

Additional Supporting Information may be found online in the supporting information tab for this article.

3.4. P-IV: ENGINEERING *PSEUDOMONAS PUTIDA* KT2440 FOR THE PRODUCTION OF ISOBUTANOL

P. putida was engineered from an isobutanol degrader to an isobutanol producer by overexpression of the Ehrlich pathway. Different alcohol dehydrogenase enzymes were compared for effective isobutanol biosynthesis from glucose. Isobutanol is an important bulk chemical in the rubber and coatings industry and can be used as a fuel additive. A yield of 22 mg isobutanol per g glucose was achieved in shake flask experiments which is the highest reported yield of isobutanol produced by *P. putida.*

R. Nitschel is the main author of this manuscript and performed the experiments and construction of the strains and plasmids with assistance of I. Welsch and N. T. Wirth. C. Massner contributed with plasmid construction and F. Borges added ideas for decarboxylase enzymes. A. Ankenbauer supported with metabolite analysis, assisted with ideas for micro-aerobic experiments and proofread the manuscript. N. Ahmad and S. McColm constructed the pSEVA-based plasmids under supervision of I. Fotheringham. R. Takors supervised the work and proofread the manuscript. B. Blombach (corresponding author) supervised this study and edited the manuscript.

RESEARCH ARTICLE

Engineering *Pseudomonas putida* KT2440 for the production of isobutanol

Robert Nitschel[1] | **Andreas Ankenbauer[1]** | **Ilona Welsch[1]** | **Nicolas T. Wirth[1]** | **Christoph Massner[1]** | **Naveed Ahmad[2]** | **Stephen McColm[2]** | **Frédéric Borges[3]** | **Ian Fotheringham[2]** | **Ralf Takors[1]** | **Bastian Blombach[1,4]** (iD)

[1]Institute of Biochemical Engineering, University of Stuttgart, Stuttgart, Germany

[2]Ingenza Ltd., Roslin Innovation Centre, Charnock Bradley Building, Easter Bush Campus, Roslin, UK

[3]Laboratoire d'Ingénierie des Biomolécules (LIBio), Université de Lorraine, Nancy, France

[4]Microbial Biotechnology, Campus Straubing for Biotechnology and Sustainability, Technical University of Munich, Straubing, Germany

Correspondence
Bastian Blombach, Microbial Biotechnology, Technical University of Munich, Schulgasse 22, 94315 Straubing, Germany
Email: bastian.blombach@tum.de

Abstract

We engineered *P. putida* for the production of isobutanol from glucose by preventing product and precursor degradation, inactivation of the soluble transhydrogenase SthA, overexpression of the native *ilvC* and *ilvD* genes, and implementation of the feedback-resistant acetolactate synthase AlsS from *Bacillus subtilis*, ketoacid decarboxylase KivD from *Lactococcus lactis*, and aldehyde dehydrogenase YqhD from *Escherichia coli*. The resulting strain *P. putida* Iso2 produced isobutanol with a substrate specific product yield ($Y_{Iso/S}$) of 22 ± 2 mg per gram of glucose under aerobic conditions. Furthermore, we identified the ketoacid decarboxylase from *Carnobacterium maltaromaticum* to be a suitable alternative for isobutanol production, since replacement of *kivD* from *L. lactis* in *P. putida* Iso2 by the variant from *C. maltaromaticum* yielded an identical $Y_{Iso/S}$. Although *P. putida* is regarded as obligate aerobic, we show that under oxygen deprivation conditions this bacterium does not grow, remains metabolically active, and that engineered producer strains secreted isobutanol also under the non-growing conditions.

KEYWORDS

isobutanol, ketoacid decarboxylase, metabolic engineering, microaerobic, *Pseudomonas putida*

1 | INTRODUCTION

Biofuel production from renewable feed stocks is of special importance because of the finite nature of the currently used crude oil derivatives and growing concerns about climate change [1]. Isobutanol is an attractive alternative to the employed fossil fuels. It has several advantages such as a higher energy density, compatibility with existing engines, lower vapor pressure and volatility, as well as a lower corrosivity compared to bio-ethanol [2,3]. Furthermore, isobutanol is used in the chemical industry and can be used to produce the gaseous alkene precursor isobutene [4].

Isobutanol can be synthesized via the branched-chain amino acid biosynthesis and the so-called Ehrlich pathway to convert pyruvate to isobutanol (Figure 1). The first step in this route is the conversion of two pyruvate molecules to

2-acetolactate catalyzed by the acetolactate synthase (AlsS), which is usually feedback inhibited by the branched-chain amino acids L-valine, L-leucine, and L-isoleucine. However, AlsS from *Bacillus subtilis* has been shown to be feedback-resistant and therefore has been applied for isobutanol production in several studies [5,6]. Then, 2-acetolactate is reduced to 2,3-dihydroxyisovalerate and subsequently converted to 2-ketoisovalerate (2-KIV) by the ketoacid reductoisomerase IlvC and dihydroxyacid dehydratase IlvD, respectively. Finally, isobutanol is synthesized from 2-KIV in two more reaction steps of the Ehrlich pathway. The decarboxylation of 2-KIV to isobutyraldehyde is catalyzed by ketoacid decarboxylases (KDCs) that are not widespread in nature. Especially KivD from *Lactococcus lactis* has been proved as an efficient variant in, e.g. *E. coli* and *C. glutamicum* [5,7]. The last step from isobutyraldehyde to isobutanol requires an aldehyde reductase or alcohol dehydrogenase. A number of NADH and NADPH dependent enzymes are available that catalyze this reaction [8].

Several microorganisms have been engineered for isobutanol production such as *E. coli*, *C. glutamicum*, *B. subtilis*, and yeast such as *Saccharomyces cerevisiae* [5,7,9,10]. Although highly efficient *E. coli* and *C. glutamicum* strains have been constructed [6,7], the relatively low tolerance of most microbial systems against isobutanol hampers commercialization of isobutanol production processes. In contrast, pseudomonads have an intrinsic tolerance against organic compounds and solvents [11,12] making them promising candidates for isobutanol production.

Among them, *Pseudomonas putida* is a Gram-negative, saprophytic soil bacterium with a genome size of 6.18 Mbp [13]. It has been reported to promote plant growth, prevent plant diseases, and can efficiently remove organic soil pollutants and environmental contaminants [14]. *P. putida* features a versatile metabolism using the Entner–Doudoroff pathway for glucose catabolism, shows resistance against oxidative stress conditions, and genetic engineering tools are readily available [15–17]. The carbohydrate substrate spectrum is limited and confined to hexoses [18], however, *P. putida* has been recently engineered to concomitantly consume xylose, cellobiose, and glucose, which are the basic building blocks of the abundant polysaccharides cellulose and hemicellulose [19]. As a result of these achievements, *P. putida* has emerged as a promising candidate for industrial biotechnology [20,21]. Recent works have engineered this bacterium for the production of polyhydroxyalkanoates, the nylon precursor *cis,cis*-muconic acid [22] and aromatic compounds like *p*-coumaric acid or *trans*-cinnamate [23,24]. *P. taiwanensis* VLB120 has been applied for the production of phenol [25,26].

In this study, we engineered *P. putida* for the production of isobutanol from glucose by preventing product and precursor degradation and increasing the flux from pyruvate towards

PRACTICAL APPLICATION

The relatively low tolerance of most microbial systems against isobutanol hampers commercialization of isobutanol production processes. In contrast, pseudomonads have an intrinsic tolerance against organic compounds and solvents making them promising candidates for isobutanol production. Therefore, we engineered *Pseudomonas putida* KT2440 for the production of this alcohol by preventing product and precursor degradation and increasing the flux from pyruvate toward isobutanol. The achieved overall isobutanol yield is significantly higher compared to other engineered *P. putida* strains; however, rather low compared to tailored *E. coli* and *C. glutamicum* strains. Therefore, this study paths the way to construct more efficient *P. putida* strains for isobutanol production in future studies.

isobutanol. We identified KivD from *Carnobacterium maltaromaticum* as a suitable alternative to KivD from *L. lactis* to drive the decarboxylation of 2-ketoisovalerate and finally we showed that isobutanol production can also be achieved under oxygen deprivation conditions with this obligate aerobic bacterium.

2 | MATERIALS AND METHODS

2.1 | Bacterial strains and plasmids

Bacterial strains, their respective genotype, plasmids, and oligonucleotides used in this study are listed in Table 1.

2.2 | Media and culture conditions

E. coli DH5α was grown aerobically in Lysogeny broth (LB) complex medium containing 10 g/L tryptone, 5 g/L yeast extract, and 10 g/L NaCl [34] at 37ºC as 5 mL cultures in glass test tubes on a rotary shaker at 120 rpm (Infors AG, Bottmingen, Switzerland). *C. maltaromaticum* and *L. lactis* were grown in brain–heart infusion (BHI) broth (Carl Roth GmbH & Co. KG, Karlsruhe, Germany) at 30°C on a rotary shaker at 120 rpm. For longtime storage, *P. putida* was kept as 30% (*w/v*) glycerol stock at −70°C and was streaked out for cultivation on LB solid medium with 15 g/L agar. The first preculture of *P. putida* was prepared by inoculation of 5 mL LB medium in a test tube with a single colony. The culture was cultivated at 30°C on a rotary shaker (Edmund Bühler GmbH, Bodelshausen, Germany) at 175 rpm overnight and used to inoculate, a second overnight preculture to an optical density at 600 nm (OD$_{600}$) of 0.01–0.02 in 50 mL DeBont minimal medium (pH 7) [35], which was supplemented with
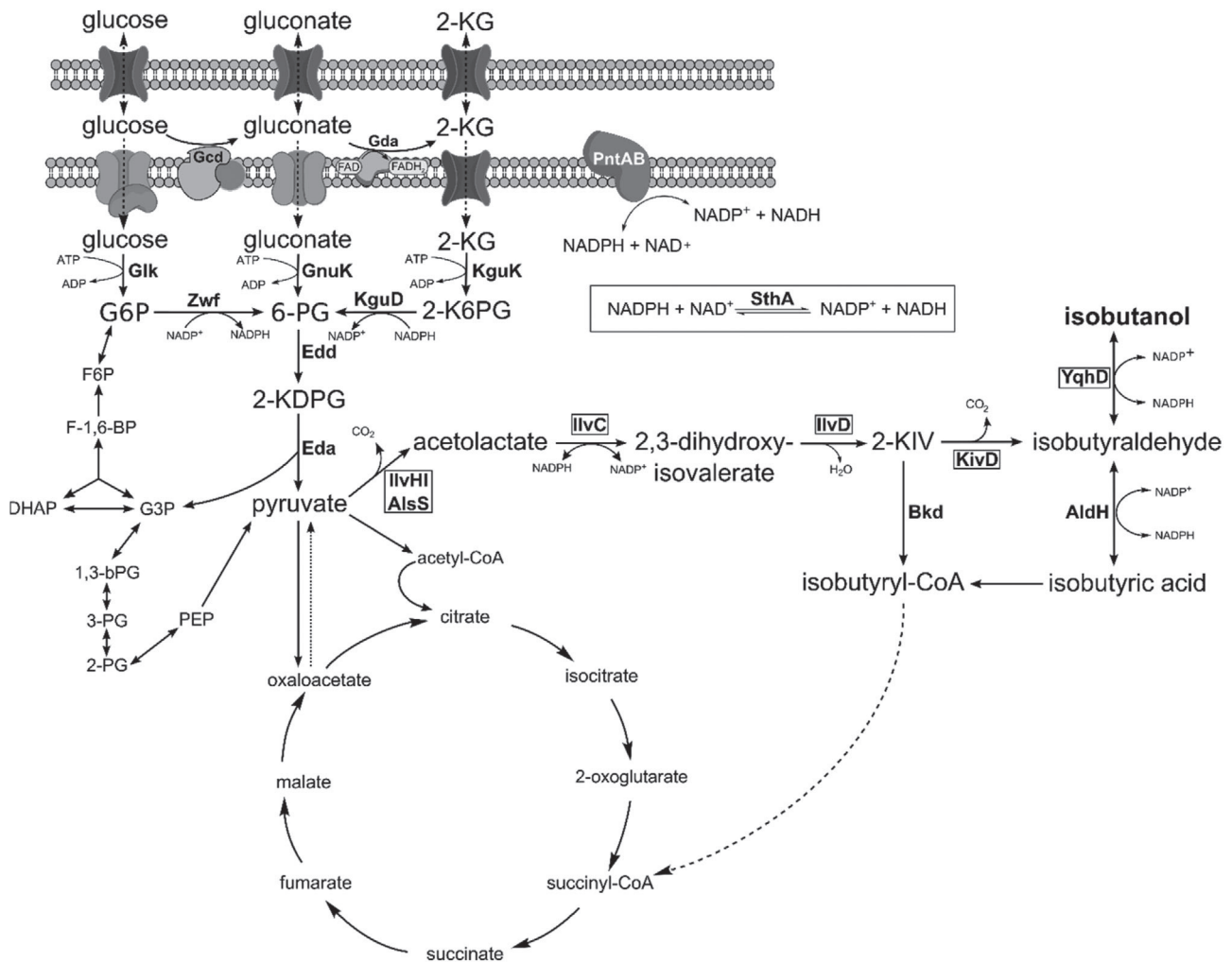
FIGURE 1 The central metabolism of *P. putida* KT2440 with the Ehrlich pathway. Abbreviations (coding genes are given in brackets): G6P: glucose-6-phosphate 2-KG: 2-ketogluconate, 2-K6PG: 2-keto-6-phosphogluconate, 6-PG: 6-phosphogluconate, 2-KDPG: 2-keto-3-deoxy-6-phosphogluconate, G3P: glyceraldehyde-3-phosphate, 1,3-bPG: 1,3-bisphosphoglycerate, 3-PG: 3-phosphoglycerate, 2-PG: 2-phosphoglycerate, PEP: phosphoenolpyruvate, DHAP: dihydroxyacetone-phosphate, F-1,6-bP: fructose-1,6-bisphosphate, F6P: fructose-6-phosphate, CoA: co-enzyme A, Gcd: glucose dehydrogenase (*gcd*), *gad*: gluconate 2-dehydrogenase (*gad*), PQQ: pyrroloquinoline quinone, Glk: glucokinase (*glk*), Zwf: glucose-6-phosphate 1-dehydrogenase (*zwf-1, zwf-2, zwf-3*), GnuK: gluconate kinase (*gnuK*), KguD: 2-6-phosphoketogluconate reductase (*kguD*), KguK: 2-ketogluconate kinase (*kguK*), Edd: 6-phosphogluconate dehydratase (*edd*), Eda: 2-keto-3-deoxy-6-phosphogluconate aldolase (*eda*), IlvHI/AlsS: acetolactacte synthase (*ilvHI/alsS*), IlvC: ketolacid reductoisomerase (*ilvC*), IlvD: dihydroxyacid dehydratase (*ilvD*), KivD: ketoacid decarboxylase (*kivD*), Bkd: branched-chain ketoacid dehydrogenase complex (*bkd*), Yqhd: aldehyde reductase (*yqhD*), AldH: aldehdye dehydyrogenases, PntAB: pyridine nucleotide transhydrogenase (membrane bound) (*pntAB*), SthA: pyridine nucleotide transhydrogenase (soluble) (*sthA*)

5.4 g/L glucose and 0.5 g/L yeast extract. Cells from the second preculture were harvested by centrifugation ($4500 \times g$, 15 min, 4°C), resuspended in DeBont medium, and used to inoculate 50 mL DeBont medium, to an OD_{600} of about 0.1–0.2. The main culture was supplemented with 5.4 g/L glucose, 0.5 g/L isobutanol, or 2.9 g/L 2-ketoisovalerate, respectively. The second pre- and main cultures were performed in 500 mL baffled Erlenmeyer flasks filled with 50 mL medium on a rotary shaker at 175 rpm at 30°C. Micro-aerobic shaking flask cultivations were carried out in sealed 100 mL Müller-Krempel bottles as 25 mL cultures that

were inoculated to an OD_{600} of 15–20. To obtain sufficient biomass, the second preculture was performed in 100 mL LB medium in a 500 mL baffled Erlenmeyer flask that was cultivated on a rotary shaker (175 rpm) overnight at 30°C. Cells from the second preculture were harvested by centrifugation ($4500 \times g$, 15 min, 4°C) and resuspended in 25 mL DeBont minimal medium (pH 7) supplemented with 5.4 g/L glucose and 15 g/L 3-morpholino-propanesulfonic acid. To induce plasmid-based gene expression, 0.2% (*w/v*) L-arabinose was supplemented. For plasmid-bearing strains, 50 µg/mL kanamycin or 50 µg/mL apramycin were added to the medium.

TABLE 1 Overview of strains, plasmids and oligonucleotides used in this study

Strain, plasmid or oligonucleotide	Relevant characteristic(s) or sequence (5′ → 3′)	Source, reference or purpose
Strains		
Pseudomonas putida KT2440	Wild type strain, DSM-6125, ATCC47054	[27]
Carnobacterium maltaromaticum LMA28		[28]
Lactococcus lactis subsp. *cremoris* MG1363		[29]
Corynebacterium glutamicum	Wild type strain ATCC13032	American type culture collection
P. putida GN346	*P. putida* KT2440 Δ*upp*, Δ*pedE*, Δ*pedI*, Δ*pedH*, Δ*aldB-I*	[30]
P. putida EP1	*P. putida* GN346 Δ*bkdAA*	This work
P. putida EP2	*P. putida* EP1 Δ*sthA*	This work
P. putida EP3	*P. putida* EP2 Δ*gcd*	This work
P. putida Iso1	*P. putida* EP1 + pIP02	This work
P. putida Iso2	*P. putida* EP2 + pIP02	This work
P. putida Iso3	*P. putida* EP2 + pIP03	This work
P. putida Iso4	*P. putida* EP2 + pIP04	This work
P. putida Iso5	*P. putida* EP3 + pIP02	This work
P. putida Iso6	*P. putida* EP2 + pIP05	This work
Plasmids		
pBB1	pACYC184/pBL1 derivative, chloramphenicol resistance, P_tac promoter and *trpA* terminator	[31]
pSA55	Expression plasmid for *adh2* of *S. cerevisae* and *kivD* of *L. lactis*	[5]
pBB1 *yqhD*	pBB1 P_tac *yqhD*	This work
pBB1 *kivD yqhD*	pBB1 P_tac *kivD yqhD*	This work
pNG413.1	pBBR1MCS2 derivative, apramycin resistance, *araC*, P_BAD, *lacZ*	[32]
pSEVA231	pBBR1 derivative, kanamycin resistance, mobilizable (*oriT*)	[33]
pIP01	pSEVA231P_tac *kivD yqhD*	This work
pIP02	pNG413 *araC* P_BAD *kivD yqhD alsS ilvC ilvD*	This work
pIP03	pIP02, *yqhD* was changed for *adhA* from *L. lactis*	This work
pIP04	pIP02, *yqhD* was changed for *adhA* from *C. glutamicum*	This work
pIP05	pIP02, *kivD* was changed for *kdcA* from *C. maltaromaticum*	This work
pEMP04	pSEVA231 P_tac *kivD yqhD alsS ilvC ilvD*	Ingenza Ltd.
pEMP012	pEMP04, *yqhD* was changed for *adhA* from *L. lactis*	This work
pEMP013	pEMP04, *yqhD* was changed for *adhA* from *C. glutamicum*	This work
pEMP014	pEMP04, *kivD* was changed for kdcA from *C. maltaromaticum*	This work
Oligonucleotide		
yqhd1	AACTGCAGAACCAATGCATTGGAGGAGACACAACA TGAACAACTTTAATCTGCACACCCCAACC	Construction of pBB1yqhd, PstI site underlined
yqhd2	CCGCTCGAGAAAGCTTAGCGGGCGGCTT CGTATATACG	Construction of pBB1yqhd, XhoI site underlined
kivd1	TCCCCCCGGGAGGAGACACAACATGTATACAGTAGGAG ATTACCTAT	Construction of pBB1 kivd yqhd, XmaI site underlined
kivd2	CCAATGCATTGGTTCTGCAGTTTTATGATTTATTTTGTTC AGCAAAT	Construction of pBB1 kivd yqhd, PstI site underlined
bkdaa1	CTGGATCCCATTCAGACCTCCATGACC	Deletion of *bkdAA*
bkdaa2	CGGCCGCTTCAGAGCTCACATGAGATGAACGA CCACAAC	Deletion of *bkdAA*
bkdaa3	TGTTGTGGTCGTTCATCTCATGTGAGCTCTG AAGCGGC	Deletion of *bkdAA*

(Continues)

TABLE 1 (Continued)

Strain, plasmid or oligonucleotide	Relevant characteristic(s) or sequence (5′ → 3′)	Source, reference or purpose
bkdaa4	GCTTGTCGACCCGTCGTCACTGCCGTAG	Deletion of *bkdAA*
bkdaagc1	GTACCGACGATGCCGCT	Verification of *bkdAA* deletion
bkdaagc2	GCCGTGCCACTAAGATGTAG	Verification of *bkdAA* deletion
stha1	GCCGCTTTGGTCCCGGATCCACAGCATCCAGTACGT CCGC	Deletion of *sthA*
stha2	GTTGAAATCGGTCTCTCCGACCTGAACGCCGCGCACA TTAAC	Deletion of *sthA*
stha3	GTTAATGTGCGCGGCGTTCAGGTCGGAGAGACCGATTT CAAC	Deletion of *sthA*
stha4	TTGCATGCCTGCAGGTCGACTGGTTGGGCAAACCCTGC TTGG	Deletion of *sthA*
sthagc1	ATGGCTATTCGACGCTGCTG	Verification of *sthA* deletion
sthagc2	ACTATGGCTGCGAACTGCTG	Verification of *sthA* deletion
gcd1	GCCGCTTTGGTCCCGGATCCTGACCTTGAGTTGTTCC TTG	Deletion of *gcd*
gcd2	GACCTGACGGAGAACCTACATTAGCCGAGT AAGCGACAC	Deletion of *gcd*
gcd3	GTGTCGCTTACTCGGCTAATGTAGGTTCTCCGTCA GGTC	Deletion of *gcd*
gcd4	TTGCATGCCTGCAGGTCGACGACAACATCAGCAACG ACC	Deletion of *gcd*
gcdgc1	GGGATGGGTTTCAATGGTTC	Verification of *gcd* deletion
gcdgc2	GGCACAAGATGTTCTCAAGG	Verification of *gcd* deletion
png1	AGCTCTAAGGAGGTTATAAAAACATATGTATACAGTAGG AGATTACC	Construction of pIP02, pIP03, pIP04 and pIP05
png2	GAGAATAGGAACTTCGAACTGCAGGTCGACTCAGAGG CCTTCCAGC	Construction of pIP02, pIP03 and pIP04
png3	AGCTCTAAGGAGGTTATAAAAACATATGTACACTGTT GGAAATTATTTGTTA	Construction of pIP05
pbb1	TCGG<u>AGCTC</u>CGCGAATTGCAAGCTGATCCG	Construction of pIP01, SacI site underlined
pbb2	ATC<u>GGATCC</u>CTTAGCGGGCGGCTTCGTAT	Construction of pIP01, BamHI site underlined
kdca1	TTGCTAAACAAAATTCATAAAACTGCAGAACCAATGC	Amplification of *kdcA* gene
kdca2	AATGCATTGGTTCTGCAGTTTTATGAATTTTGTTTAGC AAAGACTTTC	Amplification of *kdcA* gene
p41	TTGCTAAACAAAATTCATAAAACTGCAGAACCAATG CATTG	Construction of pEMP014
p42	TAATTTCCAACAGTGTACATGTTGTGTCTCCTCCCGG	Construction of pEMP014
p43	TCATTGATTTTACTAAATAAGCCAGGAGGACAGCTAT	Construction of pEMP012
p44	CGTACTACTGCTGCTTTCATGTTGTGTCTCCTCCAATGC	Construction of pEMP012
p45	GTGTGGCGATTCGTTTCTAAGCCAGGAGGACAGCTA TGAC	Construction of pEMP013
p46	TGGGGTGCAGCAGTGGTCATGTTGTGTCTCCTCCAA TGCATTG	Construction of pEMP013
adha1	GCATTGGAGGAGACACAACATGAAAGCAGCAGTA GTACG	Amplification of *adhA* gene from *L. lactis*
adha2	GTCATAGCTGTCCTCCTGGCTTATTTAGTAAAATC AATGACCATCC	Amplification of *adhA* gene from *L. lactis glutamicum*
adha3	TGCATTGGAGGAGACACAACATGACCACTGCTGCACC	Amplification of *adhA* gene from *C. glutamicum*
adha4	GTCATAGCTGTCCTCCTGGCTTAGAAACGAATCG CCACACG	Amplification of *adhA* gene from *C. glutamicum*

(Continues)

TABLE 1 (Continued)

Strain, plasmid or oligonucleotide	Relevant characteristic(s) or sequence (5′ → 3′)	Source, reference or purpose
alss1	GAGGAAAGCGGCCGCGCTCTTCGGGGCGGAGCTTGTTG	Construction of pEMP04, NotI site underlined
alss2	TTAGATCTCGAGGCTCTTCGGGCCTAGAGAGCTTTCGTTTTCATG	Construction of pEMP04, XhoI site underlined
ilvc1	GAGGAAGCGGCCGCGCTCTTCGAAGAAAGTCGCCATCATC	Construction of pEMP04, NotI site underlined
ilvc2	TTAGATCTCGAGGCTCTTCGGGCTTAGTTCTTGGTCTTGTCGAC	Construction of pEMP04, XhoI site underlined,
ilvd1	GAGGAAGCGGCCGCGCTCTTCGCGGCGCCCGTG	Construction of pEMP04, NotI site underlined
ilvd2	TTAGATCTCGAGGCTCTTCGGGCTCAGAGGCCTTCCAG	Construction of pEMP04, XhoI site underlined
pip011	GAGGAAGCGGCCGCGCTCTTCGCGTGACTGGGAAAACCCTGGCGACTAGTCTTGGACTC	Construction of pEMP04, NotI site underlined
pip012	TTAGATCTCGAGGCTCTTCGGGCTTAGCGGGCGGCTTCGTATATACGGCGGCTGA	Construction of pEMP04, XhoI site underlined

2.3 | Recombinant DNA work

Standardized cloning procedures such as PCR and DNA restrictions were carried out according to Sambrook and Russell, 2001. Plasmids were isolated from 5 mL liquid cultures using the E.Z.N.A.® Plasmid Mini Kit (Omega Bio-tek, Inc., Norcross, USA) following manufacturer's instructions. PCR fragments were purified with the NucleoSpin® Gel and PCR Clean-up Kit (Macherey-Nagel GmbH & Co. KG, Düren, Germany) according to the manufacturer's instructions. Chromosomal DNA of *E. coli* MG1655, *P. putida, C. maltaromaticum*, and *L. lactis* was isolated using the Nucleospin® Microbial DNA Kit (Macherey-Nagel GmbH & Co. KG, Düren, Germany) following the protocol of the manufacturer. Electrocompetent cells were prepared for *E. coli* and *P. putida* as described previously [53,54]. *E. coli* DH5α and *P. putida* strains were electroporated with an Eporator (Eppendorf AG, Hamburg, Germany) at 2.5 kV with 600 Ω resistance. All enzymes for recombinant DNA work were obtained from Thermo Fisher Scientific Inc. (Darmstadt, Germany) and oligonucleotides were synthesized by biomers.net GmbH (Ulm, Germany, listed in Table 3).

2.4 | Plasmid construction

yqhD was amplified from genomic DNA of *E. coli* MG1655 using the primers yqhd1/yhqd2, digested with PstI/XhoI and ligated into PstI/XhoI-digested pBB1 yielding pBB1 yqhD. *kivD* was subsequently added before *yqhD*, amplified from pSA55 with the primer pair kivd1/kivd2, digested with PstI/XmaI, and ligated into PstI/XmaI-digested pBB1

yqhd creating plasmid pBB1 kivD yqhD. P$_{tac}$, *kivD*, and *yqhD* were amplified from plasmid pBB1 kivD yqhD using the primers pbb1/pbb2. The resulting PCR fragment was digested with BamHI/SacI and subsequently ligated into BamHI/SacI-digested pSEVA231 to create plasmid pIP01. Plasmid pEMP04 was constructed using the inABLE DNA assembly method from Ingenza Ltd. The *B. subtilis alsS* and *P. putida ilvC* and *ilvD* genes were amplified using primer pairs alss1/alss2, ilvc1/ilvc2, and ilvd1/ilvd2, respectively. Additionally, a 5′ truncated version of pIP01 was amplified using primer pair pip011/pip012. The PCR products were digested using SapI and annealed oligonucleotides were ligated at each terminus. Ligation of the oligonucleotides results in the generation of 5′ and 3′ 16 nt single stranded overhangs that are complementary between fragments resulting in the DNA assembling in the predefined order. The genes of pEMP04 were amplified using the primers png1/png2 and cloned by Gibson Assembly [36] into NdeI/SalI-digested pNG413.1 yielding plasmid pIP02. *kdcA* from *C. maltaromaticum* LMA28, *adhA* from *L. lactis* MG1363, and *adhA* from *C. glutamicum* was amplified using the respective genomic DNA with the primers kdca1/kdca2, adha1/adha2, and adha3/adha4 and cloned together via Gibson Assembly with a PCR fragment from pEMP04 that was amplified with the primers p41/p42, p43/p44, or p45/p46 to construct plasmid pEMP014, pEMP012, and pEMP013. To exchange P$_{tac}$ with *araC* P$_{BAD}$ the genes of pEMP012, pEMP013 and pEMP014 were amplified using the primers png1/png2 for pEMP012/013 and png3/png2 for pEMP014 and cloned by Gibson Assembly into NdeI/SalI-digested pNG413.1, constructing the plasmids pIP03, pIP04, and pIP05.

2.5 | Determination of μ and $Y_{X/S}$

Growth rates were determined by linear regression of $\ln(OD_{600})$ plotted against time (in hours) during the exponential growth phase. Biomass yields $Y_{X/S}$ (g/g) were calculated by linear regression of the biomass concentration c_x (g/L) plotted against the respective glucose concentration (g/L) during the exponential growth phase.

2.6 | Construction of *P. putida* deletion mutants

Chromosomal deletions in *P. putida* were carried out using the 5-fluorouracil (5-FU)/*upp* counterselection system [37]. Deletions of the *bkdAA* gene (encoding the α-subunit of the ketoacid dehydrogenase complex), the *sthA* gene (encoding soluble transhydrogenase) and the *gcd* gene (encoding glucose dehydrogenase) were performed using the integration vector pJOE6261.2. The flanking regions (about 500 bp) of each gene were amplified by PCR from chromosomal DNA of *P. putida* using the primer pairs bkdaa1/bkdaa2 and bkdaa3/bkdaa4, stha1/stha2, and stha3/stha4, gcd1/gcd2 and gcd3/gcd4. The two respective PCR fragments were purified and cloned into SalI/BamHI-restricted pJOE6261.2 by Gibson Assembly. Finally, the assembly mix was used to transform *P. putida* by electroporation. The first selection was carried out on LB agar with 50 μg/L kanamycin and a kanamycin-resistant clone was afterward grown in liquid LB medium for 24 h. The second recombination event was induced by plating cells on LB agar with 50 μg/L 5-FU. Deletion mutants were identified by colony PCR using the primer pairs bkdaagc1/bkdaagc2, sthagc1/sthagc2, and gcdgc1/gcdgc2, respectively.

2.7 | Analytics

Biomass formation was measured by determination of the OD_{600} (Ultrospec 10, GE Healthcare, USA) at specific time points. The cell dry weight (g_{CDW}/L) was correlated to the OD_{600} in several independent cultivations with a correlation factor of 0.346 g_{CDW}/L per OD (data not shown). Shaking flasks were sampled directly in the incubator using an injection syringe (100 Sterican®, 0.80×120 mm, B.Braun, Melsungen, Germany). For the determination of isobutanol, 2-KIV, 2-ketogluconate (2-KG), and glucose concentrations, 2 mL of the main culture was harvested by centrifugation ($12\,100 \times g$, 5 min, room temperature (RT)) and the supernatant was analyzed via HPLC. Glucose concentrations were measured enzymatically with a test kit from r-biopharm (r-biopharm AG, Darmstadt, Germany).

2.8 | HPLC metabolite quantification

Isobutanol, 2-KIV and 2-KG were measured with a Agilent 1200 series HPLC system equipped with a Rezex ROA organic acid H (8%) column (300 by 7.8 mm, 8 μm; Phenomenex) protected by a Phenomenex guard column carbo-H (4 by 3.0 mm inside diameter) [38]. Samples and standards were treated with a phosphate precipitation protocol before HPLC measurements. More precisely, 500 μL of sample volume was mixed with 45 μL 4 M NH_3 and 50 μL 1.2 M $MgSO_4$ followed by 5 min incubation at RT and centrifugation for 5 min at $7000 \times g$. Pellets were discarded and the supernatant was mixed with 500 μL 0.1 M H_2SO_4, incubated for 15 min at RT, and centrifuged for 15 min at $7000 \times g$. The resulting supernatant was used for HPLC injection with an injection volume of 10 μL. Separation was carried out under isocratic conditions at 50°C column temperature for 60 min with 5 mM H_2SO_4 as the mobile phase at a constant flow rate of 0.4 mL/min. Detection of isobutanol, 2-KIV, and 2-KG was achieved with a refractive index detector at 32°C. Quantification of all analytes was done with a 7-point calibration curve for each component as an external reference standard.

3 | RESULTS

3.1 | Preventing product and precursor degradation

Pseudomonads are well-known for their ability to degrade a variety of organic substances to utilize them as carbon and energy sources [21]. Since the genomic repertoire provides annotated routes for the degradation of isobutanol and 2-ketoisovalerate (Figure 1), we initially characterized growth on both compounds (Figure 2). *P. putida* showed exponential growth on isobutanol with a μ of 0.27 ± 0.01 h^{-1} as well as on 2-KIV with a μ of 0.33 ± 0.01 h^{-1} that is 52% of the growth rate on glucose (Figure 2A,B). Recently, several enzymes involved in *n*-butanol degradation were identified [39] and Simon et al. [30] constructed *P. putida* Δupp $\Delta pedE$ $\Delta pedI$ $\Delta pedH$ $\Delta aldB-I$ (*P. putida* GN346) to inactivate two alcohol dehdydrogenases (PedE, PedH) and two aldehyde dehydrogenases (PedI, AldB-I) and showed that the introduced deletions prevented *n*-butanol consumption. Accordingly, *P. putida* GN346 was unable to utilize isobutanol as sole carbon and energy source (Figure 2A).

P. putida possesses a branched chain ketoacid dehydrogenase (BCKDH) complex that converts 2-ketoacids to the respective decarboxylated CoA-derivatives [40,41] which are, after further conversion steps, funneled into the TCA cycle. To prevent the consumption of the precursor 2-KIV, we inactivated the α-subunit of the BCKDH by deletion of the *bkdAA* gene in *P. putida* GN346. In contrast to the wild-type, the resulting strain *P. putida* EP1 was unable to grow on 2-KIV as carbon source (Fig. 2B), and therefore was used as basis for further strain engineering.
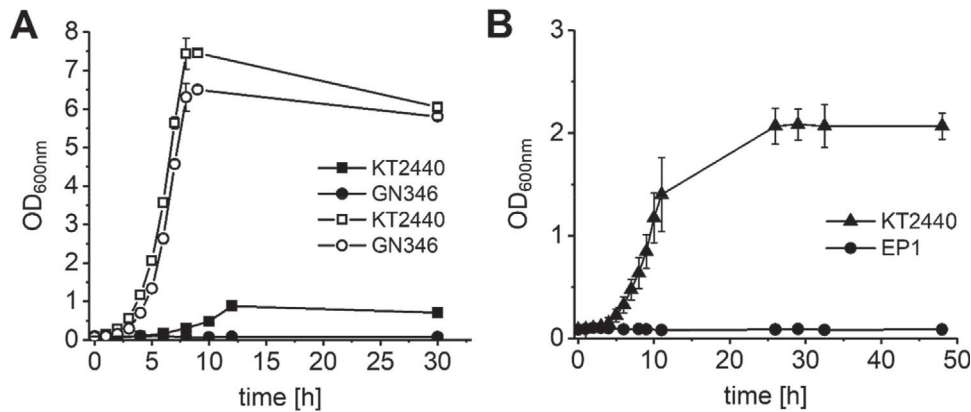
FIGURE 2 (A) Growth of *P. putida* KT2440 and *P. putida* GN346 in DeBont minimal medium containing 0.5 g/L isobutanol (filled symbols) or 5.4 g/L glucose (open symbols). (B) Growth of *P. putida* and *P. putida* EP1 in DeBont minimal medium containing 2.9 g/L 2-ketoisovalerate. Experiments were performed in triplicates and error bars represent the corresponding standard deviation

TABLE 2 Overview of growth, 2-ketogluconate (2-KG) and isobutanol production of *P. putida* and its engineered derivatives

Strain	μ [h^{-1}]	$Y_{X/S}$ [g/g]	$Y_{2\text{-KG/S}}$ [mg/g$_{GLC}$]	$Y_{Iso/S}$ [mg/g$_{GLC}$]
KT2440	0.62 ± 0.01	0.40 ± 0.01	0	0
GN346	0.59 ± 0.01	0.39 ± 0.01	0	0
Iso1	0.56 ± 0.02	0.30 ± 0.01	0	0
Iso2	0.25 ± 0.01	0.13 ± 0.01	438 ± 20	22 ± 2
Iso3	0.14 ± 0.01	0.06 ± 0.01	833 ± 100	13 ± 1
Iso4	0.19 ± 0.01	0.09 ± 0.02	771 ± 15	14 ± 0.0
Iso5	0.18 ± 0.02	0.28 ± 0.01	0	0
Iso6	0.28 ± 0.01	0.10 ± 0.01	633 ± 39	21 ± 1

3.2 | Engineering *P. putida* for isobutanol production

To drain the carbon from pyruvate to 2-KIV, we constructed a plasmid harboring the *alsS* gene encoding the acetolactate synthase from *Bacillus subtilis*, which is not feedback inhibited by branched chain amino acids, and the native *ilvCD* genes encoding the ketolacid reductoisomerase and dihydroxyacid dehydratase (Figure 1). For the conversion of 2-KIV to isobutanol, we additionally cloned *kivD* encoding the KDC from *Lactococcus lactis* and *yqhD* encoding an aldehyde reductase from *E. coli* (Fig. 1). AlsS, KivD, and YqhD were previously applied for isobutanol production in other hosts such as *C. glutamicum* and *E. coli* [5,7]. The resulting plasmid pIP02 expresses all cloned genes under control of the L-arabinose inducible P$_{BAD}$ promoter and was used to transform *P. putida* EP1 yielding *P. putida* Iso1. In minimal medium with glucose, *P. putida* Iso1 showed a $\mu = 0.56 \pm 0.02$. Although the $Y_{X/S}$ was reduced by 25% compared to the wild-type, no isobutanol was produced during the cultivation (Table 2).

The synthesis of isobutanol from glucose requires 2 mol NAD(P)H per mol isobutanol. The reduction of acetolactate is catalyzed by NADPH-dependent ketolacid

reductoisomerase (IlvC), while the conversion of isobutyraldehyde to isobutanol can be catalyzed by NAD(P)H-dependent aldehyde/alcohol dehydrogenases such as YqhD (Figure 1). Since YqhD is NADPH-dependent, the engineered iosobutanol pathway should consume 2 mol NADPH per mol isobutanol. *P. putida* possesses a membrane-bound and a soluble transhydrogenase. The latter is encoded by the *sthA* gene [42] and has in *E. coli* been reported to favor the re-oxidation of NADPH to NADP$^+$ under reduction of NAD$^+$ to NADH [43,44].

To test whether the inactivation of the soluble transhydrogenase is beneficial for isobutanol production, we deleted the *sthA* gene in *P. putida* EP1, yielding *P. putida* EP2 which was transformed with the plasmid pIP02. The resulting strain *P. putida* Iso2 showed in minimal medium containing 5.4 g/L glucose, a growth rate of 0.26 ± 0.01 h^{-1}, a $Y_{X/S}$ of of 0.13 ± 0.01 g/g, and produced 438 ± 20 mg/g$_{GLC}$ 2-KG and for the first time isobutanol with a $Y_{Iso/S}$ of 22 ± 2 mg/g$_{GLC}$ (Table 2, Figure 3). We also replaced the aldehyde reductase gene *yqhD* on the overexpression plasmid pIP02 with the *adhA* genes encoding NADH-dependent alcohol dehydrogenase variants from *Lactococcus lactis* and *Corynebacterium glutamicum*, respectively. The plasmids pIP03 and pIP04 were used to transform *P. putida* EP2, yielding *P. putida* Iso3 and Iso4,

FIGURE 3 Growth (black circles), glucose consumption (grey circles), isobutanol production (white bars) and 2-KG formation (grey bars) of *P. putida* Iso2 in DeBont minimal medium containing glucose. Experiments were performed in triplicates and error bars represent the corresponding standard deviation

which were characterized in minimal medium with glucose (Table 2). Both strains showed reduced growth rates and about 40% lower product yields compared to *P. putida* Iso2. All engineered strains with deletion of *sthA* converted 40% to 83% of the available glucose into 2-KG that was 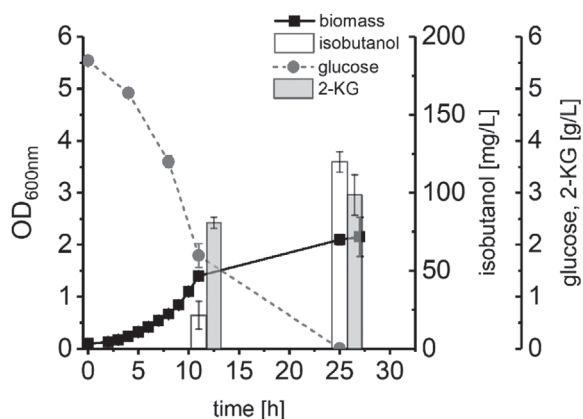secreted into the culture broth (Table 2). To avoid 2-KG secretion and to improve isobutanol production, we constructed *P. putida* EP3 by deletion of the *gcd* gene encoding periplasmatic glucose dehydrogenase in *P. putida* EP2. To construct *P. putida* Iso5, *P. putida* EP3 was transformed with the plasmid pIP02. In fact, *P. putida* Iso5 did not secrete any 2-KG, however, inactivation of GCD also abolished isobutanol production completely (Table 2).

3.3 | Ketoacid decarboxylase from *Carnobacterium maltaromaticum* is suitable for isobutanol production

The key enzyme for isobutanol production via the Ehrlich pathway is ketoacid decarboxylase (KDC) converting 2-KIV to isobutyraldehyde (Figure 1). So far, only KDC from *L. lactis* has been proven as suitable variant that efficiently catalyzes this reaction [2,5]. Recently, the genome sequence of *Carnobacterium maltaromaticum* LMA28 [28] was published that harbors a gene encoding a putative KDC. KDC from *C. maltaromaticum* shows 54% identity to the KDC enzyme from *L. lactis*. To test the suitability of KDC from *C. maltaromaticum* for isobutanol production, we replaced the *kivD* gene on plasmid pIP02 with the respective gene from *C. maltaromaticum*. Plasmid pIP05 was transformed into *P. putida* EP2 and the resulting strain *P. putida* Iso6 was characterized. *P. putida* Iso6 showed a growth rate of 0.28 $\pm$ 0.01 h^{-1}, a $Y_{X/S}$ of of 0.10 $\pm$ 0.01 g/g. and produced 633 $\pm$ 39 mg/g$_{GLC}$ 2-KG. Furthermore, *P. putida* Iso6 secreted

TABLE 3 Overview of engineered *P. putida* strains cultivated under oxygen deprivation conditions

Strain	$Y_{Iso/S}$ [mg/g$_{GLC}$]	qs [g g^{-1} h^{-1}]	$Y_{2-KG/S}$ [mg/g$_{GLC}$]
KT2440	0	0.11 $\pm$ 0.01	42 $\pm$ 32
Iso2	9 $\pm$ 1	0.14 $\pm$ 0.01	120 $\pm$ 9
Iso3	5 $\pm$ 2	0.12 $\pm$ 0.01	183 $\pm$ 8
Iso4	4 $\pm$ 1	0.13 $\pm$ 0.01	193 $\pm$ 12
Iso5	0	0.01 $\pm$ 0.00	0
Iso6	19 $\pm$ 2	0.07 $\pm$ 0.01	397 $\pm$ 14

as much isobutanol as *P. putida* Iso2 with a $Y_{Iso/S}$ of 21 $\pm$ 1 mg/g$_{GLC}$ (Table 2) showing that KDC from *C. maltaromaticum* LMA28 is a useful alternative to KDC from *L. lactis*.

3.4 | Microaerobic isobutanol production in *P. putida*

P. putida is regarded as an obligate aerobic bacterium [18]. However, since the implementation of the synthetic isobutanol pathway theoretically enables a closed redox balance, we tested the capabilities of our engineered *P. putida* strains to produce isobutanol from glucose in a zero-growth bioprocess under oxygen deprivation conditions [45]. Therefore, we inoculated *P. putida* WT and Iso2–6 to an OD$_{600}$ of 15–20 in closed bottles filled with minimal medium containing 5.4 g/L glucose and characterized substrate consumption and (by-) product formation (Table 3). In the micro-aerobic environment *P. putida* WT showed no growth, but remained metabolically active and consumed the glucose that was converted to 2-KG. With the exception of *P. putida* Iso5, all other engineered strains consumed glucose and produced isobutanol. *P. putida* Iso6 showed the best performance under oxygen deprivation conditions. Compared to the WT the q_S was reduced by 37% and *P. putida* Iso6 produced about 10% less isobutanol compared to the aerobic shaking flask experiments (Table 3).

4 | DISCUSSION

P. putida is an emerging host for industrial biotechnology [46–48]. However, this bacterium is also known to efficiently metabolize a broad range of substrates including amino and organic acids and alcohols [21]. As shown here, *P. putida* grows rapidly on isobutanol as well as on its precursor 2-KIV. Although *P. putida* KT2440 possesses four aldehyde dehydrogenases and about 10 alcohol dehydrogenases, Simon et al. [30] showed that deletion of the two alcohol dehydrogenase genes *pedE* and pedH and the two aldehyde dehydrogenases genes *pedI* and *aldB-I* is sufficient to prevent *n*-butanol degradation. Accordingly, we found that this strain background also prevents growth on

the branched-chain alcohol isobutanol. *P. putida* possesses a branched chain ketoacid dehydrogenase complex that converts 2-ketoacids to the respective decarboxylated CoA-derivatives [40,41]. As expected and also observed for *P. taiwanensis* VLB120 [41], inactivation of the BCKDH abolished growth on 2-ketoisovalerate. To avoid auxotrophies, we relinquished the inactivation of the L-valine forming transaminase IlvE, the 2-isopropylmalate synthase LeuA and the 2-ketoisovalerate hydroxymethyltransferase PanB as has been applied to improve isobutyric acid production with *P. taiwanensis* strain VLB120 [41].

Since AHAIR is usually NADPH-dependent, the synthesis of one molecule of isobutanol either requires two molecules of NADPH or one NADH plus one NADPH molecule depending on the applied alcohol/aldehyde dehydrogenase variant for the reduction of isobutyraldehyde to isobutanol. Optimization of NAD(P)H availability has already been shown to be a crucial factor for isobutanol production with other hosts such as *E. coli* and *C. glutamicum* [6,49]. Recently, Nikel et al. [16] showed that *P. putida* cells growing on glucose exhibit a slight catabolic overproduction of reducing power and run a biochemical cycle that favors NADPH formation. Therefore, we applied in our experiments the broad-substrate range NADPH-dependent aldehyde reductase YqhD [50], which has also been successfully applied for isobutanol production with *E. coli* [8]. However, expression of the synthetic pathway in *P. putida* Iso1 to channel pyruvate toward isobutanol did not result in isobutanol production from glucose. Similar to *E. coli*, *P. putida* possesses a membrane bound (PntAB) and a soluble transhydrogenase (SthA) to balance the overall redox state of the cell (Figure 1). SthA has in *E. coli* been reported to favor the oxidation of NADPH to NADP$^+$, accompanied with the reduction of NAD$^+$ to NADH [43,44]. To improve NADPH availability, we inactivated SthA that resulted in isobutanol formation in *P. putida* Iso2 under aerobic conditions. Accordingly, expression of two *adhA* genes encoding NADH-dependent alcohol dehydrogenases from *L. lactis* and *C. glutamicum*, which have previously been shown to be suitable for isobutanol production [7,8], instead of YqhD, led to significantly reduced isobutanol yields in the Δ*sthA* background (Table 2).

Inactivation of SthA resulted in isobutanol production, however, also in the secretion of significant amounts of 2-KG. In *P. putida* a majority of the glucose is converted in the periplasm by glucose dehydrogenase (Gcd) to gluconate, which is transported to the cytoplasm and activated by the gluconate kinase to feed the Entner–Doudoroff pathway with 6-phosphogluconate. Usually, only a small fraction of gluconate is converted in the periplasm by gluconate dehydrogenase to 2-KG, which is subsequently transported into the cytoplasm to finally form 6-phosphogluconate via 2-KG kinase and 2-ketogluconate-6-P reductase [16]. Since deletion of *gcd* abolished 2-KG production completely, the synthesis of this molecule occurs solely in the periplasm via the described route. The accumulation of 2-KG in the culture broth indicates a transport inhibition of gluconate and/or 2-KG from the periplasm to the cytoplasm by an unknown mechanism and/or an inhibition or limitation of the ATP-dependent conversion to the phosphorylated derivatives. The latter might result as consequence of a perturbed redox state due to the inactivated transhydrogenase SthA.

P. putida is an obligate aerobic bacterium, however, in a bioelectrochemical system *P. putida* was metabolically active under anoxic conditions when an electron mediator was applied for redox balancing in a high-yield 2-KG production system [51,52]. Since isobutanol synthesis enables regeneration of NAD(P)$^+$, we cultivated *P. putida* WT and the engineered derivatives under microaerobic conditions. All strains showed no growth (data not shown) but with the exception of *P. putida* Iso5, remained metabolically active and *P. putida* Iso2-4 and 6 also secreted 2-KG, isobutanol, and further unidentified products. However, according to the zero-growth the q_S values are low compared to aerobic conditions (e.g. for *P. putida* WT 0.11 vs. 1.55 g g^{-1} h^{-1}) . The capability of *P. putida* to remain metabolically active opens the possibility to develop dual-phase production processes that comprise an aerobic growth phase for rapid biomass formation and a micro-aeobic or anaerobic production phase [45].

This study paths the way to construct more efficient *P. putida* strains for isobutanol production in future studies. The overall isobutanol yield is significantly higher compared to other engineered *P. putida* strains [41], however, rather low compared to tailored *E. coli* and *C. glutamicum* strains [49]. Product and precursor degradation can be prevented by the presented deletions in this study, however, improving NAD(P)H and pyruvate availability [49] will be crucial to achieve high-yield isobutanol production strains.

ACKNOWLEDGEMENTS

CONFLICT OF INTEREST

The authors have declared no conflict of interest.

ORCID

Bastian Blombach 🔟

https://orcid.org/0000-0002-2996-2049

REFERENCES

1. Tiffany, D., Nelson, E., Tilman, D., Hill, J., et al., Environmental, economic, and energetic costs and benefits of biodiesel and ethanol biofuels. *Proc. Natl. Acad. Sci. USA* 2006, *103*, 11206–11210.

2. Eikmanns, B.J. and Blombach, B., Isobutanol, in: Bisaria, V. S., Kondo, A. (Eds.), *Bioprocessing of Renewable Resources to Commodity Bioproducts*, John Wiley & Sons, Inc., Weinheim 2014, pp. 327–352.

3. Chen, C.-T. and Liao, J.C., Frontiers in microbial 1-butanol and isobutanol production. *FEMS Microbiol. Lett.* 2016, *363*, fnw020.

4. Wilson, J., Gering, S., Pinard, J., Lucas, R., et al., Bio-production of gaseous alkenes: ethylene, isoprene, isobutene. *Biotechnol. Biofuels* 2018, *11*, 234.

5. Atsumi, S., Hanai, T., Liao, J.C., Non-fermentative pathways for synthesis of branched-chain higher alcohols as biofuels. *Nature* 2008, *451*, 86–89.

6. Bastian, S., Liu, X., Meyerowitz, J.T., Snow, C.D., et al., Engineered ketol-acid reductoisomerase and alcohol dehydrogenase enable anaerobic 2-methylpropan-1-ol production at theoretical yield in *Escherichia coli. Metab. Eng.* 2011, *13*, 345–352.

7. Blombach, B., Riester, T., Wieschalka, S., Ziert, C., et al., *Corynebacterium glutamicum* tailored for efficient isobutanol production. *Appl. Environ. Microbiol.* 2011, *77*, 3300–3310.

8. Atsumi, S., Wu, T.Y., Eckl, E.M., Hawkins, S.D., et al., Engineering the isobutanol biosynthetic pathway in *Escherichia coli* by comparison of three aldehyde reductase/alcohol dehydrogenase genes. *Appl. Microbiol. Biotechnol.* 2010, *85*, 651–657.

9. Li, S., Huang, D., Li, Y., Wen, J., et al., Rational improvement of the engineered isobutanol-producing *Bacillus subtilis* by elementary mode analysis. *Microb. Cell Fact.* 2012, *11*, 101.

10. Matsuda, F., Ishii, J., Kondo, T., Ida, K., et al., Increased isobutanol production in *Saccharomyces cerevisiae* by eliminating competing pathways and resolving cofactor imbalance. *Microb. Cell Fact.* 2013, *12*, 119.

11. Kieboom, J., Dennis, J.J., de Bont, J.A.M., Zijlstra, G.J., Identification and molecular characterization of an efflux pump involved in *Pseudomonas putida* S12 solvent tolerance. *J. Biol. Chem.* 1998, *273*, 85–91.

12. Udaondo, Z., Duque, E., Fernández, M., Molina, L., et al., Analysis of solvent tolerance in *Pseudomonas putida* DOT-T1E based on its genome sequence and a collection of mutants. *FEBS Lett.* 2012, *586*, 2932–2938.

13. Belda, E., van Heck, R.G.A., José Lopez-Sanchez, M., Cruveiller, S., et al., The revisited genome of *Pseudomonas putida* KT2440 enlightens its value as a robust metabolic chassis. *Environ. Microbiol.* 2016, *18*, 3403–3424.

14. Regenhardt, D., Heuer, H., Heim, S., Fernandez, D.U., et al., Pedigree and taxonomic credentials of *Pseudomonas putida* strain KT2440. *Environ. Microbiol.* 2002, *4*, 912–915.

15. Nikel, P.I., Martínez-García, E., de Lorenzo, V., Biotechnological domestication of pseudomonads using synthetic biology. *Nat. Rev. Microbiol.* 2014, *12*, 368–79.

16. Nikel, P.I., Chavarria, M., Fuhrer, T., Sauer, U., et al., *Pseudomonas putida* KT2440 strain metabolizes glucose through a cycle formed by enzymes of the Entner-Doudoroff, Embden-Meyerhof-Parnas, and pentose phosphate pathways. *J. Biol. Chem.* 2015, *290*, 25920–25932.

17. Udaondo, Z., Ramos, J.-L., Segura, A., Krell, T., et al., Regulation of carbohydrate degradation pathways in *Pseudomonas* involves a versatile set of transcriptional regulators. *Microb. Biotechnol.* 2018, *11*, 442–454.

18. dos Santos, V.A.P.M., Heim, S., Moore, E.R.B., Stratz, M., et al., Insights into the genomic basis of niche specificity of *Pseudomonas putida* KT2440. *Environ. Microbiol.* 2004, *6*, 1264–1286.

19. Dvořák, P. and de Lorenzo, V., Refactoring the upper sugar metabolism of *Pseudomonas putida* for co-utilization of cellobiose, xylose, and glucose. *Metab. Eng.* 2018, *48*, 94–108.

20. Poblete-Castro, I., Becker, J., Dohnt, K., dos Santos, V.M., et al., Industrial biotechnology of *Pseudomonas putida* and related species. *Appl. Microbiol. Biotechnol.* 2012, *93*, 2279–2290.

21. Nikel, P.I. and de Lorenzo, V., *Pseudomonas putida* as a functional chassis for industrial biocatalysis: From native biochemistry to *trans*-metabolism. *Metab. Eng.* 2018, *50*, 142–155.

22. Kohlstedt, M., Starck, S., Barton, N., Stolzenberger, J., et al., From lignin to nylon: Cascaded chemical and biochemical conversion using metabolically engineered *Pseudomonas putida. Metab. Eng.* 2018, *47*, 279–293.

23. Calero, P., Jensen, S.I., Nielsen, A.T., Broad-Host-Range ProUSER vectors enable fast characterization of inducible promoters and optimization of *p*-coumaric acid production in *Pseudomonas putida* KT2440. *ACS Synth. Biol.* 2016, *5*, 741–753.

24. Molina-Santiago, C., Cordero, B.F., Daddaoua, A., Udaondo, Z., et al., *Pseudomonas putida* as a platform for the synthesis of aromatic compounds. *Microbiology* 2016, *162*, 1535–1543.

25. Köhler, K.A.K., Rückert, C., Schatschneider, S., Vorhölter, F.-J., et al., Complete genome sequence of *Pseudomonas* sp. strain VLB120 a solvent tolerant, styrene degrading bacterium, isolated from forest soil. *J. Biotechnol.* 2013, *168*, 729–730.

26. Wynands, B., Lenzen, C., Otto, M., Koch, F., et al., Metabolic engineering of *Pseudomonas taiwanensis* VLB120 with minimal genomic modifications for high-yield phenol production. *Metab. Eng.* 2018, *47*, 121–133.

27. Bagdasarian, M., Lurz, R., Ruckert, B., Franklin, F.C., et al., Specific-purpose plasmid cloning vectors. II. Broad host range, high copy number, RSF 1010-derived vectors, and a host-vector system for gene cloning in *Pseudomonas. Gene* 1981, *16*, 237–247.

28. Cailliez-Grimal, C., Chaillou, S., Anba-Mondoloni, J., Loux, V., et al., Complete chromosome sequence of *Carnobacterium maltaromaticum* LMA 28. *Genome Announc.* 2013, *1*, e00115-12.

29. Wegmann, U., O'Connell-Motherway, M., Zomer, A., Buist, G., et al., Complete genome sequence of the prototype lactic acid bacterium *Lactococcus lactis* subsp. *cremoris* MG1363. *J. Bacteriol.* 2007, *189*, 3256–3270.

30. Simon, O., Klebensberger, J., Mükschel, B., Klaiber, I., et al., Analysis of the molecular response of *Pseudomonas putida* KT2440 to the next-generation biofuel n-butanol. *J. Proteomics* 2015, *122*, 11–25.

31. Krause, F.S., Blombach, B., Eikmanns, B.J., Metabolic engineering of *Corynebacterium glutamicum* for 2-ketoisovalerate production. *Appl. Environ. Microbiol.* 2010, *76*, 8053–8061.

32. Graf, N. and Altenbuchner, J., Functional characterization and application of a tightly regulated MekR/P *mekA* expression system in *Escherichia coli* and *Pseudomonas putida. Appl. Microbiol. Biotechnol*. 2013, *97*, 8239–8251.

33. Silva-Rocha, R., Martínez-García, E., Calles, B.N., Chavarría, M., et al., The Standard European Vector Architecture (SEVA): a coherent platform for the analysis and deployment of complex prokaryotic phenotypes. *Nucleic Acids Res*. 2012, *41*, 666–675.

34. Sambrook, J. and Russell, D.W., *Molecular cloning: a laboratory manual*., 3rd ed., Cold Spring Harbor Laboratory Press, Cold Spring Harbor 2001.

35. Hartmans, S., Smits, J.P., van der Werf, M.J., Volkering, F., et al., Metabolism of styrene oxide and 2-phenylethanol in the styrene-degrading *Xanthobacter* strain 124X. *Appl. Environ. Microbiol.* 1989, *55*, 2850–2855.

36. Gibson, D.G., Young, L., Chuang, R.-Y., Venter, J.C., et al., Enzymatic assembly of DNA molecules up to several hundred kilobases. *Nat. Methods* 2009, *6*, 343–345.

37. Graf, N. and Altenbuchner, J., Development of a method for markerless gene deletion in *Pseudomonas putida. Appl. Environ. Microbiol.* 2011, *77*, 5549–5552.

38. Buchholz, J., Schwentner, A., Brunnenkan, B., Gabris, C., et al., Platform Engineering of *Corynebacterium glutamicum* with reduced pyruvate dehydrogenase complex activity for improved production of L-lysine, L-valine, and 2-ketoisovalerate. *Appl. Environ. Microbiol.* 2013, *79*, 5566–5575.

39. Vallon, T., Simon, O., Rendgen-Heugle, B., Frana, S., et al., Applying systems biology tools to study n -butanol degradation in *Pseudomonas putida* KT2440. *Eng. Life Sci.* 2015, *15*, 760–771.

40. Sokatch, J.R., McCully, V., Roberts, C.M., Purification of a branched-chain keto acid dehydrogenase from *Pseudomonas putida. J. Bacteriol.* 1981, *148*, 647–652.

41. Lang, K., Zierow, J., Buehler, K., Schmid, A., Metabolic engineering of *Pseudomonas* sp. strain VLB120 as platform biocatalyst for the production of isobutyric acid and other secondary metabolites. *Microb. Cell Fact.* 2014, *13*, 2.

42. Nikel, P.I., Pérez-Pantoja, D., de Lorenzo, V., Pyridine nucleotide transhydrogenases enable redox balance of *Pseudomonas putida* during biodegradation of aromatic compounds. *Environ. Microbiol.* 2016, *18*, 3565–3582.

43. Sauer, U., Canonaco, F., Heri, S., Perrenoud, A., et al., The soluble and membrane-bound transhydrogenases UdhA and PntAB have divergent functions in NADPH metabolism of *Escherichia coli**. *J. Biol. Chem.* 1998, *273*, 85–91.

44. Fuhrer, T. and Sauer, U., Different biochemical mechanisms ensure network-wide balancing of reducing equivalents in microbial metabolism. *J. Bacteriol.* 2009, *191*, 2112–2121.

45. Lange, J., Takors, R., Blombach, B., Zero-growth bioprocesses: A challenge for microbial production strains and bioprocess engineering. *Eng. Life Sci.* 2017, *17*, 27–35.

46. Nikel, P.I., Chavarría, M., Danchin, A., de Lorenzo, V., From dirt to industrial applications: *Pseudomonas putida* as a Synthetic Biology chassis for hosting harsh biochemical reactions. *Curr. Opin. Chem. Biol.* 2016, *34*, 20–29.

47. Martínez-García, E. and de Lorenzo, V., Molecular tools and emerging strategies for deep genetic/genomic refactoring of *Pseudomonas. Curr. Opin. Biotechnol.* 2017, *47*, 120–132.

48. Martínez-García, E. and de Lorenzo, V., *Pseudomonas putida* in the quest of programmable chemistry. *Curr. Opin. Biotechnol.* 2019, *59*, 111–121.

49. Blombach, B. and Eikmanns, B.J., Current knowledge on isobutanol production with *Escherichia coli*, *Baciullus subtilis* and *Corynebacterium glutamicum. Bioeng. Bugs* 2011, *2*, 346–350.

50. Jarboe, L.R., YqhD: a broad-substrate range aldehyde reductase with various applications in production of biorenewable fuels and chemicals. *Appl. Microbiol. Biotechnol.* 2011, *89*, 249–257.

51. Lai, B., Yu, S., Bernhardt, P. V, Rabaey, K., et al., Anoxic metabolism and biochemical production in *Pseudomonas putida* F1 driven by a bioelectrochemical system. *Biotechnol. Biofuels* 2016, *9*, 39.

52. Yu, S., Lai, B., Plan, M.R., Hodson, M.P., et al., Improved performance of *Pseudomonas putida* in a bioelectrochemical system through overexpression of periplasmic glucose dehydrogenase. *Biotechnol. Bioeng.* 2018, *115*, 145–155.

53. Dower, W. J., Miller, J. F. and Ragsdale, C. W., High efficiency transformation of *E.coli* by high voltage electroporation. *Nucleic Acids Res.* 1988, *16*, 6127–6145.

54. Choi, K. H., Kumar, A. and Schweizer, H. P., A 10-min method for preparation of highly electrocompetent *Pseudomonas aeruginosa* cells: Application for DNA fragment transfer between chromosomes and plasmid transformation. *J. Microbiol. Methods* 2006, *64*, 391–397.

3.5. P-V: Micro-aerobic Production of Isobutanol with Engineered *Pseudomonas putida*

Isobutanol production with *P. putida* was scaled up from shake flask to a fed-batch cultivation in a 30 L bioreactor. Metabolite and flux analysis revealed intracellular redox imbalances that were caused by high NADPH demand in the production pathway. The cells counteracted by the exorbitant formation of 2-ketogluconic acid to maintain the electron supply for the electron transport chain. A novel approach of micro-aerobic conditions in the bioreactor doubled the isobutanol yield from the predecessor publication (**P-IV**) and paves the way for innovative low-oxygen applications with *P. putida.*

A. Ankenbauer is the main author of this manuscript and performed the experiments. R. Nitschel and T. Müller assisted during the experiments and proofread the manuscript. R. Nitschel contributed valuable ideas for the experimental work. T. Müller helped with evaluation of the results. A. Teleki supervised and developed the LC-MS metabolite quantification method with assistance of L. Favilli. T. Müller and A. Teleki drafted the chapter "LC-MS based analysis of intracellular metabolites". B. Blombach supervised and proofread the study. R. Takors (corresponding author) supervised this study, contributed ideas, and edited the manuscript.

RESEARCH ARTICLE

Micro-aerobic production of isobutanol with engineered *Pseudomonas putida*

Andreas Ankenbauer[1] [iD] | Robert Nitschel[1] | Attila Teleki[1] | Tobias Müller[1] |
Lorenzo Favilli[1] | Bastian Blombach[2] [iD] | Ralf Takors[1]

[1] Institute of Biochemical Engineering, University of Stuttgart, Stuttgart, Germany

[2] Microbial Biotechnology, Campus Straubing for Biotechnology and Sustainability, Technical University of Munich, Straubing, Germany

Correspondence
Prof. Ralf Takors, Institute of Biochemical Engineering, University of Stuttgart, Allmandring 31, 70569 Stuttgart, Germany.
Email: takors@ibvt.uni-stuttgart.de

We dedicate our contribution to the 70th anniversary of Prof. Dr. Thomas Bley.

Abstract

Pseudomonas putida KT2440 is emerging as a promising microbial host for biotechnological industry due to its broad range of substrate affinity and resilience to physicochemical stresses. Its natural tolerance towards aromatics and solvents qualifies this versatile microbe as promising candidate to produce next generation biofuels such as isobutanol. In this study, we scaled-up the production of isobutanol with *P. putida* from shake flask to fed-batch cultivation in a 30 L bioreactor. The design of a two-stage bioprocess with separated growth and production resulted in 3.35 $g_{isobutanol}$ L^{-1}. Flux analysis revealed that the NADPH expensive formation of isobutanol exceeded the cellular catabolic supply of NADPH finally causing growth retardation. Concomitantly, the cell counteracted to the redox imbalance by increased formation of 2-ketogluconic thereby providing electrons for the respiratory ATP generation. Thus, *P. putida* partially uncoupled ATP formation from the availability of NADH. The quantitative analysis of intracellular pyridine nucleotides $NAD(P)^+$ and $NAD(P)H$ revealed elevated catabolic and anabolic reducing power during aerobic production of isobutanol. Additionally, the installation of micro-aerobic conditions during production doubled the integral glucose-to-isobutanol conversion yield to 60 $mg_{isobutanol}$ $g_{glucose}^{-1}$ while preventing undesired carbon loss as 2-ketogluconic acid.

KEYWORDS
2-ketogluconic acid, micro-aerobic, isobutanol, NADPH, *Pseudomonas putida*

1 | INTRODUCTION

The global market for isobutanol is anticipated to grow by 6.4% annually reaching USD 1.6 billion in 2027 (reportsanddata.com/press-release/global-isobutanol-

market). Being mainly produced by petrochemical synthesis, isobutanol primarily serves as chemical intermediate (46.5% in 2019) in particular for coating solvents or butyl rubber [1]. Besides, isobutanol can be used as drop-in additive for gasoline and serves as precursor to produce aviation fuel. The C4 alcohol exhibits a higher combustion power, a lower vapor pressure, and a lower

Abbreviations: 2-KG, 2-ketogluconic acid; KIV, 2-ketoisovalerate

corrosive impact compared to ethanol [1, 2]. However, regarding the need to reduce the human carbon footprint by establishing a circular economy, industry seeks for bio-based isobutanol production from renewable feedstocks. Accordingly, microbial isobutanol production from glucose has been established in several organisms [3, 4] such as *Escherichia coli* [5, 6], *Bacillus subtilis* [7], and *Corynebacterium glutamicum* [8, 9] under aerobic or anaerobic conditions. Nevertheless, the toxicity of isobutanol to these organisms is a major drawback preventing their use for industrial scale production with even further improved key performance values [4, 10].

Therefore, bacterial organisms such as *Pseudomonas putida* with a natural tolerance towards toxic compounds and alcohols like butanol and ethanol could be an alternative production host [11–13]. The Gram-negative soil bacterium *P. putida* KT2440, certified as HV1 [14] is genetically accessible [15] and endowed with a versatile metabolism that originates from its ability to colonize harsh environments [16, 17]. Moreover, *P. putida* exhibits a broad range of substrate affinity which is essential for the consumption of complex harvest residuals such as lignocellulose and oils [18, 19]. The cyclic nature of glucose oxidation via the combined EDEMP pathway [20, 21] allows *P. putida* to adjust NADPH formation, a trait that is beneficial to counteract oxidative stress. As recently shown, *P. putida* is also well-endowed to withstand transient substrate starvation conditions that may occur in large-scale bioreactors thanks to the rapid access to intracellular 3-hydroxyalkanoate storage buffers [22].

These metabolic advantages render *P. putida* a suitable microbial platform for isobutanol production which was successfully shown in shake flask cultures [23]. The authors engineered the *P. putida* GN346 mutant [13], that is unable to degrade n-butanol, for the overproduction of isobutanol from glucose via the NADPH dependent Ehrlich pathway. Besides isobutanol, high accumulation of the by-product 2-ketogluconic acid (2-KG) (>0.4 $g_{2\text{-KG}}$ g_{glc}^{-1}) was observed for *P. putida* Iso2 and engineered derivatives [23]. The problem of unwanted 2-KG formation also occurred with *P. putida* engineered for *cis,cis*-muconic acid production [24, 25]. *P. putida* KT2440 is known to oxidize glucose to gluconate (glt) and to 2-KG in the periplasm via glucose dehydrogenase (Gcd) and gluconate dehydrogenase (Gad) [21, 26]. However, the deletion of *gcd* in the isobutanol producer *P. putida* Iso2 not only stopped 2-KG production but isobutanol formation, too [23].

Since anaerobic conditions improved isobutanol production in *E. coli* [6] and *C. glutamicum* [9] through increased supply of NADPH, Nitschel et al. [23] tested *P. putida's* capability of converting glucose into isobutanol

PRACTICAL APPLICATION

To meet the steadily growing demand for isobutanol as chemical precursor or fuel additive, biotechnological production approaches from renewable feedstocks are in the focus of research and industry. In contrast to bacterial strains that are sensitive to extracellular alcohol, *Pseudomonas putida* exhibits a natural tolerance towards solvents and other toxic chemicals. Therefore, we exploited this superiority with the previously engineered *P. putida* Iso2 strain to achieve high isobutanol titers with different fed-batch strategies. By installing a micro-aerobic production environment in the bioreactor, the balance between cellular NADPH formation and demand was improved resulting in enhanced isobutanol yields. Since carbon uptake and intracellular accumulation of succinic acid was observed during oxygen depletion, this study paves the way for innovative micro-aerobic applications using the strict aerobic microbe *P. putida*.

during micro-aerobic conditions in sealed shake flasks. The authors observed minimal metabolic activity even though *P. putida* KT2440 is not capable of anaerobic respiration to control its energy and redox balance in the absence of oxygen [15, 27]. Different studies already aimed to enable *P. putida* for anoxic carbon conversion, e.g. by knocking-in a fermentative pathway [28] or by using a redox mediator in a bioelectrochemical system [29, 30]. However, none of these attempts resulted in anaerobic growth which would require sophisticated strain engineering [31]. Further advances were achieved by creating an anaerotolerant *P. putida* strain that showed growth under micro-oxic conditions [32]. Our study focuses on the scale-up of isobutanol production with *P. putida* from shake flask to fed-batch cultivations in a 30 L stirred tank reactor. Aerobic and micro-aerobic conditions are installed to evaluate the supply of the critical electron donor NADPH as a key to improve substrate-to-isobutanol yields. Additionally, the cellular ATP management is quantified.

2 | MATERIALS AND METHODS

2.1 | Strain and medium

The *P. putida* Iso2 strain that was engineered for isobutanol production from glucose [23] was applied in all

experiments. The strain is based on the GN346 variant [13] of *P. putida* KT2440 with additional deletions of *bkdAA* and *sthA*. Furthermore, it harbours the arabinose inducible plasmid pIP02 (pNG413 *araC* P_{BAD} *kivD yqhD alsS ilvC ilvD*) for overexpression of the Ehrlich pathway and the route from pyruvate to 2-ketoisovalerate (KIV) as part of the branched-chain amino acid pathway. The cultivation medium was adopted from Vallon et al. [33] and Davis et al. [34] and contained (per liter): 4.7 g $(NH_4)_2SO_4$, 0.8 g $MgSO_4 \cdot 7 H_2O$, 0.04 g $CaCl_2 \cdot 2 H_2O$, 0.5 g NaCl, 4 g KH_2PO_4; and trace elements (per liter): 4 mg $ZnSO_4 \cdot 7 H_2O$, 2 mg $MnCl_2 \cdot 4 H_2O$, 30 mg $Na_3C_6H_5O_7 \cdot 2 H_2O$, 2 mg $CuSO_4 \cdot 5 H_2O$, 0.04 mg $NiCl_2 \cdot 6 H_2O$, 0.06 mg $Na_2MoO_4 \cdot 2 H_2O$, 0.6 mg H_3BO_3, 20 mg $FeSO_4 \cdot 7 H_2O$ (Merck, Darmstadt, Germany). 50 $mg_{apramycin}$ L^{-1} were added to ensure plasmid selection.

2.2 | Cultivation

The seed train for each bioreactor fermentation was started with a preculture that was inoculated from the working cell bank (33% glycerol stock, stored at −70°C). The first preculture was cultivated in a 500 mL baffled shake flask containing 50 mL of minimal medium (pH 7) with 6 g glucose, 10 g 3-morpholino-propanesulfonic acid (MOPS), and 0.5 g yeast extract (VWR International, Radnor, Pennsylvania) per liter. After approx. 10 h of incubation (130 rpm, 30°C), cells from the first preculture were used to inoculate the second preculture in a 5 L shaking flask containing 500 mL minimal medium with 6 $g_{glucose}$ L^{-1} and 10 g_{MOPS} L^{-1}. After incubation for 14 h, the total volume of the second preculture (about 0.8 g_X L^{-1}) was used to start batch cultivation in a 30 L stirred tank reactor (STR) (Bioengineering, Wald, Switzerland) containing 8 L minimal medium (inoculum included) with 15 $g_{glucose}$ L^{-1}, at 30°C with total pressure of 1.5 bar. The initial aeration was started at 1 L min^{-1} and increased stepwise to 8 L min^{-1} during the batch phase. Also, the initial stirrer speed of 300 min^{-1} was adjusted to maintain the dissolved oxygen (DOT) above 15%. During fermentation, the pH was controlled at 6.9 using 25% NH_4OH (Carl Roth, Karlsruhe, Germany). After initially supplied glucose was consumed an exponential feed consisting of 600 g glucose and 12.5 g $MgSO_4$ per liter controlled the biomass growth rate at a predefined value. Additionally, five-fold trace elements were supplemented during the fed-batch phase. Peristaltic pumps (120U, Watson-Marlow GmbH, Rommerskirchen, Germany) were used for liquid feeding. Furthermore, the plasmid was induced by adding 1.57 $g_{arabinose}$ L^{-1} to the medium. Three different process strategies were performed in this study comprising a reference process (*Process R*), a process with fast grow-

ing cells (*Process F*) and a process with immediate micro-aerobic condition after plasmid induction (*Process MA*). The micro-aerobic environment (DOT < 1%) was installed by switching from submerse aeration to head-space aeration. Striped-out isobutanol was trapped from the exhaust gas in 10 L deionized water (adopted from Inokuma et al. [35]). This gas washing setup yielded an isobutanol recovery of 96.3% over 12 h in a reference experiment. The O_2 and CO_2 volume fractions in the off gas was determined with a combined O_2/CO_2 gas sensor (BlueSens Gas Sensor GmbH, Herten, Germany).

2.3 | Determination of biomass and extracellular metabolites

4×1 mL of biosuspension was centrifuged with 20,000 g for 5 min at 4°C, washed twice with demineralized water, transferred into pre-weighed glass vials (1.5 mL, VWR International, Radnor, Pennsylvania) and eventually dried at 105°C for 24 h. The weight of the remaining biomass was determined using a micro balance (XP26 Delta Range®, Mettler Toledo, Gießen, Germany). The organic acids, glucose, and gluconate in the supernatant were quantified using enzyme kits (r-biopharm AG, Darmstadt, Germany). 2-ketogluconic acid, 2-ketoisovalerate, and isobutanol were measured using an isocratic HPLC equipped with the RI detector (1200Series, Agilent, Santa Clara, CA, USA) and a Rezex ROA-Organic Acid H^+ (300 × 7.8 mm) column (Phenomenex, Aschaffenburg, Germany) at 50°C. 0.4 mL min^{-1} of 5 mM H_2SO_4 was used as mobile phase for the separation of the HPLC analytes. The extracellular concentrations of L-valine, L-isoleucine, and L-leucine were determined according to the amino acid detection protocol described by Buchholz et al. [36].

2.4 | LC-MS based analysis of intracellular metabolites

Targeted metabolome analyses of intracellular *P. putida* extracts were based on previous HILIC-ESI-MS studies [37, 38]. The inactivation of samples and preparation of cellular extracts was performed according following adapted procedure: 0.5 mL of biosuspension were directly mixed to 1.5 mL pre-cooled (-40°C) quenching solution (60% methanol (v/v), 133 mM ammonium acetate/pH 9.2) and immediately centrifugated for 45 s at 20,000 g in a pre-cooled rotor (-20°C). Cell pellets were frozen in liquid nitrogen and stored at -70°C. The frozen pellets were resuspended in pre-cooled (-20°C) extraction buffer consisting of methanol (66% v/v), ammonium acetate (100 mM/pH 9.2), L-norvaline (0.15 mM), and 3-mercaptopropionic

acid (2.5 mM). Added volumes were adjusted to achieve constant biomass concentrations (c_X = 10–15 g L^{-1}). During resuspension, sample temperature was kept below -20°C by rotational vortexing and chilling in a constantly cooled cryostat (-40°C). Subsequently, the same volume of pre-cooled chloroform (-20°C) was added and mixed properly. Next, the samples were incubated for 1 h at -20°C and 1 h at room temperature in a rotary overhead-shaker and remaining cell debris were separated by centrifugation (10 min at 20,000 g and 4°C). The upper H$_2$O/methanol phase (polar metabolites) was stored at -70°C until measurement.

Measurements were performed on an Agilent 6410B Triple-Quad LC-MS/MS system. Sample preparation and chromatographic separation by alkaline polymer-based zwitterionic hydrophilic interaction chromatography (ZIC-pHILIC) were performed as previously described [37]. Central carbon metabolites were analyzed with high selectivity in multiple reaction monitoring (MRM) mode with high selectivity and pre-optimized precursor-to-product ion transitions with a mass resolution of 0.1 u and adapted MS/MS parameters [38]. Pyridine nucleotide factors were analyzed with higher sensitivity in selective ion monitoring (SIM) mode with a mass resolution of 0.3 u and analog MS parameters. System control, acquisition, and analysis of data were performed by usage of commercial MassHunter B.06.00 software.

2.5 | Calculation of ATP formation and demand

The total ATP generation of the cell is based on the direct phosphorylation on substrate level $q_{ATP,S}$ (Equation 2) via carbon uptake $q_{S,in}$ (Equation 1) and on the oxidative phosphorylation via the respiratory chain $q_{ATP,O}$ (Equation 3). According to recent published carbon fluxes [39], a net formation of 2.67 mol$_{ATP}$ mol$_{glucose}$$^{-1}$ via direct phosphorylation is assumed from glucose based carbon uptake in *P. putida*. The P/O ratio (1.33 mol$_{ATP}$ mol$_{oxygen}$$^{-1}$ [40]) links the oxygen uptake to the ATP formation via oxidative phosphorylation through the electron transport chain and the proton gradient that fuels the ATP synthase. Electrons to reduce oxygen in *P. putida* cannot only be transferred by NADH or FADH$_2$ but also via pyrroloquinoline (PQQ) by oxidation of glucose to gluconate and 2-ketogluconic acid [41]. In accordance, the electron flux via glucose oxidation to 2-KG was shown in anaerobically cultivated *P. putida* F1 [29]. The authors illustrated that the incomplete oxidation of glucose to 2-KG is an alternative route for *P. putida* to generate ATP ($q_{ATP,alt}$). The enzyme complex in the electron transport chain creates a proton gradient through the electron flux which drives the ATP synthase. 2 e$^-$ are

released per molecule of glt and 4 e$^-$ per molecule of 2-KG formed from glucose that can be used to finally reduce oxygen (Equation 4). In contrast to the ATP generation, the total growth related ATP demand can be determined by Equation 5 [40].

$$q_{S,in} = q_S - q_{glt} - q_{2KG} \tag{1}$$

$$q_{ATP,S} = 2.67 * q_{S,in} \tag{2}$$

$$q_{ATP,O} = q_{O2} * 2 * P/O \tag{3}$$

$$q_{ATP,alt} = q_{2KG} * 2 * P/O + q_{glt} * P/O \tag{4}$$

$$q_{ATP} = \mu * 85 \ mmol_{ATP} * g_X^{-1} + 3.96 \ mmol_{ATP} * g_X^{-1} * h^{-1} \tag{5}$$

2.6 | In silico calculation of NADPH demand

The total NADPH supply was estimated using the ratio of 1.7 mol$_{NADPH}$ mol$_{glucose}$$^{-1}$, and a NADPH surplus of 14 to 21% was assumed for growth on glucose [21, 39, 42]. The additional NADPH demand in the isobutanol production pathway was calculated based on the extracellular uptake and formation rates of KIV, L-valine and isobutanol. If uptake of KIV was detected, it was assumed to serve as precursor for isobutanol and L-valine. Furthermore, the intracellular flux distribution from KIV to L-valine and to isobutanol was estimated to mirror the ratio of secreted isobutanol per L-valine during aerobic production. During micro-aerobic condition, no growth occurred, and stationary conditions were assumed. Then, NADPH demands for isobutanol production and 2-KG uptake via KguD should equal NADPH formation via the enzymes Zwf, Icd and MaeB. Recently published carbon fluxes [39] and the following stoichiometries were used for carbon and NADPH balancing:

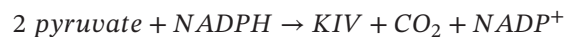$$G6P + NADP^+ \rightarrow 6PG + NADPH$$

$$2KG + NADPH \rightarrow 6PG + NADP^+$$

$$Isocitrate + NADP^+ \rightarrow 2-oxoglutarate + CO_2 + NADPH$$

$$Malate + NADP^+ \rightarrow pyruvate + CO_2 + NADPH$$
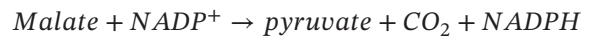
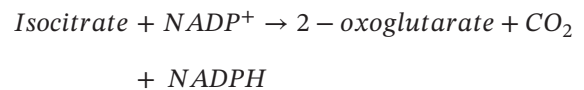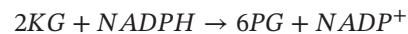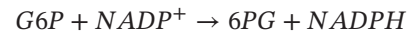$$2 \ pyruvate + NADPH \rightarrow KIV + CO_2 + NADP^+$$

TABLE 1 Comparison of process parameters from the reference *Process R*, the *Process F* with fast growing cells and the micro-aerobic *Process MA*

Process strategy	μ_{max} [h^{-1}]	$Y_{X/S,max}$ [g g^{-1}]	$\mu_{fed-batch}$ [h^{-1}]	$Y_{X/S,fed-batch}$ [g g^{-1}]	$Y_{2-KG/S}$ [g g^{-1}]	$Y_{P/S}$ [g g^{-1}]	$q_{P,max}$ [mmol g^{-1} h^{-1}]
Process R	0.29 ± 0.03 (4)	0.16 ± 0.01 (4)	0.13 ± 0.01 (3)	0.32 ± 0.03 (3)	0.254	0.025	0.39
Process MA					**0.003**	**0.060**	**1.27**
Process F			0.22	0.37	0.623	0.022	0.65

Yields are given as product formed per glucose consumed. Standard deviation and number of replicates (in brackets) are shown after each value. Bold numbers indicate the best results. Since the batch phase was comparable in *Process R, Process F*, and *Process MA*, the mean values for μ_{max} and $Y_{X/S,max}$ are shown. The same applies fort the comparable fed-batch phase in *Process R* and *Process MA*.

$$KIV \ + \ glutamate \ \rightarrow Lvaline + 2 - oxoglutarate$$

$$2 - oxoglutarate + \ NADPH \rightarrow glutamate + \ NADP^+$$

$$KIV + NADPH \rightarrow isobutanol + CO_2 + NADP^+$$

3 | RESULTS

3.1 | Scale-up of microbial isobutanol production with *P. putida* Iso2

To increase biomass concentration and to monitor the growth and production performance of the metabolically engineered *P. putida* Iso2 strain [23] producing the non-native metabolite isobutanol, the cultivation process was scaled-up from shake flask to a 30 L stirred tank bioreactor. Growth and production were separated in two stages to analyse the effect of plasmid encoded overexpression of the isobutanol pathway on the phenotype and metabolism. Cells were cultivated under controlled conditions in the bioreactor with 8 L of initial working volume. Three different process strategies were performed. As illustrated in Figure 1A, each process consists of a batch and fed-batch phase (*growth phase)* and a post-induction phase (*production phase*). Figure 1B shows the time course of different product concentrations and the isobutanol yield with respect to the time of plasmid induction ($t = 0$h). The reference process is entitled as "*Process R*" and was accomplished in the following manner: During the batch process (until -13 h), cells grew with a maximum specific growth rate of 0.29 (± 0.03) h^{-1} showing a biomass specific yield of 0.16 g$_X$ g$_{glucose}$$^{-1}$ (Table 1) and accumulated 1.7 g$_{2-KG}$ L^{-1}. In the subsequent glucose limited fed-batch phase (from -13 to 0 h) cells grew with μ_{fb} = 0.13 h^{-1}. Cell density reached 12 g$_X$ L^{-1} and 8.3 g L^{-1} of the precursor 2-ketoisovalerate (KIV) for the isobutanol pathway accumulated during the fed-batch phase. The feed profiles, glucose concentrations, and DOT levels are shown in the Figure S1. Next, the inducer arabinose (1.57 g L^{-1}) was added to the broth to initiate the production of isobutanol ($t = 0$h). During *production phase I*, extracellular isobu-

tanol accumulated to 1.7 g$_{isobutanol}$ L^{-1}, but the growth rate decreased to 0.02 h^{-1} within 8 h. Concomitantly, cells started to accumulate 22 g$_{2-KG}$ L^{-1}, and 2.1 g$_{L-valine}$ L^{-1}. Extracellular KIV concentrations remained for the first 4 h of production but declined afterwards due to cellular consumption. In *production phase II* (from 8 to 12 h), the submerse aeration was switched to head-space aeration to install micro-aerobic conditions. The resulting oxygen deprivation led to only minimal secretion of 2-KG and L-valine while the isobutanol titer increased further from 1.7 to 2.4 g L^{-1} which was accompanied by consumption of KIV. In total, 943 g glucose were consumed to produce 23.1 g isobutanol within 38 h leading to a yield of 22 mg$_{isobutanol}$ g$_{glucose}$$^{-1}$ (refer to Table 1).

Figure 2 illustrates the uptake and formation rates of the substrates and products in all three process strategies before (0 h) and after plasmid induction (2-12 h). In the reference *Process R*, the biomass specific glucose consumption rate rose from 1.95 to 2.95 mmol$_{glucose}$ g$_X$$^{-1}$ h^{-1} during *production phase I* even though the growth rate declined from 0.13 to 0.02 h^{-1}. Simultaneously, the 2-KG production rate increased significantly to 2.0 mmol$_{2-KG}$ g$_X$$^{-1}$ h^{-1} which led to a persistent decline of carbon uptake (total of C-6 sugars). Nevertheless, the maximum isobutanol production rate of 0.39 mmol$_{isobutanol}$ g$_X$$^{-1}$ h^{-1} was observed within the first 2 h after induction, accompanied by a maximum L-valine excretion of 0.24 mmol$_{valine}$ g$_X$$^{-1}$ h^{-1}. The highest KIV consumption rate of 0.95 mmol$_{KIV}$ g$_X$$^{-1}$ h^{-1} was measured in the micro-aerobic *production phase II* in which isobutanol production rate (0.17 mmol$_{isobutanol}$ g$_X$$^{-1}$ h^{-1}) was still half of the maximum rate.

3.2 | High growth rates lead to increased product and by-product formation

With the aim to increase the biomass specific isobutanol production rate, fast cell growth of 0.22 h^{-1} that is close to μ_{max} was installed during the fed-batch phase (from -10.9 to 0 h) in *Process F* by adjusting the glucose feed (see Figure 1). The plasmid encoded isobutanol production was started with 16.6 g$_X$ L^{-1} biomass concentration ($t = 0$ h). Within
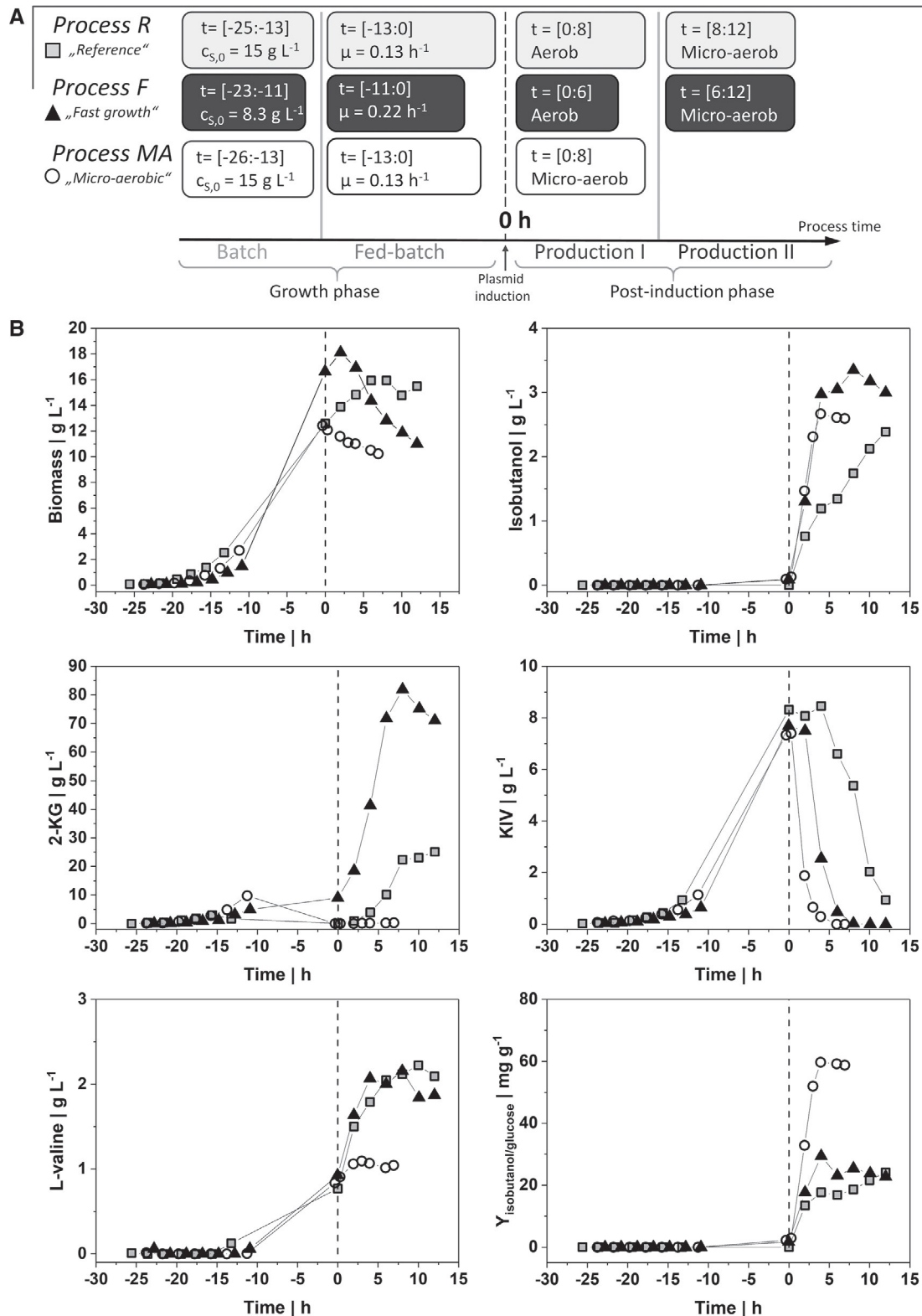
FIGURE 1 (A) Schematic overview of the three different process strategies applied in this study. *Process R* serves as reference process. After the batch and fed-batch phase, plasmid was induced and isobutanol production was monitored. After 8 h, submerse aeration was switched to headspace aeration. In contrast, fast growing cells were induced in *Process F* and micro-aerobic condition was installed after 6 h. Additionally, constant micro-aerobic condition was installed in *Process MA* 20 min after plasmid induction. The time span of each phase is given in brackets. (B) Time course of biomass concentration, extracellular concentrations of isobutanol, 2-KG, L-valine, 2-ketoisovalerate (KIV), and isobutanol per glucose yield $Y_{isobutanol/glucose}$. Each plot displays the reference *Process R* (grey square), the *Process F* (black triangle), and one replicate of the *Process MA* (circle). The process time (h) is given in relation to the induction of the plasmid (dotted vertical line)
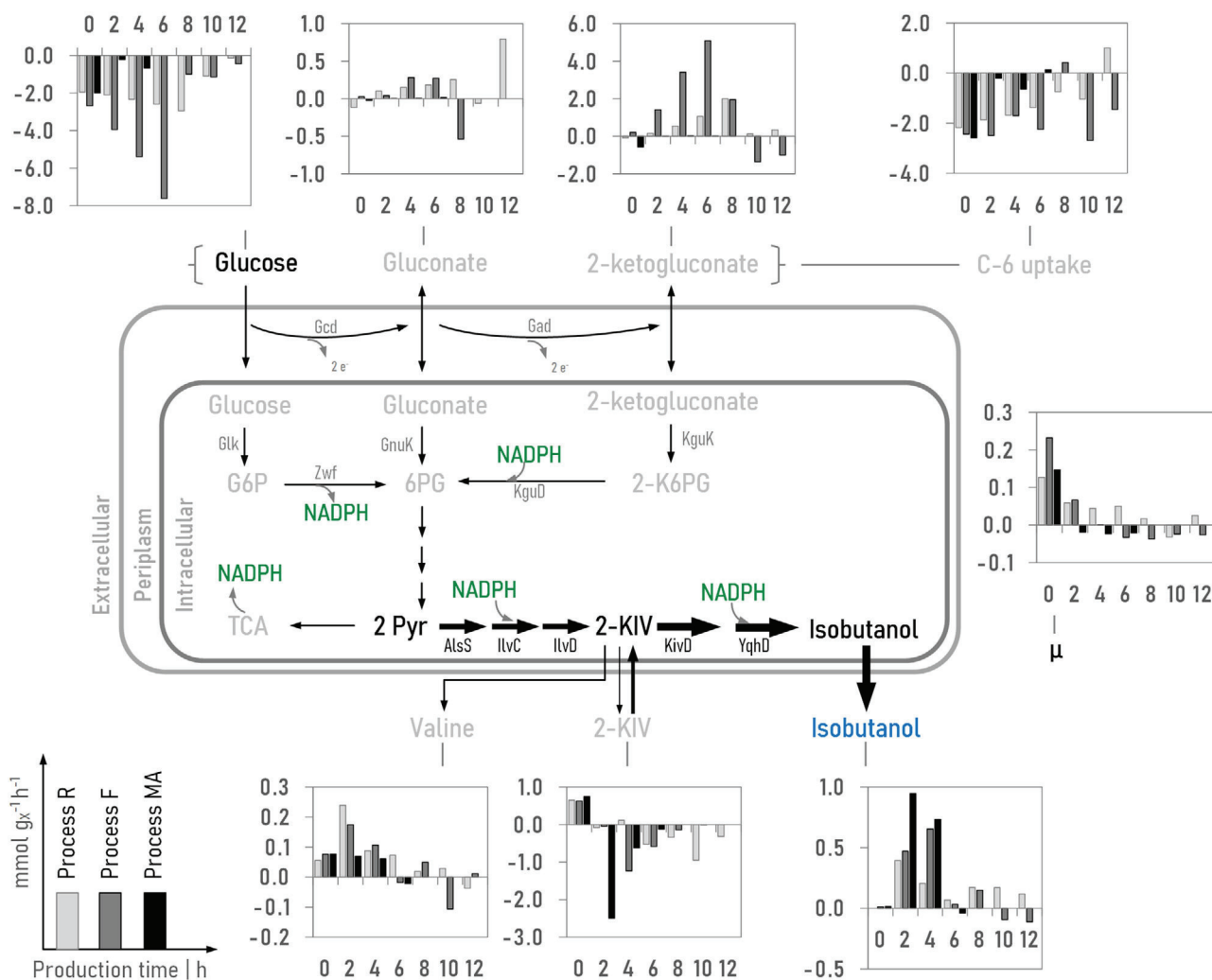
FIGURE 2 Uptake (negative) rates of carbon sources and formation (positive) rates of products (in mmol g_X^{-1} h^{-1}) as well as growth rates during production of isobutanol in the reference *Process R* (grey bar), in *Process F* (dark grey bar) and in one replicate of *Process MA* (black bar). Time point 0 h equals the reference condition before induction of the plasmid. Micro-aerobic condition was installed in *Process R* 8 h, in *Process F* 6 h, and in *Process MA* 20 min after plasmid induction. Abbreviations (coding genes are given in parentheses): C-6: difference of glucose uptake and gluconate and 2-ketogluconate formation, G6P: glucose-6-phosphate, 2-K6PG: 2-keto-6-phosphogluconate, 6PG: 6-phosphogluconate, Gcd: glucose dehydrogenase (*gcd*), Gad: gluconate 2-dehdyrogenase complex (PP3382-PP3384, PP3623, PP4232), Glk: glucokinase (*glk*), Zwf: glucose-6-phosphate 1-dehydrogenase (*zwf-1, zwf-2, zwf-3*), GnuK: gluconate kinase (*gnuK*), KguD: 2-6-phosphoketogluconate reductase (*kguD*), KguK: 2-ketogluconate kinase (*kguK*), AlsS: acetolactacte synthase (*ilvHI/alsS*), IlvC: ketol-acid reductoisomerase (*ilvC*), IlvD: dihydroxyacid dehydratase (*ilvD*), KivD: alpha-ketoisovalerate decarboxylase (*kivD*), Yqhd: aldehyde reductase (*yqhD*)

4 h of *production phase I*, 3.0 $g_{isobutanol}$ L^{-1} accumulated. 2-KG formation increased by 3.3-fold, reaching a maximum medium concentration of 82 g_{2-KG} L^{-1} that accounts for 0.58 g_{2-KG} $g_{glucose}^{-1}$. Consequently, the total glucose consumption increased by 41% still revealing an almost equal isobutanol yield of 25 $mg_{isobutanol}$ $g_{glucose}^{-1}$ compared to the reference *Process R* (Table 1). After reaching a peak at 18.3 g_X L^{-1} biomass concentrations declined by more than 20% (from 2 to 6 h). Switching to micro-aerobic condition after 6 h only marginally affected isobutanol production. The maximum of 3.35 $g_{isobutanol}$ L^{-1} in *production phase II*

coincided with the depletion of the extracellular precursor KIV.

As illustrated in Figure 2, the high growth rate during fed-batch in *Process F* resulted in a 1.7-fold enhanced maximum isobutanol production rate of 0.65 mmol g_X^{-1} h^{-1} in relation to the reference *Process R*. Noteworthy, within *production phase I* in *Process F*, glucose consumption rate almost tripled from 2.7 to 7.6 $mmol_{glucose}$ g_X^{-1} h^{-1} and 2-KG formation rate increased by 24-fold in contrast to the uninduced cells. Interestingly, despite an increased glucose supply and consumption in *Process F*, the combined
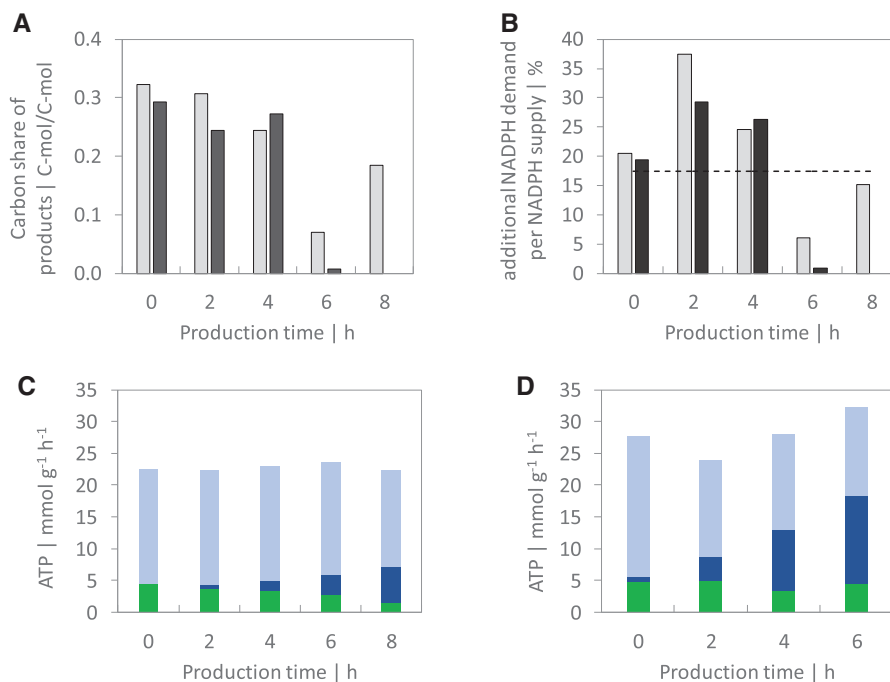
FIGURE 3 (A) Carbon share of the products KIV, L-valine, isobutanol, and CO_2 per uptake of substrates in *Process R* (grey bar) and *Process F* (dark grey bar). (B) NADPH demand for production of KIV, L-valine and isobutanol as percentage of the total NADPH supply in *Process R* (grey bar) and *Process F* (dark grey bar). The dotted line represents the theoretical NADPH surplus in *P. putida* WT. (C-D) Biomass specific ATP formation rates based on oxidative phosphorylation ($q_{ATP,O}$, sum of dark blue and light blue bar) and substrate level phosphorylation ($q_{ATP,S}$, green bar) in (C) the reference *Process R* and (D) the *Process F*. The dark blue bar represents the ATP generation based on the electron transport via oxidation of glucose to 2-KG ($q_{ATP,alt}$). The light blue bar represents the remaining part of oxidative phosphorylation via NADH and $FADH_2$ (=$q_{ATP,O}$ − $q_{ATP,alt}$). The production time in (A-D) is given with respect to induction of the plasmid whereas 0 h equals the reference condition before plasmid induction

carbon uptake of glucose, gluconate and 2-ketogluconate did not exceed 2.4 mmol g_X^{-1} h^{-1} although a maximum carbon uptake of approx. 8 mmol g_X^{-1} h^{-1} was observed during the batch phase. Even more, the growth rate declined drastically by nearly 70% within the first 2 h of *production phase I* followed by a phase of reduced cell density. During production of isobutanol, up to 0.28 mmol$_{gluconate}$ g_X^{-1} h^{-1} was measured. Additionally, extracellular accumulated KIV was almost completely consumed during *production phase I*. To conclude, the set growth rate close to μ_{max} led to increased production of isobutanol but also to exorbitantly high oxidation of glucose to 2-KG and a cessation of growth.

3.3 | Metabolic constraints during aerobic overproduction of isobutanol

As illustrated in Figure 3A, approximately 30% of the total carbon uptake during the fed-batch phase in *Process R* and *Process F* accounts for the products KIV, isobutanol, L-valine, and CO_2 that are formed in the production pathway. Hereby, most of the carbon is excreted in form of KIV. During *production phase I*, the product per substrate carbon

share in the isobutanol pathway is slightly decreased, but still above 20%. After 4 h of *production phase I*, a reduced isobutanol production rate resulted in less than 10% product formation per carbon uptake. Moreover, we calculated the additional NADPH that is consumed within the production pathway based on the product formation rates. The total NADPH supply was estimated from published NADPH production rates in *P. putida* KT2440 [21, 39]. The authors found that glucose-grown *P. putida* consumes most of the created NADPH by anabolic reactions except of a surplus of 14 to 21%. As shown in Figure 3B, the NADPH surplus (17.4% as average of literature values) covers the additional NADPH demand from overexpressed enzymes during the fed-batch phase. However, during the first 4 h of *production phase I* the additional NADPH demand exceeds the theoretical NADPH surplus which coincides with a decline of the growth rate in both processes.

Furthermore, we estimated the ATP formation of the cells based on their carbon and oxygen uptake. Additionally, the oxidation of glucose to gluconate and 2-KG releases electrons that reduce the respiratory chain component PQQ [29, 41]. In return, the proton gradient created by the electron transport chain drives the ATP synthase. Thus, the periplasmatic oxidation of glucose

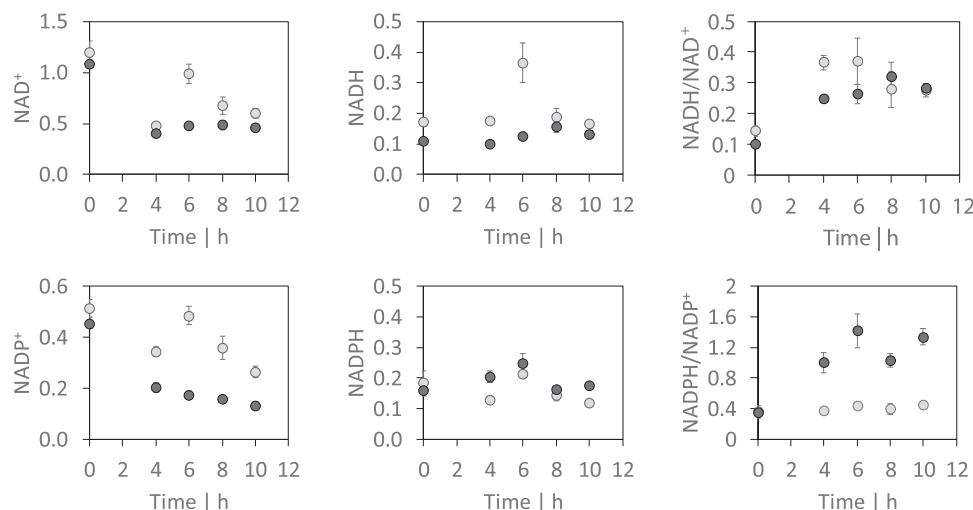**FIGURE 4** Intracellular concentrations (in μmol g_X^{-1}) of the redox cofactors NAD$^+$, NADP$^+$, NADH and NADPH and the respective redox ratios during the production phase in the reference *Process R* (grey circle) and in *Process F* (black circle). Time point 0 h equals the reference condition before induction of the plasmid

to 2-KG contributes to the overall ATP formation from oxidative phosphorylation. More precisely, Figures 3C,D illustrate the ATP formation from substrate level and oxidative phosphorylation before and after plasmid induction during aerobic production. The latter consists of electron transfers from NADH, FADH$_2$, and periplasmatic glucose oxidation. The total ATP generation in *Process R* and *Process F* remains nearly constant during *production phase I*. Remarkably, the amount of ATP generated by electrons released from the 2-KG pathway increased from 0.6 to 5.7 mmol g_X^{-1} h^{-1} in *Process R* and from 3.8 to 13.9 mmol g_X^{-1} h^{-1} in *Process F*, resulting in an ATP coverage of 50% at the end of *production phase I* in *Process F*.

Figure 4 shows absolute concentrations [μmol g_X^{-1}] of intracellular redox cofactors NAD$^+$, NADH, NADP$^+$ and NADPH that were detected in the aerobic *Process R* and *Process F*. Reduced NAD(P)H analogues are often heavily degraded under standard cold-based quenching/extraction conditions [43]. However, alkaline conditions (pH 9.2) with varying buffer concentrations and the addition of the reducing agent mercaptoethanol stabilized reduced pyridine nucleotides in solution [44]. Thus, by testing different buffer and reducing agents, we identified the supplementation of ammonium acetate to methanol as optimal quenching solution and supplementation of ammonium acetate plus 3-mercaptopropioinic acid to methanol as ideal extraction solution in regard of reliable and stabilized NAD(P)H species. This method was suitable to detect oxidized as well as reduced nucleotides. Under aerobic isobutanol production in *Process R* and *Process F*, pools of intracellular oxidized cofactors NAD$^+$ and NADP$^+$ were found to be significantly decreased in *production phase I* and *phase II* (see Figure 4). Remarkably, the level of the

reduced species NADH and NADPH remained nearly constant in both processes except for an NADH outlier after 6 h in *Process R*. Consequently, isobutanol producing *P. putida* show higher catabolic reduction charges (NADH/NAD$^+$) in both processes and slightly enhanced anabolic reduction charge in *Process F*. Further intracellular central carbon metabolites are shown in Figure S2.

3.4 | Micro-aerobic conditions increased isobutanol yield and reduced by-product formation

As shown in the reference *Process R*, switching from aerobic to micro-aerobic condition significantly reduced the by-product formation with almost unchanged product formation at the same time. Therefore, *Process MA* was performed similarly to *Process R*, but micro-aerobic condition (DOT = 0%) was installed already 20 min after plasmid induction in *production phase I*. The results of this process were validated in a biological duplicate (refer to Table S1). The related process kinetics can be drawn from Figure 1. As expected, no extracellular accumulation of 2-KG was observed in the *production phase I*. However, the biomass concentration declined considerably from 12.4 to 10.2 g_X L^{-1} during the micro-aerobic phase. Moreover, extracellular accumulated KIV was completely converted to isobutanol within 6 h after induction, resulting in a maximum titer of 2.67 $g_{isobutanol}$ L^{-1}. This process strategy yielded 60 mg$_{isobutanol}$/g$_{glucose}$ within only 4 h, which is two times higher compared to *Process F* and *Process R*. Besides, total glucose consumed was 58% less than in the reference *Process R*. Furthermore, the extracellular

TABLE 2 Carbon balance derived from the three different process strategies

Process strategy	Biomass	Isobutanol	2-KG	CO$_2$	Gluconate	2-KIV	L-valine	Sum
Process R	0.19	0.04	0.24	0.47	0.01	0.01	0.03	0.98
Process MA	0.28	0.09	0.01	0.57	0.01	0.01	0.04	1.00
Process F	0.12	0.04	0.57	0.24	0.01	0.00	0.02	1.01

Each value represents the carbon share (C-mol/C-mol) of the product based on the total glucose consumed at the end of the process.
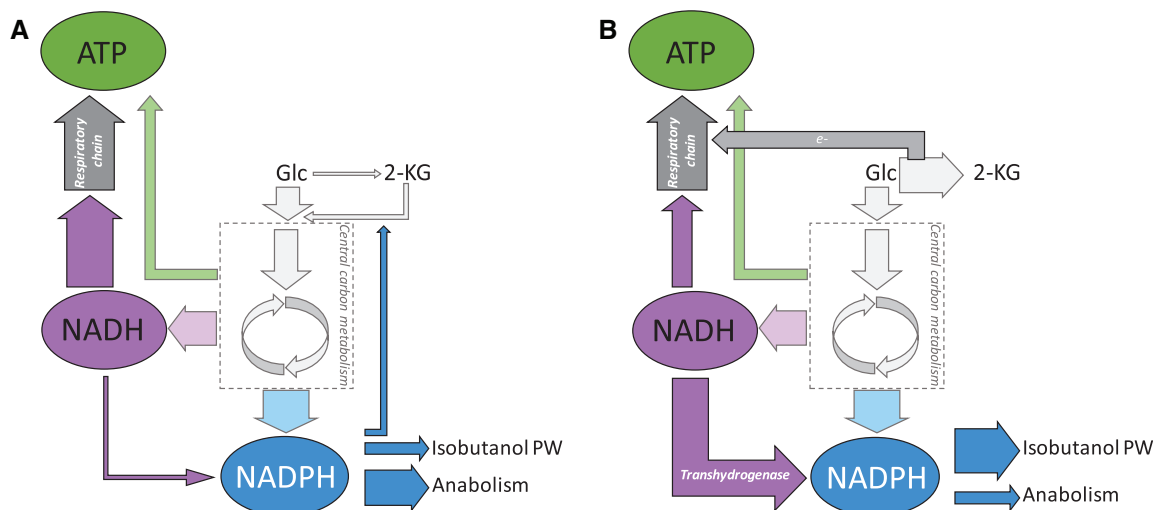
FIGURE 5 Schematic overview of assumed metabolic fluxes that are related to the intracellular pools of ATP, NADH, and NADPH (A) before induction and (B) during isobutanol formation in *P. putida* Iso2. The thickness of the arrows indicates the intensity of the related flux

by-product L-valine was approx. 50% lower than detected during both aerobic production strategies. As illustrated in Figure 2, only a minimal glucose consumption rate was observed during micro-aerobic condition in *Process MA*. Therefore, carbon uptake into the cells was only approx. 10% of aerobic carbon uptake. Concomitantly, the growth rate turned negative resulting in reduction of cell concentration. However, nearly equimolar conversion of extracellular KIV into isobutanol was observed within 4 h of oxygen limited production in *Process MA*, but isobutanol production ceased after complete consumption of KIV. The Figure S3 illustrates the intracellular concentrations of carbon metabolites and redox cofactor during micro-aerobic isobutanol production. Notably, succinic acid accumulated more than six-fold during oxygen depletion compared to aerobic growth.

In addition, carbon balance revealed that 12.8% of glucose was fuelled into the L-valine and the Ehrlich pathway, of which 9.2% accounts for isobutanol, in case of the optimized *Process MA* (Table 2). In contrast, only 4% of glucose was channelled into isobutanol during aerobic production in *Process R* and *Process F*. Even more, aerobic, fast-growing *P. putida* cells (*Process F*) lost 58% carbon into 2-KG which does only occur to a minimal extent (0.6%) under micro-aerobic production.

4 | DISCUSSION

4.1 | NADPH limitation constrains the growth-coupled isobutanol production in *P. putida*

The overexpression of the recombinant enzymes IlvD and YqhD to produce isobutanol obviously leads to an excessive demand of the cofactor NADPH in *P. putida* Iso2. This resulted in metabolic constraints affecting the cellular pools of NADPH, NADH and ATP which we depicted in Figure 5. As shown by Kohlstedt and Wittmann [39], the metabolism of *P. putida* creates a surplus of NADPH in growing cells that is most likely converted into NADH by the transhydrogenase. Interestingly, isobutanol production in *P. putida* was only possible after knockout of the transhydrogenase *stha* [23]. This genetic manipulation enabled the ample supply of NADPH for the isobutanol production pathway. As shown in Figure 3, the cofactor surplus was sufficient to cover the overproduction of KIV and L-valine during the non-induced fed-batch phase. The expression of the relative enzymes before induction most likely mirrors leaky plasmid expression. However, the overexpression of Yqhd after induction created a further NADPH sink that exceeded the NADPH surplus. As

a result, NADPH demand in the production pathway competed with anabolic processes which resulted in reduced growth in *Process R*. In fact, a 66% higher production rate in *Process F* coincided with cessation of growth. Furthermore, glucose uptake is accompanied by partial periplasmatic oxidation to gluconate and to 2-KG [21]. In contrast to recent approaches to prevent 2-KG secretion by deletion of the glucose dehydrogenase *gcd* [23–25], the glucose limited feeding strategy inhibited extracellular secretion of 2-KG before plasmid induction. However, after induction, the high NADPH demand in the isobutanol pathway competed with the NADPH dependent uptake of 2-KG and may partially explain the extracellular accumulation of this organic acid. In addition, to satisfy the extensive NADPH demand, an increased activity of the membrane bound transhydrogenase PntAB is likely to occur. This enzyme's favoured reaction is the reduction of $NADP^+$ at the expense of NADH via proton translocation [45, 46] which leads to a reduced availability of NADH for respiratory ATP generation. To satisfy the cellular ATP demand, electrons for the respiratory chain are released by periplasmatic oxidation of glucose to 2-KG [29, 41] which decouples ATP generation from the availability of NADH or $FADH_2$ as electron donor. This hypothesis is supported by the immense extracellular accumulation of 2-KG during aerobic isobutanol production that resulted in a carbon loss of up to 58%. Concomitantly, the electron supply from periplasmatic glucose oxidation contributed to total ATP generation with rising significance (Figure 3). The estimated total ATP generation in *P. putida* Iso2 is close to the theoretical demand of $15\,\text{mmol}_{\text{ATP}}\,\text{g}_X^{-1}\,\text{h}^{-1}$ at $\mu = 0.13\,\text{h}^{-1}$ and $24\,\text{mmol}_{\text{ATP}}\,\text{g}_X^{-1}\,\text{h}^{-1}$ at $\mu = 0.22\,\text{h}^{-1}$ for wildtype *P. putida* [40]. The crucial role of periplasmatic glucose oxidation during NADPH intensive product formation in *P. putida* is underlined by the lacking isobutanol production in the *Δgcd* strain [23].

These results show that cells are endowed to quickly adapt NADPH supply and energy management to current needs. Figure 4 outlines that physiological NADH and NADPH levels could be maintained for the sake of lower NAD^+ and $NADP^+$ levels which finally increased catabolic and anabolic reduction states. Still, the resulting redox ratios are in good agreement with published findings measured in *P. putida* KT2440 [47, 48]. Since NADPH is also required to counteract oxidative [49] and chemical stress [50, 51], the cellular need to maintain physiological levels or even increase the cofactor supply through rearranging metabolic fluxes [42] is important. Accordingly, the NADPH requirements for isobutanol compete with the 'life-style' of *P. putida* requiring for further systems metabolic engineering measures to succeed.

Even though the fed-batch cultivation significantly increased the isobutanol titer compared to shake flask (0.12 g L^{-1}) [23] and exceeds the product formation of engineered *Pseudomonas* sp. strain [52], the production efficiency of *P. putida* Iso2 is still not competitive with high yield aerobic or anaerobic approaches using, e.g. *E. coli* or *C. glutamicum* [3].

4.2 | Oxygen limited stationary conditions benefit NADPH dependent isobutanol formation

Processes R, *F* and *MA* vary by the installation of different post-induction aeration scenarios. In contrast to aerobic conditions that enabled growth-coupled isobutanol formation, micro-aerobic conditions limited cell growth leading to growth-decoupled isobutanol production. The dual-phase cultivation strategy, comprising aerobic biomass formation followed by micro-aerobic isobutanol production in *Process MA* substantially improved the product yield and inhibited extracellular by-product formation. Moreover, the micro-aerobic process strategy optimized NADPH dependent product formation—within the cellular capacities as illustrated above—but hampered the growth of the strict aerobic microbe *P. putida*. The controlled limitation of oxygen supply forced the cells into a stationary state as their energy generation is mainly dependent on the electron transport chain with the final electron acceptor oxygen [39]. In this case, electrons cannot be transferred by the succinate dehydrogenase to reduce FAD^+ which explains the observed intracellular accumulation of succinic acid that is seven-fold higher in *production phase I* of *Process MA* compared to the pre-induction level. In accordance, accumulation of succinic acid was also observed for anaerobic production of isobutanol in *C. glutamicum* [9]. Noteworthy, *P. putida* Iso2 showed a substantially higher volumetric isobutanol productivity of 9.5 mmol L^{-1} h^{-1} during micro-aerobic conditions compared to 4.4 mmol L^{-1} h^{-1} observed for *C. glutamicum* [9]. Furthermore, the micro-aerobic production condition in *Process MA* resulted in direct conversion of KIV into isobutanol which doubled the formation rate in contrast to *Process F* and reduced the product related NADPH costs. We estimated a lower additional NADPH demand of $1.1\,\text{mol}_{\text{NADPH}}\,\text{mol}_{\text{isobutanol}}^{-1}$ in *Process MA* compared to $1.5\,\text{mol}_{\text{NADPH}}\,\text{mol}_{\text{isobutanol}}^{-1}$ and $1.9\,\text{mol}_{\text{NADPH}}\,\text{mol}_{\text{isobutanol}}^{-1}$ in *Process R* and *Process F*, respectively. Nevertheless, metabolic activity of *P. putida* is a prerequisite for NADPH supply in a micro-aerobic environment and could potentially be monitored using exhaust gas analysis [53]. In agreement with Lai et al. [29] and Nitschel et al. [23], minimal carbon uptake to eventually generate NADPH through the central enzymes Zwf, Icd and MaeB [21, 39] was detected during oxygen depletion. We estimated a total NADPH formation of

510 mmol$_{NADPH}$ from carbon uptake versus a total demand of only 300 mmol$_{NADPH}$ needed as cofactor for Yqhd to convert isobutyraldehyde into isobutanol during 4 h of micro-aerobic production in *Process MA*. Thus, a sufficient amount of cofactors was supplied for the conversion of KIV into isobutanol in stationary *P. putida* cells.

To conclude, stationary cells and sufficient precursor supply qualifies micro-aerobic isobutanol formation in *P. putida* Iso2 as more efficient in terms of energy and NADPH demand compared to aerobic production. Moreover, the formation of 2-ketogluconic acid appears to be a unique trait in *P. putida* to balance its energy supply as a countermeasure to cofactor limitation. The novel findings of oxygen limited succinate accumulation could pave the way for innovative biotechnological applications with *P. putida*. Since micro-aerobic isobutanol production only occurred until extracellular KIV was depleted, we assume a hampered carbon flux to the precursor KIV during oxygen depletion. This bottleneck and the role of the transhydrogenase PntAB should be addressed by subsequent metabolic engineering studies to facilitate NADPH demanding product formation with *P. putida* KT2440.

Nomenclature

Y [g g$_{glucose}^{-1}$] Product yield per glucose consumed
q_i [mmol g$_X^{-1}$ h^{-1}] Biomass specific production rate of compound i

Greek symbols

μ [h^{-1}] Cell-specific growth rate

Indices

X Biomass
S Substrate glucose
O Oxygen
P Product isobutanol

CONFLICT OF INTEREST
The authors have declared no conflict of interest.

DATA AVAILABILITY STATEMENT
The data that support the findings of this study are available from the corresponding author upon reasonable request.

ORCID
Andreas Ankenbauer https://orcid.org/0000-0002-2843-683X
Bastian Blombach https://orcid.org/0000-0002-2996-2049

REFERENCES
1. Brownstein, A. M., Isobutanol in: Renewable Motor Fuels, Elsevier, 2015, pp. 47–56.
2. Dürre, P., Biobutanol: an attractive biofuel. Biotechnol. J. 2007, 2, 1525–1534.
3. Blombach, B., Eikmanns, B. J., Current knowledge on isobutanol production with *Escherichia coli*, *Bacillus subtilis* and *Corynebacterium glutamicum*. Bioeng. Bugs. 2011, 2, 346–350.
4. Chen, C.-T., Liao, J. C., Frontiers in microbial 1-butanol and isobutanol production. FEMS Microbiol. Lett. 2016, 363, fnw020.
5. Atsumi, S., Wu, T.-Y., Eckl, E.-M., Hawkins, S. D. et al. Engineering the isobutanol biosynthetic pathway in *Escherichia coli* by comparison of three aldehyde reductase/alcohol dehydrogenase genes. Appl. Microbiol. Biotechnol. 2010, 85, 651–657.
6. Bastian, S., Liu, X., Meyerowitz, J. T., Snow, C. D. et al. Engineered ketol-acid reductoisomerase and alcohol dehydrogenase enable anaerobic 2-methylpropan-1-ol production at theoretical yield in *Escherichia coli*. Metab. Eng. 2011, 13, 345–352.
7. Li, S., Wen, J., Jia, X., Engineering *Bacillus subtilis* for isobutanol production by heterologous Ehrlich pathway construction and the biosynthetic 2-ketoisovalerate precursor pathway overexpression. Appl. Microbiol. Biotechnol. 2011, 91, 577–589.
8. Smith, K. M., Cho, K.-M., Liao, J. C., Engineering *Corynebacterium glutamicum* for isobutanol production. Appl. Microbiol. Biotechnol. 2010, 87, 1045–1055.
9. Blombach, B., Riester, T., Wieschalka, S., Ziert, C. et al. *Corynebacterium glutamicum* tailored for efficient isobutanol production. Appl. Environ. Microbiol. 2011, 77, 3300–3310.
10. Jones, D. T., Woods, D. R., Acetone-butanol fermentation revisited. Microbiol. Rev. 1986, 50, 484–524.
11. Nikel, P. I., de Lorenzo, V., Robustness of *Pseudomonas putida* KT2440 as a host for ethanol biosynthesis. N. Biotechnol. 2014, 31, 562–571.

12. Ramos, J.-L., Sol Cuenca, M., Molina-Santiago, C., Segura, A., et al. Mechanisms of solvent resistance mediated by interplay of cellular factors in *Pseudomonas putida*. FEMS Microbiol. Rev. 2015, 39, 555–566.

13. Simon, O., Klebensberger, J., Mukschel, B., Klaiber, I. et al. Analysis of the molecular response of *Pseudomonas putida* KT2440 to the next-generation biofuel n-butanol. J. Proteomics. 2015, 122, 11–25.

14. Kampers, L. F. C., Volkers, R. J. M., Martins Dos Santos, V. A. P., *Pseudomonas putida* KT2440 is HV1 certified, not GRAS. Microb. Biotechnol. 2019, 12, 845–848.

15. Nelson, K. E., Weinel, C., Paulsen, I. T., Dodson, R. J. et al. Complete genome sequence and comparative analysis of the metabolically versatile *Pseudomonas putida* KT2440. Environ. Microbiol. 2002, 4, 799–808.

16. Timmis, K. N., *Pseudomonas putida*: a cosmopolitan opportunist par excellence. Environ. Microbiol. 2002, 4, 779–781.

17. Nikel, P. I., Chavarria, M., Danchin, A., de Lorenzo, V., From dirt to industrial applications: *Pseudomonas putida* as a synthetic biology chassis for hosting harsh biochemical reactions. Curr. Opin. Chem. Biol. 2016, 34, 20–29.

18. Hintermayer, S. B., Weuster-Botz, D., Experimental validation of in silico estimated biomass yields of *Pseudomonas putida* KT2440. Biotechnol. J. 2017, 12.

19. Weimer, A., Kohlstedt, M., Volke, D. C., Nikel, P. I. et al. Industrial biotechnology of *Pseudomonas putida*: advances and prospects. Appl. Microbiol. Biotechnol. 2020, 104, 7745–7766.

20. Chavarría, M., Nikel, P. I., Pérez-Pantoja, D., Lorenzo, V. de., The Entner-Doudoroff pathway empowers *Pseudomonas putida* KT2440 with a high tolerance to oxidative stress. Environ. Microbiol. 2013, 15, 1772–1785.

21. Nikel, P. I., Chavarria, M., Fuhrer, T., Sauer, U. et al. *Pseudomonas putida* KT2440 strain metabolizes glucose through a cycle formed by enzymes of the Entner-Doudoroff, Embden-Meyerhof-Parnas, and Pentose Phosphate Pathways. J. Biol. Chem. 2015, 290, 25920–25932.

22. Ankenbauer, A., Schäfer, R. A., Viegas, S. C., Pobre, V. et al. *Pseudomonas putida* KT2440 is naturally endowed to withstand industrial-scale stress conditions. Microb. Biotechnol. 2020, 13, 1145–1161.

23. Nitschel, R., Ankenbauer, A., Welsch, I., Wirth, N. T. et al. Engineering *Pseudomonas putida* KT2440 for the production of isobutanol. Eng. Life Sci. 2020, 97, 8239.

24. Johnson, C. W., Salvachúa, D., Rorrer, N. A., Black, B. A. et al. Innovative chemicals and materials from bacterial aromatic catabolic pathways. Joule. 2019, 3, 1523–1537.

25. Bentley, G. J., Narayanan, N., Jha, R. K., Salvachúa, D. et al. Engineering glucose metabolism for enhanced muconic acid production in *Pseudomonas putida* KT2440. Metab. Eng. 2020, 59, 64–75.

26. del Castillo, T., Ramos, J. L., Rodriguez-Herva, J. J., Fuhrer, T. et al. Convergent peripheral pathways catalyze initial glucose catabolism in *Pseudomonas putida*: genomic and flux analysis. J. Bacteriol. 2007, 189, 5142–5152.

27. Stanier, R. Y., Palleroni, N. J., Doudoroff, M., The aerobic pseudomonads: a taxonomic study. J. Gen. Microbiol. 1966, 43, 159–271.

28. Nikel, P. I., de Lorenzo, V., Engineering an anaerobic metabolic regime in *Pseudomonas putida* KT2440 for the anoxic biodegradation of 1,3-dichloroprop-1-ene. Metab. Eng. 2013, 15, 98–112.

29. Lai, B., Yu, S., Bernhardt, P. V., Rabaey, K. et al. Anoxic metabolism and biochemical production in *Pseudomonas putida* F1 driven by a bioelectrochemical system. Biotechnol. Biofuels. 2016, 9, 39.

30. Schmitz, S., Nies, S., Wierckx, N., Blank, L. M. et al. Engineering mediator-based electroactivity in the obligate aerobic bacterium *Pseudomonas putida* KT2440. Front. Microbiol. 2015, 6, 284.

31. Kampers, L. F. C., Koehorst, J. J., van Heck, R. J. A., Suarez-Diez, M. et al. A metabolic and physiological design study of *Pseudomonas putida* KT2440 capable of anaerobic respiration. BMC Microbiol. 2021, 21, 9.

32. Kampers, L. F. C., van Heck, R. G. A., Donati, S., Saccenti, E. et al. In silico-guided engineering of *Pseudomonas putida* towards growth under micro-oxic conditions. Microb. Cell Fact. 2019, 18, 179.

33. Vallon, T., Glemser, M., Malca, S. H., Scheps, D. et al. Production of 1-Octanol from n-Octane by *Pseudomonas putida* KT2440. Chemie Ingenieur Technik. 2013, 85, 841–848.

34. Davis, R., Duane, G., Kenny, S. T., Cerrone, F. et al. High cell density cultivation of *Pseudomonas putida* KT2440 using glucose without the need for oxygen enriched air supply. Biotechnol. Bioeng. 2015, 112, 725–733.

35. Inokuma, K., Liao, J. C., Okamoto, M., Hanai, T., Improvement of isopropanol production by metabolically engineered *Escherichia coli* using gas stripping. J. Biosci. Bioeng. 2010, 110, 696–701.

36. Buchholz, J., Graf, M., Blombach, B., Takors, R., Improving the carbon balance of fermentations by total carbon analyses. Biochemical Engineering Journal. 2014, 90, 162–169.

37. Feith, A., Teleki, A., Graf, M., Favilli, L. et al. HILIC-enabled 13C metabolomics strategies: comparing quantitative precision and spectral accuracy of QTOF High- and QQQ low-resolution mass spectrometry. Metabolites. 2019, 9, 63.

38. Teleki, A., Sánchez-Kopper, A., Takors, R., Alkaline conditions in hydrophilic interaction liquid chromatography for intracellular metabolite quantification using tandem mass spectrometry. Anal. Biochem. 2015, 475, 4–13.

39. Kohlstedt, M., Wittmann, C., GC-MS-based 13C metabolic flux analysis resolves the parallel and cyclic glucose metabolism of *Pseudomonas putida* KT2440 and *Pseudomonas aeruginosa* PAO1. Metab. Eng. 2019, 54, 35–53.

40. van Duuren, J. B. J. H., Puchalka, J., Mars, A. E., Bucker, R. et al. Reconciling in vivo and in silico key biological parameters of *Pseudomonas putida* KT2440 during growth on glucose under carbon-limited condition. BMC Biotechnol. 2013, 13, 93.

41. Ebert, B. E., Kurth, F., Grund, M., Blank, L. M. et al. Response of *Pseudomonas putida* KT2440 to increased NADH and ATP demand. Appl. Environ. Microbiol. 2011, 77, 6597–6605.

42. Nikel, P. I., Fuhrer, T., Chavarría, M., Sánchez-Pascuala, A. et al. Reconfiguration of metabolic fluxes in *Pseudomonas putida* as a response to sub-lethal oxidative stress. ISME J. 2021.1–16.

43. de Koning, W., van Dam, K., A method for the determination of changes of glycolytic metabolites in yeast on a subsecond time scale using extraction at neutral pH. Anal. Biochem. 1992, 204, 118–123.

44. Lowry, O. H., Passonneau, J., Rock, M. K., The stability of pyridine nucleotides. J. Biol Chem. 1961, 1961, 2756–2759.

45. Spaans, S. K., Weusthuis, R. A., van der Oost, J., Kengen, S. W. M., NADPH-generating systems in bacteria and archaea. Front. Microbiol. 2015, 6, 742.

46. Fuhrer, T., Sauer, U., Different biochemical mechanisms ensure network-wide balancing of reducing equivalents in microbial metabolism. J. Bacteriol. 2009, 191, 2112–2121.

47. Borrero-de Acuña, J. M., Bielecka, A., Häussler, S., Schobert, M. et al. Production of medium chain length polyhydroxyalkanoate in metabolic flux optimized *Pseudomonas putida*. Microb. Cell Fact. 2014, 13, 88.

48. Martínez-García, E., Nikel, P. I., Aparicio, T., de Lorenzo, V., *Pseudomonas* 2.0: genetic upgrading of *P. putida* KT2440 as an enhanced host for heterologous gene expression. Microb. Cell Fact. 2014, 13, 159.

49. Kim, J., Park, W., Oxidative stress response in *Pseudomonas putida*. Appl. Microbiol. Biotechnol. 2014, 98, 6933–6946.

50. Nikel, P. I., Pérez-Pantoja, D., de Lorenzo, V., Pyridine nucleotide transhydrogenases enable redox balance of *Pseudomonas putida* during biodegradation of aromatic compounds. Environ. Microbiol. 2016, 18, 3565–3582.

51. Blank, L. M., Ionidis, G., Ebert, B. E., Bühler, B. et al. Metabolic response of *Pseudomonas putida* during redox biocatalysis in the presence of a second octanol phase. FEBS J. 2008, 275, 5173–5190.

52. Lang, K., Zierow, J., Buehler, K., Schmid, A., Metabolic engineering of *Pseudomonas* sp. strain VLB120 as platform biocatalyst for the production of isobutyric acid and other secondary metabolites. Microb. Cell Fact. 2014, 13, 2.

53. Heyman, B., Tulke, H., Putri, SP., Fukusaki, E., Büchs, J., Online monitoring of the respiratory quotient reveals metabolic phases during microaerobic 2,3-butanediol production with *Bacillus licheniformis*. Eng. Life Sci. 2020; 20, 133–144

SUPPORTING INFORMATION

Additional supporting information may be found online in the Supporting Information section at the end of the article.

4. DISCUSSION

The following discussion will summarize the key findings of publication **P-I** – **P-V** and embed the different outputs in a scientific context.

4.1. *P. PUTIDA* WITHSTANDS TRANSIENT GLUCOSE AND OXYGEN STARVATION

As introduced, different stressors at the industrial scale seriously influence the performance of industry strains like *E. coli* (Lara et al., 2006a; Takors, 2012). However, only a few studies dealt with the large-scale application of *P. putida* (Elbahloul and Steinbuchel, 2009; Gorenflo et al., 2001), thus sound observations of its large-scale applicability are so far lacking. With the studies **P-II** and **P-III**, it was shown that *P. putida* KT2440 is neither compromised by fluctuating carbon nor by oscillating oxygen supply, even not by transient dual starvation conditions. Strikingly, biomass losses, which were observed in industry-scale cultivations with various other organisms (Lara et al., 2006a; Lara et al., 2006b), do not apply for *P. putida,* based on the presented observations. The stable phenotypical parameters of glucose-grown *P. putida* under both, oxygen and glucose limited conditions emphasize the versatile stress mechanism of this strain that most presumably originates from its nature as a soil-dweller with a constantly changing substrate supply. *P. putida* withstands repeated short-term glucose starvation since no significant physiological changes were monitored during the cultivation in the STR with well-defined glucose starvation in the PFR. The biomass yield, the glucose uptake rate, and the oxygen and carbon dioxide transfer rates during the STR-PFR cultivation remained comparable to the undisturbed reference condition (**P-II**). In contrast, *E. coli's* biomass yield increased by 9% under similar experimental conditions which was attributed to growth arrest in the PFR zone (Löffler et al., 2016). Since *P. putida's* biomass yield remained constant, we conclude that cells continued to grow in the malnutrition zone inside the PFR (**P-II**).

The physiological behavior changed when *P. putida* cells faced oscillating oxygen supply during exponential growth in batch cultures. Hereby the biomass yields in the perturbed STR cultivations were similar to the control experiment, but the maximum growth rate was significantly reduced from 0.5 h^{-1} by almost 50% to 0.26 h^{-1} and the glucose uptake rate was diminished by 30% when exposed to oscillating dissolved oxygen tensions in the STR batch cultivation (**P-III**). Due to its strict aerobic nature, the growth of *P. putida* is bound to the uptake of oxygen. If dissolved oxygen in the medium gets depleted due to high consumption and reduced air supply, the cells are forced into a stationary state. When oxygen is supplied back to the medium, the cells continue to grow. In the case of dual starvation of oxygen and glucose inside the PFR, the overall growth performance of *P. putida* with a growth rate of 0.2 h^{-1} was hardly affected (**P-III**). Combining the results of the STR and STR-PFR experiments with oscillating oxygen availability indicates that growth rates should not exceed 0.26 h^{-1} in large-scale applications with *P. putida* to avoid performance losses.

4.2. Omics Studies Reveal Several Stress Regulation Measurements in *P. putida*

The stress response to e.g., starvation can occur on different cellular levels. This comprises transcriptional adaptations and regulations as well as proteomic, metabolic, and energetic alterations. The prediction of regions with high expression patterns helps to identify novel ncRNAs in *P. putida*, that are expressed during carbon starvation. Since small non-coding RNAs orchestrate bacterial adaptations to different stress situations through regulation on protein and mRNA levels (Waters and Storz, 2009), their detection and purpose are of utmost interest. Within this work, 725 putative ncRNAs were detected but their diverse function remains to be discovered (**P-I**). Several of these novel small RNAs were found to have expression levels above or below the mean value during repeated glucose oscillation in the STR-PFR system. It is worth noting that the cells exhibit only minor transcriptional regulations in the steady state after 25 h of the STR-PFR cultivation since the expression pattern of the 725 ncRNAs is nearly equal or slightly above the mean value whereas high expression

patterns were found 9 hours after connection of the PFR to the STR (**P-I**). A similar correlation was found for differentially expressed genes since only 65 genes were significantly up- or downregulated in the STR-PFR steady state in contrast to 615 DEGs that were detected 15 min after connection of the PFR (**P-II**). Moreover, significant changes were found in cells at the exit of the starvation zone of the PFR. According to the heatmap, most ncRNAs show expression levels below the mean value (**P-I**). Thus, glucose depletion seems to repress the expression of ncRNAs which was also found for glucose starving *Pectobacterium atrosepticum* (Kwenda et al., 2016). Only a few ncRNAs are expressed in higher abundance at the outlet of the PFR (**P-I**). Similarly, the majority of over 900 DEGs were downregulated (537 DEGs) as a short-term response to sudden glucose starvation at the outlet of the PFR (**P-II**). The results of the performed studies (**P-I, P-II**) highlight the ability of *P. putida* to adapt to changing circumstances in the long term and to quickly react to a stress situation such as starvation with intensified alterations on the transcriptome level. *P. putida's* constant growth characteristics emphasize the long-term adaptation of transcriptional regulations.

To be more precise, the cells reacted to glucose starvation with a measure similar to the stringent response. The genes *rpoS* and *relA* were upregulated, whereas *spoT* was found to be downregulated at the exit of the PFR with concomitantly significantly increased intracellular levels of ppGpp (**P-II**). The alarmone ppGpp is known to activate the stringent response in bacteria like *E. coli* (Ferenci, 2001; Hauryliuk et al., 2015) and the same regulation is anticipated for *P. putida*. Mozejko-Ciesielska et al. (2017) showed that ppGpp levels and *rpoS* transcripts were amplified during the transition from exponential growth to the stationary phase. The elevated intracellular levels of ppGpp at the exit of the PFR (**P-II**) are similar to the *E. coli* cells under the same conditions (Löffler et al., 2016). Furthermore, the ppGpp-mediated stringent response in *P. putida* seems to address intracellular carbon through upregulation of catabolic pathways during starvation. Genes coding for amino acid catabolism were significantly upregulated in the starvation zone which is in accordance with *E. coli* (Löffler et al., 2016). Moreover, significant upregulation was found for genes belonging to the β-oxidation cycle that is part of the PHA metabolism. Indeed, cells quickly degraded intracellular 3-hydroxyalkanoates during starvation in the PFR. By metabolizing these carbon storage compounds the cells could cover almost 80% of their ATP maintenance

demand during 128 s of carbon starvation. Thus, the degradation of these PHA precursors mediated by the stringent response provides a transient carbon buffer for the cells (**P-II**). It was recently shown that the stringent response is closely connected to the synthesis of PHA under nitrogen limitation. PHA accumulation was significantly lower in a *relA/spoT* deficient strain compared to the wild type (Dabrowska et al., 2020). In this work, it was illustrated that the degradation of intracellular 3-HAs provides sufficient carbon and energy equivalents like NAD(P)H and ATP for the cell to survive short-term glucose starvation with only minimal influence on the cells' energetic state **(P-II)**.

Reversible lactate formation as external carbon buffer during short-term oxygen starvation was also observed in *C. glutamicum* (Käß et al., 2014; Limberg et al., 2017). However, under dual starvation, *P. putida* could not recover its energy charge within the residence time in the PFR, even though the levels of the stringent response mediator ppGpp were elevated. Most presumably, a lack of oxygen as final electron acceptor blocks the electron transport via succinate dehydrogenase and thereby impairs the ATP synthase. This hypothesis is supported by reduced intracellular ATP and increased AMP levels during dual starvation and downregulation of enzymes that are related to the electron transport chain (**P-III**).

Proteomics analysis further revealed downregulation of the isocitrate lyase during oscillating DOTs. A reduced flux via this enzyme was found to increase the PHA synthesis (Klinke et al., 2000), however, 3-HA or PHA analysis was not performed in oxygen disturbed experiments. In accordance with Lieder et al. (2016), proteins that belong to the orthologous group of replication, recombination and repair were found with higher abundance as response to limited oxygen availability (**P-III**).

Since the response of the cell to transient nutrient depletion implies alterations and regulations on transcriptional, translational, and metabolic levels, additional energy must be spent by the cells. Transcriptional and translational costs added 17% on the non-growth associated maintenance (NGAM) demand in *P. putida* KT2440 (**P-II**). In *E. coli* the additional spent energy was even 30% of the NGAM as a response to glucose starvation (Löffler et al., 2016). In a recent study, it was shown that the stress-response deficient strain *E. coli* SR (Michalowski et al., 2017) exhibited a similar growth

performance compared to the wild type strain in an ammonium limited STR-PFR setup and significantly reduced the transcriptional short-term response by more than 50% (Ziegler et al., 2020) which is assumed to be even more pronounced in glucose-starved cells (compare Löffler et al. (2016) and Simen et al. (2017)). Thus, the knockout of the ppGpp-related gene *relA*, which was significantly upregulated in glucose-starved *P. putida* cells (**P-II**), might also lead to a reduced waste of energy in this organism. Since a *relA/spoT* mutant strain was still able to accumulate PHAs (Mozejko-Ciesielska et al., 2017), this knockout target should not impede *P putida's* ability to address the PHA precursors as carbon buffers during transient starvation. This gene engineering target will complement the list of top ATP-consuming genes proposed in **P-II** to create a streamlined *P. putida* mutant strain with low energy demand and optimized performance under industrial-scale conditions.

4.3. DOES THE SCALE-DOWN SYSTEM REALISTICALLY REFLECT LARGE-SCALE GRADIENTS?

Recent simulation studies based on Euler-Lagrange approaches (Haringa et al., 2017; Haringa et al., 2016) for tracking the lifelines of bacterial cells inside large-scale bioreactors predict lower mixing times (Hajian et al., 2020; Kuschel et al., 2017; Kuschel and Takors, 2020) compared to 128 s that was installed as residence time inside the starvation zone of the PFR (**P-I – P-III**). To be precise, computational fluid dynamics simulations recently showed that *C. glutamicum* cells exhibit different growth rates when circulating inside a large-scale bioreactor with zones of different oxygen and glucose concentrations (Kuschel and Takors, 2020). The authors predict varying residence times in regimes with different supplies of substrates. For example, the highest frequency of regime transitions was when cells crossed a low glucose regime from a transition zone with an average of 5.5 s but maximal 75.7 s. Since different transition possibilities with different residence times were predicted, the simulated growth of *C. glutamicum* was impaired (Kuschel and Takors, 2020). In a similar study,

Hajian et al. (2020) estimated a mixing time of approx. 40 s for a 54 m³ aerated stirred tank reactor. Based on their results the authors further propose the design of double STR-PFR systems with simulated zones of (i) overflow metabolism (carbon excess), (ii) substrate limitation, and (iii) starvation to realistically mimic lifelines of the cells in scale-down studies (Hajian et al., 2020). Considering this current knowledge about more accurate mixing times and the distribution of substrate regimes inside large bioreactors, the experimental conditions in these studies (**P-I** - **P-III)** resemble a rather extreme large-scale scenario. Consequently, its well-balanced performance under these intense circumstances emphasizes the outstanding suitability of *P. putida* KT2440 for production-scale applications.

4.4. *P. putida* Produced Isobutanol Micro-aerob and Counteracted Redox Imbalances by 2-KG Formation

Due to its high tolerance to solvents and alcohols, *P. putida* KT2440 is a promising host for the microbial synthesis of isobutanol. For this purpose, the Ehrlich pathway was introduced in *P. putida* GN346 (Simon et al., 2015), since this strain is unable to consume *n*-butanol. Its inability to consume isobutanol was proven within this study. Out of the different enzymes tested, the strain *P. putida* Iso2 showed the highest glucose to isobutanol conversion (22 mg$_{isobutanol}$ g$_{glucose}^{-1}$) reaching 120 mg L^{-1} in aerobic shake flask cultures (**P-IV**). This is the highest isobutanol titer reported for pseudomonads, but not competitive with other engineered strains (refer to Table 4). Among these, particularly *E. coli* and *C. glutamicum* variants converted glucose nearly equimolar into isobutanol (Blombach and Eikmanns, 2011). The main advantage of these bacteria compared to *Pseudomonas putida* is their capability of fermentative glucose metabolism which is important to balance the cell's redox and energy state during the absence of oxygen. Concomitantly, during anaerobic conditions the availability of the growth important cofactor NADPH is increased and can be used in the overexpressed L-valine pathway. In addition, the membrane-bound

transhydrogenase PntAB (Sauer et al., 2004) turned out to be the key factor for efficient isobutanol synthesis in *E. coli* and *C. glutamicum* (Bastian et al., 2011; Blombach et al., 2011; Blombach and Eikmanns, 2011), as it translocates protons from NADH onto NADPH. Since *P. putida* is endowed with the soluble and membrane-bound transhydrogenase (Nikel et al., 2016b), aerobic isobutanol production was only possible in strains (*P. putida* Iso2-4, Iso6) with the knockout of SthA (**P-IV**) that favors the oxidation of NADPH (Sauer et al., 2004). Nevertheless, one major drawback in isobutanol-producing *P. putida* strains was an immense side product formation of the organic acid 2-ketogluconate, exceeding 400 $mg_{2\text{-}KG}$ $g_{glucose}^{-1}$. Interestingly, the carbon loss into the by-product was reduced when cells were cultivated under oxygen-limited conditions in sealed shake flasks. The strain Iso6 with *kdcA* from *C. maltaromaticum* showed, besides strain Iso2, the highest micro-aerobic titer but also a high 2-KG formation. After knocking out the pathway for 2-KG via glucose dehydrogenase Gcd, neither 2-KG nor isobutanol was detected in the culture medium (**P-IV**). Similar observations concerning 2-KG formation were made with a *cis-cis* muconic acid producing *P. putida* strain (Bentley et al., 2020; Johnson et al., 2019).

With the purpose to unravel constraints and metabolite dynamics during the isobutanol production in *P. putida,* three different fed-batch cultivations with separated growth and production phases were performed at the scale of a controlled 30 L bioreactor (**P-V**). A deeper insight into carbon fluxes revealed limitations of NADPH during aerobic production. The overproduction of the NADPH-dependent L-valine and Ehrlich pathway in *P. putida* Iso2 overstrained the cell's natural NADPH surplus (Kohlstedt and Wittmann, 2019; Nikel et al., 2021; Nikel et al., 2015) by more than double. The sudden high NADPH demand after plasmid induction led to a reduction in the growth rate, which can be explained by the competition for this cofactor through anabolic reactions and isobutanol production from pyruvate. Although no side products, except 2-KIV and, to a lower extent L-valine, were detected in the glucose-limited fed-batch before plasmid induction, the cells apparently counteracted the imbalanced redox state by the increased formation of 2-KG, resulting in over 70 $g_{2\text{-}KG}$ L^{-1} after 6 hours of production. On the one hand, the NADPH demand for isobutanol formation competes with the NADPH dependent uptake of 2-KG (Nikel et al., 2015). On the other hand, the transhydrogenase PntAB presumably converts NADH into NADPH to maintain the redox balance. This is supported by reduced $NADP^+$ levels with simultaneous constant

NADPH levels. Since NADH plays a crucial role in the electron transport chain to generate ATP, the cell counteracted the reduced NADH supply through increased electron transport by periplasmatic oxidation of glucose to 2-KG (del Castillo et al., 2007; Ebert et al., 2011) which covered approx. 50% of the cell's ATP demand. Due to this immense side product formation, the isobutanol yield was not increased in the scaled-up process, but the highest reported titer of 3.35 $g_{isobutanol}$ L^{-1} was achieved for *P. putida*.

The two main drawbacks of side product formation and NADPH limitation during isobutanol production were resolved by installing a controlled micro-aerobic environment inside the bioreactor. Metabolic active but non-growing cells enabled high isobutanol production rates during micro-aerobic conditions which almost tripled the yield from 22 $mg_{isobutanol}$ $g_{glucose}^{-1}$ in shake flasks (**P-IV**) to 60 $mg_{isobutanol}$ $g_{glucose}^{-1}$ (0.09 C-mol C-$mol_{glucose}^{-1}$) in the bioreactor (**P-V**). A striking finding was that glucose uptake and thereby probably the generation of energy equivalents was observed in sealed shake flasks and in poorly aerated bioreactor cultivations for the strict aerobic *P. putida* (**P-IV**, **P-V**). However, micro-aerobic isobutanol production was restricted to extracellular available 2-KIV that was accumulated in the aerobic phase. In addition, intracellular accumulation of industrial relevant succinic acid (Fumagalli, 2003), was observed during micro-aerobic stationary glucose consumption (**P-V**). Hence, the findings from this thesis pave the way for future promising studies to exploit micro-aerobic applications with *P. putida* KT2440.

5. CONCLUSION & OUTLOOK

P. putida KT2440 is endowed with advantageous traits for its application as an industrial workhorse. Within this thesis, *P. putida* was proven to withstand single and dual nutrient starvation that often led to reduced growth and productivity when using other industrial workhorses. The cultivation under controlled limitation conditions allowed the identification of *P. putida's* versatile stress repertoires consisting of an interplay between small non-coding RNAs, mRNA transcripts, metabolomic, and proteomic alterations, partly initiated by the stringent response. To optimally mimic large-scale inhomogeneities in lab-scale, the STR-PFR system, which was used, could be extended with a second PFR to mirror glucose-excess zones and residence times in the starvation zone might be reduced to 75 s in future studies.

The capability of enduring fluctuating oxygen supply during bioreactor cultivations and tolerating the presence of solvents or alcohols renders *P. putida* KT2440 a suitable host for e.g., biphasic cultivation strategies with *in situ* product removal using ethyl decanoate for rhamnolipid (RL) recovery (Demling et al., 2020). In this regard, ethyl decanoate was shown to work properly for rhamnolipid (RL) recovery produced by *P. putida* (Demling et al., 2020). As presented in this thesis, similar amounts of RL were secreted during 2 min intervals of oxygen oscillations compared to the ideal aerated control experiment. These findings might contribute to optimizing industrial RL production (Bator et al., 2020; Tiso et al., 2020; Weimer et al., 2020) with *P. putida*.

Despite successful scale-up and production of isobutanol in *P. putida* (0.09 C-mol$_{isobutanol}$ mol$_{glucose}^{-1}$), the results imply a bias in the production kinetic and thus constrain further economic applications. Either cells exhibit high by-product formation during aerobic conditions, or micro-aerobic isobutanol formation is dependent on the amount of 2-KIV excreted during the fed-batch phase. No further isobutanol synthesis was observed after extracellular 2-KIV was depleted. With the current price of glucose, the isobutanol production with *P. putida* Iso2 (**P-V**) would cost 0.25 € per gram of

isobutanol, which does not include other production costs. Currently, the price for isobutanol is 0.03 € per gram of isobutanol. Thus, the production efficiency must be increased more than ten-fold to achieve economic benefits on an industrial scale with *P. putida.* Since a co-feed of formate was proven to benefit NADH regeneration rates in *P. putida* grown on glucose (Zobel et al., 2017), the addition of formate to *P. putida* Iso2 cultures might increase the NADH availability during aerobic isobutanol production. Consequently, the unwanted 2-KG formation might be diminished, leading to higher isobutanol product yields. Furthermore, equimolar isobutanol to glucose yields were achieved with the exchange of the NADPH dependent by the NADH-dependent enzymes in the production pathway or by overexpression of the transhydrogenase PntAB in *E. coli* (Bastian et al., 2011). Another approach for balancing the intracellular redox state was followed by Xu et al. (2019). The authors exchanged the native isocitrate dehydrogenase with a non-native NADH dependent analog which enhanced the NADPH-demanding L-lysine synthesis in *C. glutamicum* and restored the NADPH/NADH ratio to 1. Therefore, these metabolic and genetic modifications present easy-to-implement engineering approaches in the current isobutanol producing *P. putida* strain and are recommended for future studies. In particular, the high volumetric productivity during micro-aerobic isobutanol production which is competitive to anaerobic isobutanol production with *C. glutamicum* (Blombach et al., 2011) qualifies *P. putida* Iso2 as the ideal base strain to further optimize the synthesis of this C-4 alcohol. With a streamlined isobutanol-producing *P. putida* strain that optimally performs in industrial-scale processes, the share of biofuels that contribute to the renewable energy supply can potentially be greatly increased.

References

Anjum, A., Zuber, M., Zia, K.M., Noreen, A., Anjum, M.N., Tabasum, S., 2016. Microbial production of polyhydroxyalkanoates (PHAs) and its copolymers: A review of recent advancements. International journal of biological macromolecules 89, 161–174. https://doi.org/10.1016/j.ijbiomac.2016.04.069.

Askitosari, T.D., Berger, C., Tiso, T., Harnisch, F., Blank, L.M., Rosenbaum, M.A., 2020. Coupling an Electroactive *Pseudomonas putida* KT2440 with Bioelectrochemical Rhamnolipid Production. Microorganisms 8. https://doi.org/10.3390/microorganisms8121959.

Atsumi, S., Hanai, T., Liao, J.C., 2008. Non-fermentative pathways for synthesis of branched-chain higher alcohols as biofuels. Nature 451, 86–89. https://doi.org/10.1038/nature06450.

Atsumi, S., Higashide, W., Liao, J.C., 2009. Direct photosynthetic recycling of carbon dioxide to isobutyraldehyde. Nature biotechnology 27, 1177–1180. https://doi.org/10.1038/nbt.1586.

Atsumi, S., Wu, T.-Y., Eckl, E.-M., Hawkins, S.D., Buelter, T., Liao, J.C., 2010. Engineering the isobutanol biosynthetic pathway in *Escherichia coli* by comparison of three aldehyde reductase/alcohol dehydrogenase genes. Applied microbiology and biotechnology 85, 651–657. https://doi.org/10.1007/s00253-009-2085-6.

Baez, A., Cho, K.-M., Liao, J.C., 2011. High-flux isobutanol production using engineered *Escherichia coli*: a bioreactor study with in situ product removal. Applied microbiology and biotechnology 90, 1681–1690. https://doi.org/10.1007/s00253-011-3173-y.

Bagdasarian, M., Lurz, R., Rückert, B., Franklin, F., Bagdasarian, M.M., Frey, J., Timmis, K.N., 1981. Specific-purpose plasmid cloning vectors II. Broad host range, high copy number, RSF 1010-derived vectors, and a host-vector system

References

for gene cloning in *Pseudomonas*. Gene 16, 237–247. https://doi.org/10.1016/0378-1119(81)90080-9.

Bastian, S., Liu, X., Meyerowitz, J.T., Snow, C.D., Chen, M.M.Y., Arnold, F.H., 2011. Engineered ketol-acid reductoisomerase and alcohol dehydrogenase enable anaerobic 2-methylpropan-1-ol production at theoretical yield in *Escherichia coli*. Metabolic engineering 13, 345–352. https://doi.org/10.1016/j.ymben.2011.02.004.

Bator, I., Karmainski, T., Tiso, T., Blank, L.M., 2020. Killing Two Birds With One Stone - Strain Engineering Facilitates the Development of a Unique Rhamnolipid Production Process. Frontiers in bioengineering and biotechnology, 899. https://doi.org/10.3389/fbioe.2020.00899.

Beckers, V., Poblete-Castro, I., Tomasch, J., Wittmann, C., 2016. Integrated analysis of gene expression and metabolic fluxes in PHA-producing *Pseudomonas putida* grown on glycerol. Microbial cell factories 15, 73. https://doi.org/10.1186/s12934-016-0470-2.

Bentley, G.J., Narayanan, N., Jha, R.K., Salvachúa, D., Elmore, J.R., Peabody, G.L., Black, B.A., Ramirez, K., Capite, A. de, Michener, W.E., Werner, A.Z., Klingeman, D.M., Schindel, H.S., Nelson, R., Foust, L., Guss, A.M., Dale, T., Johnson, C.W., Beckham, G.T., 2020. Engineering glucose metabolism for enhanced muconic acid production in *Pseudomonas putida* KT2440. Metabolic engineering 59, 64–75. https://doi.org/10.1016/j.ymben.2020.01.001.

Blombach, B., Eikmanns, B.J., 2011. Current knowledge on isobutanol production with *Escherichia coli*, *Bacillus subtilis* and *Corynebacterium glutamicum*. Bioengineered bugs 2, 346–350. https://doi.org/10.4161/bbug.2.6.17845.

Blombach, B., Riester, T., Wieschalka, S., Ziert, C., Youn, J.-W., Wendisch, V.F., Eikmanns, B.J., 2011. *Corynebacterium glutamicum* tailored for efficient isobutanol production. Applied and environmental microbiology 77, 3300–3310. https://doi.org/10.1128/AEM.02972-10.

Brownstein, A.M., 2015. Isobutanol, in: Renewable Motor Fuels. Elsevier, pp. 47–56.

Brynildsen, M.P., Liao, J.C., 2009. An integrated network approach identifies the isobutanol response network of *Escherichia coli*. Molecular systems biology 5, 277. https://doi.org/10.1038/msb.2009.34.

References

Buchholz, J., Graf, M., Freund, A., Busche, T., Kalinowski, J., Blombach, B., Takors, R., 2014. CO_2/HCO_3^- perturbations of simulated large scale gradients in a scale-down device cause fast transcriptional responses in *Corynebacterium glutamicum*. Applied microbiology and biotechnology 98, 8563–8572. https://doi.org/10.1007/s00253-014-6014-y.

Bylund, F., Collet, E., Enfors, S.-O., Larsson, G., 1998. Substrate gradient formation in the large-scale bioreactor lowers cell yield and increases by-product formation. Bioprocess Engineering 18, 171. https://doi.org/10.1007/s004490050427.

Campbell-Platt, G., 1994. Fermented foods — a world perspective. Food Research International 27, 253–257. https://doi.org/10.1016/0963-9969(94)90093-0.

Chatterji, D., Kumar Ojha, A., 2001. Revisiting the stringent response, ppGpp and starvation signaling. Current opinion in microbiology 4, 160–165. https://doi.org/10.1016/S1369-5274(00)00182-X.

Chavarría, M., Nikel, P.I., Pérez-Pantoja, D., Lorenzo, V. de, 2013. The Entner-Doudoroff pathway empowers *Pseudomonas putida* KT2440 with a high tolerance to oxidative stress. Environ Microbiol 15, 1772–1785. https://doi.org/10.1111/1462-2920.12069.

Chen, C.-T., Liao, J.C., 2016. Frontiers in microbial 1-butanol and isobutanol production. FEMS microbiology letters 363, fnw020. https://doi.org/10.1093/femsle/fnw020.

Chen, E.C.-H., 1978. The Relative Contribution of Ehrlich and Biosynthetic Pathways to the Formation of Fusel Alcohols. Journal of the American Society of Brewing Chemists 36, 39–43. https://doi.org/10.1094/ASBCJ-36-0039.

Chianelli, R.R., Lyons, J.E., Mills, G., 1994. Chapter 9 catalysts for liquid transportation fuels from petroleum, coal, residual oil, and biomass. Catalysis Today 22, 361–396. https://doi.org/10.1016/0920-5861(94)80110-X.

Choi, K.-Y., Wernick, D.G., Tat, C.A., Liao, J.C., 2014. Consolidated conversion of protein waste into biofuels and ammonia using *Bacillus subtilis*. Metabolic engineering 23, 53–61. https://doi.org/10.1016/j.ymben.2014.02.007.

Crater, J.S., Lievense, J.C., 2018. Scale-up of industrial microbial processes. FEMS microbiology letters 365. https://doi.org/10.1093/femsle/fny138.

References

Dabrowska, D., Mozejko-Ciesielska, J., Pokój, T., Ciesielski, S., 2020. Transcriptome Changes in *Pseudomonas putida* KT2440 during Medium-Chain-Length Polyhydroxyalkanoate Synthesis Induced by Nitrogen Limitation. International journal of molecular sciences 22. https://doi.org/10.3390/ijms22010152.

Davis, R., Duane, G., Kenny, S.T., Cerrone, F., Guzik, M.W., Babu, R.P., Casey, E., O'Connor, K.E., 2015. High cell density cultivation of *Pseudomonas putida* KT2440 using glucose without the need for oxygen enriched air supply. Biotechnology and bioengineering 112, 725–733. https://doi.org/10.1002/bit.25474.

del Castillo, T., Ramos, J.L., Rodriguez-Herva, J.J., Fuhrer, T., Sauer, U., Duque, E., 2007. Convergent peripheral pathways catalyze initial glucose catabolism in *Pseudomonas putida*: genomic and flux analysis. Journal of Bacteriology 189, 5142–5152. https://doi.org/10.1128/JB.00203-07.

Delvigne, F., Takors, R., Mudde, R., van Gulik, W., Noorman, H., 2017. Bioprocess scale-up/down as integrative enabling technology: from fluid mechanics to systems biology and beyond. Microbial biotechnology 10, 1267–1274. https://doi.org/10.1111/1751-7915.12803.

Demling, P., Campenhausen, M. von, Grütering, C., Tiso, T., Jupke, A., Blank, L.M., 2020. Selection of a recyclable in situ liquid–liquid extraction solvent for foam-free synthesis of rhamnolipids in a two-phase fermentation. Green Chem. 22, 8495–8510. https://doi.org/10.1039/D0GC02885A.

Doi, Y., Segawa, A., Kawaguchi, Y., Kunioka, M., 1990. Cyclic nature of poly(3-hydroxyalkanoate) metabolism in *Alcaligenes eutrophus*. FEMS microbiology letters 55, 165–169. https://doi.org/10.1016/0378-1097(90)90188-v.

Dürre, P., 2007. Biobutanol: an attractive biofuel. Biotechnology journal 2, 1525–1534. https://doi.org/10.1002/biot.200700168.

Dvořák, P., Nikel, P.I., Damborský, J., Lorenzo, V. de, 2017. Bioremediation 3.0: Engineering pollutant-removing bacteria in the times of systemic biology. Biotechnology advances 35, 845–866. https://doi.org/10.1016/j.biotechadv.2017.08.001.

Ebert, B.E., Kurth, F., Grund, M., Blank, L.M., Schmid, A., 2011. Response of *Pseudomonas putida* KT2440 to increased NADH and ATP demand. Applied and environmental microbiology 77, 6597–6605. https://doi.org/10.1128/AEM.05588-11.

Elbahloul, Y., Steinbuchel, A., 2009. Large-scale production of poly(3-hydroxyoctanoic acid) by *Pseudomonas putida* GPo1 and a simplified downstream process. Applied and environmental microbiology 75, 643–651. https://doi.org/10.1128/AEM.01869-08.

Enfors, S.-O., Jahic, M., Rozkov, A., Xu, B., Hecker, M., Jürgen, B., Krüger, E., Schweder, T., Hamer, G., O'Beirne, D., Noisommit-Rizzi, N., Reuss, M., Boone, L., Hewitt, C., McFarlane, C., Nienow, A., Kovacs, T., Trägårdh, C., Fuchs, L., Revstedt, J., Friberg, P.C., Hjertager, B., Blomsten, G., Skogman, H., Hjort, S., Hoeks, F., Lin, H.-Y., Neubauer, P., van der Lans, R., Luyben, K., Vrabel, P., Manelius, Å., 2001. Physiological responses to mixing in large scale bioreactors. Journal of Biotechnology 85, 175–185. https://doi.org/10.1016/S0168-1656(00)00365-5.

Escapa, I.F., García, J.L., Bühler, B., Blank, L.M., Prieto, M.A., 2012. The polyhydroxyalkanoate metabolism controls carbon and energy spillage in *Pseudomonas putida*. Environmental Microbiology 14, 1049–1063. https://doi.org/10.1111/j.1462-2920.2011.02684.x.

Eschbach, M., Schreiber, K., Trunk, K., Buer, J., Jahn, D., Schobert, M., 2004. Long-term anaerobic survival of the opportunistic pathogen *Pseudomonas aeruginosa* via pyruvate fermentation. J Bacteriol 186, 4596–4604. https://doi.org/10.1128/JB.186.14.4596-4604.2004.

European Commission, 2020. EU energy in figures: statistical pocketbook 2020. Publications Office of the European Union.

Ferenci, T., 2001. Hungry bacteria - definition and properties of a nutritional state. Environ Microbiol 3, 605–611. https://doi.org/10.1046/j.1462-2920.2001.00238.x.

Fleming, A., 1929. On the Antibacterial Action of Cultures of a *Penicillium*, with Special Reference to their Use in the Isolation of *B. influenzae* Br J Exp Pathol 10, 226–236.

References

Fuhrer, T., Sauer, U., 2009. Different biochemical mechanisms ensure network-wide balancing of reducing equivalents in microbial metabolism. Journal of Bacteriology 191, 2112–2121. https://doi.org/10.1128/JB.01523-08.

Fulco, A.J., 1983. Fatty acid metabolism in bacteria. Progress in Lipid Research 22, 133–160. https://doi.org/10.1016/0163-7827(83)90005-X.

Fumagalli, C., 2003. Succinic Acid and Succinic Anhydride, in: Kirk, R.E., Othmer, D.F. (Eds.), Encyclopedia of chemical technology. Wiley, New York, NY.

Gentry, D.R., Hernandez, V.J., Nguyen, L.H., Jensen, D.B., Cashel, M., 1993. Synthesis of the stationary-phase sigma factor sigma s is positively regulated by ppGpp. J Bacteriol 175, 7982–7989. https://doi.org/10.1128/jb.175.24.7982-7989.1993.

Gorenflo, V., Schmack, G., Vogel, R., Steinbüchel, A., 2001. Development of a Process for the Biotechnological Large-Scale Production of 4-Hydroxyvalerate-Containing Polyesters and Characterization of Their Physical and Mechanical Properties. Biomacromolecules 2, 45–57. https://doi.org/10.1021/bm0000992.

Gottesman, S., Storz, G., 2011. Bacterial small RNA regulators: versatile roles and rapidly evolving variations. Cold Spring Harbor perspectives in biology 3. https://doi.org/10.1101/cshperspect.a003798.

Gross, T., 1995. Introductory microbiology, 1st ed. Chapman & Hall, London, 414 pp.

Hajian, C.S.S., Zieringer, J., Takors, R., 2020. Euler-Lagrangian Simulations: A Proper Tool for Predicting Cellular Performance in Industrial Scale Bioreactors. Advances in biochemical engineering/biotechnology. https://doi.org/10.1007/10_2020_133.

Hara, K.Y., Kondo, A., 2015. ATP regulation in bioproduction. Microbial cell factories 14, 198. https://doi.org/10.1186/s12934-015-0390-6.

Hardiman, T., Lemuth, K., Keller, M.A., Reuss, M., Siemann-Herzberg, M., 2007. Topology of the global regulatory network of carbon limitation in *Escherichia coli*. Journal of Biotechnology 132, 359–374. https://doi.org/10.1016/j.jbiotec.2007.08.029.

References

Haringa, C., Deshmukh, A.T., Mudde, R.F., Noorman, H.J., 2017. Euler-Lagrange analysis towards representative down-scaling of a 22 m 3 aerobic *S. cerevisiae* fermentation. Chemical Engineering Science 170, 653–669. https://doi.org/10.1016/j.ces.2017.01.014.

Haringa, C., Tang, W., Deshmukh, A.T., Xia, J., Reuss, M., Heijnen, J.J., Mudde, R.F., Noorman, H.J., 2016. Euler-Lagrange computational fluid dynamics for (bio)reactor scale down: An analysis of organism lifelines. Eng. Life Sci. 16, 652–663. https://doi.org/10.1002/elsc.201600061.

Hauryliuk, V., Atkinson, G.C., Murakami, K.S., Tenson, T., Gerdes, K., 2015. Recent functional insights into the role of (p)ppGpp in bacterial physiology. Nature reviews. Microbiology 13, 298–309. https://doi.org/10.1038/nrmicro3448.

Herbert, D., Elsworth, R., Telling, R.C., 1956. The continuous culture of bacteria; a theoretical and experimental study. Journal of general microbiology 14, 601–622. https://doi.org/10.1099/00221287-14-3-601.

Hermann, B.G., Patel, M., 2007. Today's and tomorrow's bio-based bulk chemicals from white biotechnology: a techno-economic analysis. Applied biochemistry and biotechnology 136, 361–388. https://doi.org/10.1007/s12010-007-9031-9.

Hermann, M., Teleki, A., Weitz, S., Niess, A., Freund, A., Bengelsdorf, F.R., Dürre, P., Takors, R., 2021. Identifying and Engineering Bottlenecks of Autotrophic Isobutanol Formation in Recombinant *C. ljungdahlii* by Systemic Analysis. Frontiers in bioengineering and biotechnology 9, 647853. https://doi.org/10.3389/fbioe.2021.647853.

Higashide, W., Li, Y., Yang, Y., Liao, J.C., 2011. Metabolic engineering of *Clostridium cellulolyticum* for production of isobutanol from cellulose. Appl. Environ. Microbiol. 77, 2727–2733. https://doi.org/10.1128/AEM.02454-10.

Hintermayer, S.B., Weuster-Botz, D., 2017. Experimental validation of in silico estimated biomass yields of *Pseudomonas putida* KT2440. Biotechnology journal 12. https://doi.org/10.1002/biot.201600720.

Hortsch, R., Corvo, P., 2020. The Biorefinery Concept: Producing Cellulosic Ethanol from Agricultural Residues. Chemie Ingenieur Technik 92, 1803–1809. https://doi.org/10.1002/cite.202000203.

References

Hsiang, S., Kopp, R.E., 2018. An Economist's Guide to Climate Change Science. Journal of Economic Perspectives 32, 3–32. https://doi.org/10.1257/jep.32.4.3.

Huijberts, G.N., Eggink, G., Waard, P.d., Huisman, G.W., Witholt, B., 1992. *Pseudomonas putida* KT2442 cultivated on glucose accumulates poly(3-hydroxyalkanoates) consisting of saturated and unsaturated monomers. Appl. Environ. Microbiol. 58, 536–544.

Humphrey, A., 1998. Shake Flask to Fermentor: What Have We Learned? Biotechnol. Prog. 14, 3–7. https://doi.org/10.1021/bp970130k.

IEA, 2020. World Energy Balances: Overview. https://www.iea.org/reports/world-energy-balances-overview (last accessed 02. October 2021).

Johnson, C.W., Salvachúa, D., Rorrer, N.A., Black, B.A., Vardon, D.R., St. John, P.C., Cleveland, N.S., Dominick, G., Elmore, J.R., Grundl, N., Khanna, P., Martinez, C.R., Michener, W.E., Peterson, D.J., Ramirez, K.J., Singh, P., VanderWall, T.A., Wilson, A.N., Yi, X., Biddy, M.J., Bomble, Y.J., Guss, A.M., Beckham, G.T., 2019. Innovative Chemicals and Materials from Bacterial Aromatic Catabolic Pathways. Joule 3, 1523–1537. https://doi.org/10.1016/j.joule.2019.05.011.

Jones, D.T., Woods, D.R., 1986. Acetone-butanol fermentation revisited. Microbiological Reviews 50, 484–524.

Junker, B.H., 2004. Scale-up methodologies for *Escherichia coli* and yeast fermentation processes. Journal of bioscience and bioengineering 97, 347–364. https://doi.org/10.1016/S1389-1723(04)70218-2.

Kampers, L.F.C., Koehorst, J.J., van Heck, R.J.A., Suarez-Diez, M., Stams, A.J.M., Schaap, P.J., 2021. A metabolic and physiological design study of *Pseudomonas putida* KT2440 capable of anaerobic respiration. BMC microbiology 21, 9. https://doi.org/10.1186/s12866-020-02058-1.

Kampers, L.F.C., van Heck, R.G.A., Donati, S., Saccenti, E., Volkers, R.J.M., Schaap, P.J., Suarez-Diez, M., Nikel, P.I., Martins Dos Santos, V.A.P., 2019a. In silico-guided engineering of *Pseudomonas putida* towards growth under micro-oxic conditions. Microbial cell factories 18, 179. https://doi.org/10.1186/s12934-019-1227-5.

References

Kampers, L.F.C., Volkers, R.J.M., Martins Dos Santos, V.A.P., 2019b. *Pseudomonas putida* KT2440 is HV1 certified, not GRAS. Microbial biotechnology 12, 845–848. https://doi.org/10.1111/1751-7915.13443.

Kar, T., Destain, J., Thonart, P., Delvigne, F., 2010. Impact of scaled-down on dissolved oxygen fluctuations at different levels of the lipase synthesis pathway of *Yarrowia lipolytica*. Biotechnologie, Agronomie, Société et Environnement 14, 523–529.

Kar, T., Destain, J., Thonart, P., Delvigne, F., 2012. Scale-down assessment of the sensitivity of *Yarrowia lipolytica* to oxygen transfer and foam management in bioreactors: investigation of the underlying physiological mechanisms. Journal of industrial microbiology & biotechnology 39, 337–346. https://doi.org/10.1007/s10295-011-1030-8.

Käß, F., Junne, S., Neubauer, P., Wiechert, W., Oldiges, M., 2014. Process inhomogeneity leads to rapid side product turnover in cultivation of *Corynebacterium glutamicum*. Microbial cell factories 13, 6. https://doi.org/10.1186/1475-2859-13-6.

Kim, J., Park, W., 2014. Oxidative stress response in *Pseudomonas putida*. Applied microbiology and biotechnology 98, 6933–6946. https://doi.org/10.1007/s00253-014-5883-4.

King, D.A., 2004. Environment. Climate change science: adapt, mitigate, or ignore? Science (New York, N.Y.) 303, 176–177. https://doi.org/10.1126/science.1094329.

Klinke, S., Dauner, M., Scott, G., Kessler, B., Witholt, B., 2000. Inactivation of isocitrate lyase leads to increased production of medium-chain-length poly(3-hydroxyalkanoates) in *Pseudomonas putida*. Appl Environ Microbiol 66, 909–913. https://doi.org/10.1128/aem.66.3.909-913.2000.

Kohlstedt, M., Starck, S., Barton, N., Stolzenberger, J., Selzer, M., Mehlmann, K., Schneider, R., Pleissner, D., Rinkel, J., Dickschat, J.S., Venus, J., van B J H Duuren, J., Wittmann, C., 2018. From lignin to nylon: Cascaded chemical and biochemical conversion using metabolically engineered *Pseudomonas putida*. Metabolic engineering 47, 279–293. https://doi.org/10.1016/j.ymben.2018.03.003.

References

Kohlstedt, M., Wittmann, C., 2019. GC-MS-based 13C metabolic flux analysis resolves the parallel and cyclic glucose metabolism of *Pseudomonas putida* KT2440 and *Pseudomonas aeruginosa* PAO1. Metabolic engineering 54, 35–53. https://doi.org/10.1016/j.ymben.2019.01.008.

Kuschel, M., Siebler, F., Takors, R., 2017. Lagrangian Trajectories to Predict the Formation of Population Heterogeneity in Large-Scale Bioreactors. Bioengineering (Basel, Switzerland) 4. https://doi.org/10.3390/bioengineering4020027.

Kuschel, M., Takors, R., 2020. Simulated oxygen and glucose gradients as a prerequisite for predicting industrial scale performance a priori. Biotechnology and bioengineering 117, 2760–2770. https://doi.org/10.1002/bit.27457.

Kwenda, S., Gorshkov, V., Ramesh, A.M., Naidoo, S., Rubagotti, E., Birch, P.R.J., Moleleki, L.N., 2016. Discovery and profiling of small RNAs responsive to stress conditions in the plant pathogen *Pectobacterium atrosepticum*. BMC genomics 17, 47. https://doi.org/10.1186/s12864-016-2376-0.

Lai, B., Yu, S., Bernhardt, P.V., Rabaey, K., Virdis, B., Krömer, J.O., 2016. Anoxic metabolism and biochemical production in *Pseudomonas putida* F1 driven by a bioelectrochemical system. Biotechnology for biofuels 9, 39. https://doi.org/10.1186/s13068-016-0452-y.

Lan, E.I., Liao, J.C., 2013. Microbial synthesis of n-butanol, isobutanol, and other higher alcohols from diverse resources. Bioresource technology 135, 339–349. https://doi.org/10.1016/j.biortech.2012.09.104.

Lang, K., Zierow, J., Buehler, K., Schmid, A., 2014. Metabolic engineering of *Pseudomonas sp.* strain VLB120 as platform biocatalyst for the production of isobutyric acid and other secondary metabolites. Microbial cell factories 13, 2. https://doi.org/10.1186/1475-2859-13-2.

Lange, J., Münch, E., Müller, J., Busche, T., Kalinowski, J., Takors, R., Blombach, B., 2018. Deciphering the Adaptation of *Corynebacterium glutamicum* in Transition from Aerobiosis via Microaerobiosis to Anaerobiosis. Genes 9. https://doi.org/10.3390/genes9060297.

Lange, J., Takors, R., Blombach, B., 2017. Zero-growth bioprocesses: A challenge for microbial production strains and bioprocess engineering. Engineering in Life Sciences 17, 27–35. https://doi.org/10.1002/elsc.201600108.

Lara, A.R., Galindo, E., Ramírez, O.T., Palomares, L.A., 2006a. Living With Heterogeneities in Bioreactors: Understanding the Effects of Environmental Gradients on Cells. MB 34, 355–382. https://doi.org/10.1385/MB:34:3:355.

Lara, A.R., Leal, L., Flores, N., Gosset, G., Bolivar, F., Ramirez, O.T., 2006b. Transcriptional and metabolic response of recombinant *Escherichia coli* to spatial dissolved oxygen tension gradients simulated in a scale-down system. Biotechnology and bioengineering 93, 372–385. https://doi.org/10.1002/bit.20704.

Li, H., Opgenorth, P.H., Wernick, D.G., Rogers, S., Wu, T.-Y., Higashide, W., Malati, P., Huo, Y.-X., Cho, K.M., Liao, J.C., 2012. Integrated electromicrobial conversion of CO_2 to higher alcohols. Science 335, 1596. https://doi.org/10.1126/science.1217643.

Li, S., Wen, J., Jia, X., 2011. Engineering *Bacillus subtilis* for isobutanol production by heterologous Ehrlich pathway construction and the biosynthetic 2-ketoisovalerate precursor pathway overexpression. Applied microbiology and biotechnology 91, 577–589. https://doi.org/10.1007/s00253-011-3280-9.

Lieder, S., Jahn, M., Koepff, J., Muller, S., Takors, R., 2016. Environmental stress speeds up DNA replication in *Pseudomonas putida* in chemostat cultivations. Biotechnology journal 11, 155–163. https://doi.org/10.1002/biot.201500059.

Limberg, M.H., Schulte, J., Aryani, T., Mahr, R., Baumgart, M., Bott, M., Wiechert, W., Oldiges, M., 2017. Metabolic profile of 1,5-diaminopentane producing *Corynebacterium glutamicum* under scale-down conditions: Blueprint for robustness to bioreactor inhomogeneities. Biotechnol. Bioeng. 114, 560–575. https://doi.org/10.1002/bit.26184.

Lin, P.P., Mi, L., Morioka, A.H., Yoshino, K.M., Konishi, S., Xu, S.C., Papanek, B.A., Riley, L.A., Guss, A.M., Liao, J.C., 2015. Consolidated bioprocessing of cellulose to isobutanol using *Clostridium thermocellum*. Metabolic engineering 31, 44–52. https://doi.org/10.1016/j.ymben.2015.07.001.

References

Lin, P.P., Rabe, K.S., Takasumi, J.L., Kadisch, M., Arnold, F.H., Liao, J.C., 2014. Isobutanol production at elevated temperatures in thermophilic *Geobacillus thermoglucosidasius*. Metabolic engineering 24, 1–8. https://doi.org/10.1016/j.ymben.2014.03.006.

Löffler, M., Simen, J.D., Jager, G., Schaferhoff, K., Freund, A., Takors, R., 2016. Engineering *E. coli* for Large-Scale Production - Strategies Considering ATP Expenses and Transcriptional Responses. Metabolic engineering. https://doi.org/10.1016/j.ymben.2016.06.008.

Lorantfy, B., Jazini, M., Herwig, C., 2013. Investigation of the physiological response to oxygen limited process conditions of *Pichia pastoris* Mut+ strain using a two-compartment scale-down system. Journal of bioscience and bioengineering 116, 371–379. https://doi.org/10.1016/j.jbiosc.2013.03.021.

Lorenzo, V. de, 2008. Systems biology approaches to bioremediation. Current Opinion in Biotechnology 19, 579–589. https://doi.org/10.1016/j.copbio.2008.10.004.

Love, M.I., Huber, W., Anders, S., 2014. Moderated estimation of fold change and dispersion for RNA-seq data with DESeq2. Genome Biol 15, 550.

M. Patel, M. Crank, V. Dornberg, B. Hermann, L. Roes, B. Hüsing, L.S. van Overbeek, F. Terragni, E. Recchia, Patel, M., Crank, M., Dornberg, V., Hermann, B., Roes, L., Hüsing, B., van Overbeek, L.S., Terragni, F., Recchia, E., 2006. Medium and long-term opportunities and risk of the biotechnological production of bulk chemicals from renewable resources - The potential of white biotechnology. Utrecht University, Department of Science, Technology and Society (STS) / Copernicus Institute. Utrecht University, Department of Science, Technology and Society (STS) / Copernicus Institute, Utrecht, -UR - https://library.wur.nl/webquery/wurpubs/reports/411452.

Marketysers Global Consulting LLP, 2020. Isobutanol Market To Reach USD 1.56 Billion By 2027. https://www.reportsanddata.com/press-release/global-isobutanol-market (last accessed 02. October 2021).

Matsuda, F., Ishii, J., Kondo, T., Ida, K., Tezuka, H., Kondo, A., 2013. Increased isobutanol production in *Saccharomyces cerevisiae* by eliminating competing

pathways and resolving cofactor imbalance. Microbial cell factories 12, 119. https://doi.org/10.1186/1475-2859-12-119.

Michaelis, L., Menten, M.L., 1913. Kinetik der Invertinwirkung. Biochem. Zeitung 1913, 333–369.

Michalowski, A., Siemann-Herzberg, M., Takors, R., 2017. *Escherichia coli* HGT: Engineered for high glucose throughput even under slowly growing or resting conditions. Metabolic engineering 40, 93–103. https://doi.org/10.1016/j.ymben.2017.01.005.

Monod, J., 1949. The Growth of Bacterial Cultures. Annual review of microbiology 3, 371–394. https://doi.org/10.1146/annurev.mi.03.100149.002103.

Monod, J., 1950. La technique de culture continue: Théorie et applications. Annales de L'Institut Pasteur, 184–204.

Mozejko-Ciesielska, J., Dabrowska, D., Szalewska-Palasz, A., Ciesielski, S., 2017. Medium-chain-length polyhydroxyalkanoates synthesis by *Pseudomonas putida* KT2440 relA/spoT mutant: Bioprocess characterization and transcriptome analysis. AMB Express 7, 92. https://doi.org/10.1186/s13568-017-0396-z.

Mozejko-Ciesielska, J., Pokoj, T., Ciesielski, S., 2018. Transcriptome remodeling of *Pseudomonas putida* KT2440 during mcl-PHAs synthesis: effect of different carbon sources and response to nitrogen stress. Journal of industrial microbiology & biotechnology 45, 433–446. https://doi.org/10.1007/s10295-018-2042-4.

Nakazawa, T., 2002. Travels of a *Pseudomonas*, from Japan around the world. Environ Microbiol 4, 782–786. https://doi.org/10.1046/j.1462-2920.2002.00310.x.

Nelson, K.E., Weinel, C., Paulsen, I.T., Dodson, R.J., Hilbert, H., Martins dos Santos, V.A.P., Fouts, D.E., Gill, S.R., Pop, M., Holmes, M., Brinkac, L., Beanan, M., DeBoy, R.T., Daugherty, S., Kolonay, J., Madupu, R., Nelson, W., White, O., Peterson, J., Khouri, H., Hance, I., Chris Lee, P., Holtzapple, E., Scanlan, D., Tran, K., Moazzez, A., Utterback, T., Rizzo, M., Lee, K., Kosack, D., Moestl, D., Wedler, H., Lauber, J., Stjepandic, D., Hoheisel, J., Straetz, M., Heim, S., Kiewitz, C., Eisen, J.A., Timmis, K.N., Düsterhöft, A., Tümmler, B., Fraser, C.M., 2002. Complete genome sequence and comparative analysis of the metabolically

versatile *Pseudomonas putida* KT2440. Environ Microbiol 4, 799–808. https://doi.org/10.1046/j.1462-2920.2002.00366.x.

Neubauer, P., Haggstrom, L., Enfors, S.O., 1995. Influence of substrate oscillations on acetate formation and growth yield in *Escherichia coli* glucose limited fed-batch cultivations. Biotechnology and bioengineering 47, 139–146. https://doi.org/10.1002/bit.260470204.

Neubauer, P., Junne, S., 2010. Scale-down simulators for metabolic analysis of large-scale bioprocesses. Current Opinion in Biotechnology 21, 114–121. https://doi.org/10.1016/j.copbio.2010.02.001.

Nikel, P.I., Chavarria, M., Danchin, A., Lorenzo, V. de, 2016a. From dirt to industrial applications: *Pseudomonas putida* as a Synthetic Biology chassis for hosting harsh biochemical reactions. Current opinion in chemical biology 34, 20–29. https://doi.org/10.1016/j.cbpa.2016.05.011.

Nikel, P.I., Chavarria, M., Fuhrer, T., Sauer, U., Lorenzo, V. de, 2015. *Pseudomonas putida* KT2440 Strain Metabolizes Glucose through a Cycle Formed by Enzymes of the Entner-Doudoroff, Embden-Meyerhof-Parnas, and Pentose Phosphate Pathways. The Journal of biological chemistry 290, 25920–25932. https://doi.org/10.1074/jbc.M115.687749.

Nikel, P.I., Fuhrer, T., Chavarría, M., Sánchez-Pascuala, A., Sauer, U., Lorenzo, V. de, 2021. Reconfiguration of metabolic fluxes in *Pseudomonas putida* as a response to sub-lethal oxidative stress. The ISME journal. https://doi.org/10.1038/s41396-020-00884-9.

Nikel, P.I., Lorenzo, V. de, 2013. Engineering an anaerobic metabolic regime in *Pseudomonas putida* KT2440 for the anoxic biodegradation of 1,3-dichloroprop-1-ene. Metabolic engineering 15, 98–112. https://doi.org/10.1016/j.ymben.2012.09.006.

Nikel, P.I., Lorenzo, V. de, 2014. Robustness of *Pseudomonas putida* KT2440 as a host for ethanol biosynthesis. New biotechnology 31, 562–571. https://doi.org/10.1016/j.nbt.2014.02.006.

References

Nikel, P.I., Martinez-Garcia, E., Lorenzo, V. de, 2014. Biotechnological domestication of *pseudomonads* using synthetic biology. Nature reviews. Microbiology 12, 368–379. https://doi.org/10.1038/nrmicro3253.

Nikel, P.I., Pérez-Pantoja, D., Lorenzo, V. de, 2016b. Pyridine nucleotide transhydrogenases enable redox balance of *Pseudomonas putida* during biodegradation of aromatic compounds. Environmental Microbiology 18, 3565–3582. https://doi.org/10.1111/1462-2920.13434.

Novick, A., Szilard, L., 1950. Description of the Chemostat. Science 112, 715–716. https://doi.org/10.1126/science.112.2920.715.

Panikov, N.S., 1995. Microbial growth kinetics, 1st ed. Chapman & Hall, London, 378 pp.

Pasteur, L., 1862. Quelques résultats nouveaux relatifs aux fermentations acétique et butyrique. Bull Soc Chim Paris, 52–53.

Pirt, S.J., 1974. The theory of fed batch culture with reference to the penicillin fermentation. J. Appl. Chem. 24, 415–424. https://doi.org/10.1002/JCTB.2720240706.

Pirt, S.J., 1979. FED-BATCH CULTURE OF MICROBES. Ann NY Acad Sci 326, 119–125. https://doi.org/10.1111/j.1749-6632.1979.tb14156.x.

Poblete-Castro, I., Binger, D., Rodrigues, A., Becker, J., Martins Dos Santos, V.A.P., Wittmann, C., 2013. In-silico-driven metabolic engineering of *Pseudomonas putida* for enhanced production of poly-hydroxyalkanoates. Metabolic engineering 15, 113–123. https://doi.org/10.1016/j.ymben.2012.10.004.

Poblete-Castro, I., Escapa, I.F., Jäger, C., Puchalka, J., Lam, C.M.C., Schomburg, D., Prieto, M.A., Martins dos Santos, V.A.P., 2012. The metabolic response of *P. putida* KT2442 producing high levels of polyhydroxyalkanoate under single- and multiple-nutrient-limited growth: highlights from a multi-level omics approach. Microbial cell factories 11, 34. https://doi.org/10.1186/1475-2859-11-34.

Poblete-Castro, I., Rodriguez, A.L., Lam, C.M.C., Kessler, W., 2014. Improved production of medium-chain-length polyhydroxyalkanoates in glucose-based fed-batch cultivations of metabolically engineered *Pseudomonas putida* strains. Journal of microbiology and biotechnology 24, 59–69.

Potrykus, K., Cashel, M., 2008. (p)ppGpp: Still magical? Annual review of microbiology 62, 35–51. https://doi.org/10.1146/annurev.micro.62.081307.162903.

Prieto, A., Escapa, I.F., Martínez, V., Dinjaski, N., Herencias, C., La Peña, F. de, Tarazona, N., Revelles, O., 2016. A holistic view of polyhydroxyalkanoate metabolism in *Pseudomonas putida*. Environmental Microbiology 18, 341–357. https://doi.org/10.1111/1462-2920.12760.

Qiu, M., Shen, W., Yan, X., He, Q., Cai, D., Chen, S., Wei, H., Knoshaug, E.P., Zhang, M., Himmel, M.E., Yang, S., 2020. Metabolic engineering of *Zymomonas mobilis* for anaerobic isobutanol production. Biotechnology for biofuels 13, 15. https://doi.org/10.1186/s13068-020-1654-x.

Raghavan, P., Vivekanandan, M., 1999. Bioremediation of oil-spilled sites through seeding of naturally adapted *Pseudomonas putida*. International Biodeterioration & Biodegradation 44, 29–32. https://doi.org/10.1016/S0964-8305(99)00048-7.

Ramos, J.-L., Sol Cuenca, M., Molina-Santiago, C., Segura, A., Duque, E., Gomez-Garcia, M.R., Udaondo, Z., Roca, A., 2015. Mechanisms of solvent resistance mediated by interplay of cellular factors in *Pseudomonas putida*. FEMS microbiology reviews 39, 555–566. https://doi.org/10.1093/femsre/fuv006.

Ramos-González, M.I., Molin, S., 1998. Cloning, Sequencing, and Phenotypic Characterization of the rpoS Gene from *Pseudomonas putida* KT2440. Journal of Bacteriology 180, 3421–3431.

Rarbach, M., Söltl, Y., 2013. sunliquid(®): Sustainable and competitive cellulosic ethanol from agricultural residues. Chimia 67, 732–734. https://doi.org/10.2533/chimia.2013.732.

Riesenberg, D., Guthke, R., 1999. High-cell-density cultivation of microorganisms. Applied microbiology and biotechnology 51, 422–430. https://doi.org/10.1007/s002530051412.

Rühl, J., Schmid, A., Blank, L.M., 2009. Selected *Pseudomonas putida* strains able to grow in the presence of high butanol concentrations. Appl. Environ. Microbiol. 75, 4653–4656. https://doi.org/10.1128/AEM.00225-09.

Ruth, K., Roo, G. de, Egli, T., Ren, Q., 2008. Identification of two acyl-CoA synthetases from *Pseudomonas putida* GPo1: One is located at the surface of

polyhydroxyalkanoates granules. Biomacromolecules 9, 1652–1659. https://doi.org/10.1021/bm8001655.

Sauer, U., Canonaco, F., Heri, S., Perrenoud, A., Fischer, E., 2004. The soluble and membrane-bound transhydrogenases UdhA and PntAB have divergent functions in NADPH metabolism of *Escherichia coli*. J. Biol. Chem. 279, 6613–6619. https://doi.org/10.1074/jbc.M311657200.

Sauer, U., Fischer, R., Dürre, P., 1993. Solvent formation and its regulation in strictly anaerobic bacteria. Curr. Top. Mol. Genet 1, 337–351.

Schmitz, S., Nies, S., Wierckx, N., Blank, L.M., Rosenbaum, M.A., 2015. Engineering mediator-based electroactivity in the obligate aerobic bacterium *Pseudomonas putida* KT2440. Frontiers in microbiology 6, 284. https://doi.org/10.3389/fmicb.2015.00284.

Schweder, T., Krüger, E., Xu, B., Jürgen, B., Blomsten, G., Enfors, S.-O., Hecker, M., 1999. Monitoring of genes that respond to process-related stress in large-scale bioprocesses. Biotechnol. Bioeng. 65, 151–159. https://doi.org/10.1002/(SICI)1097-0290(19991020)65:2<151:AID-BIT4>3.3.CO;2-M.

Simen, J.D., Löffler, M., Jager, G., Schaferhoff, K., Freund, A., Matthes, J., Muller, J., Takors, R., 2017. Transcriptional response of *Escherichia coli* to ammonia and glucose fluctuations. Microbial biotechnology. https://doi.org/10.1111/1751-7915.12713.

Simon, O., Klebensberger, J., Mukschel, B., Klaiber, I., Graf, N., Altenbuchner, J., Huber, A., Hauer, B., Pfannstiel, J., 2015. Analysis of the molecular response of *Pseudomonas putida* KT2440 to the next-generation biofuel n-butanol. Journal of proteomics 122, 11–25. https://doi.org/10.1016/j.jprot.2015.03.022.

Smith, K.M., Cho, K.-M., Liao, J.C., 2010. Engineering *Corynebacterium glutamicum* for isobutanol production. Applied microbiology and biotechnology 87, 1045–1055. https://doi.org/10.1007/s00253-010-2522-6.

Sohn, S.B., Kim, T.Y., Park, J.M., Lee, S.Y., 2010. In silico genome-scale metabolic analysis of *Pseudomonas putida* KT2440 for polyhydroxyalkanoate synthesis,

degradation of aromatics and anaerobic survival. Biotechnology journal 5, 739–750. https://doi.org/10.1002/biot.201000124.

Soini, J., Ukkonen, K., Neubauer, P., 2008. High cell density media for *Escherichia coli* are generally designed for aerobic cultivations – consequences for large-scale bioprocesses and shake flask cultures. Microbial cell factories 7, 26. https://doi.org/10.1186/1475-2859-7-26.

Spaans, S.K., Weusthuis, R.A., van der Oost, J., Kengen, S.W.M., 2015. NADPH-generating systems in bacteria and archaea. Frontiers in microbiology 6, 742. https://doi.org/10.3389/fmicb.2015.00742.

Stanier, R.Y., Palleroni, N.J., Doudoroff, M., 1966. The aerobic *pseudomonads*: a taxonomic study. Journal of general microbiology 43, 159–271. https://doi.org/10.1099/00221287-43-2-159.

Steen, A., Utkür, F.Ö., Borrero-de Acuña, J.M., Bunk, B., Roselius, L., Bühler, B., Jahn, D., Schobert, M., 2013. Construction and characterization of nitrate and nitrite respiring *Pseudomonas putida* KT2440 strains for anoxic biotechnical applications. J Biotechnol 163, 155–165. https://doi.org/10.1016/j.jbiotec.2012.09.015.

Sudarsan, S., Dethlefsen, S., Blank, L.M., Siemann-Herzberg, M., Schmid, A., 2014. The functional structure of central carbon metabolism in *Pseudomonas putida* KT2440. Applied and environmental microbiology 80, 5292–5303. https://doi.org/10.1128/AEM.01643-14.

Sun, Z., Ramsay, J.A., Guay, M., Ramsay, B.A., 2006. Automated feeding strategies for high-cell-density fed-batch cultivation of *Pseudomonas putida* KT2440. Applied microbiology and biotechnology 71, 423–431. https://doi.org/10.1007/s00253-005-0191-7.

Sweere, A., Luyben, K., Kossen, N., 1987. Regime analysis and scale-down: Tools to investigate the performance of bioreactors. Enzyme and Microbial Technology 9, 386–398. https://doi.org/10.1016/0141-0229(87)90133-5.

Takors, R., 2012. Scale-up of microbial processes: impacts, tools and open questions. Journal of Biotechnology 160, 3–9. https://doi.org/10.1016/j.jbiotec.2011.12.010.

References

Timilsina, G.R., 2014. Biofuels in the long-run global energy supply mix for transportation. Philosophical transactions. Series A, Mathematical, physical, and engineering sciences 372, 20120323. https://doi.org/10.1098/rsta.2012.0323.

Tiso, T., Ihling, N., Kubicki, S., Biselli, A., Schonhoff, A., Bator, I., Thies, S., Karmainski, T., Kruth, S., Willenbrink, A.-L., Loeschcke, A., Zapp, P., Jupke, A., Jaeger, K.-E., Büchs, J., Blank, L.M., 2020. Integration of Genetic and Process Engineering for Optimized Rhamnolipid Production Using *Pseudomonas putida*. Frontiers in bioengineering and biotechnology, 976. https://doi.org/10.3389/fbioe.2020.00976.

Tolan, J.S., 2002. Iogen's process for producing ethanol from cellulosic biomass. Clean Techn Environ Policy 3, 339–345. https://doi.org/10.1007/s10098-001-0131-x.

Traxler, M.F., Zacharia, V.M., Marquardt, S., Summers, S.M., Nguyen, H.-T., Stark, S.E., Conway, T., 2011. Discretely calibrated regulatory loops controlled by ppGpp partition gene induction across the 'feast to famine' gradient in *Escherichia coli*. Molecular Microbiology 79, 830–845. https://doi.org/10.1111/j.1365-2958.2010.07498.x.

Uchino, K., Saito, T., Gebauer, B., Jendrossek, D., 2007. Isolated poly(3-hydroxybutyrate) (PHB) granules are complex bacterial organelles catalyzing formation of PHB from acetyl coenzyme A (CoA) and degradation of PHB to acetyl-CoA. Journal of Bacteriology 189, 8250–8256. https://doi.org/10.1128/JB.00752-07.

Vallon, T., Simon, O., Rendgen-Heugle, B., Frana, S., Mückschel, B., Broicher, A., Siemann-Herzberg, M., Pfannenstiel, J., Hauer, B., Huber, A., Breuer, M., Takors, R., 2015. Applying systems biology tools to study n -butanol degradation in *Pseudomonas putida* KT2440. Eng. Life Sci. 15, 760–771. https://doi.org/10.1002/elsc.201400051.

Verkerk, K.A., Jaeger, B., Finkeldei, C.-H., Keim, W., 1999. Recent developments in isobutanol synthesis from synthesis gas. Applied Catalysis A: General 186, 407–431. https://doi.org/10.1016/S0926-860X(99)00158-1.

References

Viegas, S.C., Arraiano, C.M., 2008. Regulating the regulators: How ribonucleases dictate the rules in the control of small non-coding RNAs. RNA biology 5, 230–243. https://doi.org/10.4161/rna.6915.

Wang, Z., Gerstein, M., Snyder, M., 2009. RNA-Seq: a revolutionary tool for transcriptomics. Nature reviews. Genetics 10, 57–63. https://doi.org/10.1038/nrg2484.

Waters, L.S., Storz, G., 2009. Regulatory RNAs in bacteria. Cell 136, 615–628. https://doi.org/10.1016/j.cell.2009.01.043.

Weimer, A., Kohlstedt, M., Volke, D.C., Nikel, P.I., Wittmann, C., 2020. Industrial biotechnology of *Pseudomonas putida*: advances and prospects. Applied microbiology and biotechnology 104, 7745–7766. https://doi.org/10.1007/s00253-020-10811-9.

Weizmann, C., 1916. Production of acetone and alcohol by bacteriological processes: US-Patent.

Xing, Z., Kenty, B.M., Li, Z.J., Lee, S.S., 2009. Scale-up analysis for a CHO cell culture process in large-scale bioreactors. Biotechnology and bioengineering 103, 733–746. https://doi.org/10.1002/bit.22287.

Xu, J.-Z., Ruan, H.-Z., Chen, X.-L., Zhang, F., Zhang, W., 2019. Equilibrium of the intracellular redox state for improving cell growth and L-lysine yield of *Corynebacterium glutamicum* by optimal cofactor swapping. Microbial cell factories 18, 65. https://doi.org/10.1186/s12934-019-1114-0.

Yamanè, T., Shimizu, S., 1984. Fed-batch techniques in microbial processes, in: Agrawal, P. (Ed.), Bioprocess parameter control: With 28 tables, vol. 30. Springer, Berlin, pp. 147–194.

Yu, S., Lai, B., Plan, M.R., Hodson, M.P., Lestari, E.A., Song, H., Krömer, J.O., 2018. Improved performance of *Pseudomonas putida* in a bioelectrochemical system through overexpression of periplasmic glucose dehydrogenase. Biotechnol. Bioeng. 115, 145–155. https://doi.org/10.1002/bit.26433.

Ziegler, M., Zieringer, J., Takors, R., 2020. Transcriptional profiling of the stringent response mutant strain *E. coli* SR reveals enhanced robustness to large-scale conditions. Microbial biotechnology. https://doi.org/10.1111/1751-7915.13738.

Zobel, S., Kuepper, J., Ebert, B., Wierckx, N., Blank, L.M., 2017. Metabolic response of *Pseudomonas putida* to increased NADH regeneration rates. Eng. Life Sci. 17, 47–57. https://doi.org/10.1002/elsc.201600072.

APPENDIX

A. SUPPLEMENTARY MATERIAL TO P-II

Supplementary File

Pseudomonas putida KT2440 is naturally endowed to withstand industrial-scale stress conditions

Author names and affiliations:

Andreas Ankenbauer[1], Richard A. Schäfer[1], Sandra C. Viegas[2], Vânia Pobre[2], Björn Voß[1], Cecília M. Arraiano[2] and Ralf Takors[1,*]

[1]University of Stuttgart, Institute of Biochemical Engineering, Allmandring 31, 70569 Stuttgart, Germany

[2]Universidade Nova de Lisboa, Instituto de Tecnologia Química e Biológica António Xavier, Av. da República, EAN, 2780-157 Oeiras, Portugal.

*Corresponding author. Email address: takors@ibvt.uni-stuttgart.de

Supplementary Tables

Table S1 Energy balance for central metabolic precursors. "Energy produced" is calculated from glucose until precursor. "ATP produced" summarizes the energy produced based on the P/O ratio of 1.33. Negative values indicate consumption

Precursor	Energy produced			ATP produced
	ATP	NADH	NADPH	
E4P	-1	0	1	0.33
G3P	-1	0	0	-1
3PG	0	1	0	1.33
PEP	0	1	0	1.33
Pyr	0.5	0.5	0	1.17
Acetyl-CoA	0.5	1.5	0	2.495
AKG	0	2	1	3.99
OAA	-0.5	0.5	0	0.17
PRPP	-2	0	1	-0.67
Formate	0	0	-1	-1.33

Table S2 Energy costs for de novo synthesis of nucleotide triphosphates (NTP). Calculation is based on the P/O ratio of 1.33.

NTP	Precursor				Energy required			ATP costs
	PRPP	Formate	3PG	AKG	ATP	NADH	NADPH	netto
ATP	0.5	0.5	0.5	1	3	-0.5	1	0.01
GTP	1	1	1	1	3	-2	1	-1.65
CTP	0	0	0	1	5	0	1	2.34
UTP	0	0	0	1	4	0	1	1.34

Table S3 Energy costs for amino acids (AA) based on their respective precursors. Total ATP costs summarize energy produced from glucose to precursor (see Table S1) and from precursor to AA. Amino acid composition for P. putida KT2440 is derived from Sohn et al. (2010)

AA	Precursors									Energy produced			ATP costs	AA composition, g/100g protein
	E4P	PEP	3PG	Pyr	AcCoA	AKG	OAA	G3P	PRPP	ATP	NADH	NADPH		
Ala	0	0	0	1	0	0	0	0	0	0	0	0	-1.17	9.6
Arg	0	0	0	0	1	2	0	0	0	-4	0	-3	-2.49	5.5
Asn	0	0	0	0	0	1	0	0	0	-2	0	-1	-0.66	4.5
Asp	0	0	0	0	0	1	0	0	0	0	0	-1	-2.66	4.5
Cys	0	0	1	0	0	0	0	0	0	0	1	0	-2.66	1.7
Glu	0	0	0	0	0	1	0	0	0	0	0	-1	-2.66	4.9
Gln	0	0	0	0	0	1	0	0	0	-1	0	-1	-1.66	4.9
Gly	0	0	1	0	0	0	0	0	0	0	1	0	-2.66	11.5
His	0	0	0	0	0	0	0	0	1	-1	2	0	-0.99	1.8
Ile	0	0	0	1	0	0	1	0	0	-2	0	-3	4.66	5.4
Leu	0	0	0	2	1	0	0	0	0	0	1	-1	-4.83	8.4
Lys	0	0	0	1	0	1	0	0	0	-1	0	-3	-0.17	6.4
Met	0	0	0	0	0	0	1	0	0	-3	0	-5	9.49	2.9
Phe	1	2	0	0	0	0	0	0	0	-1	0	-1	-0.66	3.5
Pro	0	0	0	0	0	1	0	0	0	-1	0	-3	1.00	4.1
Ser	0	0	1	0	0	0	0	0	0	0	1	0	-2.66	4
Thr	0	0	0	0	0	0	1	0	0	-2	0	-2	4.50	4.7
Trp	1	2	1	-1	0	0	0	-1	1	-1	1	-1	-2.49	1.1
Tyr	1	2	0	0	0	0	0	0	0	-1	1	-1	-1.99	2.6
Val	0	0	0	2	0	0	0	0	0	0	0	-1	-1.00	7.9

Table S4 Carbon share of biomass, PHA and CO_2 ($\pm$ standard deviation from three biological replicates) based on glucose uptake rate at μ = 0.194 $\pm$ 0.01 h^{-1}. Carbon composition of biomass was taken from van Duuren, Jozef B J H et al. (2013)

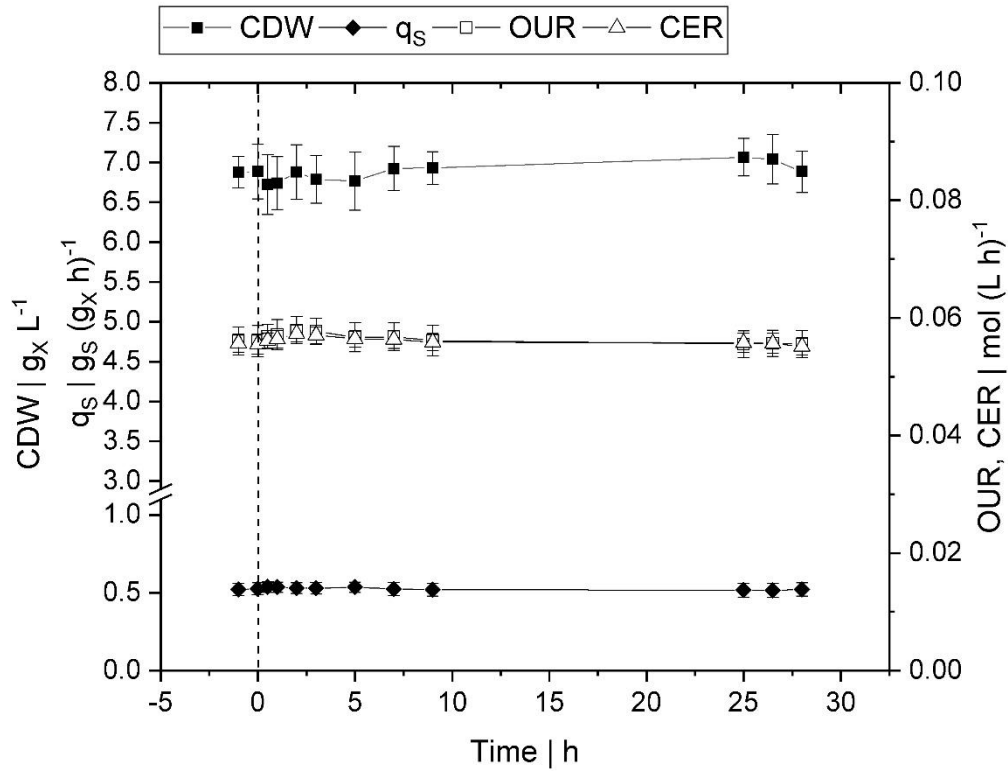| Condition	PHA free Biomass	PHA	CO_2	Sum
STR (Ref.)	47.8 $\pm$ 2.6	0.6 $\pm$ 0.2	48.6 $\pm$ 2.6	96.9 $\pm$ 5.4
STR+PFR (25 h)	48.3 $\pm$ 2.3	0.5 $\pm$ 0	48.7 $\pm$ 2.7	97.5 $\pm$ 5

Supplementary Figures

Figure S1 Physiological kinetics of P. putida KT2440 cultivated in a glucose-limited chemostat before and after the connection of the PFR (time point 0 h). Error bars represent the standard deviation of three biological replicates.

Equation	y = a + b*x
Plot	C10
Weight	Instrumental
Intercept	-0.13384 ± 0.02092
Slope	0.01422 ± 2.84565E-4
Residual Sum of Squares	1.37267
Pearson's r	0.9996
R-Square(COD)	0.9992
Adj. R-Square	0.9988
Equation	y = a + b*x
Plot	C12
Weight	Instrumental
Intercept	-0.13638 ± 0.00199
Slope	0.0086 ± 9.43357E-5
Residual Sum of Squares	2.4794
Pearson's r	0.99982
R-Square(COD)	0.99964
Adj. R-Square	0.99952
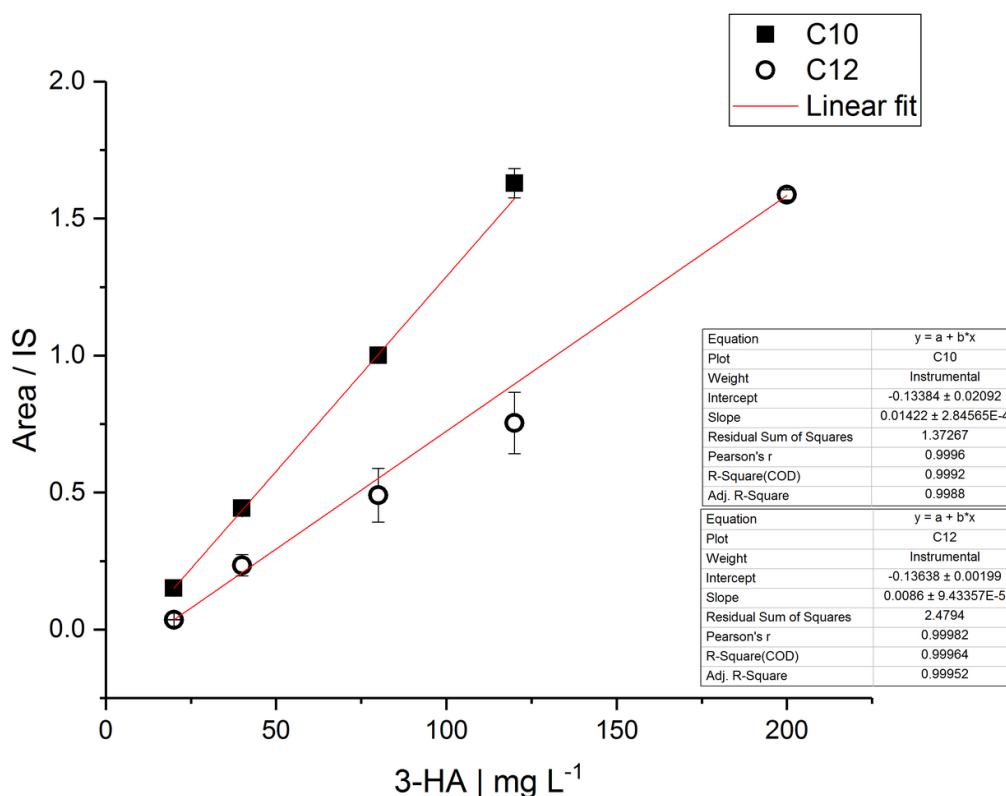
Figure S2 Calibration fit for GC standards. Derivatized 3-hydroxydecanoate and 3-hydroxydodecanoate were measured via GC FID. For normalization purpose, each area was normalized by the respective area of the internal standard (IS). This calibration range was suitable to determine the 3-HA concentrations in the extracted cultivation samples.

Supplementary Section

Plug flow reactor characterization

Characterization of the plug flow reactor compartment was performed with tracer experiments according to Löffler et al. (2016) and Buchholz et al. (2014) with overpressure of 0.5 bar and aeration (0.1 L min^{-1}) before port P1. The calculated mean residence time τ and its variance σ^2 are listed in Table S5 along with the respective Bodenstein number *Bo* (George et al., 1993; Levenspiel, 1999). According to George et al. (1993) *Bo* >10 is sufficient to negate back-mixing, thus plug-flow behavior can be assumed in the PFR compartment.

Table S5 Parameters for characterizing the plug flow reactor.

Sample port	τ	σ	Bo
	s	s^2	-
P1	34.9	128.8	18.8
P2	61.7	541.2	14.0
P3	77.3	298.7	40.0
P4	101.7	338.0	61.2
P5	128.4	843.2	39.1

Statistical analysis of 3-HA determination

Measurements of 3-HAs were performed in two out of three independent biological replicates. Concerning the detection of biomass specific C10 and C12 concentrations, relatively high differences between the duplicates were detected (see Table S6). However, despite of an apparent trend of a reduced pool size at the end of the PFR (102-128 s) in contrast to the entrance (0-35 s) in each individual experiment, statistical analysis did not reveal significance. *p*-values based on one-way analysis of variance (ANOVA) are presented at the end of Table S6.

Table S6 measured values of intracellular 3-HA concentrations in experiment 1 (Exp. 1) and experiment 2 (Exp. 2), mean values and standard deviation (SD) in relation to the residence time in the PFR.

	C10, mg/g$_X$				C12, mg/g$_X$			
Residence time in PFR, s	Exp. 1	Exp. 2	Mean	SD	Exp. 1	Exp. 2	Mean	SD
0	3.46	4.47	3.97	0.72	4.56	4.27	4.42	0.20
35	3.45	5.15	4.30	1.20	4.11	5.01	4.56	0.64
62	3.40	4.68	4.04	0.91	3.69	4.25	3.97	0.40
77	2.65	3.68	3.16	0.73	2.65	3.46	3.05	0.58
102	2.98	4.12	3.55	0.81	3.04	3.33	3.19	0.21
128	2.92	3.78	3.35	0.60	3.24	3.76	3.50	0.37
p-value (ANOVA)	0.74				0.05			

Data Processing

In this study, the raw paired-end sequencing reads consist of 36 samples divided into 12 measurements with three replicates each. In total, this results in about 520 million reads, making up between 9 and 25 million reads per sample (see Supplementary Data, tab 'statistics'). For the preprocessing, TRIMMOMATIC v0.39 (Bolger et al., 2014) was applied to remove remaining technical sequences within the reads using the provided TruSeq2 adapter files (https://github.com/timflutre/trimmomatic/). In addition to the quality and length requirements, the seeds were allowed to have 2 mismatches that would still lead to a full match. For the palindrome clip threshold and the simple clip threshold we specified cutoffs of 25 and 10, respectively. The minimum adapter length was decreased to 1 enabling the removal of very short adapter fragments. Furthermore, the reads were quality trimmed using a sliding window approach in which the reads are scanned in windows (of size 4) and clipped once the average quality score (Phred) within the window falls below 20 ('SLIDINGWINDOW:4:20'). In the end, only reads that still consist of forward and reverse reads were subjected to the further analysis. Figure S3 illustrates the proportion of the raw reads after the preprocessing and alignment procedure. Similarly, Figure S4 shows the proportion of all aligned reads that were assigned (uniquely) to features in the coding sequence. We provide the corresponding values in the Supplementary Data sheet 'statistics'.
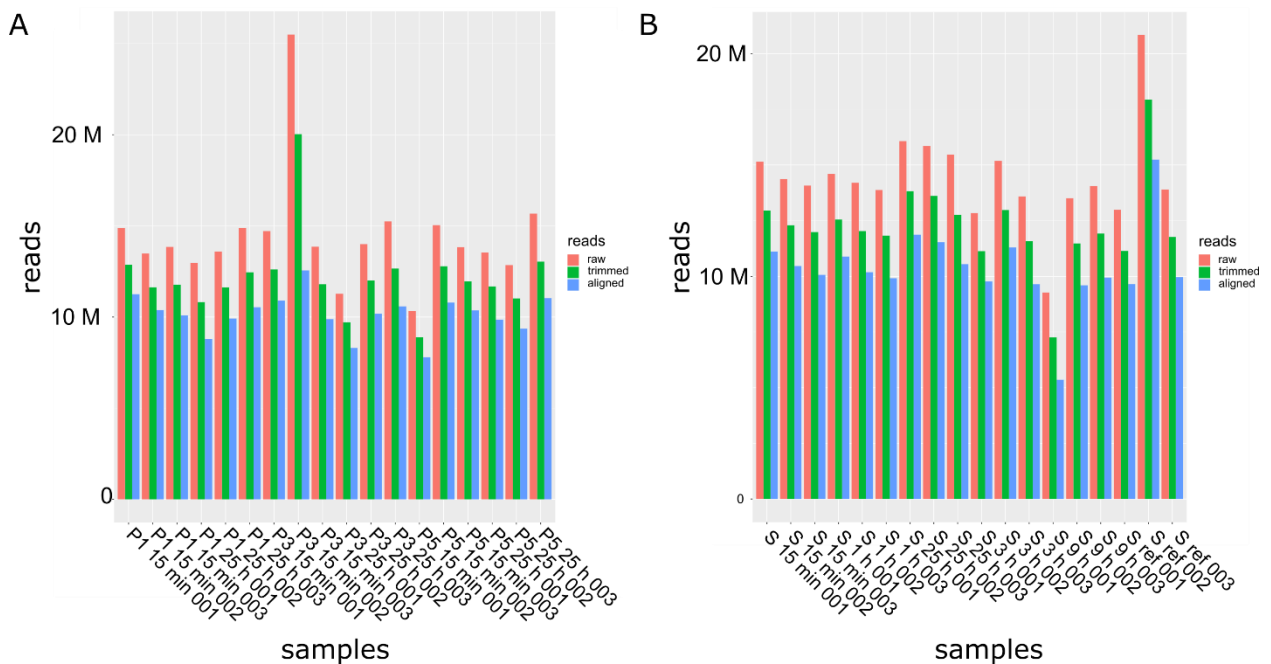

Figure S3 Read distribution of the samples withdrawn from the PFR (A) and the STR (B). The bars correspond to the read number before (raw) and after preprocessing (trimmed) as well as after the sequence alignment (aligned).
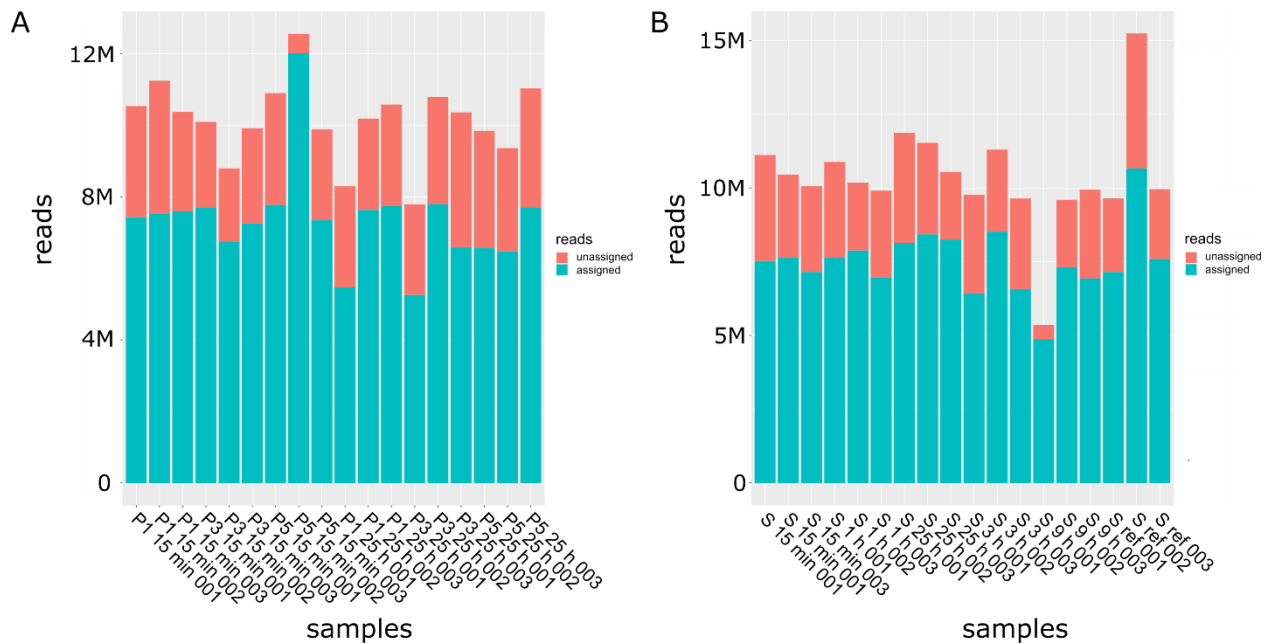
Figure S4 Portion of assigned features to the total number of aligned reads for samples withdrawn from the PFR (A) and STR (B).

Differential Expression Analysis

At first, the data was inspected by performing a principal component analysis (PCA) on the samples. Initially, we transformed the count data using the regularized log transformation (rlog) to eliminate the dependence of the variance of the values to their mean. This results in count values on the $\log_2$ scale normalized to library size that are approximately homoskedastic (having constant variance along the range of mean values). For that, we used the function `rlogTransformation` and applied a blind dispersion estimation by setting `blind=TRUE` in order to compare the samples in an unbiased manner (neglecting the information about experimental groups). This transformation is delineated in Figure S5 A in which the standard deviation across samples is plotted against the mean after transformation. We took the mean of the replicates of each sample selected 1000 genes that exhibit the highest standard deviation across samples. Subsequently, the variance stabilized data was transposed to perform the principal component analysis on the samples using the function `prcomp` from the R Stats Package. In Figure S5 B, the calculated coordinates of the individuals (samples) were plotted on the principal components. In accordance to the scree plot (Figure S5 C), the first

two principal components explain about 81% of the variation. The transcriptional changes along the PFR at 15 min and 25 h exhibit different expression profiles on the first principal component (PC1), in which both time points could be divided into clearly separate clusters on the second principal component (PC2). Likewise, we can observe a change in the transcriptomic profile, shortly after connecting the PFR to the STR. In particular, the STR samples at the reference state (STR-Ref) and after 15 min (STR-15min) are positioned on the opposite ends along the PC2. Similar profiles in the STR at 9 h and 25 h indicate a steady state (green ellipse) that reflects the adaptation of the organism. Furthermore, the close proximity of the samples in the STR and the first port of the PFR (PFR1) at the corresponding time points are in accordance to the time interval between sampling. Finally, Figure S5 D list the top 20 genes that contribute the most to the variance in PC1 and PC2.
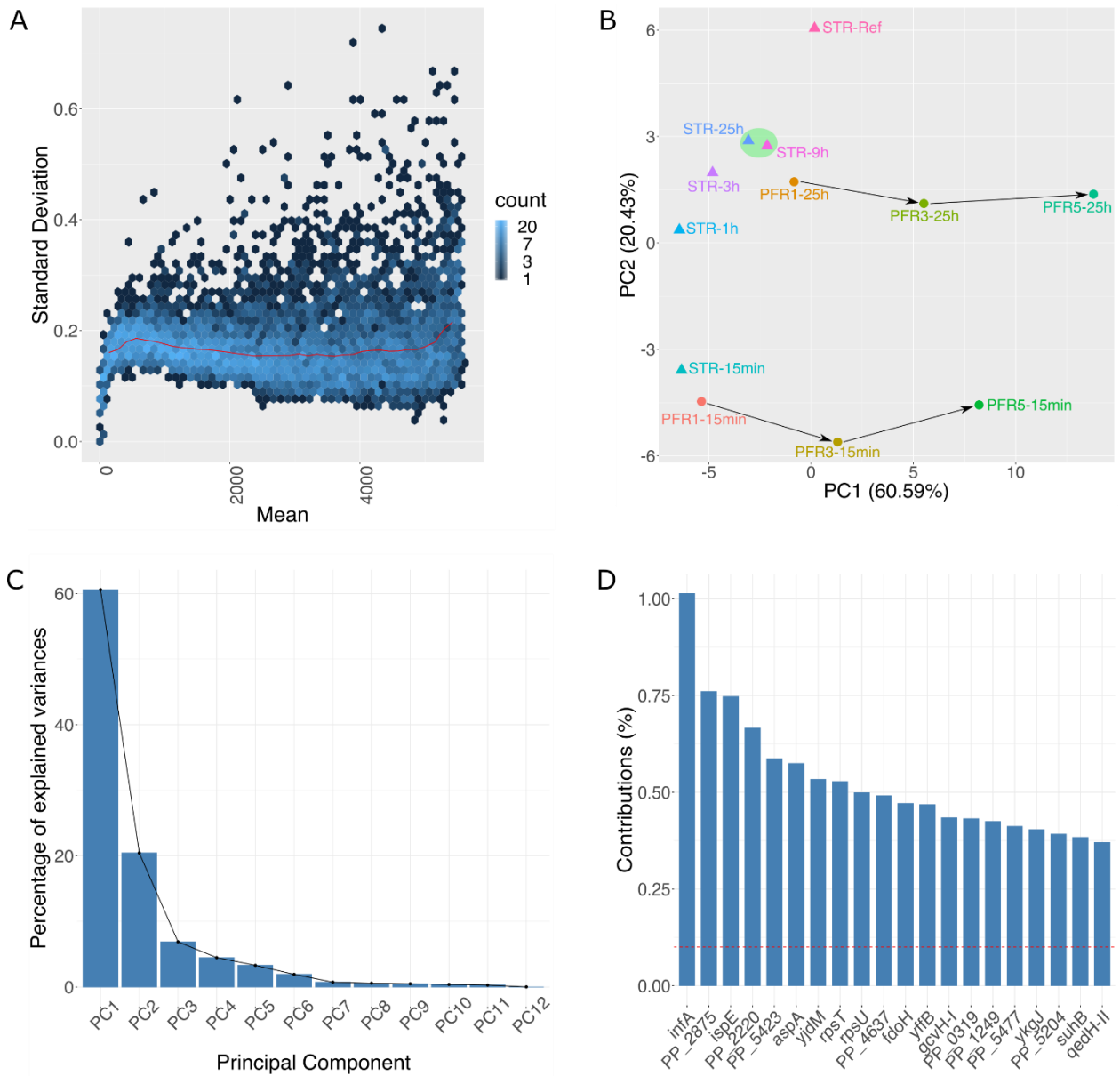
Figure S5 (A) Scatterplot of the standard deviation across samples against the mean (calculated gene-wise) using the regularized log transformation. The red line depicts the running median estimator (window-width 10%). If there is no variance-mean dependence, then the line should be approximately horizontal. (B) Individuals (samples) of 12 process time points plotted on principal component 1 (PC1) and 2 (PC2). Circles and squares correspond to the location of the sampling in the PFR and STR, respectively. Arrows follow the adaptation trajectories within the PFR. A potential steady state is indicated by the green ellipse. (C) Scree plot of the PCA illustrating the contribution of each principal component to the variance. (D) Barplot of the top 20 variables (genes) contributing to the variability of PC1 and PC2. The red reference line corresponds to the expected value if the contribution where uniform and is considered as important in contributing to the dimension.

Furthermore, we tested for outliers in the data using the Cook's distance for every gene and for every sample as a measure of how much a single sample is influencing the fitted coefficients for a gene. As illustrated in Figure S6, all samples exhibit similar distances indicating no isolated large counts.
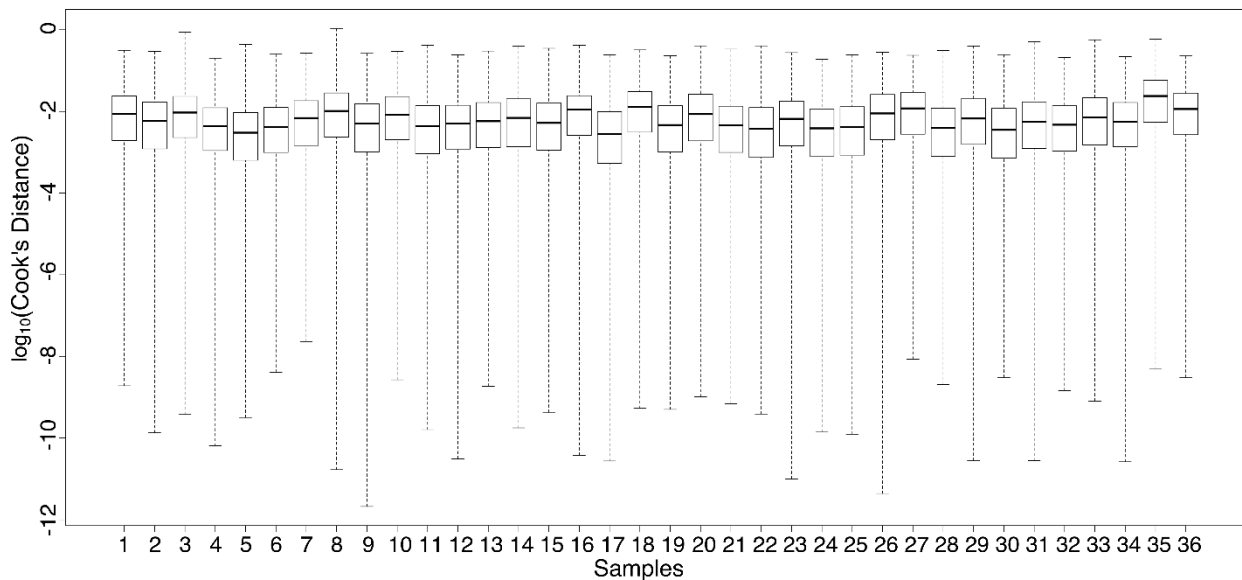

Figure S6 Boxplot of the Cook's distances to see if one sample is consistently higher than the others (this is not the case)

Gene Set Enrichment Analysis (GSEA)

We utilized GAGE (Luo et al., 2009) to perform the gene set enrichment analysis on the data. For that, we obtained the Gene Ontology term annotations for *P. putida* from the Pseudomonas genome database and used the rlog transformed raw count data, similar to the principal component analysis. We configured GAGE to conduct group-on-group comparisons (`compare="as.group"`) between the reference and target condition identical to the differential expression analysis using t-test statistics (`use.fold=F`). The gene sets were considered to be significantly different with an FDR q-value <0.05 corrected after Benjamini an Hochberg (1995). As illustrated in Figure S7, the analysis revealed 18 gene sets that exhibit a significant difference in at least one sample. The only significant downregulation occurs at PFR sample port P1 at 15 min with a moderate t-statistic of signal transduction, phosphorylation and transferase activity that are not affected in other samples. In PFR sample

port P3 at 15 min the gene sets for *catalytic activity*, *metabolic process*, *oxidoreductase activity* and the *oxidation-reduction* are upregulated that are further dominant in the PFR at 25 h. Interestingly, these gene sets are also upregulated in the STR at 25 h. Furthermore, we observe the gene sets for *RNA binding, ribosome, intracellular, translation* only being upregulated in the beginning of the process (15 min, 1 h). The underlying data is provided in the Supplementary Data (see tab 'GSEA')

Molecular function

A phosphorelay sensor kinase activity

B magnesium ion binding

C RNA binding

D structural constituent of ribosome

E catalytic activity

N oxidoreductase activity

O oxidoreductase activity,
   acting on the aldehyde or oxo group of donors,
   NAD or NADP as acceptor

P transferase activity,
   transferring phosphorus-containing groups

Biological Process

I translation

J tRNA aminoacylation for protein translation

K signal transduction

L metabolic process

M phosphorylation

Q oxidation-reduction process

R bacterial-type flagellum-dependent cell motility

Cellular component

F intracellular
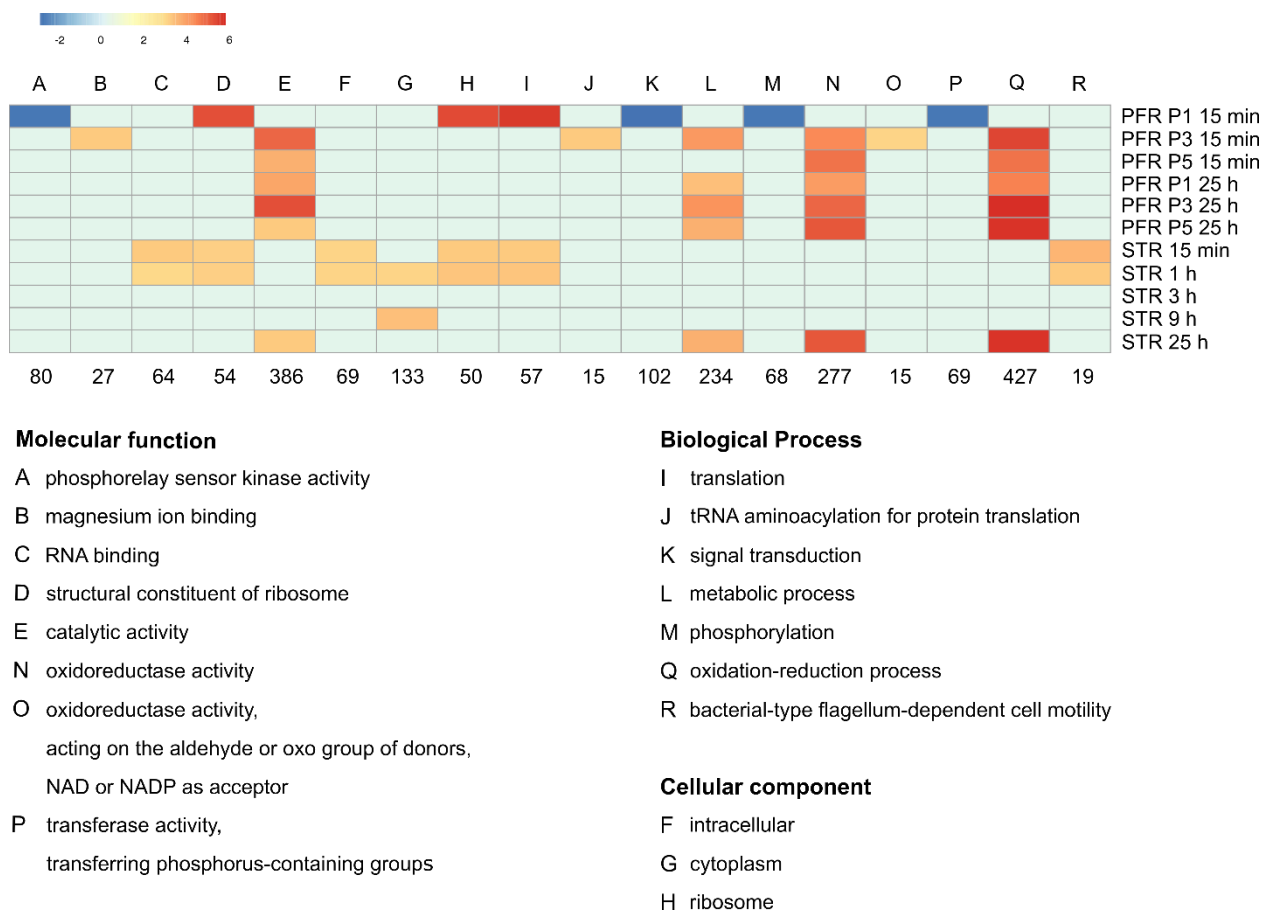
G cytoplasm

H ribosome

Figure S7 Results of the gene set enrichment analysis of both the short-term and long-term response. For that, samples (rows) withdrawn from the PFR (P1, P3, P5) were compared with the samples of the STR at the corresponding time points and samples withdrawn from the STR were compared to the reference condition in the STR. Gene sets were considered as significantly different with an FDR q-value <0.05, shown as cells with the value of the t-statistic (indicated by the color scale) from GAGE indicating the magnitude of gene set level changes. Numbers at the bottom correspond to the size of the gene sets.

References

Benjamini, Yoav and Hochberg, Yosef (1995) Controlling the False Discovery Rate: A Practical and Powerful Approach to Multiple Testing. *Journal of the Royal Statistical Society. Series B (Methodological)* **57** (1): 289–300.

Bolger, A.M., Lohse, M., Usadel, B., 2014. Trimmomatic: a flexible trimmer for Illumina sequence data. Bioinformatics (Oxford, England) 30 (15), 2114–2120. 10.1093/bioinformatics/btu170.

Buchholz, J., Graf, M., Freund, A., Busche, T., Kalinowski, J., Blombach, B., Takors, R., 2014. CO_2 /HCO_3^- perturbations of simulated large scale gradients in a scale-down device cause fast transcriptional responses in Corynebacterium glutamicum. Applied microbiology and biotechnology 98 (20), 8563–8572. 10.1007/s00253-014-6014-y.

George, S., Larsson, G., Enfors, S.-O., 1993. A scale-down two-compartment reactor with controlled substrate oscillations: Metabolic response of Saccharomyces cerevisiae. Bioprocess Engineering 9 (6), 249–257. 10.1007/BF01061530.

Levenspiel, O., 1999. Chemical reaction engineering, 3rd ed. Wiley, Hoboken, NJ, 668 pp.

Liao, Y., Smyth, G.K., Shi, W., 2014. featureCounts: an efficient general purpose program for assigning sequence reads to genomic features. Bioinformatics 30 (7), 923–930. 10.1093/bioinformatics/btt656.

Löffler, M., Simen, J.D., Jager, G., Schaferhoff, K., Freund, A., Takors, R., 2016. Engineering E. coli for Large-Scale Production - Strategies Considering ATP Expenses and Transcriptional Responses. Metabolic engineering. 10.1016/j.ymben.2016.06.008.

Luo, W., Friedman, M.S., Shedden, K., Hankenson, K.D., Woolf, P.J., 2009. GAGE: generally applicable gene set enrichment for pathway analysis. BMC Bioinformatics 10 (1), 1–17. 10.1186/1471-2105-10-161.

Sohn, S.B., Kim, T.Y., Park, J.M., Lee, S.Y., 2010. In silico genome-scale metabolic analysis of Pseudomonas putida KT2440 for polyhydroxyalkanoate synthesis, degradation of aromatics and anaerobic survival. Biotechnology journal 5 (7), 739–750. 10.1002/biot.201000124.

van Duuren, Jozef B J H, Puchalka, J., Mars, A.E., Bucker, R., Eggink, G., Wittmann, C., Dos Santos, Vitor A P Martins, 2013. Reconciling in vivo and in silico key biological parameters of Pseudomonas putida KT2440 during growth on glucose under carbon-limited condition. BMC biotechnology 13, 93. 10.1186/1472-6750-13-93.

Winsor, G.L., Griffiths, E.J., Lo, R., Dhillon, B.K., Shay, J.A., Brinkman, F.S.L., 2016. Enhanced annotations and features for comparing thousands of Pseudomonas genomes in the Pseudomonas genome database. Nucleic Acids Res 44 (D1), D646-53. 10.1093/nar/gkv1227.

B. SUPPLEMENTARY MATERIAL TO P-III

Supporting Information for

Pseudomonas putida KT2440 endures temporary oxygen limitations

Philipp Demling[1], Andreas Ankenbauer[2], Bianca Klein[3], Stephan Noack[3], Till Tiso[1*], Ralf Takors[2], Lars M. Blank[1*]

1   Institute of Applied Microbiology (iAMB), Aachen Biology and Biotechnology (ABBt), RWTH Aachen University, Worringer Weg 1, 52074 Aachen

2   Institute of Biochemical Engineering, University of Stuttgart, Allmandring 31, 70569 Stuttgart

3   Institute of Bio- and Geosciences, Biotechnology (IBG-1), Forschungszentrum Jülich GmbH, Leo-Brandt-Straße 1, 52425 Jülich, Germany

* Corresponding authors:

Lars M. Blank, Worringer Weg 1, 52074 Aachen; lars.blank@rwth-aachen.de, Phone: +49 241 80 26600

Till Tiso, Worringer Weg 1, 52074 Aachen, E-Mail: till.tiso@rwth-aachen.de, Phone: +49 241 80 26629

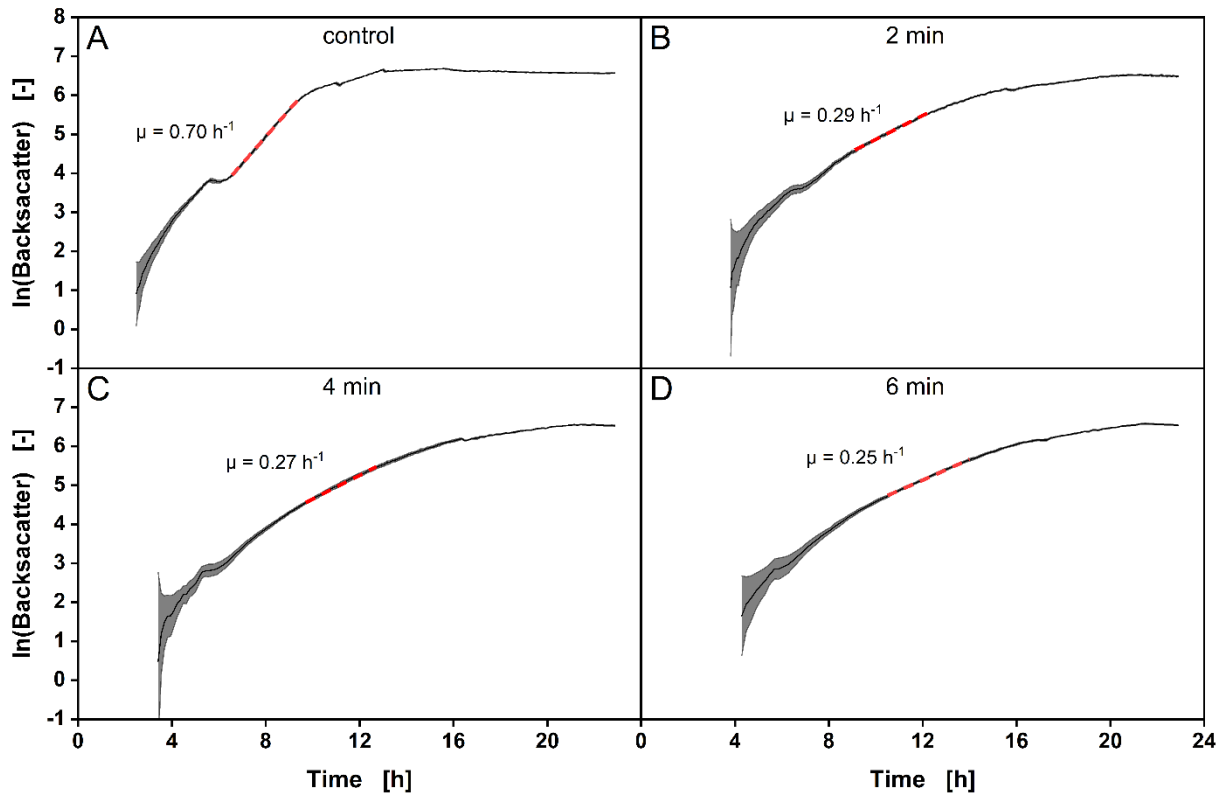Running title: *P. putida* endures temporary O_2 limitation

Figure A1 Logarithmic backscatter signal over time of cultivations of P. putida KT2440 in microtiter plates at different intervals of oscillating agitation. (A) control, (B) 2 min oscillation, (C) 4 min oscillation, (D) 6 min oscillation. The red dashed lines indicate regions used for the determination of the growth rate. Shaded areas represent the standard deviation of measurements from five independent experiments.
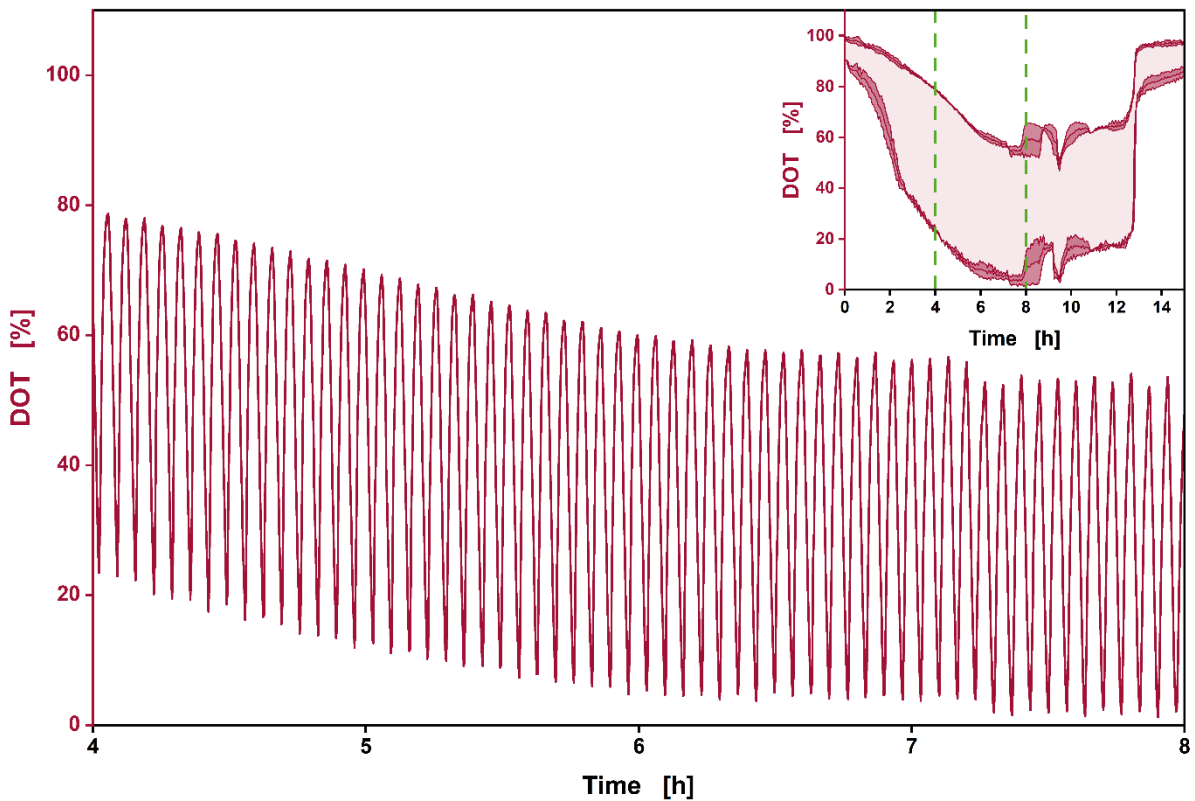

Figure A2 Close view of the DOT signal of an STR cultivation of *P. putida* KT2440 subjected to an oscillating agitation and aeration at an interval of 2 min. The depicted section of the cultivation ranges from 4 h to 8 h as illustrated by the green dashed lines in the graph of the entire cultivation in the top right corner. Only one replicate is shown for clarity.
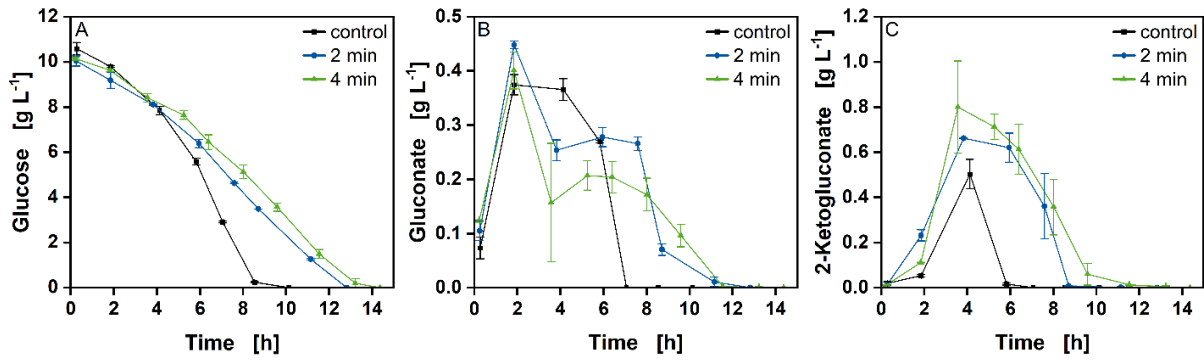
Figure A3 Cultivations of *P. putida* KT2440 at different intervals of oscillating aeration and agitation. (A) glucose, (B) gluconate, and (C) 2-ketogluconate concentrations for the control cultivations (black squares), 2 min intervals of oscillation (blue circles), and 4 min intervals of oscillation over the duration of the cultivation. Error bars represent errors derived from two independent experiments. Note the different scales of the y-axes.

Figure A4 Cultivations of *P. putida* KT2440 SK4 at different intervals of oscillating aeration and agitation. (A) glucose, (B) gluconate, and (C) 2-ketogluconate concentrations for the control cultivations (black squares) and 2 min intervals of oscillation (blue circles) over the duration of the cultivation. Error bars represent errors derived from two independent experiments. Note the different scales of the y-axes.
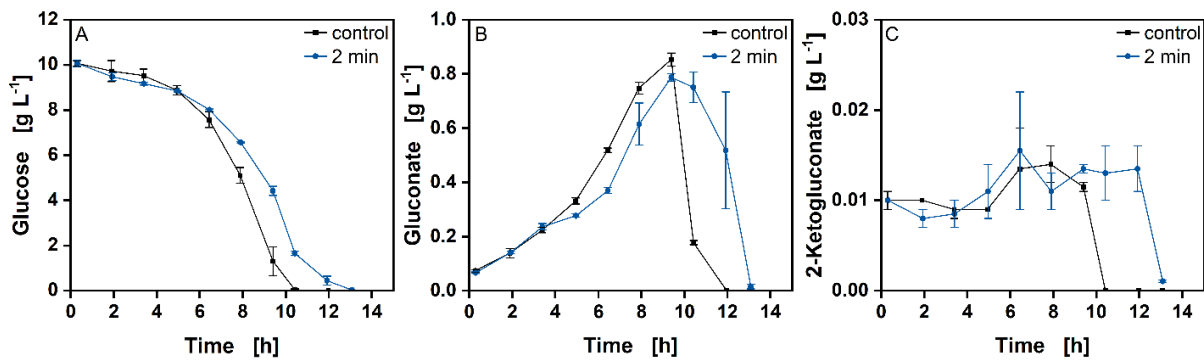
Table A1 Significantly altered proteins of *P. putida* KT2440 subjected to 2 min intervals of oscillation compared to control cultivations at t1 and t2.

ID [†]	Annotation [†]	fold change	p-value	COG
t₁				
PP_4116	isocitrate lyase AceA	0.228	0.00062	C
PP_2679	quinoprotein ethanol dehydrogenase PedH	0.230	0.0001	G
PP_4487	acetyl-CoA synthetase AcsA-I	0.230	0.00027	I
PP_5365	fatty acid methyltransferase	0.400	0.02716	M
PP_2675	cytochrome c-type protein	0.468	0.00931	C
PP_2680	aldehyde dehydrogenase AldB-II	0.473	8.72E-06	C
PP_2677	hypothetical protein	0.496	0.03697	S
PP_3839	alcohol dehydrogenase AdhP	2.092	0.00799	P
PP_3924	hypothetical protein	2.132	0.00319	L
PP_5391	hypothetical protein	2.162	0.00028	S
PP_0485	single-stranded DNA-binding protein (ssb)	2.395	0.00199	L
PP_2132	universal stress protein	2.404	4.77E-05	T
PP_1000	ornithine carbamoyltransferase ArcB	2.437	0.00092	E
PP_3420	sensor histidin kinase	2.816	0.01354	L
t₂				
PP_4116	isocitrate lyase AceA	0.368	0.00987	C
PP_2679	quinoprotein ethanol dehydrogenase PedH	0.437	0.00568	G
PP_4487	acetyl-CoA synthetase AcsA-I	0.436	0.01131	I
PP_0625	chaperone protein ClpB	2.701	0.04893	O

† According to pseudomonas.com (Winsor et al., 2016)
‡ Clusters of orthologous groups (COG). According to the COG database(Tatusov et al., 1997) retrieved via eggnog 5.0.0.
  COGs: C - Energy production and conversion, E - Amino acid transport and metabolism, G - Carbohydrate transport and metabolism, I - Lipid transport and metabolism, L - Replication, recombination, and repair, M - Cell wall/membrane/envelope biogenesis, O - Post-translational modification, protein turnover, and chaperones, P - Inorganic ion transport and metabolism, S - Unknown function, T - Signal transduction mechanism.

References

Tatusov RL, Koonin EV, Lipman DJ. 1997. A genomic perspective on protein families. *Science* 278(5338):631. *doi:* 10.1126/science.278.5338.631.

Winsor GL, Griffiths EJ, Lo R, Dhillon BK, Shay JA, Brinkman FSL. 2016. Enhanced annotations and features for comparing thousands of *Pseudomonas* genomes in the *Pseudomonas* genome database. *Nucleic acids research* 44(D1):D646-D653. *doi:* 10.1093/nar/gkv1227.

C. SUPPLEMENTARY MATERIAL TO P-V

Supplementary file

Micro-aerobic production of isobutanol with engineered *Pseudomonas putida*

Andreas Ankenbauer[1]

Robert Nitschel[1]

Attila Teleki[1]

Tobias Müller[1]

Lorenzo Favilli[1]

Bastian Blombach[2]

Ralf Takors[1]

[1]Institute of Biochemical Engineering, University of Stuttgart, Allmandring 31, 70569 Stuttgart, Germany

[2]Microbial Biotechnology, Campus Straubing for Biotechnology and Sustainability, Technical University of Munich, Straubing, Germany

Correspondence: Prof. Ralf Takors (takors@ibvt.uni-stuttgart.de). Institute of Biochemical Engineering, University of Stuttgart, Allmandring 31, 70569 Stuttgart, Germany.

Supplementary Process Characteristics

Figure S 1 shows the extracellular glucose concentrations, the dissolved oxygen tensions, and the Feed rates in the *Process R*, *Process F*, and *Process MA*. Table S 1 lists the process related results from the biological duplicate of *Process MA*.
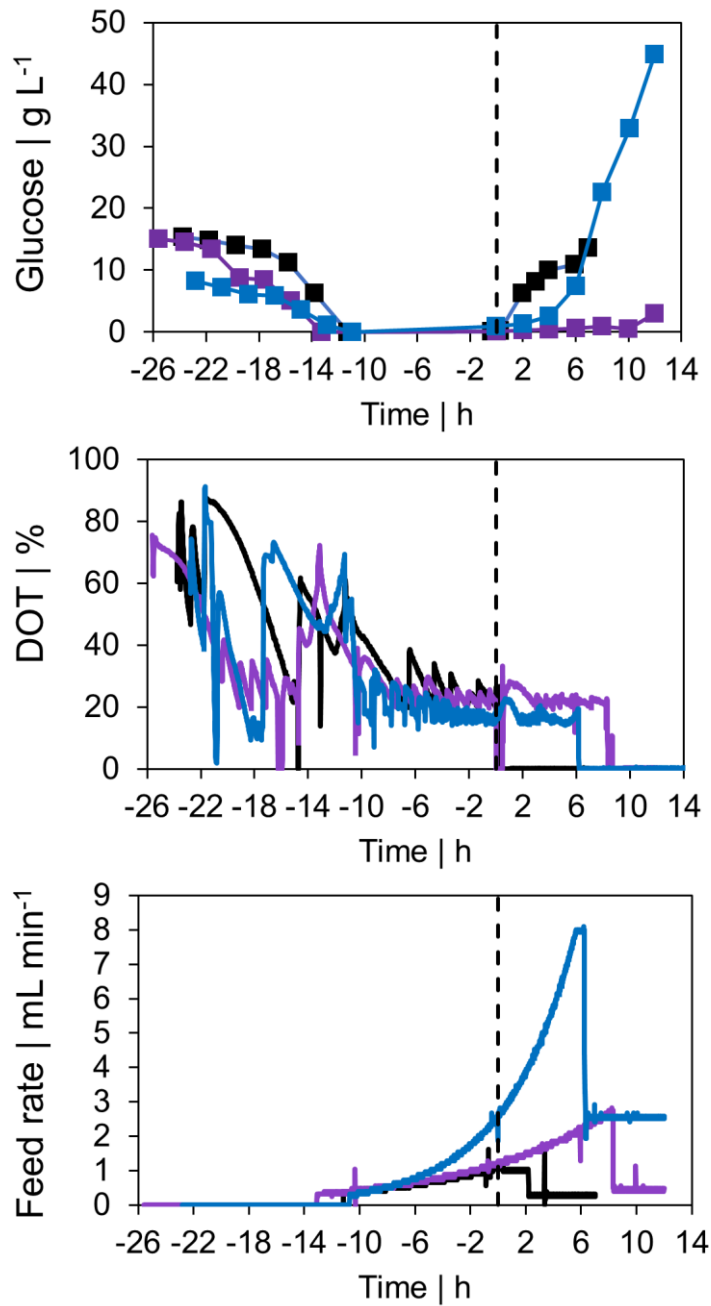

Figure S 1 Extracellular glucose concentrations, dissolved oxygen tensions (DOT), and the feed rates in Process R (purple), Process F (blue), and Process MA (black)

Time [h]		Biomass [g L⁻¹]		Isobutanol [g L⁻¹]		2-KG [g L⁻¹]		KIV [g L⁻¹]		L-valine [g L⁻¹]		Y_{PS} [mg g⁻¹]		DOT [%]	
-24.1	-23.8	0.1	0.1	0.0	0.0	0.2	0.1	0.1	0.1	0.0	0.0	0.0	0.0	41.7	66.8
-22.1	-21.8	0.1	0.1	0.0	0.0	0.4	0.2	0.1	0.1	0.0	0.0	0.0	0.0	60.2	52.8
-20.1	-19.8	0.2	0.2	0.0	0.0	0.9	0.7	0.2	0.1	0.0	0.0	0.0	0.0	48.1	79.0
-18.1	-17.8	0.5	0.3	0.0	0.0	1.7	1.5	0.3	0.2	0.0	0.0	0.0	0.0	49.6	58.3
-16.1	-15.8	1.0	0.8	0.0	0.0	3.3	2.8	0.4	0.4	0.0	0.0	0.0	0.0	58.0	31.8
-14.1	-13.8	1.9	1.3	0.0	0.0	5.3	4.9	0.9	0.6	0.0	0.0	0.0	0.0	33.0	54.2
-13.3	-11.3	2.4	2.7	0.0	0.0	5.9	9.8	0.9	1.1	0.1	0.0	0.0	0.0	60.3	56.0
0.0	-0.4	12.5	12.4	0.1	0.1	0.5	0.0	6.4	7.3	1.0	0.8	2.1	2.2	26.3	22.7
0.3	0.3	12.5	12.1	0.1	0.1	0.5	0.0	6.3	7.4	1.1	0.9	2.5	2.9	24.1	26.6
2.0	1.9	11.2	11.6	1.5	1.5	0.5	0.0	4.2	1.9	1.2	1.1	20.5	32.9	0.1	0.0
3.0	3.0	11.1	11.1	1.9	2.3	0.3	0.2	1.0	0.7	1.2	1.1	42.7	52.0	0.0	0.3
4.0	3.9	10.6	11.0	1.9	2.7	0.3	0.2	0.4	0.3	1.3	1.1	55.6	59.7	0.0	0.2
6.0	5.9	10.2	10.5	2.6	2.6	0.4	0.2	0.2	0.0	1.1	1.0	49.4	59.2	0.5	0.1
8.0	6.9	10.2	10.2	2.5	2.6	0.4	0.3	0.0	0.0	1.1	1.0	49.0	58.8	0.3	0.1

Table S 1 Comparison of relevant product concentrations and yields that were determined in the biological duplicate experiment of Process MA. The process time is given in relation to the point of plasmid induction. The grey columns represent the results shown in the manuscript.

Intracellular metabolite quantification

Figure S 2 illustrates intracellular metabolite levels that were determined before and during aerobic isobutanol production in *P. putida* Iso2.
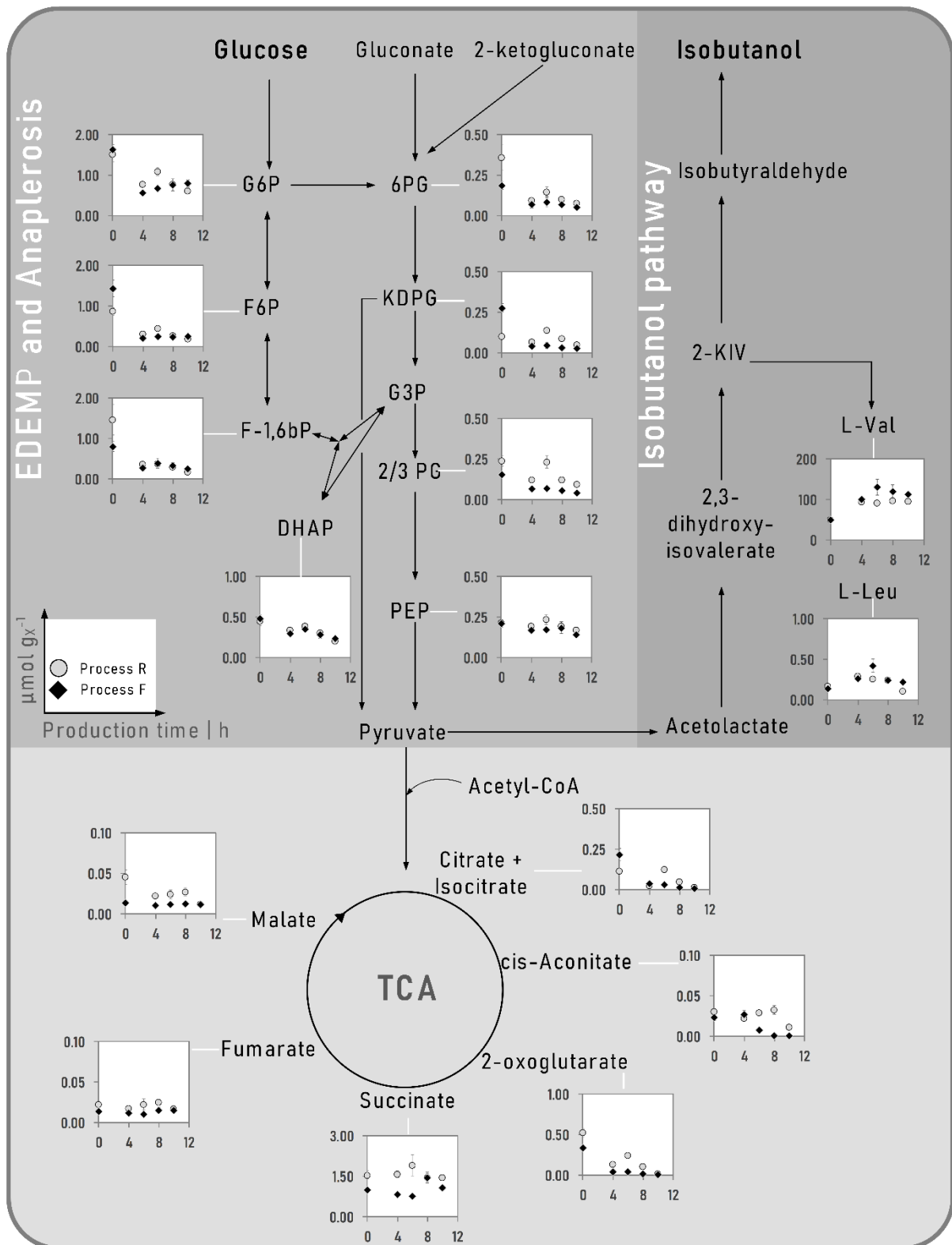
Figure S 2 Intracellular concentrations (in µmol gx^{-1}) of different metabolites in isobutanol producing P. putida Iso2 cells under aerobic fed-batch conditions in the reference Process R (◐) and Process F (◆). Time point 0 h equals the reference condition before induction of the plasmid. Micro-aerobic condition was installed after 8 h in Process R and after 6 h in Process F, respectively. Abbreviations: G6P: glucose-6-phosphate, 6PG: 6-phosphogluconate, KDPG: 2-keto-3-deoxy-6-phosphogluconate, G3P: glyceraldehyde-3-phosphate, 2/3 PG: 3-phosphoglycerate and 2-phosphoglycerate, PEP: phosphoenolpyruvate, DHAP: dihydroxyacetone-phosphate, F-1,6-bP: fructose-1,6-bisphosphate, F6P: fructose-6-phosphate, CoA: co-enzyme A, TCA: tricarboxylic acid cycle, L-Leu: L-leucine, L-Val: L-valine, 2-KIV: 2-ketoisovalerate

Figure S 3 shows intracellular metabolite concentrations after 4 hours of micro-aerobic condition in contrast to the aerobic level before plasmid induction in *Process MA*.
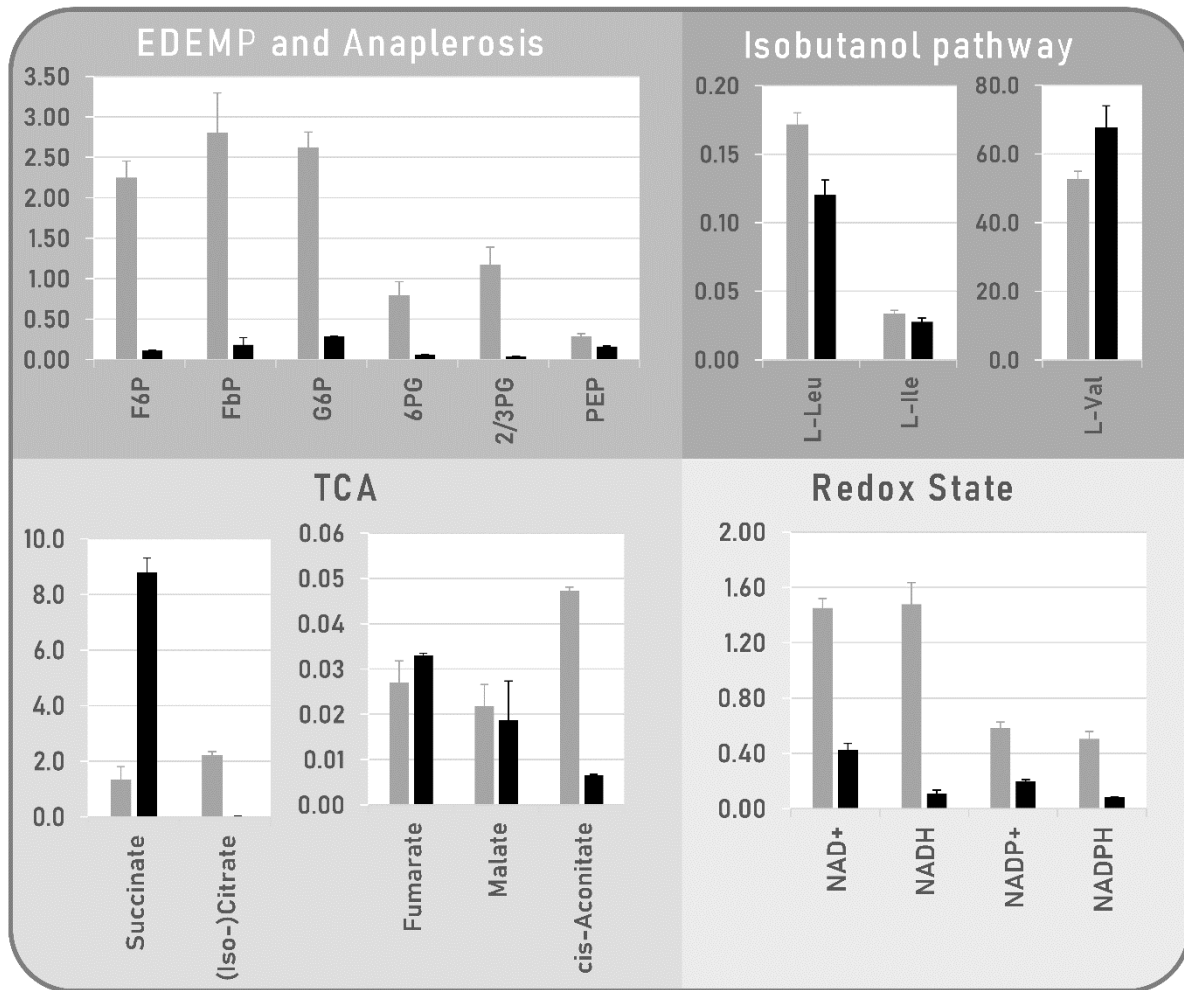

Figure S 3 Comparison of intracellular concentrations (in µmol g$_X^{-1}$) of different metabolites in isobutanol producing P. putida Iso2 cells under micro-aerobic condition (black bars) in contrast to aerobic growing cells (grey bars) in Process MA. Abbreviations as addition to Figure S2: L-Ile: L-isoleucine